

**LANTHANIDE-DOPED NANOPARTICLES AS THE ACTIVE OPTICAL MEDIUM IN  
POLYMER-BASED DEVICES**

PROEFSCHRIFT

ter verkrijging van  
de graad van doctor aan de Universiteit Twente,  
op gezag van rector magnificus,  
prof.dr.F. A. van Vught,  
volgens besluit van het College voor Promoties  
in het openbaar te verdedigen  
op vrijdag 6 februari 2004 om 16.45 uur

door

**Jan Willem Stouwdam**

geboren op 29 december 1974

te Ijsselmuiden

Dit proefschrift is goedgekeurd door:

Promotor Prof.dr.ir.D. N. Reinhoudt

Assistent-promotor Prof.dr.ir.F. C. J. M. van Veggel



Dit onderzoek is financieel gesteund door het gebied Chemische Wetenschappen van de Nederlandse Organisatie voor Wetenschappelijk Onderzoek

ISBN 90-365-2011-8

## *Table of contents*

<b>CHAPTER 1</b> .....	<b>1</b>
General introduction .....	1
1.1 References.....	3
<b>CHAPTER 2</b> .....	<b>5</b>
Luminescence of lanthanide ions.....	5
2.1 General introduction .....	6
2.2 Luminescence of trivalent lanthanide ions .....	7
2.3 Quenching processes.....	10
2.3.1 Multi-phonon emission.....	10
2.3.2 Energy transfer between lanthanide ions .....	11
2.3.3 Cross-relaxation .....	11
2.3.4 Up-conversion.....	12
2.4 Lanthanide luminescence in inorganic materials.....	13
2.5 Lanthanide luminescence in organic materials.....	14
2.6 Nanoparticles .....	16
2.6.1 Synthesis of nanoparticles in organic solution .....	16
2.6.2 Synthesis of semiconductor nanoparticles.....	17
2.6.3 Synthesis of metal nanoparticles.....	19
2.6.4 Lanthanide-doped nanoparticles .....	19
2.6.5 Lanthanide ions in semiconductor nanoparticles.....	23
2.6.6 Synthesis of mono-disperse nanoparticles.....	24
2.7 Optical amplifiers .....	25
2.7.1 1550 nm fiber amplifiers.....	27
2.7.2 1300 nm fiber amplifiers.....	27
2.7.3 Other wavelength amplifiers.....	28
2.8 Polymer-based optical amplifiers .....	29
2.9 Electroluminescence .....	31
2.10 Outlook .....	33
2.11 References.....	33
<b>CHAPTER 3</b> .....	<b>41</b>
Synthesis of lanthanide(III)-doped nanoparticles .....	41

3.1 Introduction .....	42
3.2 Results and discussion .....	42
3.2.1 Luminescence of $\text{Eu}^{3+}$ -doped nanoparticles .....	47
3.2.2 Strongly visible-emitting ions $\text{Tb}^{3+}$ , $\text{Dy}^{3+}$ , and $\text{Sm}^{3+}$ .....	52
3.2.3 Weakly visible-emitting ions $\text{Pr}^{3+}$ , $\text{Tm}^{3+}$ , and $\text{Ho}^{3+}$ .....	54
3.2.4 Determination of the quantum yield .....	56
3.2.5 Near-infrared emitting ions .....	57
3.3 Conclusions .....	65
3.4 Experimental section .....	65
3.5 References and notes .....	68
<b>CHAPTER 4.....</b>	<b>71</b>
Surface effects on the luminescence of lanthanide(III)-doped nanoparticles.....	71
4.1 Introduction .....	72
4.2 Results and discussion .....	73
4.2.1 Quenching by solvents .....	73
4.2.2 Influence of the refractive index.....	74
4.2.3 Concentration quenching.....	75
4.2.4 Modeling of the luminescence lifetime .....	76
4.2.5 Nanoparticles with different sizes .....	82
4.3 Conclusions .....	88
4.4 Experimental section .....	88
4.5 References and notes .....	88
Appendix 4.A .....	90
4.A.1 Modeling the luminescence decay.....	90
4.1 References and notes .....	92
<b>CHAPTER 5.....</b>	<b>93</b>
Surface modification of lanthanide(III)-doped nanoparticles .....	93
5.1 Introduction .....	94
5.2 Results and discussion .....	95
5.2.1 Surface modification of $\text{LaF}_3$ and $\text{LaPO}_4$ nanoparticles.....	95
5.2.2 Synthesis of core-shell nanoparticles of $\text{LaF}_3$ .....	100
5.3 Conclusions .....	106
5.4 Experimental section .....	106

5.5 References and notes .....	108
<b>CHAPTER 6 .....</b>	<b>111</b>
Synthesis of lanthanide(III)-doped semiconductor nanoparticles .....	111
6.1 Introduction.....	112
6.2 Results and discussion .....	113
6.2.1 Characterization of Eu <sup>3+</sup> -doped nanoparticles.....	113
6.2.2 Quenching in lanthanide-doped TiO <sub>2</sub> nanoparticles.....	117
6.2.3 Lanthanide ions emitting in the Near-Infrared .....	119
6.2.4 A LED with TiO <sub>2</sub> :Eu nanoparticles.....	120
6.3 Conclusions.....	121
6.4 Experimental section.....	122
6.5 References and notes .....	123
<b>CHAPTER 7 .....</b>	<b>125</b>
Polymer waveguide amplifiers doped with LaF <sub>3</sub> :Nd nanoparticles. ....	125
7.1 Introduction.....	126
7.2 Results and discussion .....	129
7.2.1 PMMA waveguides .....	129
7.2.2 SU-8 waveguides .....	132
7.2.3 Modeling of the amplification .....	137
7.3 Outlook: Optimization of the device structure .....	138
7.4 Conclusions.....	141
7.5 Experimental section.....	141
7.6 References and notes .....	142
Appendix 7.A.....	144
7.1 Modeling of the Nd <sup>3+</sup> optical amplification.....	144
7.2 References.....	147
Summary.....	149
Samenvatting .....	153
Dankwoord.....	157
Curriculum Vitae .....	159





# CHAPTER 1

## *General introduction*

In the current age of information technology the demand for fast transport of a large amount of data over long distances is constantly growing. The use of glass fibers for optical telecommunication has been a very important step in increasing the bandwidth and speed of data transport and these glass fibers have almost completely replaced conventional electric data transport in copper cables. Glass fibers could only be used to their full potential after the introduction of optical amplifiers to compensate for the small optical losses that occur in these fibers.<sup>1</sup> Optical amplifiers allow for the direct amplification of optical signals, without the conversion to electrical signals. The active luminescent material in optical amplifiers is often one of the lanthanide ions, because they have the appropriate optical transitions. The major advantages of the lanthanide ions are the long luminescence lifetime and the high quantum efficiency that can be achieved at the major telecommunication wavelengths of 1300 and 1530 nm. The  $\text{Er}^{3+}$ -doped fiber amplifier (EDFA) is the most commonly used amplifier, because the optical transition of the  $\text{Er}^{3+}$  ion at 1530 nm coincides with the minimum loss window of optical glass fibers. To cover the complete low-loss window, other lanthanide ions also attract a lot of attention, like  $\text{Pr}^{3+}$  and  $\text{Nd}^{3+}$  for amplification around 1300 nm and  $\text{Tm}^{3+}$  for amplification around 1450 nm.<sup>2,3</sup> A large number of optical components are needed for the manipulation of optical signals, but combining these components with glass fiber technology is very expensive. The use of planar waveguide technology would have significant advantages in reducing the cost

of integrated systems with the use of lithographic techniques.<sup>4</sup> Polymers are interesting materials for the use in planar waveguides, because of the low fabrication cost of devices and the flexibility these polymers offer in their processing.<sup>5</sup> Also needed in these integrated waveguide structures are optical amplifiers, for the compensation of optical losses that occur during the manipulation of the data signals and of the intrinsic losses of the device. Polymer-based optical amplifiers have to be developed, but the use of lanthanide ions as the luminescent material in these polymer-based amplifiers has some drawbacks. The luminescence of lanthanide ions, especially the ions emitting at the wavelengths that are of interest for telecommunication, is quenched significantly in organic materials, due to the high vibrational energies of the chemical bonds in the polymer. In order to increase the luminescence of the lanthanide ions in polymer-based materials, the ion has to be shielded from the polymer environment and one way to do this is by the synthesis of organic complexes, in which an organic ligand is coordinated to the lanthanide ion.<sup>6</sup> Reducing the amount of organic bonds in close proximity to the lanthanide ion has improved the luminescence slightly, but still quenching is the dominant process.<sup>7</sup>

Therefore, the goal of this thesis is to improve the luminescence properties of lanthanide ions in an organic solution or polymer, by doping them in the core of inorganic nanoparticles. These nanoparticles are soluble in organic solvents, but at the same time they can provide an environment around the lanthanide ion that reduces quenching. Generally, lanthanide ions have good optical properties in inorganic matrices, like glasses and crystals, and long luminescence lifetimes and high quantum yields are observed in these materials. Doping of the lanthanide ions in the core of nanoparticles would give the lanthanide ion the luminescence properties found in inorganic materials, but at the same time the nanoparticles could be processed as an organic compound.

An overview of the luminescence of lanthanide ions will be given in chapter 2. The luminescence of different ions in a variety of hosts will be discussed and it will focus on the doping of lanthanide ions in nanoparticles. The synthesis and properties of different nanoparticles will be discussed in detail.

The synthesis and optical characterization of nanoparticles doped with lanthanide ions are discussed in chapter 3, as a way to improve the luminescence of lanthanide ions in an organic solution. The nanoparticles have organic ligands coordinated to the surface that provide stability of the nanoparticles and give the nanoparticles solubility in organic solvents. The small size of the nanoparticles minimizes scattering and optically clear solutions can be made. Nanoparticles doped with a range of lanthanide ions were prepared giving rise to different luminescence

spectra. The difference in luminescence spectra will be discussed in terms of the different crystal symmetries of the nanoparticles that were prepared.

In chapter 4, the influence of the environment on the luminescence properties of the lanthanide ions doped in the nanoparticles will be discussed. Due to the small size of the nanoparticles the surface has a major influence on the luminescence of the lanthanide ions and a model will be described that deals with the influence of surface quenching. Differently sized nanoparticles are synthesized and it is shown that the optical properties of the lanthanide ions are strongly size dependent.

The modification of the surface of the nanoparticles is discussed in chapter 5. The surface of the nanoparticles is not only important for the optical properties of the lanthanide ions, but it also determines the solubility of the nanoparticles. Control over the surface properties is an important tool for the use of these materials in polymer-based technology and several methods to change the surface bound ligands are discussed. The growth of an inorganic shell around the nanoparticles is described as a simple way to improve the luminescence properties of the doped lanthanide ions.

Chapter 6, describes the synthesis of semiconductor nanoparticles doped with lanthanide ions. The low absorption coefficients and the narrow absorption lines of the lanthanide ions make direct excitation of the lanthanide ions inefficient. Semiconductor materials can have broad absorption bands with high absorption coefficients at wavelengths ranging from the UV to the near-infrared (NIR) and energy transfer from the semiconductor host material to the lanthanide ion could provide alternative excitation pathways. Semiconductor nanoparticles can be excited in polymer light-emitting diodes (LEDs) and the doping of lanthanide ions in the nanoparticles could generate lanthanide luminescence directly from electricity.

Optical amplification in a polymer waveguide is reported for the first time at an important telecommunication wavelength of 1320 nm. The fabrication of planar polymer-based optical amplifiers is described in chapter 7, using Nd<sup>3+</sup>-doped nanoparticles synthesized as described in this thesis. It is shown that these nanoparticles are promising materials for polymer amplifiers. Modeling of the amplification results shows that the gain of these polymer-based optical amplifiers might be close to the gain that was obtained in Nd<sup>3+</sup>-doped glass fiber amplifiers.

## 1.1 References

<sup>1</sup> Polman, A. *Phys. B* **2001**, *300*, 78.

- <sup>2</sup> Digonnet, M. J. F. *Rare earth doped fiber laser and amplifiers*; Dekker: New York, 1993.
- <sup>3</sup> Soga, K.; Wang, W.; Riman, R. E.; Brown, J. B.; Mikeska, K. R. *J. Appl. Phys.* **2003**, *93*, 2946.
- <sup>4</sup> Miya, T. *IEEE J. Sel. Top. Quantum Electron.* **2000**, *6*, 38.
- <sup>5</sup> (a) Chen, R. T. *Opt. Laser Technol.* **1993**, *25*, 347; (b) Schacklette, L. W.; Blomquist, R.; Deng, J. M.; Ferm, P. M.; Maxfield, M.; Mato, J.; Zou, H. *Adv. Funct. Mater.* **2003**, *13*, 453; (c) Zhou, M. *Opt. Eng.* **2002**, *1*, 1631.
- <sup>6</sup> Parker, D.; Gareth Williams, J. A. *J. Chem. Soc., Dalton Trans.* **1996**, *18*, 3613.
- <sup>7</sup> (a) Hebbink, G. A.; Reinhoudt, D. N.; van Veggel, F. C. J. M. *Eur. J. Org. Chem.* **2001**, *21*, 4101; (b) Hasegawa, Y.; Ohkubo, T.; Sogabe, K.; Kawamura, Y.; Wada, Y.; Makashima, N.; Yanagida, S. *Angew. Chem. Int. Ed.* **2000**, *39*, 357.

# CHAPTER 2

## *Luminescence of lanthanide ions*

*The luminescence of lanthanide ions has a large technological importance in a variety of materials like phosphor lamps, displays, lasers, and optical amplifiers. Usually, the best hosts for these lanthanide ions are inorganic materials like crystals and glasses, because lanthanide ions generally show high quantum yields in these hosts. However, the use of organic materials could have significant advantages over these inorganic materials in terms of the processability and costs. In this chapter, some of the characteristics of the lanthanide ions will be described and how these ions are already being used in organic environment. Furthermore, an overview is given on optical amplifiers with lanthanide ions, since this will be a focus in the remainder of this thesis.*

## 2.1 General introduction

Most of the lanthanide ions were discovered in the early 19<sup>th</sup> and some in the 20<sup>th</sup> century,<sup>1</sup> but since this fairly recent discovery the technological importance of the ions has been growing rapidly. Although they are also called rare earth ions, they are not as rare as this name would suggest. The ions are abundant in the earths crust, but they do not have the tendency to form concentrated ore deposits.<sup>2</sup> A wide variety of minerals, which can be found on a few places in the world, do contain rare earth elements at relatively high concentration, in different compositions.<sup>3</sup> The lighter ions have a higher abundance in these ores and consequently have lower prices. The ions have a wide variety of technological importance in for instance permanent magnets, catalysis, batteries, and optics.<sup>4</sup> The optical properties of lanthanide ions became important when techniques were developed to separate the different lanthanide ions to high purity. Cathode ray tubes of computers and color televisions use europium as the red phosphor<sup>5</sup> and in fiber optic telecommunication, erbium ions are used in laser amplifiers to enhance optical signals.<sup>6</sup> It is especially this laser action of lanthanide ions that is the subject of this thesis.

The ions are extremely stable under laser action, because the optical transitions involve electronic transitions within the ion itself. No chemical bonds are involved so degradation does not occur. The long luminescence lifetime of the lanthanide ions makes laser action relatively easy to achieve with cheap pump sources.<sup>7</sup> The luminescence of the ions is widely studied in inorganic hosts, like crystals or glasses.<sup>8</sup> These host materials are often fabricated at high temperatures and with sometimes high-cost materials. For optical glass fiber technology, the high costs of integration of the optical components can even exceed the fabrication costs of the components itself. This has clear disadvantages especially in short range telecommunication, where the optical signals have to be processed in a large number of optical components. Integration of these components on a single chip could reduce the costs significantly. Polymers are attracting interest for integrated optical systems and research is going on to investigate the use of lanthanide luminescence in polymer materials.<sup>9</sup> Polymers have the advantage that they can be processed at low temperatures and with standard techniques it is relatively easy to make different structures. This would make it possible to integrate a wide variety of optical components like splitters, couplers, multiplexers, and amplifiers lowering the cost of optical systems. Polymer-based optical amplifiers have to be developed for the compensation of optical losses that occur in the integrated systems. Lanthanide ions could be used as the luminescent material in these amplifiers, but then the ions have to be incorporated in the polymer matrix. The

solubility of the ions in organic materials is low and one way to circumvent this problem is by the synthesis of lanthanide complexes, which are soluble in organic materials. A disadvantage of the use of these complexes is that the good optical properties these lanthanide ions have in inorganic materials are largely reduced in the organic complexes.<sup>10</sup> The high vibrational energies of the chemical bonds in organic complexes are efficient quenchers of lanthanide luminescence. In order to use lanthanide ions in a polymer matrix, they have to be shielded from the organic environment in order to have good luminescence properties.

## 2.2 Luminescence of trivalent lanthanide ions

The lanthanides are the elements following lanthanum in the periodic table. In this range of elements the  $4f$  shell is successively filled. These  $4f$  electrons are shielded from the environment by the filled  $5s$  and  $5p$  shells. Since the valence electrons are the same for all the ions, they all show very similar reactivity and coordination behavior.<sup>4</sup>

This thesis will focus on the luminescence of the trivalent lanthanide ions, but a few ions in the series also show luminescence in the divalent state ( $\text{Eu}^{2+}$ ,  $\text{Sm}^{2+}$ ).<sup>11</sup> Since luminescence of the trivalent lanthanide ions arises from transitions within the  $4f$  shell and because this shell is shielded by filled  $5s$  and  $5p$  shells, the absorption and emissions of the ions are only slightly affected by the environment. The transitions within the  $4f$  state are parity forbidden, but due to mixing with allowed transitions, like the  $4f$ - $5d$  transitions, they do occur. As a result of the forbidden character, absorption coefficients are low and luminescence lifetimes are long, ranging from microseconds up to several milliseconds. Figure 2.1 shows the energy levels of the  $4f$  configurations. Three lanthanide ions are not shown in this figure and of these ions;  $\text{La}^{3+}$  and  $\text{Lu}^{3+}$  have a completely empty and a completely filled  $4f$  shell, respectively, and therefore have no optical transitions and  $\text{Ce}^{3+}$  has one electron and one  $4f$  level just above the ground state.  $\text{Ce}^{3+}$  has the lowest oxidation potential of the lanthanide ions making the allowed  $4f$ - $5d$  transitions possible in the UV.  $\text{Y}^{3+}$  is usually also treated as a lanthanide ion, because of similar reactivity and coordination behavior. This ion also has no optical transitions, but luminescent lanthanide ions are often incorporated in host materials with  $\text{Y}^{3+}$  ions. The energy levels are denoted as  $(^{2S+1})\Gamma_J$  (Russel-Saunders notation), where  $S$  is the spin multiplicity,  $\Gamma$  the orbital angular momentum, and  $J$  the total angular momentum. Due to the effective shielding of the  $4f$  electrons, the crystal field has almost no effect on the energy of the levels. For this reason this energy level diagram can be used for lanthanide ions in all sorts of host materials. In principle this could lead to very similar emission and absorption spectra for the same lanthanide ion in a range of

different hosts, but symmetry and quenching will have an effect on the emission properties as discussed further in this chapter.



Figure 2.1: Energy level diagrams of the lanthanide ions.<sup>12</sup>

Table 2.1 gives some important emissions of lanthanide ions and their technological interest. The selection rules for the different transitions are influenced by the symmetry of the environment. The nature of the transitions varies from pure magnetic dipole transitions to pure electric dipole transitions and mixtures of the two. The emission spectrum of the  $\text{Eu}^{3+}$  ion is strongly influenced by the symmetry of the surroundings. The main emissions of this ion occur from the  $^5\text{D}_0$  to the  $^7\text{F}_J$  ( $J = 0-6$ ) levels. The  $^5\text{D}_0 \rightarrow ^7\text{F}_1$  transition is a pure magnetic dipole transition, which is practically independent of the symmetry of the surroundings and the strength can be calculated theoretically. The transitions to the  $^7\text{F}_{0, 3, 5}$  levels are forbidden both in magnetic and electric dipole schemes and are usually very weak in the emission spectrum. The remaining transitions to the  $^7\text{F}_{2, 4, 6}$  levels are pure electric dipole transitions and they are strongly dependent on the symmetry of the environment. In a crystal site with inversion symmetry the electric dipole transitions are strictly forbidden and the  $^5\text{D}_0 \rightarrow ^7\text{F}_1$  transition is usually the dominant emission line. In a site without inversion symmetry the strength of the electric dipole transitions is higher. The  $^5\text{D}_0 \rightarrow ^7\text{F}_2$  transition is usually the strongest emission line in this case,



because transitions with  $\Delta J = \pm 2$  are hypersensitive to small deviations from inversion symmetry.<sup>13</sup> The symmetry around the lanthanide ion can thus be obtained from the shape of the emission spectrum of the  $\text{Eu}^{3+}$  ion. The other lanthanide ions have transitions that are usually mixtures of electric and magnetic dipole transitions and the effects of the symmetry are less pronounced.

Table 2.1: Important emission lines of some lanthanide ions.

Ion	Transition	Wavelength (nm)	Application
$\text{Pr}^{3+}$	$^1\text{G}_4 \rightarrow ^3\text{H}_5$	1300	Optical amplifier
$\text{Nd}^{3+}$	$^4\text{F}_{3/2} \rightarrow ^4\text{I}_{11/2}$	1064	Solid state lasers
$\text{Eu}^{3+}$	$^5\text{D}_0 \rightarrow ^7\text{F}_2$	615	Displays, lighting
$\text{Tb}^{3+}$	$^5\text{D}_4 \rightarrow ^7\text{F}_5$	545	Lighting
$\text{Dy}^{3+}$	$^6\text{F}_{11/2} + ^6\text{H}_{9/2} \rightarrow ^6\text{H}_{15/2}$	1300	Optical amplifier
$\text{Er}^{3+}$	$^4\text{I}_{13/2} \rightarrow ^4\text{I}_{15/2}$	1530	Optical amplifier
$\text{Tm}^{3+}$	$^3\text{H}_4 \rightarrow ^3\text{F}_4$	1480	Optical amplifier
$\text{Yb}^{3+}$	$^2\text{F}_{5/2} \rightarrow ^2\text{F}_{7/2}$	980	Sensitizer

The symmetry also has an influence on the radiative lifetime of the  $^5\text{D}_0$  level. The radiative lifetime is the time for the luminescence to drop to  $1/e$  in intensity in absence of quenching. In the case of a  $\text{Eu}^{3+}$  ion without inversion symmetry the rate of the forced electric dipole transition is higher than in the case of a  $\text{Eu}^{3+}$  ion with inversion symmetry. This automatically means that the radiative lifetime of a  $\text{Eu}^{3+}$  ion in a site with inversion symmetry is longer. Radiative lifetimes of lanthanide ions have been calculated with several methods, of which the Judd-Ofelt theory is the most popular.<sup>14</sup> In this theory the strength of the electric dipole transitions are calculated from the absorption spectrum and these strengths can be related to the radiative lifetime. Werts *et al.* have formulated an equation to calculate the radiative lifetime of the  $\text{Eu}^{3+}$  ion from the shape of the emission spectrum (Equation 2.1).<sup>15</sup>

$$\frac{1}{\tau_R} = A_{\text{MD},0} n^3 \left( \frac{I_{\text{tot}}}{I_{\text{MD}}} \right) \quad (\text{Eq. 2.1})$$

In this equation, the strength of the magnetic dipole transition ( $I_{MD}$ ) is compared to the intensity of the total spectrum ( $I_{tot}$ ).  $A_{MD,0}$  is the spontaneous emission probability of the  ${}^5D_0 \rightarrow {}^7F_1$  transition in vacuo and  $n^3$  is a correction for the refractive index.  $A_{MD,0}$  could be calculated and was found to be  $14.65 \text{ s}^{-1}$ .

## 2.3 Quenching processes

### 2.3.1 Multi-phonon emission

Non-radiative processes can also play an important role. The energy of the excited state can be taken up by the surroundings in the form of vibrational energy, often referred to as phonon emission. The effectiveness of this process depends on the availability of high-energy vibrations in the surroundings and the energy difference between the energy levels of the lanthanide ion. The fundamental vibrations of the chemical bonds in the surroundings and the energy of the vibration are determined by the reduced mass of a bond. Especially bonds with hydrogen have a small reduced-mass and therefore high vibrational energies. These bonds are therefore able to take up large amounts of energy and effectively quench lanthanide ions with large separations between the energy levels. The visible emitting ions  $\text{Eu}^{3+}$  and  $\text{Tb}^{3+}$  have large gaps between the emissive  ${}^5D_0$  and  ${}^5D_4$  level of  $12,000$  and  $15,000 \text{ cm}^{-1}$ , respectively, but still these ions and especially  $\text{Eu}^{3+}$  are quenched substantially when the ions are dissolved in water (vibrational energy:  $\nu_{\max} 3500 \text{ cm}^{-1}$ ). The quenching efficiency is strongly dependent on the number of vibrational quanta that are needed to bridge the gap between the lowest emitting level and the highest non-emitting level of the lanthanide ion. The intensity of the vibronic transition is dependent on the square overlap integral (Franck-Condon factor) of the initial and final vibrational states and this overlap decreases rapidly as the number of vibrational quanta increases.<sup>16</sup> This is summarized in the theory of the energy gap law.<sup>17</sup> The observation of luminescence of a lanthanide ion in solvents with high vibrational energies (water) is dependent on the energy difference between the lowest radiative level and the highest non-radiative level. For example,  $\text{Tb}^{3+}$  in water shows reasonable luminescence but  $\text{Eu}^{3+}$  luminescence is almost completely quenched. The  $\text{Eu}^{3+}$  ion is quenched by energy transfer to the 4<sup>th</sup> overtone of the OH bonds, while the  $\text{Tb}^{3+}$  ion is quenched by energy transfer to the 5<sup>th</sup> overtone of the OH bond. Another important factor governing the efficiency of quenching is the distance between the lanthanide ion and the quencher group. Quenching occurs through a dipole-dipole interaction in a Förster-type mechanism.<sup>18</sup> In this Förster mechanism the interaction between the lanthanide ion (donor) and the quenching site (acceptor) only occurs when the energy levels of the donor and

acceptor are resonant. The donor and acceptor do not have to have overlap of their wave functions, but the process is strongly distance dependent. For dipole-dipole interactions the rate of quenching has a distance dependence of  $r^{-6}$ .<sup>10</sup>

### 2.3.2 Energy transfer between lanthanide ions

Another factor in the quenching of lanthanide ions is the interaction between the lanthanide ions, of the same or different type. Two different lanthanide ions can transfer energy when they have similar separations between the energy levels. The small mismatch in energy can be compensated for by the emission or uptake of a phonon. Energy transfer of one lanthanide ion can be used to enhance luminescence of the other lanthanide ion. For example the lanthanide couple  $\text{Yb}^{3+}$ - $\text{Er}^{3+}$ , where the  $\text{Yb}^{3+}$  ion is excited at 980 nm and then transfers its energy to the  $\text{Er}^{3+}$  ion. The advantage of co-doping with  $\text{Yb}^{3+}$  is that the  $\text{Yb}^{3+}$  ions have a much higher absorption cross-section at 980 nm.<sup>19</sup> The optical gain of an amplifier co-doped with both these ions can be increased compared to an amplifier with only  $\text{Er}^{3+}$  ions.<sup>20</sup> Another example is the  $\text{Tm}^{3+}$ - $\text{Ho}^{3+}$  couple, where  $\text{Tm}^{3+}$  is used as the sensitizer and  $\text{Ho}^{3+}$  as the emitter around 2  $\mu\text{m}$ . The  $\text{Tm}^{3+}$  ion has an absorption peak around 790 nm, a wavelength where a lot of cheap semiconductor pump lasers are available. Pumping at this wavelength leads to an excited  $\text{Tm}^{3+}$  ion in the  $^3\text{H}_4$  level, which self-quenches to the  $^3\text{F}_4$  level producing two  $\text{Tm}^{3+}$  ions excited in the  $^3\text{F}_4$  level. Energy transfer from the  $^3\text{F}_4$  level of  $\text{Tm}^{3+}$  to the  $^5\text{I}_7$  level of  $\text{Ho}^{3+}$  could theoretically lead to two excited  $\text{Ho}^{3+}$  ions per absorbed photon.<sup>21</sup> The same energy transfer process could also be used to enhance laser action of  $\text{Tm}^{3+}$  around 1480 nm.<sup>22</sup> Pumping of the  $\text{Tm}^{3+}$  ion into the  $^3\text{H}_4$  level can lead to  $\text{Tm}^{3+}$  emission at 1480 nm by radiative decay to the  $^3\text{F}_4$  level. If this  $^3\text{F}_4$  level is relatively long lived, which is the case in some host materials, it is difficult to create a population inversion between the  $^3\text{H}_4$  and  $^3\text{F}_4$  level. Co-doping with  $\text{Ho}^{3+}$  leads to a fast depopulation of the  $^3\text{F}_4$  level making population inversion possible.

### 2.3.3 Cross-relaxation

In a cross-relaxation process two ions that are closely together interact and exchange energy. Examples of these processes are given in Figure 2.2 for  $\text{Eu}^{3+}$  and  $\text{Pr}^{3+}$ . A  $\text{Eu}^{3+}$  ion in the  $^5\text{D}_1$  excited state can transfer its energy to a neighboring  $\text{Eu}^{3+}$  ion promoting it to the  $^7\text{F}_3$  level. This leads to one ion in the  $^5\text{D}_0$  excited state and one in the  $^7\text{F}_3$  level. In the case of  $\text{Pr}^{3+}$ , the  $^3\text{P}_0$  level can be quenched by cross-relaxation leading to an ion in the  $^3\text{H}_6$  and an ion in the  $^1\text{D}_2$  level.

The  $^1D_2$  level can be quenched again by cross-relaxation leading to an ion in the  $^1G_4$  state and an ion in the  $^3F_3$  level.

Energy migration is another form of cross-relaxation between two ions of the same sort. The excited state energy levels of two identical ions are resonant, so the energy can be transferred to the neighboring ion by cross-relaxation and travel through the material hopping from one ion to the other. An increase in the doping concentration leads to a faster energy migration through the material, making the chance of meeting a quenching site higher. For reasons of cross-relaxation and energy migration, high doping concentrations often lead to a decrease in luminescence intensity and luminescence lifetime.

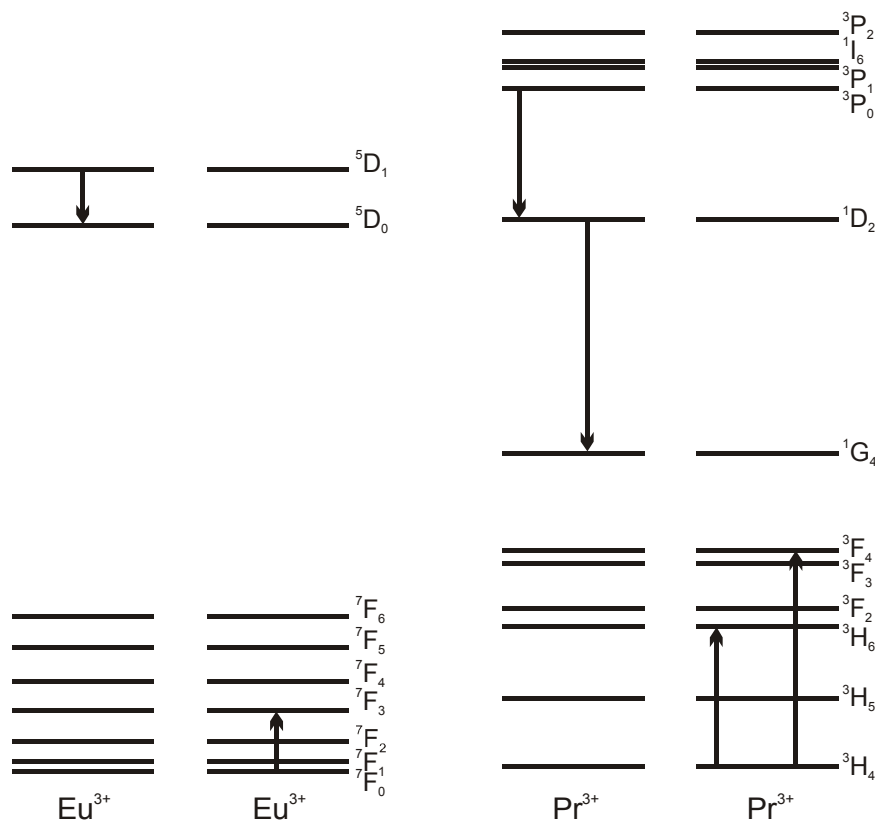


Figure 2.2: Cross-relaxation processes in  $\text{Eu}^{3+}$  and  $\text{Pr}^{3+}$ .

### 2.3.4 Up-conversion

Up-conversion is a process in which an excited state of a lanthanide ion is promoted to a higher energy level by the absorption of another photon or by cross-relaxation between two excited states. Up-conversion materials are of interest for the generation of high energy, blue or UV- emitting lasers that are pumped with low cost red or near-infrared pump lasers. Up-conversion phenomena can be found in most lanthanide ions using the appropriate conditions like the right pumping wavelengths and the right host materials. Up-conversion can also reduce

the efficiency of lasers and amplifiers, when the desired excited state is depleted by cross-relaxation or excited state absorption. Up-conversion by cross-relaxation can be the gain limiting factor in  $\text{Er}^{3+}$ -doped amplifiers with a high concentration of  $\text{Er}^{3+}$  ions.<sup>23</sup> This up-conversion process can clearly be seen by the green light emitted from the amplifier under NIR light pumping. For this reason the concentration of  $\text{Er}^{3+}$  ions in an amplifier has to be low, resulting in very long amplifiers to achieve sufficient gain.

## 2.4 Lanthanide luminescence in inorganic materials

The luminescence in inorganic materials is generally characterized by high quantum yields and therefore long luminescence lifetimes. There are, however, circumstances where the quantum yields of these inorganic materials are lowered. For the visible emitting ions high quantum yields can be reached in almost all inorganic materials as long as the purity is good and water can be excluded from the material. Recently, interest for long wavelength lasers in the near- and mid-infrared has focused the attention on lanthanide ions that emit between 1.5-5  $\mu\text{m}$ . These lasers could have applications as surgical instruments, and as eye safe lasers. Ions that are of interest for emission in this region are  $\text{Ho}^{3+}$  at 2  $\mu\text{m}$ <sup>24</sup> and 2.9  $\mu\text{m}$ ,<sup>25</sup> and  $\text{Er}^{3+}$  at 2.7  $\mu\text{m}$ <sup>26</sup> and 3.5  $\mu\text{m}$ .<sup>27</sup> For emission at these wavelengths, the separation between the energy levels becomes so small that the vibrational energies of the inorganic materials can also quench the luminescence. In order to observe efficient lanthanide luminescence at these wavelengths, materials with low phonon energies have to be used. A summary of some widely used inorganic materials with their phonon energies is given in Table 2.2. Silica glass fibers are mostly used for optical telecommunication, but this material has relatively high phonon energies. This means that some of the optical transitions of lanthanide ions are quenched by multi-phonon relaxation. When quenching occurs other glasses are used, like fluoride and chalcogenide glasses. The materials used for lanthanide luminescence can be divided in two main groups, glasses and crystals. Crystals are especially important for solid state lasers, for example Nd:YAG crystals for a solid state laser operating at 1064 nm.<sup>28</sup> Crystals were also important for the determination of the luminescence properties of lanthanide ions. In crystals, the  $\text{Ln}^{3+}$  ions can exist in a single well-defined crystal site. In this way the emission and absorption spectra of the lanthanide ions can be related to the symmetry of the crystal site and important information can be obtained about the energy of the levels.

Table 2.2: Phonon energies of some common inorganic materials used as hosts for luminescent lanthanide ions.<sup>29,30,31</sup>

Material	Phonon energy (cm <sup>-1</sup> )
Phosphate glass	1200
Silica glass	1100
Fluoride glass	550
Chalcogenide glass	400
LaPO <sub>4</sub>	1050
YAG	860
YVO <sub>4</sub>	600
LaF <sub>3</sub>	300
LaCl <sub>3</sub>	200

Examples of these studies in the literature and of relevance in this thesis are given for LaF<sub>3</sub><sup>32</sup> and YVO<sub>4</sub>.<sup>33</sup> Crystals doped with lanthanide ions can also be used to study energy migration between lanthanide ions.<sup>34</sup> Glass hosts doped with lanthanide ions are interesting materials for telecommunication where they can be integrated with un-doped optical glass fiber. In these glasses the lanthanide ions do not have a fixed crystal site, which leads to inhomogeneous line broadening. General problems can be the limited solubility of lanthanide ions in the glass and clustering of the ions at higher concentration. The luminescence properties of the lanthanide ions are reduced when they cluster, because of cross-relaxation. At low concentrations, luminescence lifetimes of Er<sup>3+</sup> can go up to 15 ms and this long lifetime is beneficial for the use in optical amplifiers.<sup>6</sup> Sol-gel processing has been used to make planar waveguides for integrated optics.<sup>35</sup> These integrated planar waveguides have to be of limited length and as a consequence the concentration of Er<sup>3+</sup> has to be increased. A way to circumvent the problems of cross-relaxation is by co-doping with other trivalent ions, like Al<sup>3+</sup>, that do not influence the luminescence of the lanthanide ion.<sup>36</sup>

## 2.5 Lanthanide luminescence in organic materials

In order to use the luminescence of the lanthanide ions in an organic environment, the ions have to be solubilized in organic solution. One way to do this is by the formation of complexes

with organic ligands. Charged ligands can compensate for the charge of the lanthanide ions and the organic groups on the ligand give the complex solubility in organic solvents and polymers.<sup>37</sup>

A general problem of the use of lanthanide complexes is that the organic groups are close to the lanthanide ion. This close proximity of organic groups leads to efficient quenching of the excited lanthanide ions, especially for the NIR-emitting ions. In our group, lanthanide complexes based on terphenyl and calix[4]arene ligands were used.<sup>38</sup> Some of these structures are depicted in Figure 2.3.

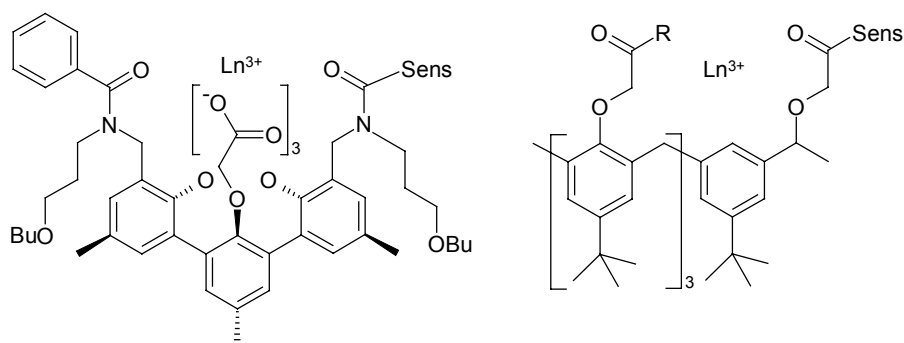


Figure 2.3: Lanthanide complexes: (left) terphenyl-based, (right) calix[4]arene-based. Sens = a sensitizer attached to the complex, that can absorb the light and transfer its energy to the lanthanide ion.

These organic complexes can have a sensitizer attached in close proximity to the lanthanide ion. Different sensitizers can be attached, that have high absorption coefficients and that can transfer their energy to the lanthanide ion, giving the lanthanide ion overall a high effective absorption coefficient. Visible emitting ions, like  $\text{Eu}^{3+}$  and  $\text{Tb}^{3+}$ , can have high quantum yields in these complexes and they find applications in biological immuno assays.<sup>39</sup> Lifetimes of these visible emitting lanthanide complexes are in the order of milliseconds and quantum yields of up to 15 % have been reached, depending on the solvent used.<sup>40</sup> In deuterated solvent the quantum yields are usually higher because quenching by OH groups is decreased. Complexes with NIR-emitting ions have much lower quantum yields. Luminescence lifetimes measured for  $\text{Yb}^{3+}$ ,  $\text{Nd}^{3+}$ , and  $\text{Er}^{3+}$  in a calix[4]arene complex were 12  $\mu\text{s}$ , 0.9  $\mu\text{s}$ , and 1.3  $\mu\text{s}$ , respectively.<sup>41</sup> In terphenyl complexes these lifetimes are of the same order of magnitude. For  $\text{Yb}^{3+}$ ,  $\text{Nd}^{3+}$ , and  $\text{Er}^{3+}$ , luminescence lifetimes of 19  $\mu\text{s}$ , 2  $\mu\text{s}$ , and 3  $\mu\text{s}$ , respectively, were measured with some variation for the solvent used.<sup>40b,42</sup> An estimation of the quantum yield of these complexes was made by comparing the luminescence lifetime of the complexes with radiative lifetimes reported in the literature. For  $\text{Yb}^{3+}$  and  $\text{Nd}^{3+}$  the quantum yields are approximately 1 % and for  $\text{Er}^{3+}$  this is well below 0.5 %. One way of increasing the

luminescence lifetime of the NIR-emitting ions in organic complexes is by decreasing the vibrational energies of the organic bonds that are in close proximity to the lanthanide ions by deuteration,<sup>43</sup> or fluorination<sup>44</sup> of the ligand. Deuteration of the terphenyl ligand gave a 2-3 fold increase in the luminescence lifetime of the three NIR-emitting ions.<sup>45</sup> Other groups have also used deuteration and fluorination of the organic ligands in order to increase the luminescence lifetime of the lanthanide ions.<sup>10,46</sup> The lifetimes of important ions like Nd<sup>3+</sup> and Er<sup>3+</sup> are still only several microseconds and for other ions like Pr<sup>3+</sup>, Ho<sup>3+</sup> and Tm<sup>3+</sup> it is very difficult to observe NIR luminescence in organic systems.

In order to reduce quenching of the lanthanide ion by the organic groups, the distance between the excited lanthanide ion and the organic environment has to be increased. A possible way to do this is by doping the lanthanide ion in the core of an inorganic nanoparticle that is stabilized by organic ligands. In these nanoparticles the lanthanide ion is in an environment that could give all the advantages of lanthanide luminescence in an inorganic environment, but with the solubility in organic solvent, because of the adsorbed organic monolayer.

## 2.6 Nanoparticles

### 2.6.1 Synthesis of nanoparticles in organic solution

Colloidal gold was prepared for the first time by M. Faraday in 1857 and the properties of this nanosized material have been studied since then.<sup>47</sup> Aqueous solutions containing silver and gold nanoparticles have been used to coat various substrates with thin films of metals. Control over the size and the size distribution of the nanoparticles have been important subjects in nanoparticle research. Control over the size of the nanoparticles is important, because the properties of the nanoparticles are strongly dependent on the size. Most nanoparticle solutions are prepared in aqueous phases and stabilization of the nanoparticles is usually achieved by surface charges on the nanoparticles that keep them separated from each other. In this way, aggregation of the particles into insoluble large aggregates is prevented. A good method to synthesize relatively mono-disperse gold nanoparticles in water has been described using citrate as a reducing agent and as a stabilizer.<sup>48</sup> The synthesis of nanoparticles that are soluble in organic solvents became an important subject of research after the synthesis of CdSe nanoparticles by Bawendi *et al.*<sup>49</sup> and the synthesis of gold nanoparticles by Brust *et al.*<sup>50</sup> These nanoparticles are stabilized by organic ligands that have a coordinating group that binds to the nanoparticle surface and bulky organic tails that separate the particles. A schematic picture of



such a nanoparticle is shown in Figure 2.4. In this case the stabilization is not by charges on the surface, but because of the bulkiness of the organic ligands. Stabilization of nanoparticles with these organic ligands is so successful that the particles can be precipitated from the solution, dried, and be resolubilized in organic solvent. Most of the synthesis methods aim to have a good control over the particle size and size distribution.

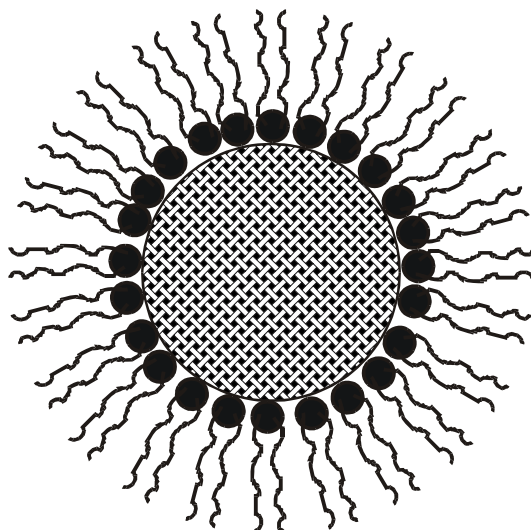


Figure 2.4: Schematic representation of a nanoparticles stabilized with organic ligands.

### 2.6.2 Synthesis of semiconductor nanoparticles

Semiconductor nanoparticles have interesting properties that are markedly different from the bulk. Excitation of a semiconductor leads to the generation of an electron and a hole. This electron and hole can combine to form a bound electron-hole pair, also referred to as an exciton. This exciton has a certain size, known as the Bohr exciton radius and for most semiconductors the Bohr radius is in the order of a few nanometers. When the size of the nanoparticles approaches the size of the Bohr exciton radius, the charge carriers have to be treated quantum mechanically. The conduction and valence bands split into discrete levels and the band-gap increases with decreasing particle size, leading to a blue shift in the absorption and emission spectrum. Nanoparticles that show these phenomena are often called quantum dots, because they show quantum confinement. The size of the exciton is now limited to the size of the nanoparticles, so the charges will be present on the surface of the nanoparticles. Passivation of the surface is therefore very important to observe luminescence. CdS nanoparticles have been prepared from aqueous solutions,<sup>51</sup> but these generally suffer from low quantum yields due to the bad surface passivation and difficulties to control the size distribution. The synthesis of CdE (E = S, Se, Te) nanoparticles reported by Bawendi *et al.* was performed in TOPO ( trioctylphosphine oxide) as the coordinating ligand and solvent.<sup>49</sup> An organometallic precursor, CdMe<sub>2</sub> was

injected into a hot solution of TOPO together with a chalcogenide source in the form of TOP(E) or bis(trimethylsilyl)E (E = S, Se, Te). Decomposition of these precursors leads to the growth of nanoparticles. The reaction temperature and the reaction time determine the size of the nanoparticles. This procedure yields nanoparticles that can be isolated, dried, and re-dispersed in organic solvents and with a relatively high luminescence quantum yield. Improvements in the reactants and coordinating solvents followed later. The highly toxic and air sensitive CdMe<sub>2</sub> could be replaced by CdO without changing the optical properties of the nanoparticles.<sup>52</sup> The introduction of other coordinating ligands like stearic acid and hexadecyl amine together with TOPO resulted in even better control over the nanoparticles growth and size distribution.<sup>53</sup> With the addition of hexylphosphonic acid not only control over the size of the nanoparticles, but shape control could also be obtained.<sup>54</sup> The stronger binding of this ligand to the particles surface gave rod-like nanoparticles when the concentration was as low as 5 %. The phosphonic acid ligand slows down the reaction rate and as a result the concentration of reactive monomer is high which leads to a preferential growth of one of the crystal surfaces and using this ligand even arrows, teardrop, and branched-tetrapod structures could be prepared.<sup>55</sup> Semiconductor nanoparticles of different materials have been synthesized and with their different bandgaps and sizes the emissions can be tuned from the blue till the NIR. Some of these materials are summarized in Table 2.3.

*Table 2.3: Semiconductor nanoparticles with emissions at different wavelengths.*

Semiconductor	Wavelength region (nm)	Reference
ZnSe	370-420	56
CdS	400-450	52a
CdSe	450-650	53b
CdTe	520-700	57
HgTe	800-1700	58
PbS	1000-1600	59
PbSe	1200-2000	60

With these semiconductor nanoparticles the telecommunication window can also be completely covered, but these particles have a drawback in comparison with lanthanide ions and that is the short luminescence lifetime. The lifetime of these particles ranges from several nanoseconds up to 1  $\mu$ s, making it more difficult to create a population inversion. Despite this

drawback, optical gain of CdSe nanoparticles has been reported for a close packed crystal.<sup>61</sup> The termination of the surface is very important to obtain nanoparticles with high quantum yields. A large fraction of the atoms is located at the surface and these atoms are not all fully coordinated. The exciton is located at the surface most of the time due to the reduced size of the nanoparticles and thus quenching at the surface generally plays an important role. The use of strongly coordinating groups to the surface of the nanoparticles can decrease the non-radiative effects and high quantum yields can be obtained under certain circumstances. The quantum yield of the nanoparticles could be improved significantly when the surface is coated with an inorganic shell. These core-shell particles consist of a core of small band-gap semiconductor surrounded by a shell of larger band-gap semiconductor.<sup>62</sup> In these core-shell nanoparticles, the hole is confined to the core of the particles while the electron can travel over the whole particle. Because of the absence of the hole at the particles surface the quantum yields could be increased up to 80 %. Examples of these core-shell particles are CdSe/ZnSe,<sup>63</sup> CdSe/ZnS,<sup>64</sup> HgTe/CdS<sup>65</sup>, and InP/ZnS<sup>66</sup>, but many more examples can be given.

### 2.6.3 Synthesis of metal nanoparticles

Gold nanoparticles synthesized by Brust *et al.* were made in a two phase system. To a solution of HAuCl<sub>4</sub> in water, a toluene solution of the phase-transfer agent tetraoctylammonium bromide and a thiol as the ligand, was added.<sup>50</sup> The gold ions transfer to the organic phase where they are reduced by the addition of sodium borohydride in the aqueous phase, leading to the formation of gold nanoparticles. The size of the particles can be controlled to some extent by the ratio of thiol ligand to gold ions, but the size distribution of the particles is generally large. Improvements in the synthesis method have lead nanoparticles with a narrower size distribution. The synthesis of other metal nanoparticles, like Ag, Pd, and Pt nanoparticles has been described, using similar methods.<sup>67</sup> A special class of metal nanoparticles that gained considerable interest are magnetic nanoparticles. Nanoparticles with a sufficiently narrow size distribution spontaneously form 2D superlattices that could have applications in magnetic data storage. Several procedures have been described to produce mono-disperse nanoparticles of Co<sup>68</sup> and FePt.<sup>69</sup> These usually involve high boiling point solvents together with a coordinating ligand, like oleic acid.

### 2.6.4 Lanthanide-doped nanoparticles

Several procedures have been described for the synthesis of lanthanide-doped nanoparticles and novel properties of the luminescence of lanthanide ions in these nanoscale

materials have been reported. Most lanthanide-doped nanoparticles are made via high temperature procedures leading to small crystallites without any surface capping. Particles of  $\text{Y}_2\text{O}_3:\text{Eu}^{70}$  and  $\text{Y}_2\text{SiO}_5:\text{Eu}^{71}$  have been prepared at temperatures of 1000 °C and more. These nanoparticles are not soluble in organic solvents, because they lack the solubilizing surface groups, but due to an enlarged surface area and small domain of the crystal itself, different properties compared to the bulk materials are observed. First of all, the emission lines in nanocrystalline materials show extra inhomogeneous broadening.<sup>72</sup> Not all crystal sites are the same, especially due to the enormous increase in surface sites compared to bulk sites. The increase in surface area was found to be an advantage for  $\text{Y}_2\text{O}_3:\text{Eu}$  nanoparticles excited with cathode rays.<sup>73</sup> The synthesized nanocrystalline materials have a much better surface termination than the powdered bulk material leading to higher luminescence efficiency. A blue shift in the peak emission wavelength when decreasing the particle size was also reported for  $\text{Y}_2\text{O}_3$  nanoparticles doped with  $\text{Eu}^{3+}$ .<sup>70b</sup>  $\text{Y}_2\text{O}_2\text{S}$  nanoparticles doped with  $\text{Er}^{3+}$  showed a population of the energy levels that was only observed in nanocrystalline materials and not in the bulk.<sup>74</sup> Laser excitation of the  $\text{Er}^{3+}$  ions in nanocrystals at a temperature below 7 K, leads to a saturation of the levels just above the ground state. Figure 2.5 shows a schematic and simplified excitation spectrum of  $\text{Er}^{3+}$  emission in bulk and nanocrystalline  $\text{Y}_2\text{O}_2\text{S}$  at 2.6 K.

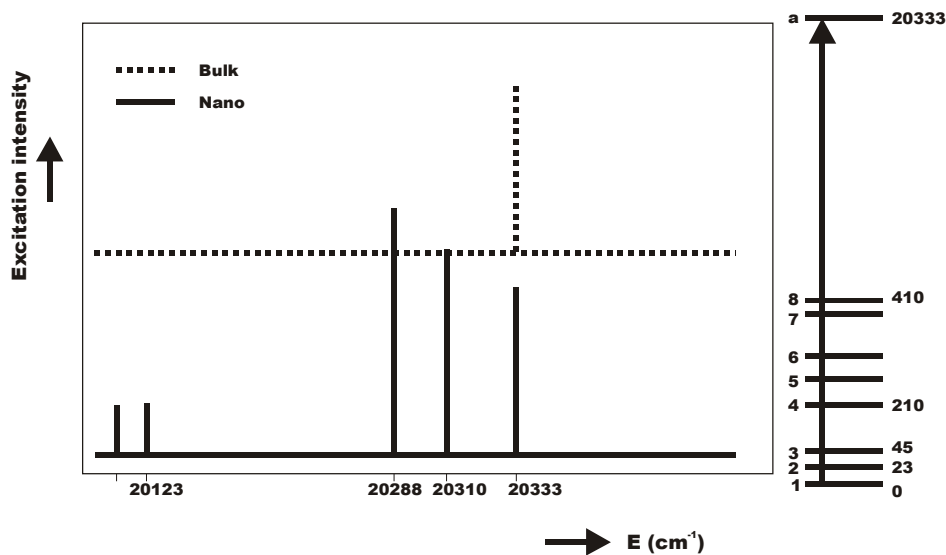


Figure 2.5: Schematic excitation spectrum of  $\text{Y}_2\text{O}_2\text{S}:\text{Er}$  nanoparticles and bulk  $\text{Y}_2\text{O}_2\text{S}:\text{Er}$  at 7 K.

The excitation spectrum of the bulk material only shows a single line at  $20,333 \text{ cm}^{-1}$  from the absorption of the lowest level of the ground state to level **a** of the excited state. In the nanocrystals absorptions from level **2**, **3**, **4**, and **5** were also observed in the excitation spectrum of the  $\text{Er}^{3+}$  emission. At low temperatures, the levels just above the ground state become

populated, because after excitation the ion does not fully decay to the ground state. The explanation that was given for this behavior is the absence of the very small phonon energies in nanocrystals because of the “ending” character of the crystal domain. The vibrational modes in a nanocrystal become discrete and are no longer band-like as in bulk materials. In bulk materials the higher levels of the ground state decay very rapidly to the lowest level even at low temperatures. A similar effect was found for  $\text{Eu}_2\text{O}_3$  nanoparticles.<sup>75</sup> A lot of energy transfer processes rely on the matching of the energy levels by the uptake or emission of low energy phonons. The absence of low energy phonons can have a significant effect on efficiency of energy transfer processes in nanoparticles.<sup>76</sup>

The symmetry of the lanthanide site can also be changed in nanocrystalline materials.<sup>77</sup> Decreasing the size of  $\text{YBO}_3:\text{Eu}$  nanoparticles lead to an increase of the  ${}^5\text{D}_0 \rightarrow {}^7\text{F}_2$  emission peak compared to the other emission lines indicating that the symmetry around the  $\text{Eu}^{3+}$  ion is lowered. A similar effect was found for 14 nm sized  $\text{YVO}_4:\text{Eu}$  particles.<sup>78</sup> These nanoparticles were excited using a narrow laser line and the excitation wavelength was slowly scanned over an absorption peak. Different  $\text{Eu}^{3+}$  sites with different site symmetries and corresponding different luminescence lifetimes were found. The sites with decreased site symmetry were attributed to surface sites, so the lower lifetimes are found at the nanoparticle surface. Lanthanide-doped nanoparticles also offer the possibility to change the environment around the lanthanide ion, while keeping the lanthanide ion in the same crystal site. This proved to be valuable in the determination of the influence of the refractive index on the luminescence lifetime. The influence of the refractive index on the luminescence lifetime of  $\text{Eu}^{3+}$  organic complexes was studied by varying the solvent in which the complex was dissolved.<sup>79</sup> In these complexes special care has to be taken that the coordination of the lanthanide is not changed when changing the solvent. In nanoparticles, the ions are doped inside the crystal and local coordination of the ion is not changed when varying the solvent.  $\text{Y}_2\text{O}_3:\text{Eu}$  particles showed a correlation between the refractive index and the luminescence lifetime of the  $\text{Eu}^{3+}$  ion, when the particles were dispersed in different environments.<sup>80</sup>

Lanthanide-doped nanoparticles that are soluble in solvents that form optically clear solutions have also been reported.  $\text{YVO}_4:\text{Eu}$  nanoparticles were synthesized by a precipitation from aqueous solution using different stabilizing groups, like sodium hexametaphosphate,<sup>81</sup> citrate<sup>82</sup>, or by adjusting the pH.<sup>83</sup> These particles are soluble in water and show strong  $\text{Eu}^{3+}$  luminescence. Due to the sensitivity of the  $\text{Eu}^{3+}$  ion on the symmetry of the environment it can clearly be seen from the emission spectrum that the ion is doped in the same site as in the bulk

material. The  $\text{Eu}^{3+}$  ion is in an  $\text{Y}^{3+}$  crystal site giving the  $\text{Eu}^{3+}$  ion  $D_{2d}$  symmetry.  $\text{YVO}_4:\text{Eu}$  is a well-known phosphor that was used in cathode ray tubes before it was replaced by the more efficient  $\text{Y}_2\text{O}_2\text{S}:\text{Eu}$  phosphor.  $\text{YVO}_4:\text{Eu}$  particles can be excited in the UV where the  $\text{VO}_4$  groups have a charge transfer band, caused by a ligand to metal charge transfer in the V-O bond. The  $\text{VO}_4$  groups can transfer their excitation energy to the  $\text{Eu}^{3+}$  ions leading to  $4f$  line emission of the lanthanide ion. The energy transfer processes in these nanoparticles have been studied by temperature-dependent spectroscopy and luminescence lifetime studies.<sup>84</sup> It was concluded that energy transfer to  $\text{Eu}^{3+}$  occurs only from  $\text{VO}_4$  groups adjacent to the  $\text{Eu}^{3+}$  center and that quenching of the excited  $\text{VO}_4$  groups at the surface of the particles is the main reason for the low quantum yield of 15 %. The quantum yield was later improved by the transfer of the nanoparticles in  $\text{D}_2\text{O}$  and by the growth of a silicate shell around the nanoparticles.<sup>85</sup> Quenching of these nanoparticles could be studied by varying the concentration of  $\text{Eu}^{3+}$  in the nanoparticles. The best quantum yields were observed when the concentration of  $\text{Eu}^{3+}$  was 5 %, but when surface quenching was an important process the highest quantum yields were observed at a higher  $\text{Eu}^{3+}$  content. Silicate coated nanoparticles with the highest quantum yield had a  $\text{Eu}^{3+}$  concentration of around 5 %, close to the value for bulk  $\text{YVO}_4:\text{Eu}$ , indicating that surface quenching is strongly reduced in these nanoparticles.

Haase *et al.* synthesized nanoparticles of  $\text{LaPO}_4$  doped with  $\text{Eu}^{3+}$  or with the combination  $\text{Ce}^{3+}$  and  $\text{Tb}^{3+}$  in coordinating organic solvents<sup>86,87</sup> and via a hydrothermal procedure.<sup>88</sup> The nanoparticles synthesized in the coordinating solvent tris(ethylhexyl)phosphate are soluble in polar organic solvents like DMF and DMSO. After the addition of some tetraalkylammonium hydroxide they are also soluble in methanol. From the emission spectrum of  $\text{Eu}^{3+}$ -doped particles it could be concluded that the  $\text{Eu}^{3+}$  ion is inside the particle, because of the similarity with the bulk spectrum. The  $\text{Eu}^{3+}$  ions can be excited in the UV (260 nm) via a charge-transfer band originating from the Eu-O bond. In the  $\text{Ce}^{3+}$  and  $\text{Tb}^{3+}$  particles the  $\text{Ce}^{3+}$  ions acts as a sensitizer for the  $\text{Tb}^{3+}$  emission, because  $\text{Ce}^{3+}$  has an allowed  $4f-5d$  transition in the UV (at  $\approx 274$  nm). This allowed transition has a high absorption coefficient and the quantum yield of particles doped with this ion could be determined. The emission spectrum of the particles consists of  $\text{Ce}^{3+}$  emission in the UV, and  $\text{Tb}^{3+}$  emission in the green. The quantum yield was up to 42 % for only the  $\text{Tb}^{3+}$  emission and 61 % if also the  $\text{Ce}^{3+}$  emission was taken into account. This value is among the highest quantum yields for organically capped nanoparticles. The luminescence decays of  $\text{Eu}^{3+}$ - and  $\text{Tb}^{3+}$ -doped nanoparticles were not mono-exponential and a model to fit the luminescence decay was described. This model takes into account quenching from randomly distributed quenchers inside the nanoparticles. The luminescence lifetimes for both ions are

several milliseconds. Recently, the luminescence of  $\text{Er}^{3+}$ -doped  $\text{LuPO}_4$  co-doped with  $\text{Yb}^{3+}$  was reported.<sup>89</sup> Energy transfer from  $\text{Yb}^{3+}$  to the  $\text{Er}^{3+}$  ion was demonstrated and in another publication energy transfer from  $\text{Yb}^{3+}$  was used to obtain up-conversion luminescence of  $\text{Er}^{3+}$  and  $\text{Tm}^{3+}$  in a nanoparticle solution, which demonstrates the good shielding of the lanthanide ions in these nanoparticles.<sup>90</sup>

Synthesis of these  $\text{YVO}_4$  and  $\text{LaPO}_4$  nanoparticles solutions were performed at relatively low temperatures compared to the synthesis of the bulk powders, but the particles are still highly crystalline and show similar spectroscopic properties as the bulk materials.<sup>91</sup>

### 2.6.5 Lanthanide ions in semiconductor nanoparticles

The shielding of lanthanide ions could be achieved by doping them in the core of nanoparticles and as a result the luminescence properties of the ions in an organic environment could be improved. Semiconductor nanoparticles have the advantage of high molar absorption coefficients and the possibility to excite them with charge carriers generated by electricity. Doping of lanthanide ions in semiconductor nanoparticles could have enormous advantages over the doping in nanoparticles of isolator host materials. Energy transfer from the semiconductor host to the lanthanide ion would have the advantage of a broad excitation band for photo-excitation and offer the possibility of electroluminescence of the lanthanide ion. At the same time the lanthanide ion is shielded from the organic environment. Energy transfer from semiconductor nanoparticles to lanthanide ions has been reported in a large number of publications. The best-known example is the energy transfer of silicon nanoparticles to  $\text{Er}^{3+}$  ions doped in silicon-enriched  $\text{SiO}_2$  waveguides.<sup>92</sup> Energy transfer of other semiconductor nanoparticles to other lanthanide ions is also described, like from  $\text{CdS}$  to  $\text{Eu}^{3+}$  and  $\text{SnO}_2$  to  $\text{Eu}^{3+}$ .<sup>93,94</sup> These examples are all in solid state glasses or sol-gel derived samples. Reports about the doping of lanthanide ions in nanoparticles passivated by organic ligands have also appeared. The doping of  $\text{Tb}^{3+}$  ions in  $\text{ZnS}$  nanoparticles was described in several papers.<sup>95</sup> Okamoto *et al.* reported luminescence studies on  $\text{CdS}$  doped with  $\text{Eu}^{3+}$ ,<sup>96</sup> and  $\text{ZnS}$  doped with  $\text{Eu}^{3+}$  was reported by Qu *et al.*<sup>97</sup> The results of these studies have been under discussion lately when Bol *et al.* tried to reproduce the results.<sup>98</sup> They conclude that the lanthanide ions are not incorporated in the nanoparticles, but probably adsorbed at the surface. The excitation spectra of their reaction products are dominated by the  $4f$  absorption bands of the lanthanide ions as proof that no energy transfer takes place from the semiconductor host to the lanthanide ion.

### 2.6.6 Synthesis of mono-disperse nanoparticles

It is important to control the size and size distribution of the nanoparticles during the synthesis. The properties of nanoparticles strongly depend on the size and therefore mono-disperse nanoparticle solutions are necessary to study the size-dependent properties. Mono-disperse nanoparticle solutions are also necessary to control the organization on substrates or in 3D space.<sup>99</sup> Control of the size and size distribution of nanoparticles during the synthesis can be obtained by confinement in tight cavities, like zeolites, dendrimers, or reversed micelles. In reversed micelles the size of the water pools can be controlled, and with the size of the water pools the size of the nanoparticles.<sup>100</sup> In coordinating solvents the size distribution of semiconductor nanoparticles is kept low by fast injection of the precursors. A rapid injection of the precursor leads to the formation of a high concentration of monomer and to a fast growth of nanoparticles with a small size distribution. When the reaction proceeds, the monomer concentration becomes lower due to the reaction and an increase in size distribution is observed. Narrow size distributions can be obtained by maintaining a high monomer concentration as was stated in the theory “focusing of the size distribution”.<sup>101</sup> Another mechanism for lowering the size distribution is by Ostwaldt ripening. In this mechanism the larger particles grow by consuming the smaller particles, because the smaller particles have a larger surface area making them less stable.<sup>102</sup> This theory was demonstrated with the synthesis of mono-disperse gold nanoparticles by heating preformed gold nanoparticles in a surfactant mixture.<sup>103</sup> The heating lead to a narrowing of the size distribution and an increase of the size from 2 to 5 nm. This is apparently the most stable size under these conditions, because starting with larger nanoparticles also results in nanoparticles with a size of 5 nm and a relatively narrow size distribution.<sup>104</sup> The desired size distribution is not in all cases obtained directly after the synthesis and the most popular method to decrease the size distribution of a nanoparticle solution is by size-selective precipitation. In this procedure, the nanoparticles are in a solution and a non-solvent is slowly added to the solution until a precipitate starts to form. This precipitate should consist of the largest particles, because these have the largest surface area and are the first to destabilize in solution. This method is time consuming, because it often has to be repeated several times and the yield of the desired size is very low.



## 2.7 Optical amplifiers

Optical amplifiers consist of a waveguide in which optical signals can be amplified without the conversion to an electrical signal.<sup>105</sup> These amplifiers are of technological importance, because of the fast amplification and because they allow for the simultaneous amplification of multiple wavelengths of light. A schematic optical amplifier is shown in Figure 2.6. The waveguiding material has a higher refractive index than the surroundings and due to total internal reflection the light is guided through the waveguide. The waveguides can be made of glass fiber, but in Figure 2.6 a planar waveguide is shown. These planar waveguides can be made on solid substrates with the use of lithographic techniques and they can play an important role in the integration of optical components. The waveguide has to be doped with a luminescent material, in our case the lanthanide ion, that can amplify light by stimulated emission. A four-level laser scheme is shown in Figure 2.6, which can be applied to most lanthanide ions. The lanthanide ion can be excited from level **4**, the ground state, to level **1** the excited state. From level **1** it decays non-radiatively and very fast to the luminescent level **2**. Spontaneous and stimulated emission is possible from level **2** to level **3**, followed by a rapid deactivation to the ground state.

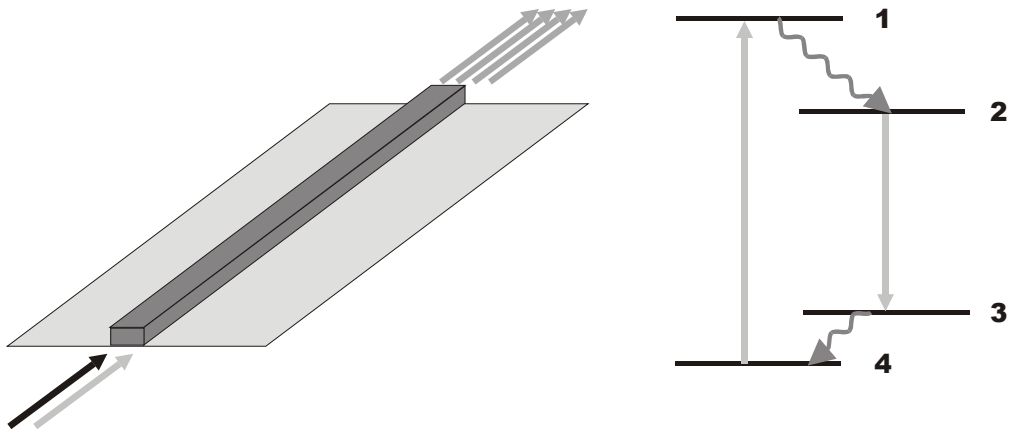


Figure 2.6: Schematic representation of an optical amplifier and the luminescence processes playing a role in the luminescent material. The scheme is for a four-level lasing medium with process  $4 \rightarrow 1$  the ground state absorption,  $2 \rightarrow 3$  spontaneous and stimulated emission and the processes  $1 \rightarrow 2$  and  $3 \rightarrow 4$  fast non-radiative decays.

The scheme shows a four-level system applicable to most lanthanide ions, but for instance  $\text{Er}^{3+}$  operates in a three-level system. In a three-level system level **3** is missing and emission goes directly to the ground state. For net optical gain a population inversion has to be created between level **2** and **3** (or the ground state for a three-level system). If this is the case, a signal can be

amplified by stimulated emission resulting in more photons with the same frequency, the same phase, and the same direction. A long living level 2 (long luminescence lifetime) is beneficial to reduce the pumping power, because with a long luminescence lifetime it takes less pump power to maintain a population inversion. Optical amplifiers are necessary to compensate for losses in telecommunication fibers. The wavelengths of interest are determined by the losses of the silica fibers used for telecommunication. The loss spectrum of an optical fiber is schematically shown in Figure 2.7. The losses increase because of Rayleigh scattering at shorter wavelengths by small inhomogeneities in the glass fiber. The minimum loss is between 1300 and 1600 nm with a peak at 1400 nm. This peak is caused by the vibrational overtone of OH groups from water that is trapped into the fiber during the production. In current optical fibers this peak can be reduced, making this wavelength also available for telecommunication.<sup>106</sup> At longer wavelengths the losses increase again due to the vibrational energies of the chemical bonds. The wavelength region most interesting for telecommunication is therefore between 1300 and 1600 nm and optical amplifiers operating at these wavelengths are of most interest.

A disadvantage of the use of glass fibers is that it is difficult to couple them to other optical components, like splitters, multiplexers, etc. Due to this problem there is a large interest in making these optical amplifiers on chips so integration is achieved more easily on the same chip. Materials, which combine good optical properties with the low cost fabrication on planar substrates, are under development.

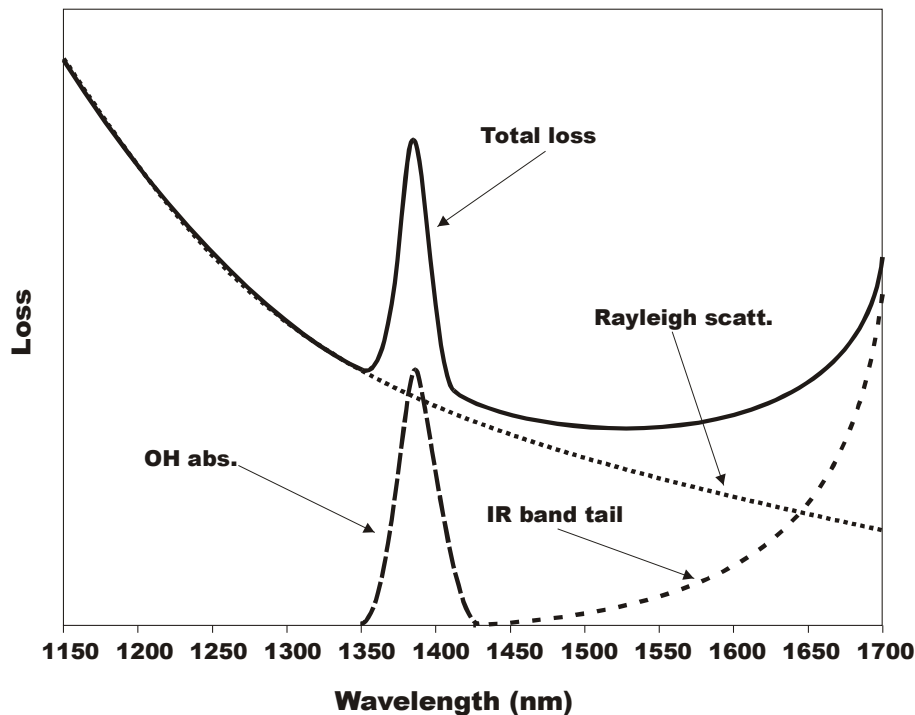


Figure 2.7: Schematic loss spectrum of an optical telecommunication fiber.

### 2.7.1 1550 nm fiber amplifiers.

The success of long-range optical telecommunication can, for a large part, be ascribed to the development of the erbium-doped fiber amplifier (EDFA). These fiber amplifiers operate in the low loss window around 1550 nm due to the  $^4I_{13/2} \rightarrow ^4I_{15/2}$  transition of  $Er^{3+}$ . In silica fiber a large gain of 30-50 dB (1,000-100,000 times signal increase) can be obtained over a 80 nm wide bandwidth. The amplification wavelengths and bandwidth can be varied slightly by changing the glass material in which the  $Er^{3+}$  ions are doped. The concentration of  $Er^{3+}$  ions has to be low in order to prevent cross-relaxation of the  $Er^{3+}$  ions, which would lead to lower efficiency of the amplifier. Due to the low  $Er^{3+}$  concentration, the amplifier has to be very long (several meters) to obtain sufficient gain. The  $Er^{3+}$  ion operates in a three-level system and as a result the transmission wavelength is also an absorption wavelength. For this reason population inversion has to be complete over the entire length of the amplifier or else signal loss by absorption would take place.

### 2.7.2 1300 nm fiber amplifiers.

A lot of optical fibers installed are single mode fibers at 1300 nm, because at 1300 nm silica fibers have their dispersion minimum. Dispersion leads to a spreading of the optical signal because the velocity of light is dependent on the wavelength. As a result the best wavelength to emit signals through a silica fiber would be 1300 nm. The demand for optical amplifiers at this wavelength is obvious and among the lanthanide ions,  $Nd^{3+}$ ,  $Pr^{3+}$ , and  $Dy^{3+}$  have transitions at these wavelengths.

The  $Nd^{3+}$  ion was the first lanthanide ion reported, that exhibits optical gain around 1300 nm.<sup>107</sup>  $Nd^{3+}$  was an interesting ion at that time, because a lot was known about the luminescence and the ion generally shows high quantum efficiencies in various hosts. In the same year optical gain was demonstrated in a ZBLAN ( $ZrF_4$ - $BaF_2$ - $LaF_3$ - $AlF_3$ - $NaF$ ) fiber doped with 1000 ppm  $Nd^{3+}$ .<sup>108</sup> A maximum gain of 32 % at 1354 nm was obtained with a pump power of 688 mW at 514 nm. The wavelength of maximum gain was red-shifted compared to the luminescence maximum, which is caused by excited state absorption. The energy level diagram of  $Nd^{3+}$  is shown in Figure 2.8. This energy level diagram shows the pumping of  $Nd^{3+}$  at 795 nm to the  $^4F_{5/2}$  level, followed by a rapid decay to the emissive  $^4F_{3/2}$  level. From this level emissions to the  $^4I_{9/2}$  level around 880 nm, to the  $^4I_{11/2}$  level around 1060 nm, and to the  $^4I_{13/2}$  level around 1330 nm are possible. The emissions to the first two levels are generally stronger than emission to the

$^4I_{13/2}$  level, and spontaneous emission in the waveguide at 880 and 1060 nm can be amplified in the same way as the signal (ASE) and in this way deplete the excited state population. Filtering out emissions at these wavelengths can reduce amplified spontaneous emission, but signal gain never exceeded 10 dB. Together with the disadvantage that the gain spectrum is at longer wavelength than the desired 1.3  $\mu\text{m}$  because of ESA, the research for optical amplifiers in the 1.3  $\mu\text{m}$  window has been focused on other lanthanide ions.

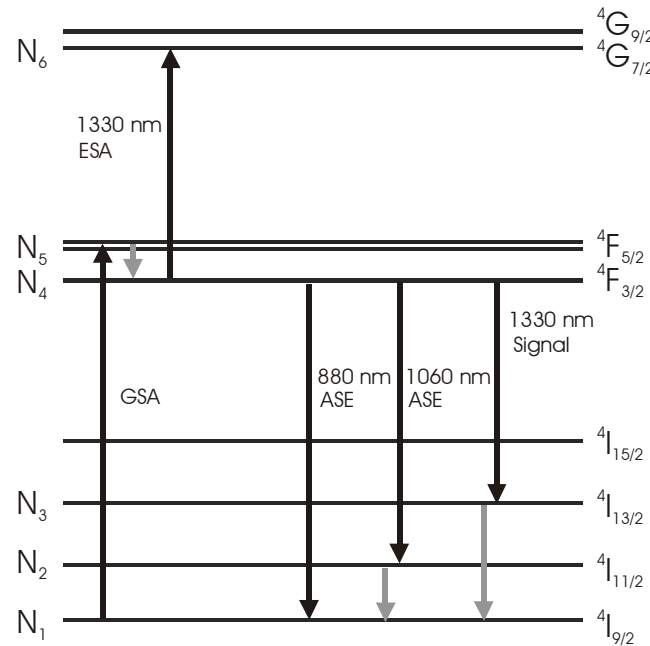


Figure 2.8: Energy level diagram of Nd<sup>3+</sup> ions. GSA is the ground state absorption, ESA is the excited state absorption, and ASE the amplified spontaneous emission processes.

Other possible lanthanide ions for optical amplification around 1300 nm are praseodymium and dysprosium. Pr<sup>3+</sup> shows emission around 1300 nm from the  $^1G_4 \rightarrow ^3H_5$  transition and Dy<sup>3+</sup> from the  $^6H_{9/2} \rightarrow ^6H_{15/2}$  transition. The efficiency of emission is strongly dependent on the phonon energy of the host material for both ions, because the energy levels are close together. Silica glass is therefore an unsuitable host for these ions, but chalcogenide glasses and fluoride glasses are.<sup>109</sup> Sol-gel processing of LaF<sub>3</sub> and LaCl<sub>3</sub> has obtained materials with high quantum yields for Pr<sup>3+</sup> and Dy<sup>3+</sup>.<sup>110</sup> Pr<sup>3+</sup>-doped fiber amplifiers with a gain exceeding 30 dB have been reported.<sup>7</sup>

### 2.7.3 Other wavelength amplifiers

To increase the bandwidth of today's telecommunication, amplification at other wavelengths is also investigated. The Tm<sup>3+</sup> ion, with emissions around 1220 nm and 1470 nm, could be used in optical amplifiers as well.<sup>29</sup> A problem with the 1470 wavelength is that this is a

four-level system of which the lifetime of the upper level is shorter than the lifetime of the lower level, making it difficult to obtain population inversion. Ways to circumvent this problem is by up-conversion pumping,<sup>111</sup> or the use of Ho<sup>3+</sup> co-doping.<sup>22</sup> An energy transfer process of Tm<sup>3+</sup> to Ho<sup>3+</sup> can decrease the luminescence lifetime of the lower laser level, making it possible to create population inversion.

## 2.8 Polymer-based optical amplifiers

Polymers for telecommunication have been prepared with good optical properties needed at the required wavelengths between 1300 and 1600 nm. Two important factors contributing to optical losses can be identified; absorption and scattering. The most important factors for the absorption losses are the overtones of the vibrations of organic bonds in polymers. They can give rise to absorptions in the telecommunication windows, leading to high losses. Especially CH and OH bonds commonly found in organic materials have strong absorptions between 1100 and 1700 nm. Some wavelengths of important vibrational overtones are given Table 2.4.<sup>112</sup> The strength of the absorptions decreases about an order of magnitude between each harmonic order. Bonds with the smallest reduced mass, like CH bonds, have the highest vibrational energies and the third overtone absorption is around 1200 nm. Polymers with CF bonds only show overtone orders of 5-7 in the telecommunication region and therefore have very low absorptions at these wavelengths. Partial or complete fluorination of the polymers has often been applied to decrease the absorption losses.

Scattering losses are another factor contributing to the loss of polymers. Scattering can occur from differently sized objects and experimental data can be fitted with an empirical law (Equation 2.2)

$$\alpha_{\text{scatter}} = A + B/\lambda^2 + D/\lambda^4 \quad (\text{Eq. 2.2})$$

in which A is the contribution of large particles ( $> \lambda$ ), B the contribution from inhomogeneities on the order of  $\lambda$  in size (Mie scattering), and D the contribution from small inhomogeneities ( $< \lambda$ , Rayleigh scattering). For the small inhomogeneities, the losses due to scattering are strongly wavelength dependent, so exclusion of the larger particles from the polymer by filtering the polymer solutions can strongly reduce scattering at the long

telecommunication wavelength. Other problems that could occur with polymers are the generally low thermal stability and high moisture sensitivity.

In order to compensate for the losses in polymer-based integrated circuits, amplifiers have to be integrated as well. Some polymer-based optical amplifiers have been fabricated, using lanthanide ions as the active luminescent material.  $\text{Nd}^{3+}$  ions have been used for polymer-based optical amplifiers around 1060 nm. In general  $\text{Nd}^{3+}$  shows the highest quantum yield of NIR-emitting lanthanide ions in organic environment, because it has the largest gap between the excited state and the lower lying energy levels. This transition around 1060 usually shows the strongest emission and is likely to be the first to show optical gain. A few reports have focused on this wavelength.

Table 2.4: Wavelengths and relative intensities of important vibrational overtones compared to the CH vibration.

Bond	Overtone order	Wavelength (nm)	Intensity (relative)
C-H		3390	1
C-H	1	1729	$7.2 \cdot 10^{-2}$
C-H	2	1176	$6.8 \cdot 10^{-3}$
C-D	2	1541	$1.6 \cdot 10^{-3}$
C-D	3	1174	$1.3 \cdot 10^{-4}$
C-F	4	1626	$6.4 \cdot 10^{-6}$
C-F	5	1361	$1.9 \cdot 10^{-7}$
C-F	6	1171	$6.4 \cdot 10^{-9}$
C=O	2	1836	$1.2 \cdot 10^{-2}$
C=O	3	1382	$4.3 \cdot 10^{-4}$
C=O	4	1113	$1.8 \cdot 10^{-5}$
O-H	1	1438	$7.2 \cdot 10^{-2}$

Karve *et al.* made a polymer waveguide of polyimide doped with  $\text{NdCl}_3$  with channel widths of  $50 \times 7 \mu\text{m}$  and 5 cm length.<sup>113</sup> The waveguides were made by alternately spin-coating a layer of doped polyimide and a layer of un-doped polyimide to reduce the losses of the polymer film. A signal of 1064 nm was coupled in at one side of the waveguide and the pumping laser operating at 800 nm was coupled in the waveguide on the other side. The gain was calculated by comparing the signal intensity when the pump was off to the signal intensity when

the pump was on. With a pump power of 110 mW and a signal power of 90 mW a signal gain of 8 dB was found. An *et al.* reported optical gain of a photolime gel waveguide doped with  $\text{NdCl}_3$  and chlorophenol red.<sup>114</sup> The pump and signal lasers were coupled into the waveguide using a prism coupling setup. With a pump power of 50 mW at 796 nm, a maximum gain of 3.8 dB at 1064 nm was obtained. Different polymers of fluorinated polyimides,<sup>115</sup> doped with  $\text{Nd}^{3+}$  complexes were reported, but no optical gain was reported for these materials. A calculation of the gain of a polymer-based amplifier with a visible emitting  $\text{Sm}^{3+}$  complex was reported by Koeppen *et al.*<sup>116</sup> For a fiber with a diameter of 1.5  $\mu\text{m}$ , an optical gain of over 20 dB was calculated at a wavelength of 644 nm. To date, no polymer-based optical amplifiers have been reported that show gain at the important telecommunication wavelengths.

The use of large colloids in polymer-based amplifiers has been considered.  $\text{SiO}_2$  colloids with sizes of 240 and 360 nm have been doped with  $\text{Er}^{3+}$  ions by ion implantation.<sup>117</sup> These colloids show a long luminescence lifetime of 17 ms for the  $\text{Er}^{3+}$  luminescence and a quantum yield of 80 % was estimated. Spin-coating of a layer of PMMA over the colloids resulted in a large reduction of the optical losses, but more careful matching of the refractive index of the polymer and the  $\text{SiO}_2$  colloids is necessary for waveguide fabrication. Large  $\text{Cr}^{3+}$ -doped particles were also incorporated in a polymer matrix.<sup>118</sup> These particles were in the order of 1  $\mu\text{m}$  and the refractive index of the polymer was closely matched to the index of the particles. Although the losses of the film were substantial, optical gain at 1.23  $\mu\text{m}$  could be measured. A signal increase by a factor of 2 was observed at a pump power of 7 W from a Nd:YAG laser operating at 1064 nm.

Recently, amplification of an organic dye at 1.3  $\mu\text{m}$  was reported, by doping the dye in a sol-gel matrix.<sup>119</sup> The emission intensity did not show a linear relationship with the pump power and an apparent gain of 11  $\text{cm}^{-1}$  was estimated by amplified spontaneous emission measurements using a one-dimensional amplifier model. Narrowing of the emission band could not be observed, which was attributed to the small gain.

## 2.9 Electroluminescence

Electroluminescence is the generation of light directly from electricity by applying a voltage over a thin layer of luminescent material. Holes are injected at the anode, electrons at the cathode and due to the applied electric field the holes and electrons travel through the layer. The holes and electrons can combine to a bound electron-hole pair (exciton) and form an excited

state. This excited state can decay by the emission of a photon. The luminescent material can be an inorganic material, small organic molecules, or a polymer. These polymer light-emitting diodes (LEDs) are fabricated as schematically shown in Figure 2.9. The transparent anode of most LEDs is composed of a glass substrate with a layer of ITO on top, so the light can escape out of the device on this side. The emissive layer is sandwiched between the cathode and the anode with a typical layer thickness of 100 nm. Metals with a low oxidation potential, like Ca, Mg, or Al, can be evaporated on top of the emissive layer to form the cathode. Another possibility is to use liquid metal alloys as the cathode.<sup>120</sup> Other layers can be added to improve the electron and hole injection in the device.

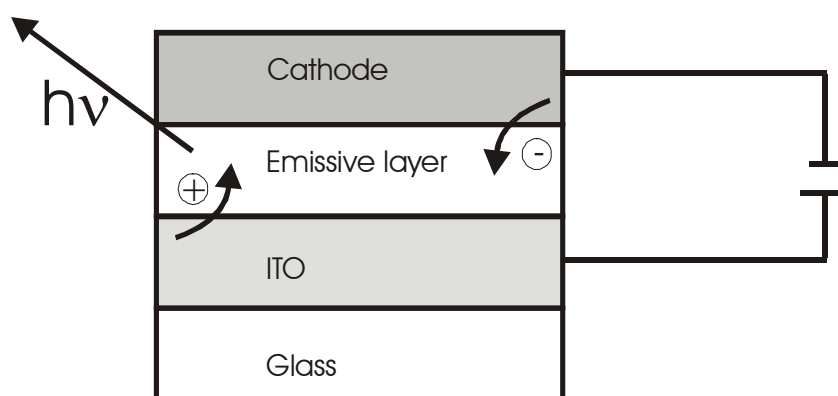


*Figure 2.9: Simple scheme of a light-emitting diode (LED). Several more layers can be added to improve electron and hole injection into the device and more than one emissive layer can be used.*

In principle this scheme could be used to excite lanthanide ions, having the advantage that a laser would no longer be necessary to excite the lanthanide ions. Electroluminescent lanthanide complexes have been reported, which emit in the visible and NIR.<sup>121</sup> Efficiencies of the NIR-emitting lanthanide complexes are generally low due to the low quantum yield of the organic complexes.<sup>122</sup> For more efficient lanthanide electroluminescence the quantum yield of the lanthanide ion itself in organic environment has to be increased. The problems are similar to the problems found using photo-excitation.

Semiconductor nanoparticles can be excited in light-emitting diodes leading to the direct generation of light from electricity. This principle was first shown using CdSe nanoparticles and PPV as a polymer layer.<sup>123</sup> A semiconductor polymer poly(*p*-phenylenevinylene) (PPV) was used as a hole transport layer on which the emissive layer of CdSe nanocrystals was spin-coated. On top of the CdSe layer the magnesium anode was evaporated, which was covered with a layer of silver to prevent oxidation in air. The efficiency of this device was later improved by using



core-shell nanoparticles of CdSe covered with a layer of CdS.<sup>124</sup> More examples of visible emitting semiconductor nanoparticles of ZnS and CdS in polymer substrates were reported.<sup>125</sup> Similar electroluminescent devices, that emit in the NIR, using nanoparticles of InAs<sup>126</sup> and PbS<sup>59</sup> were also reported.

## 2.10 Outlook

In this chapter an overview was given on the luminescence of lanthanide ions with a focus on the use of these ions in optical amplifiers. Lanthanide-doped fiber amplifiers have become a very important technology that has been developed in a relatively short period of time, of about 20 years. The major drawbacks of the glass fibers used, is the relatively expensive fabrication technology and the difficulties to integrate different optical components. The research on integrated planar polymer waveguide technology is growing. In order to make planar polymer waveguides successful, optical amplifiers have to be developed to compensate for losses in the waveguides and lanthanide ions seem to be the first choice since these luminescent materials are so important in glass technology. However, the luminescence of lanthanide ions in organic materials is not efficient due to the high-energy vibrations of the organic bonds surrounding the lanthanide ion. In this thesis the doping of lanthanide ions into nanoparticles is described as a way to improve the luminescence efficiency of the ions and to show that these materials can be used to make a polymer-based optical amplifier operating at a telecommunication wavelength. Haase *et al.* reported the efficient luminescence of LaPO<sub>4</sub> nanoparticles doped with visible emitting ions and in this thesis the properties of these nanoparticles doped with near-infrared emitting ions have been investigated. The near-infrared emitting ions generally show more efficient luminescence in materials with lower phonon energies than LaPO<sub>4</sub> and therefore the synthesis of nanoparticles with other host materials has also been investigated.

## 2.11 References

- <sup>1</sup> *CRC Handbook of Chemistry and Physics 64<sup>th</sup> ed.* ed. Weast, R. C., 1983-1984, Baco Raton, Florida, USA.
- <sup>2</sup> Jones, A. P.; Wall, F. *Rare earth minerals: chemistry, origin, and ore deposits*; Chapman and Hall: London, 1996.

3 Look at [www.molycorp.com](http://www.molycorp.com) the largest manufacturer of lanthanide ions in the western world.

4 Cotton, S. *Lanthanides and Actinides*; Macmillan Education: Basingstoke, 1991.

5 Feldmann, C.; Jüstel, T.; Ronda, C. R.; Schmidt, P. J. *Adv. Funct. Mater.* **2003**, *13*, 511.

6 Becker, P. C.; Olsson, N. A.; Simpson, J. R. *Erbium doped amplifiers: fundamentals and technology*; Academic Press: San Diego, 1999.

7 Dignonnet, M. J. F. *Rare earth doped fiber laser and amplifiers*; Dekker: New York, 1993.

8 Blasse, G.; Grabmaier, B. C. *Luminescent materials*; Springer: Berlin, 1994.

9 (a) Slooff, L. H.; van Blaaderen, A.; Polman, A.; Hebbink, G. A.; Klink, S. I.; van Veggel, F. C. J. M.; Reinhoudt, D. N.; Hofstraat, J. W. *Appl. Phys. Rev.* **2002**, *91*, 3955; (b) Kuriki, K.; Nishihara, S.; Nishizawa, Y.; Tagaya, A.; Koike, Y. *J. Opt. Soc. Am. B* **2002**, *19*, 1844; (c) Chen, R. T. *Opt. Laser Technol.* **1993**, *25*, 347.

10 Ermolaev, V. L.; Sveshnikova, E. B. *Russ. Chem. Rev.* **1994**, *63*, 905.

11 Dorenbos, P. J. *Lumin.* **2003**, *104*, 239.

12 Carnall, W. T.; Goodman, G. L.; Rajnak, K.; Rana, R. S. *J. Chem. Phys.* **1989**, *90*, 3443.

13 Kirby, A. F.; Richardson, F. S. *J. Phys. Chem.* **1983**, *87*, 2544.

14 (a) Judd, B. R. *Phys. Rev.* **1962**, *127*, 750; (b) Ofelt, G. S. *J. Chem. Phys.* **1962**, *37*, 511.

15 Werts, M. H. V.; Jukes, R. T. F.; Verhoeven, J. W. *Phys. Chem. Chem. Phys.* **2002**, *4*, 1542.

16 Gilbert, A.; Baggot, J. *Essentials of molecular photochemistry*; Blakwell Scientific Publications: London, 1991.

17 Stein, G.; Würzburg, E. *J. Chem. Phys.* **1975**, *62*, 208.

18 Förster, T. *Discuss. Faraday Soc.* **1959**, *27*, 7.

19 Strohhofer, C.; Polman, A. *Opt. Mater.* **2003**, *21*, 705.

20 (a) Strohhofer, C.; Polman, A. *J. Appl. Phys.* **2001**, *90*, 4314; (b) Townsend, J. E.; Barnes, W. L.; Jedrzejewski, K. P. *Electron. Lett.* **1991**, *27*, 1958.

21 (a) Walsh, B. M.; Barnes, N. P.; Di Bartolo, B. *J. Lumin.* **1997**, *75*, 89; (b) Walsh, B. M.; Barnes, N. P.; Di Bartolo, B. *J. Lumin.* **2000**, *90*, 39.

22 Song, J. H.; Heo, J.; Park, S. H. *J. Appl. Phys.* **2003**, *93*, 9441.

23 Kik, P. G.; Polman, A. *J. Appl. Phys.* **2003**, *93*, 5008.

24 Brierly, M. C.; France, P. W.; Millar, C. A. *Electron. Lett.* **1988**, *24*, 539.

25 Wetenkamp, L. *Electron. Lett.* **1990**, *26*, 883.

26 Yanagita, H.; Masuda, I.; Yamashita, T.; Toratani, H. *Electron. Lett.* **1990**, *26*, 1836.

27 Többen, H. *Electron. Lett.* **1992**, *28*, 1361.

28 Reisfeld, R.; Jorgensen, C. K. *Lasers and excited states of rare earths*; Springer: Berlin, 1977.

29 Soga, K.; Wang, W.; Riman, R. E.; Brown, J. B.; Mikeska, K. R. *J. Appl. Phys.* **2003**, *93*, 2946.

- 30 Hewak, D. W.; Deol, R. S.; Wang, J.; Wylangowski, G.; Medeiros, J. A.; Samson, B. N.; Laming, R. I.; Brocklesby, W. S.; Payne, D. N.; Jha, A.; Poulain, M.; Otero, S.; Surinach, S.; Baro, M. D. *Electron. Lett.* **1993**, *29*, 237.
- 31 Taylor, E. R.; Ng, L. N.; Sessions, N. P.; Buerger, H. J. *Appl. Phys. Lett.* **2002**, *92*, 112.
- 32 Carnall, W. T.; Goodman, G. L.; Rajnak, K.; Rana, R. S. *J. Chem. Phys.* **1989**, *90*, 3443.
- 33 Brecher, C.; Samelson, H.; Lempicki, A.; Riley, R.; Peters, T. *Phys. Rev.* **1967**, *155*, 178.
- 34 Blasse, G. *Prog. Solid St. Chem.* **1988**, *18*, 79 and references therein.
- 35 Huang, W.; Syms, R. R. A.; Yeatman, E. M.; Ahmad, M. M.; Clapp, T. V.; Ojha, S. M. *IEEE Photon. Tech. Lett.* **2002**, *14*, 959.
- 36 (a) Arai, K.; Namikawa, H.; Kumata, K.; Honda, T.; Ishii, Y.; Handa, T. *J. Appl. Phys.* **1986**, *59*, 3430; (b) Zhou, Y.; Lam, Y. L.; Wang, S. S.; Liu, H. L.; Kam, C. H.; Chan, Y. C. *Appl. Phys. Lett.* **1997**, *71*, 587; (c) Ryu, C. K.; Choi, H.; Kim, K. *Appl. Phys. Lett.* **1995**, *66*, 2496.
- 37 Parker, D.; Gareth Williams, J. A. *J. Chem. Soc., Dalton Trans.* **1996**, *18*, 3613.
- 38 Hebbink, G. A.; Klink, S. I.; Oude Alink, P. G. B.; van Veggel, F. C. J. M. *Inorg. Chim. Acta.* **2001**, *317*, 114.
- 39 Hemmilä, I. K. *Applications of Fluorescence in Immunoassays*; Wiley and Sons: New York, **1991**.
- 40 (a) Klink, S. I.; Grave, L.; Reinhoudt, D. N.; van Veggel, F. C. J. M.; Werts, M. H. V.; Geurts, F. A. J.; Hofstraat, J. W. *J. Phys. Chem. A* **2000**, *104*, 5457; (b) Klink, S. I.; Hebbink, G. A.; Grave, L.; Peters, F. G. A.; van Veggel, F. C. J. M.; Reinhoudt, D. N.; Hofstraat, J. W. *Eur. J. Org. Chem.* **2000**, *10*, 1923.
- 41 Hofstraat, J. W.; Oude Wolbers, M. P.; van Veggel, F. C. J. M.; Reinhoudt, D. N.; Werts, M. H. V.; Verhoeven, J. W. *J. Fluoresc.* **1998**, *8*, 301.
- 42 (a) Klink, S. I.; Keizer, H.; Hofstraat, H. W.; van Veggel, F. C. J. M. *Synth. Met.* **2002**, *127*, 213; (b) Klink, S. I.; Oude Alink, P. O.; Grave, L.; Peters, F. G. A.; Hofstraat, J. W.; Geurts, F.; van Veggel, F. C. J. M. *J. Chem. Soc., Perkin Trans. 2* **2001**, *3*, 363.
- 43 Browne, W. R.; Vos, J. G. *Coord. Chem. Rev.* **2001**, *219-221*, 761.
- 44 Yanagida, S.; Hasegawa, Y.; Murakoshi, K.; Wada, Y.; Nakashima, N.; Yamanaka, T. *Coord. Chem. Rev.* **1998**, *171*, 461.
- 45 Hebbink, G. A.; Reinhoudt, D. N.; van Veggel, F. C. J. M. *Eur. J. Org. Chem.* **2001**, *21*, 4101.
- 46 Hasegawa, Y.; Ohkubo, T.; Sogabe, K.; Kawamura, Y.; Wada, Y.; Makashima, N.; Yanagida, S. *Angew. Chem. Int. Ed.* **2000**, *39*, 357.
- 47 Faraday, M. *Philos. Trans. R. Soc.* **1857**, *147*, 145.
- 48 Turkevich, J.; Garton, G.; Stevenson, P. C. *J. Colloid Sci.* **1954**, *9*, 26.
- 49 Murray, C. B.; Norris, D. J.; Bawendi, M. G. *J. Am. Chem. Soc.* **1993**, *115*, 8706.

- 50 Brust, M.; Walker, M.; Bethell, D.; Schiffrin, D. J.; Whyman, R. *J. Chem. Soc., Chem. Commun.* **1994**, 7, 801.
- 51 (a) Weller, H. *Adv. Mater.* **1993**, 5, 88; (b) Weller, H. *Angew. Chem. Int. Ed. Engl.* **1993**, 32, 41; (c) Henglein, A. *Chem. Rev.* **1989**, 89, 1861.
- 52 (a) Peng, Z. A.; Peng, X. *J. Am. Chem. Soc.* **2001**, 123, 183; (b) Peng, Z. A.; Peng, X. *J. Am. Chem. Soc.* **2002**, 124, 3343.
- 53 (a) Qu, L.; Peng, X. *J. Am. Chem. Soc.* **2002**, 124, 2049; (b) Peng, Z. A.; Peng, X. *J. Am. Chem. Soc.* **2001**, 123, 1389; (c) Qu, L.; Peng, Z. A.; Peng, X. *Nano Lett.* **2001**, 1, 333.
- 54 (a) Peng, X.; Manna, L.; Yang, W.; Wickham, J.; Scher, E.; Kadavanich, A.; Alivisatos, A. P. *Nature*, **2000**, 404, 59; (b) Peng, Z. A.; Peng, X. *J. Am. Chem. Soc.* **2001**, 123, 1389.
- 55 Manna, L.; Scher, E. C.; Alivisatos, A. P. *J. Am. Chem. Soc.* **2000**, 122, 12700.
- 56 Cumberland, S. L.; Hanif, K. M.; Javier, A.; Khitrov, G. A.; Strouse, G. F.; Woessner, S. M.; Yun, C. S. *Chem. Mater.* **2002**, 14, 1576.
- 57 Talapin, D. V.; Haubold, S.; Rogach, A. L.; Kornowski, A.; Haase, M.; Weller, H. *J. Phys. Chem. B* **2001**, 105, 2260.
- 58 Harrison, M. T.; Kershaw, S. V.; Burt, M. G.; Rogach, A. L.; Kornowski, A.; Eychmüller, A.; Weller, H. *Pure Appl. Chem.* **2000**, 72, 295.
- 59 Bakueva, L.; Musikhin, S.; Hines, M. A.; Chang, T. W. F.; Tzolov, M.; Scholes, G. D.; Sargent, E. H. *Appl. Phys. Lett.* **2003**, 82, 2895.
- 60 Wehrenberg, B. L.; Wang, C.; Guyot-Sionnest, P. *J. Phys. Chem. B* **2002**, 106, 10634.
- 61 (a) Klimov, V. I.; Mikhailovsky, A. A.; Xu, S.; Malko, A. V.; Hollingworth, J. A.; Leatherdale, C. A.; Eisler, H. J.; Bawendi, M. G. *Science* **2000**, 290, 314; (b) Htoon, H.; Hollingworth, J. A.; Malko, A. V.; Dickerson, R.; Klimov, V. I. *Appl. Phys. Lett.* **2003**, 82, 4776.
- 62 Peng, X.; Schlamp, M. C.; Kadavanich, A. V.; Alivisatos, A. P. *J. Am. Chem. Soc.* **1997**, 119, 7019.
- 63 (a) Danek, M.; Jensen, K. F.; Murray, C. B.; Bawendi, M. G. *Chem. Mater.* **1996**, 8, 173; (b) Hoener, C. F.; Allan, K. A.; Bard, A. J.; Campion, A.; Fox, M. A.; Mallouk, T. E.; Webber, S. E.; White, J. M. *J. Phys. Chem.* **1992**, 96, 3812.
- 64 Dabbousi, B. O.; Rodriguez-Viejo, J.; Mikulec, F. V.; Heine, J. R.; Mattoussi, H.; Ober, R.; Jensen, K. F.; Bawendi, M. G. *J. Phys. Chem. B* **1997**, 101, 9463.
- 65 Harrison, M. T.; Kershaw, S. V.; Rogach, A. L.; Kornowski, A.; Eychmüller, A.; Weller, H. *Adv. Mater.* **2000**, 12, 123.
- 66 Borchert, H.; Haubold, S.; Haase, M.; Weller, H.; McGinley, C.; Riedler, M.; Möller, T. *Nano Lett.* **2002**, 2, 151.

- 67 (a) Korgel, B. A.; Fitzmaurice, D. *Adv. Mater.* **1998**, *10*, 661; (b) Thomas, P. J.; Kulkarni, G. U.; Rao, C. N. R. *J. Phys. Chem. B* **2000**, *104*, 8138; (c) Martin, J. E.; Wilcoxon, J. P.; Odinek, J.; Provencio, P. *J. Phys. Chem. B* **2002**, *106*, 971.
- 68 (a) Petit, C.; Taleb, A.; Pileni, M. P. *J. Phys. Chem. B* **1999**, *103*, 1805; (b) Puentes, V. F.; Krishnan, K. M.; Alivisatos, A. P. *Science* **2001**, *291*, 2115; (c) Sun, S.; Murray, C. B. *J. Appl. Phys.* **1999**, *85*, 4325.
- 69 Sun, S.; Murray, C. B.; Weller, D.; Folks, L.; Moser, A. *Science* **2000**, *287*, 1989.
- 70 (a) Ye, T.; Guiwen, Z.; Weiping, Z.; Shangda, X. *Mater. Res. Bull.* **1997**, *32*, 501; (b) Li, Q.; Gao, L.; Yan, D. *Nanostruct. Mater.* **1997**, *8*, 825; (c) Bihari, B.; Eilers, H.; Tissue, B. M. *J. Lumin.* **1997**, *75*, 1.
- 71 Yin, M.; Zhang, W.; Xia, S.; Krupa, J. C. *J. Lumin.* **1996**, *68*, 335.
- 72 (a) Williams, D. K.; Bihari, B.; Tissue, B. M.; McHale, J. M. *J. Phys. Chem. B* **1998**, *102*, 916; (b) Eilers, H.; Tissue, B. M. *Chem. Phys. Lett.* **1996**, *251*, 74.
- 73 Wakefield, G.; Holland, E.; Dobson, P. J.; Hutchison, J. L. *Adv. Mater.* **2001**, *13*, 1557.
- 74 Liu, G. K.; Zhuang, H. Z.; Chen, X. Y. *Nano Lett.* **2002**, *2*, 535.
- 75 (a) Yang, H. S.; Hong, K. S.; Feofilov, S. P.; Tissue, B. M.; Meltzer, R. S.; Dennis, W. M. *J. Lumin.* **1999**, *83-84*, 139; (b) Tissue, B. M. *Chem. Mater.* **1998**, *10*, 2837.
- 76 Chen, X. Y.; Zhuang, H. Z.; Liu, G. K.; Li, S.; Niedbala, R. S. *J. Appl. Phys.* **2003**, *94*, 5559.
- 77 (a) Wei, Z.; Sun, L.; Liao, C.; Yan, C.; Huang, S. *Appl. Phys. Lett.* **2002**, *80*, 1447; (b) Wei, Z.; Sun, L.; Liao, C.; Jiang, X.; Yan, C. *J. Mater. Chem.* **2002**, *12*, 3665; (c) Wei, Z.; Sun, L.; Liao, C.; Jiang, X.; Yan, C. *J. Appl. Phys.* **2003**, *93*, 9783.
- 78 Yan, C. H.; Sun, L. D.; Liao, C. S.; Zhang, Y. X.; Lu, Y. Q.; Huang, S. H.; Lü, S. Z. *Appl. Phys. Lett.* **2003**, *82*, 3511.
- 79 (a) Schuurmans, F. J. P.; Lagendijk, A. *J. Appl. Phys.* **2000**, *113*, 8; (b) Schuurmans, F. J. P.; de Lang, D. T. N.; Wegdam, G. H.; Sprik, R.; Lagendijk, A. *Phys. Rev. Lett.* **1998**, *80*, 5077.
- 80 (a) Meltzer, R. S.; Feofilov, S. P.; Tissue, B.; Yuan, H. B. *Phys. Rev. B* **1999**, *60*, 14012; (b) Meltzer, R. S.; Yen, W. M.; Zheng, H.; Feofilov, S. P.; Dejneka, M. J.; Tissue, B.; Yuan, H. B. *J. Lumin.* **2001**, *94-95*, 217.
- 81 Huignard, A.; Gacoin, T.; Boilot, J. P. *Chem. Mater.* **2000**, *12*, 1090.
- 82 Huignard, A.; Buisette, V.; Laurent, G.; Gacoin, T.; Boilot, J. P. *Chem. Mater.* **2002**, *14*, 2264.
- 83 Riwotzki, K.; Haase, M. *J. Phys. Chem. B* **1998**, *102*, 10129.
- 84 Riwotzki, K.; Haase, M. *J. Phys. Chem. B* **2001**, *105*, 12709.
- 85 Huignard, A.; Buisette, V.; Franville, A. C.; Gacoin, T.; Boilot, J. P. *J. Phys. Chem. B* **2003**, *107*, 6754.
- 86 Riwotzki, K.; Meysamy, H.; Kornowski, A.; Haase, M. *J. Phys. Chem. B* **2000**, *104*, 2824.

- 87 Riwozki, K.; Meyssamy, H.; Schnablegger, H.; Kornowski, A.; Haase, M. *Angew. Chem. Int. Ed.* **2001**, *40*, 573.
- 88 Meyssamy, H.; Riwozki, K.; Kornowski, A.; Naused, S.; Haase, M. *Adv. Mater.* **1999**, *11*, 840.
- 89 Lehmann, O.; Meyssamy, H.; Kömpe, K.; Schnablegger, H.; Haase, M. *J. Phys. Chem. B* **2003**, *107*, 7449.
- 90 Heer, S.; Lehmann, O.; Haase, M.; Güel, H. U. *Angew. Chem. Int. Ed.* **2003**, *42*, 3179.
- 91 Haase, M.; Riwozki, K.; Meyssamy, H.; Kornowski, A. *J. Alloy. Compd.* **2000**, *303-304*, 191.
- 92 (a) Fujii, M.; Yoshida, M.; Kanzawa, Y.; Hayashi, S.; Yamamoto, K. *Appl. Phys. Lett.* **1997**, *71*, 1198; (b) Kik, P. G.; Polman, A. *Mat. Sci Eng. B* **2001**, *81*, 3; (c) Han, H. S.; Seo, S. Y.; Shin, J. H. *Appl. Phys. Lett.* **2001**, *79*, 4568.
- 93 (a) Selvan, S. T.; Hayakawa, T.; Nogami, M.; Möller, M. *J. Non-Cryst. Solids* **2001**, *291*, 137; (b) Hayakawa, T.; Selvan, S. T.; Nogami, M. *J. Sol-Gel Sci. Techn.* **2000**, *19*, 779.
- 94 Nogami, M.; Enomoto, T.; Hayakawa, T. *J. Lumin.* **2002**, *97*, 147.
- 95 (a) Bhargava, R. N. *J. Lumin.* **1996**, *70*, 85; (b) Goldburt, E. T.; Bhargava, R. N. *J. SID.* **1996**, *4*, 365; (c) Kane, R. S.; Cohen, R. E.; Silbey, R. *Chem. Mater.* **1999**, *11*, 90; (d) Ihara, M.; Igarashi, T.; Kusonoki, T.; Ohno, K. *J. Electrochem. Soc.* **2000**, *147*, 2355.
- 96 Okamoto, S.; Kobayashi, M.; Kanemitsu, Y.; Kushida, T. *Phys. Stat. Sol. B* **2002**, *229*, 481.
- 97 Qu, S. C.; Zhou, W. H.; Liu, F. Q.; Chen, N. F.; Wang, Z. G.; Pan, H. Y.; Yu, D. P. *Appl. Phys. Lett.* **2002**, *80*, 3605.
- 98 Bol, A. A.; van Beek, R.; Meijerink, A. *Chem. Mater.* **2002**, *14*, 1121.
- 99 Maenosono, S.; Okubo, T.; Yamaguchi, Y. *J. Nanoparticle Res.* **2003**, *5*, 5.
- 100 Pileni, M. P. *J. Phys. Chem.* **1993**, *97*, 6961.
- 101 Peng, X.; Wickham, J.; Alivisatos, A. P. *J. Am. Chem. Soc.* **1998**, *120*, 5343.
- 102 Stella, A.; Cheyssac, P.; Kofman, R. *Science and technology of thin films*, Ed. Maticotta, F. C.; Ottaviani, G. World scientific, Singapore, Vol. 57, **1996**, p57.
- 103 (a) Maye, M. M.; Zheng, W. X.; Leibowitz, F. L.; Ly, N. K.; Zhong, C. J. *Langmuir* **2000**, *16*, 490; (b) Zhong, C. J.; Zheng, W. X.; Leibowitz, F. L.; Eichelberger, H. H. *J. Chem. Soc., Chem. Commun.* **1999**, *13*, 1211; (c) Maye, M. M.; Zhong, C. J. *J. Mater. Chem.* **2000**, *10*, 1895.
- 104 Lin, X. M.; Sorensen, C. M.; Klabunde, K. J. *J. Nanoparticles Res.* **2000**, *2*, 157.
- 105 Sudo, S. *Optical fiber amplifiers: Materials, Devices and Applications*; Artec House, Inc: Boston, 1997.
- 106 For example the Allwave™ optical fiber by Lucent Technologies.
- 107 Miniscalco, W. J.; Andrews, L. J.; Thompson, B. A. *Electron. Lett.* **1988**, *24*, 28.
- 108 Brierley, M. C.; Millar, C. A. *Electron. Lett.* **1988**, *24*, 438.

- <sup>109</sup> (a) Samson, B. N.; Medeiros Neto, J. A.; Laming, R. I.; Hewak, D. W. *Electron. Lett.* **1994**, *30*, 1617; (b) Wei, K.; Machewirth, D. P.; Wenzel, J.; Snitzer, E.; Sigel, G. H. *Opt. Lett.* **1994**, *19*, 904.
- <sup>110</sup> Ballato, J.; Riman, R. E.; Snitzer, E. *Opt. Lett.* **1997**, *22*, 691.
- <sup>111</sup> Komukai, T.; Yamamoto, T.; Sugawa, T.; Miyajima, Y. *IEEE J. Quant. Electron.* **1995**, *31*, 1880.
- <sup>112</sup> Ma, H.; Jen, A. K. Y.; Dalton, L. R. *Adv. Mater.* **2002**, *14*, 1339.
- <sup>113</sup> Karve, G.; Bihari, B.; Chen, R. T. *Appl. Phys. Lett.* **2000**, *77*, 1253.
- <sup>114</sup> An, D.; Yue, Z.; Chen, R. T. *Appl. Phys. Lett.* **1998**, *72*, 2806.
- <sup>115</sup> Lin, S.; Feuerstein, J.; Mickelson, A. R. *J. Appl. Phys.* **1996**, *79*, 2868.
- <sup>116</sup> Koeppen, C.; Yamada, S.; Jiang, G.; Garito, A. F.; Dalton, L. R. *J. Opt. Soc. Am. B* **1997**, *14*, 155.
- <sup>117</sup> Slooff, L. H.; de Dood, M. J. A.; van Blaaderen, A.; Polman, A. *Appl. Phys. Lett.* **2000**, *76*, 3682.
- <sup>118</sup> Barber, D. B.; Pollock, C. R.; Beecroft, L. L.; Ober, C. K. *Opt. Lett.* **1997**, *22*, 1247.
- <sup>119</sup> Casalboni, M.; de Matteis, F.; Merlo, V.; Proposito, P.; Russo, R.; Schutzmann, S. *Appl. Phys. Lett.* **2003**, *83*, 416.
- <sup>120</sup> Gao, F. G.; Bard, A. J. *J. Am. Chem. Soc.* **2000**, *122*, 7426.
- <sup>121</sup> (a) Slooff, L. H.; Polman, A.; Cacialli, F.; Friend, R. H.; Hebbink, G. A.; van Veggel, F. C. J. M.; Reinhoudt, D. N. *Appl. Phys. Lett.* **2001**, *78*, 2122; (b) Kido, J.; Okamoto, Y. *Chem. Rev.* **2002**, *102*, 2357; (c) Kang, T. S.; Harrison, B. S.; Bouguettaya, M.; Foley, T. J.; Boncella, J. M.; Schanze, K. S.; Reynolds, J. R. *Adv. Funct. Mater.* **2003**, *13*, 205.
- <sup>122</sup> Kang, T. S.; Harrison, B. S.; Foley, T. J.; Knefely, A. S.; Boncella, J. M.; Reynolds, J. R.; Schanze, K. S. *Adv. Mater.* **2003**, *15*, 1093.
- <sup>123</sup> Colvin, V. L.; Schlamp, M. C.; Alivisatos, A. P. *Nature*, **1994**, *370*, 354.
- <sup>124</sup> Schlamp, M. C.; Peng, X.; Alivisatos, A. P. *J. Appl. Phys.* **1997**, *82*, 5837.
- <sup>125</sup> (a) Yang, Y.; Xue, S.; Liu, S.; Huang, J.; Shen, J. *Appl. Phys. Lett.* **1996**, *69*, 377; (b) Dabbousi, B. O.; Bawendi, M. G.; Onitsuka, O.; Rubner, M. F. *Appl. Phys. Lett.* **1995**, *66*, 1316; (c) Gao, M.; Richter, B.; Kirstein, S.; Möhwald, H. *J. Phys. Chem. B* **1998**, *102*, 4096.
- <sup>126</sup> Tessler, N.; Medvedev, V.; Kazes, M.; Kan, S.; Banin, U. *Science* **2002**, *295*, 1506.





# CHAPTER 3

## Synthesis of lanthanide(III)-doped nanoparticles\*

*This chapter describes the synthesis of lanthanide(III)-doped nanoparticles. In these nanoparticles the lanthanide ion is shielded from the surrounding organic environment to improve the luminescence properties. Visible and near-infrared (NIR)-emitting lanthanide ions have been doped in nanoparticles of LaPO<sub>4</sub>:Ln, LaF<sub>3</sub>:Ln and LaVO<sub>4</sub>:Ln. The Eu<sup>3+</sup> ion was used as a probe for the doping site of the lanthanide ion, because the luminescence of this ion is sensitive to the symmetry of the local environment. Other lanthanide ions emitting in the visible and NIR could also be doped in these nanoparticles. Generally, the luminescence of the ions is comparable to that of the bulk materials. For the first time, Ho<sup>3+</sup> is reported to show luminescence in an organic solution, in the visible and in the NIR, indicating the good shielding of the lanthanide ion. The lifetimes of the Eu<sup>3+</sup> and NIR-emitting ions indicate a high quantum yield, compared to the same ions in organic complexes.*

---

\* The major part of the work in this chapter was published: Stouwdam, J. W.; van Veggel, F. C. J. M. *Nano Lett.* **2002**, 2, 733; Hebbink, G. A.; Stouwdam, J. W.; Reinhoudt, D. N.; van Veggel, F. C. J. M. *Adv. Mater.* **2002**, 14, 1147; Stouwdam, J. W.; Hebbink, G. A.; Huskens, J.; van Veggel, F. C. J. M. *Chem. Mater.* **2003**, 15, 4604.

### 3.1 Introduction

The luminescence of lanthanide ions has found important commercial applications in displays,<sup>1</sup> optical amplifiers,<sup>2</sup> and lasers,<sup>3</sup> as described in chapter 2. There is a growing interest to use this luminescence in polymer-based materials, because of the easy processing of polymers and ease of integrating different optical components. The luminescence of these lanthanide ions arises from transitions within the  $4f$  electron shell. These transitions are parity forbidden, leading to low absorption cross-sections and long luminescence lifetimes. However, this long-lived excited state can be quenched very efficiently in the presence of the high-energy vibrations of organic solvents, polymers, or ligands, thus hampering the application in polymer-based devices. Therefore, to use lanthanide luminescence in an organic environment it is important to shield the lanthanide ion from the organic surroundings. Shielding of the lanthanide ion<sup>4</sup> can be achieved by doping it in the inorganic part of nanoparticles, that should still be soluble in organic solvents. Good solubility is generally achieved by having organic groups on the outside of the nanoparticles. Most nanoparticles doped with lanthanide ions are made in high temperature procedures leading to nanoparticles without organic groups on the surface and, therefore, they have no solubility in solvents.<sup>5</sup>

Only very few examples of these lanthanide-doped nanoparticles that have a good solubility in organic solvents have been reported.<sup>6,7</sup> Haase and co-workers have synthesized nanoparticles of  $\text{LaPO}_4$  doped with the visible emitting ions  $\text{Eu}^{3+}$  and  $\text{Tb}^{3+}$ , but the near-infrared (NIR) emitting ions have received little attention. Lanthanide ions emitting at wavelengths between 1300 and 1600 nm are of interest for optical telecommunication, because at these wavelengths the silica-based optical fibers have their maximum transparency.<sup>8</sup> Nanoparticles with dimensions of a few nanometers are small enough to minimize scattering in polymer films.<sup>9</sup> The largest contribution to scattering in polymer films originates from particles with a size comparable to the wavelength of light, or bigger (Mie scattering). Nanoparticles have a size much smaller than the wavelength of light and when clustering of the nanoparticles in a polymer film is prevented, scattering should be minimal.

### 3.2 Results and discussion

**Characterization.** Nanoparticles of  $\text{LaPO}_4$  were prepared using a literature procedure from the hydrated  $\text{LnCl}_3$  salts and phosphoric acid.<sup>6</sup> The growth of the nanoparticles is controlled by the coordinating solvent tris(ethylhexyl)phosphate and protonated trioctylamine. During the reaction some of the solvent is hydrolyzed and the resulting bis(ethylhexyl)phosphate coordinates

to the surface. The coordination of this molecule to the surface was shown by  $^1\text{H}$  NMR spectroscopy and MS-FAB on the nanoparticle product. Broadened signals were observed at 0.9 and 1.3 ppm in the  $^1\text{H}$  NMR spectrum, from the ethyl hexyl chains and MS-FAB analysis showed a peak at 321.2 of the de-protonated bis(ethylhexyl)phosphate. The  $\text{LaF}_3$  and  $\text{LaVO}_4$  nanoparticles were synthesized using a procedure similar to a literature procedure for the synthesis of  $\text{LaF}_3$  nanoparticles.<sup>10</sup> Ligands **1** or **2** depicted in Figure 3.1 were used for the synthesis of the lanthanide-doped luminescent nanoparticles.<sup>11</sup> To a solution of one of these ligands and  $\text{NaF}$  or  $\text{Na}_3\text{VO}_4$  in a water/ethanol mixture was added dropwise a solution of the  $\text{Ln}(\text{NO}_3)_3$  salts in water. The dithiophosphate head-group of the ligand coordinates weakly to the lanthanide ions allowing the growth of the nanoparticles, but coordinates strongly enough to prevent the nanoparticles from aggregating.<sup>12</sup>

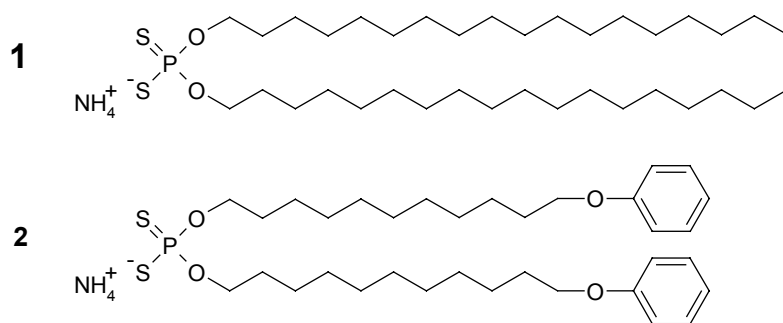


Figure 3.1: Ligands used for the synthesis of  $\text{LaF}_3$  and  $\text{LaVO}_4$  nanoparticles.

In all cases the doping concentration of the luminescent lanthanide ions is 5 % of the total lanthanide ion concentration, unless stated otherwise. Different nanoparticles, with different host materials were made because these nanoparticles all offer a different symmetry site to the lanthanide ion and because the maximum phonon energies differ for these materials, from  $300\text{ cm}^{-1}$  for  $\text{LaF}_3$ , about  $800\text{ cm}^{-1}$  for  $\text{LaVO}_4$ , to  $1050\text{ cm}^{-1}$  for  $\text{LaPO}_4$ . Especially the low-phonon energies of the  $\text{LaF}_3$  host could have advantages for the NIR-emitting ions, because multi-phonon emission is minimized in this material. The nanoparticles were characterized using transmission electron microscopy (TEM) by evaporating a drop of nanoparticle solution on a carbon coated copper grid. Figure 3.2 shows typical TEM pictures of  $\text{LaF}_3:\text{Eu}$ ,  $\text{LaVO}_4:\text{Eu}$ , and  $\text{LaPO}_4:\text{Eu}$  nanoparticles. The morphologies of the nanoparticles are independent of the doping ion. The high crystallinity of the nanoparticles can clearly be seen, despite the fact that the nanoparticles were synthesized at relatively low temperatures, i.e. below  $200^\circ\text{C}$ . The average sizes of the nanoparticles are 6.3, 7.9, and 4.3 nm for the  $\text{LaF}_3$ ,  $\text{LaVO}_4$ , and  $\text{LaPO}_4$  nanoparticles, respectively (note the different scale bars).

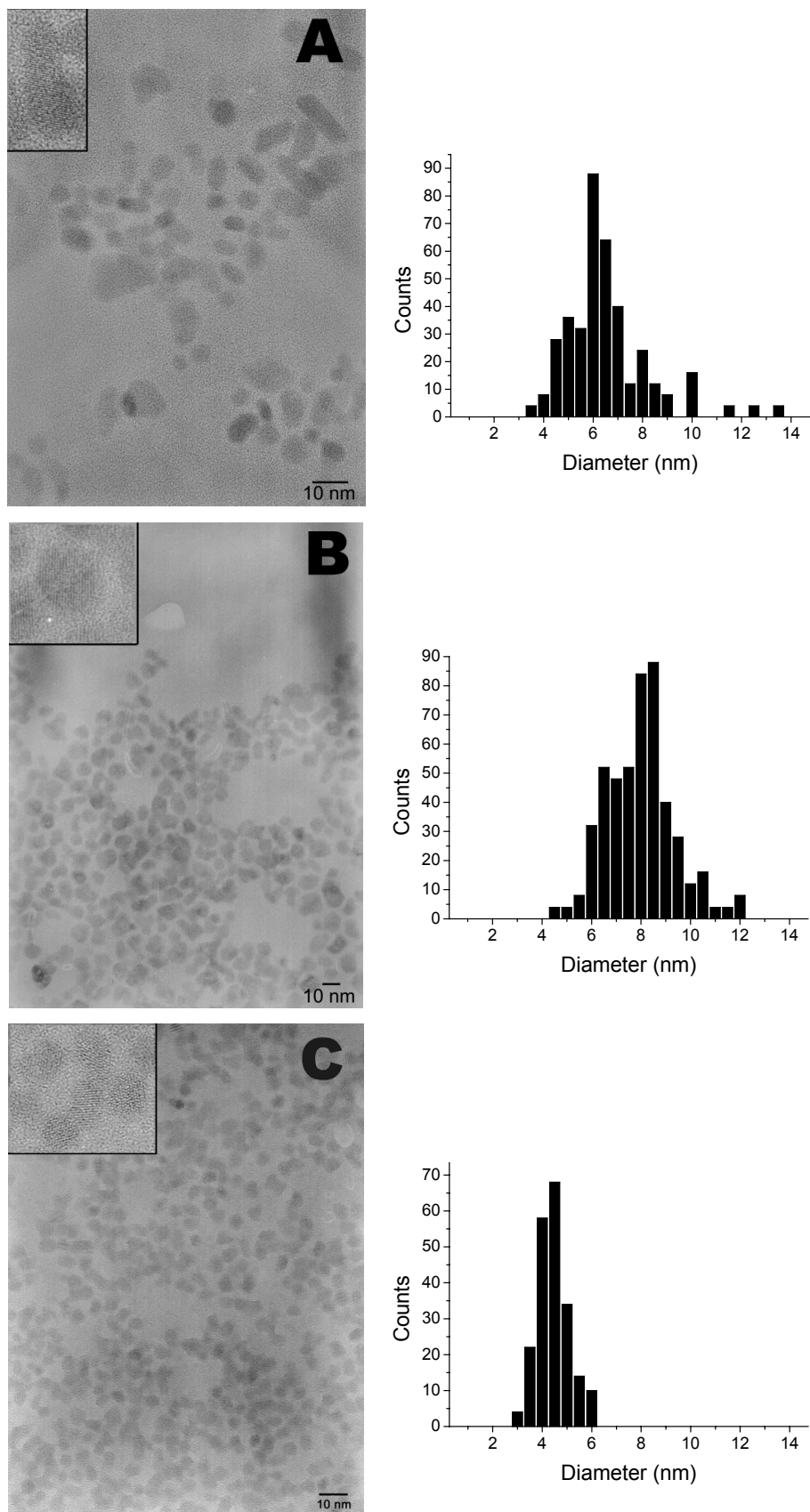


Figure 3.2: TEM pictures of (A)  $\text{LaF}_3:\text{Eu}$ , (B)  $\text{LaVO}_4:\text{Eu}$ , and (C)  $\text{LaPO}_4:\text{Eu}$  nanoparticles with the corresponding size distribution. The insets show high magnifications of single nanoparticles in which the crystallinity of the nanoparticles can be seen.

The size distribution (standard deviation) of the LaF<sub>3</sub> nanoparticles is 28 %, much larger than for the other two. The size distributions of the LaVO<sub>4</sub> and LaPO<sub>4</sub> nanoparticles are 17 % and 15 %, respectively. Moreover, the LaF<sub>3</sub> nanoparticles are less spherical in shape with aspect ratios between 1 and 3. The spherical and elongated nanoparticles both consist of one crystal domain, so the elongated nanoparticles are not formed by aggregation of multiple nanoparticles. In the size distribution histograms the sizes of the elongated nanoparticles were determined by averaging of the long and short axis. The sizes of the nanoparticles are sufficiently small to prevent scattering when the nanoparticles are incorporated in a polymer matrix.<sup>13</sup> An estimation of the number of luminescent ions in the nanoparticles can be made taking into account the density of the host material and the average size of the nanoparticles. Assuming spherical nanoparticles, and using a density of LaF<sub>3</sub> of 5.94 g/cm<sup>3</sup>,<sup>14</sup> the number of La<sup>3+</sup> atoms in the LaF<sub>3</sub> nanoparticles is about 2400. At a doping concentration of 5 % the number of luminescent ions is approximately 120 per LaF<sub>3</sub> nanoparticle. For the smaller LaPO<sub>4</sub> nanoparticles the number of luminescent ions will be slightly less and for the bigger LaVO<sub>4</sub> nanoparticles it will be slightly more. The elemental composition of the nanoparticles was determined using X-ray fluorescence (XRF) and combustion elemental analysis. The results are summarized in Table 3.1. In the nanoparticles the same ratio of lanthanide ions as applied in the synthesis was found, reflecting the similar reactivity of the lanthanide ions.

*Table 3.1: Elemental composition of lanthanide-doped nanoparticles (weight %)*

Particle	La <sup>a</sup>	Ln <sup>a</sup>	P <sup>a</sup>	V <sup>a</sup>	C <sup>b</sup>	H <sup>b</sup>	S <sup>b</sup>	N <sup>b</sup>
LaF <sub>3</sub> :Eu ligand <b>1</b>	30.96	1.61	2.64	-	35.96	6.63	6.18	-
LaF <sub>3</sub> :Eu ligand <b>2</b>	n. d. <sup>c</sup>	n. d. <sup>c</sup>	n. d. <sup>c</sup>	-	15.23	2.29	3.82	0.14
LaVO <sub>4</sub> :Eu ligand <b>1</b>	18.46	1.17	4.48	9.24	44.62	7.88	6.70	-
LaF <sub>3</sub> :Nd	24.76	1.23	3.48	-	42.49	7.76	5.76	-
LaF <sub>3</sub> :Er	24.20	1.35	3.48	-	43.59	7.62	6.48	-
LaF <sub>3</sub> :Ho	35.41	1.94	2.94	-	33.07	7.76	5.72	-
LaPO <sub>4</sub> :Nd	41.97	2.42	12.19	-	6.33	2.16	-	1.01
LaPO <sub>4</sub> :Er	41.80	2.36	12.56	-	5.57	2.63	-	1.20
LaPO <sub>4</sub> :Pr	41.97	2.35	12.52	-	6.30	2.17	-	1.01

a) measured with XRF

b) measured with combustion elemental analysis.

c) n. d. is not determined

Apart from the nanoparticle core, organic groups on the outside of the nanoparticles like tetramethyl ammonium ions and ethylhexyl chains for the  $\text{LaPO}_4$  nanoparticles and the coordinated dithiophosphate ligand for the  $\text{LaF}_3$  and  $\text{LaVO}_4$  nanoparticles were detected. The  $\text{LaF}_3$  nanoparticles synthesized with the two different ligands show a different amount of ligand present after the synthesis. Ligand **2** is much less abundant compared to the  $\text{LaF}_3$  core, although there is still a small amount of free ligand present, indicated by the 0.14 % of nitrogen in the elemental analysis. For the nanoparticles synthesized with ligand **1**, no free ligand is present, because no nitrogen has been detected. The presence of lanthanide complex can also be excluded, because this could not be detected with mass spectroscopy (FAB and MALDI). For the  $\text{LaF}_3$  nanoparticles it is likely that the surface consists of  $\text{Ln}^{3+}$  ions, because these can coordinate to the ligand that stabilizes the nanoparticle. The coordination of the ligand to the surface of the nanoparticles can be seen from the broadened signals of the ligand in the  $^1\text{H}$  NMR spectrum. Fluoride could not be detected with EA and XRF, so no information could be obtained about the amount of  $\text{F}^-$  in the  $\text{LaF}_3$  nanoparticles. In the case of  $\text{LaPO}_4$  nanoparticles the ratio of Ln/P is smaller than one, indicating that the surface of the nanoparticles consists of phosphate groups. The presence of tetramethylammonium ions in the  $^1\text{H}$  NMR spectrum is consistent with this, because these positively charged ions could coordinate to the phosphate groups.

Some representative IR spectra of the nanoparticles are shown in Figure 3.3. The IR spectra of  $\text{LaF}_3$  and  $\text{LaVO}_4$  nanoparticles synthesized with ligand **1** are very similar in the high frequency range of the IR spectrum.

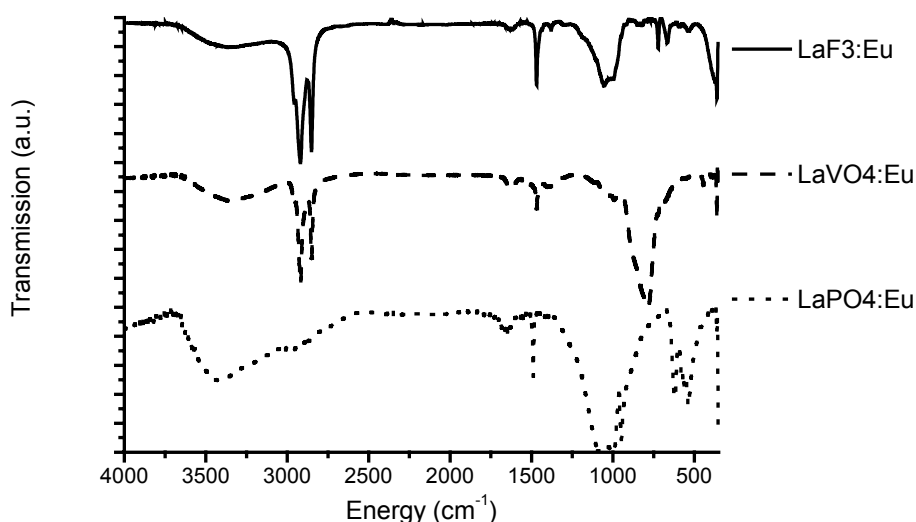


Figure 3.3: IR spectra of the  $\text{LaF}_3$ ,  $\text{LaVO}_4$ , and  $\text{LaPO}_4$  nanoparticles. The  $\text{LaF}_3$  and  $\text{LaVO}_4$  nanoparticles were synthesized using ligand **1**.

The CH stretching vibrations of the organic ligand are visible around  $3000\text{ cm}^{-1}$ . Above  $3000\text{ cm}^{-1}$  a broad band is visible caused by water that is probably coordinated to the surface of the nanoparticles.  $\text{LaF}_3$  is not a hygroscopic material so incorporation of water in the crystal lattice is not likely. The surface  $\text{LaVO}_4$  nanoparticles can be terminated with V-OH bonds, giving rise to a broad band above  $3000\text{ cm}^{-1}$ . Differences between the  $\text{LaF}_3$  and  $\text{LaVO}_4$  nanoparticles are observed at lower energy. The  $\text{LaVO}_4$  nanoparticles show a broad band peaking at  $780\text{ cm}^{-1}$  of the host lattice absorption. In the spectrum of the  $\text{LaF}_3$  nanoparticles the onset of an absorption can be seen at  $350\text{ cm}^{-1}$ . The reported value of  $300\text{ cm}^{-1}$  for host lattice absorption lies out of the range of our spectrometer.<sup>15</sup> The host lattice absorption corresponds to the maximum phonon energies surrounding the lanthanide ion and the lower these maximum phonon energies are, the lower the quenching by multi-phonon emission is by the host lattice. For the  $\text{LaPO}_4$  nanoparticles the broad band of host lattice absorption is at  $1050\text{ cm}^{-1}$ . At higher energy a broad band similar to the other two nanoparticles is observed above  $3000\text{ cm}^{-1}$ , which can be ascribed to coordinated water and to the surface P-OH bonds. A small series of peaks can be seen below  $3000\text{ cm}^{-1}$ , ascribed to the small amount of coordinated organic ligands in the form of ethylhexyl chains.

### 3.2.1 Luminescence of $\text{Eu}^{3+}$ -doped nanoparticles

**$^5\text{D}_0$   $\text{Eu}^{3+}$  emission.** The  $\text{Eu}^{3+}$  ion was used as a probe for the symmetry of the crystal site in which the ion is located. Typical  $\text{Eu}^{3+}$  emission originating from the  $^5\text{D}_0$  and  $^5\text{D}_1$  levels was observed after excitation at 397 nm for  $\text{LaF}_3:\text{Eu}$ , 280 nm for  $\text{LaVO}_4:\text{Eu}$ , and 260 nm for  $\text{LaPO}_4:\text{Eu}$ . The  $\text{Eu}^{3+}$  ion in  $\text{LaF}_3$  has to be excited directly in a  $4f$  absorption line of the ion itself. These absorption lines have a low absorption coefficient and so a high concentration of nanoparticles has to be used in order to obtain sufficient luminescence.  $\text{YVO}_4:\text{Eu}$  is a well known phosphor for display purposes, because of an intense red emission originating primarily from the  $^5\text{D}_0 \rightarrow ^7\text{F}_2$  transition.  $\text{YVO}_4$  nanoparticles could be synthesized using ligands **1** or **2** and  $\text{Y}(\text{NO}_3)_3$ , but the luminescence of these nanoparticles was weak.  $\text{LaVO}_4$  nanoparticles showed much stronger luminescence using this synthesis method and in the remainder of this chapter  $\text{LaVO}_4$  is used as the host material instead of  $\text{YVO}_4$ . The bad results for the  $\text{YVO}_4$  nanoparticles could be a result of different coordination of the ligand to the  $\text{Y}^{3+}$  ions. The ion is smaller in size and has a higher affinity for oxygen than sulfur compared to the lanthanide ions. This difference in affinity could have an influence on the reaction, because the nanoparticle growth is controlled by the lanthanide sulfur interaction of the ligand.

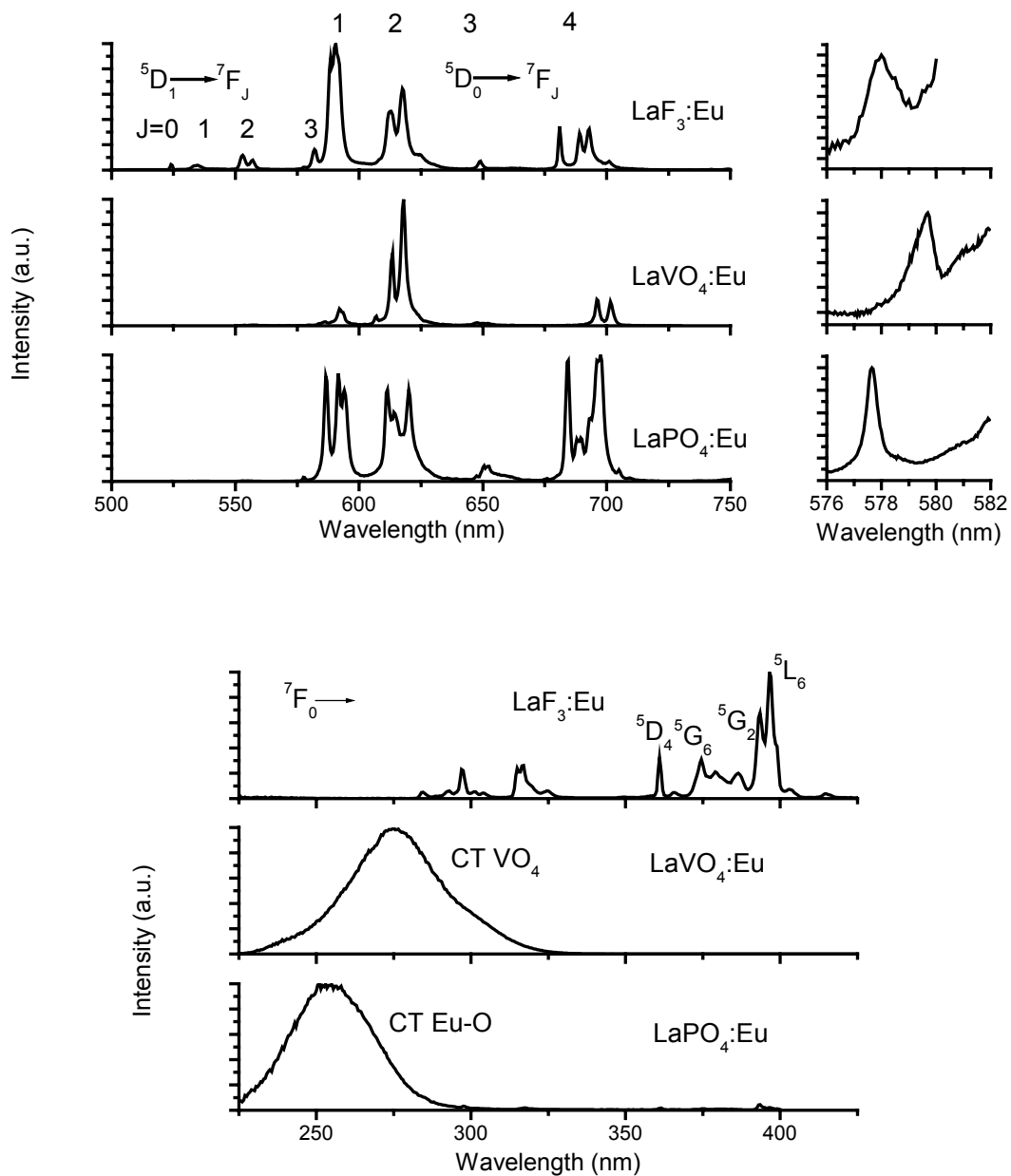


Figure 3.4: Emission (up) and excitation (down) spectra of LaF<sub>3</sub>:Eu, LaVO<sub>4</sub>:Eu, and LaPO<sub>4</sub>:Eu. An enlargement of the  $^5D_0 \rightarrow ^7F_0$  emission peak is shown on the top right.

The Eu<sup>3+</sup> emission spectrum shows that the symmetry site in both materials is the same because differences in the emission spectrum were not observed. The distances between the lanthanide ions can be a little larger, because of the increased size of the host cation. The LaVO<sub>4</sub>:Eu and LaPO<sub>4</sub>:Eu nanoparticles can be excited in a charge transfer band. In the LaVO<sub>4</sub> nanoparticles the charge transfer is in the V-O bond and in the LaPO<sub>4</sub> nanoparticles it is in the Eu-O bond. Deactivation of the charge transfer state leads to an excited Eu<sup>3+</sup> ion. Due to the low



reduction potential of  $\text{Eu}^{3+}$  this band occurs at wavelengths above 200 nm in the  $\text{LaPO}_4$  nanoparticles. The  $\text{LaVO}_4$  nanoparticles have the advantage that the charge transfer band of the  $\text{VO}_4$  group is independent of the doping ion, making it possible to excite almost all lanthanide ions using the charge transfer band of the  $\text{VO}_4$  group. The ratio of the different peaks of the  ${}^5\text{D}_0 \rightarrow {}^7\text{F}_J$  ( $J = 1, 2$ ) transitions in the  $\text{Eu}^{3+}$  emission spectrum gives information about the symmetry of the crystal site in which the ion is located. This confirms that the doping ion is present in a  $\text{La}^{3+}$  crystal site giving the  $\text{Eu}^{3+}$  ion  $C_2$  symmetry in  $\text{LaF}_3$ ,  $D_{2d}$  symmetry in  $\text{LaVO}_4$ , and  $C_1$  symmetry in  $\text{LaPO}_4$  nanoparticles, the same as for the bulk materials.<sup>16,17,18</sup> In the  $\text{LaVO}_4$  nanoparticles the  $\text{Eu}^{3+}$  ion has no inversion symmetry, so the  ${}^5\text{D}_0 \rightarrow {}^7\text{F}_2$  transition is clearly the dominating emission band. In the other two nanoparticles there is more inversion symmetry and especially in the  $\text{LaF}_3$  nanoparticles the  ${}^5\text{D}_0 \rightarrow {}^7\text{F}_1$  transition is the dominating emission band. The emission peak of the  ${}^5\text{D}_0 \rightarrow {}^7\text{F}_0$  transition gives information on the number of different  $\text{Eu}^{3+}$  sites present. Both levels are non-degenerate, so a single  $\text{Eu}^{3+}$  center should give rise to one emission peak. In all three samples one emission peak was observed for the  ${}^5\text{D}_0 \rightarrow {}^7\text{F}_0$  around 578 nm, leading to the conclusion that all  $\text{Eu}^{3+}$  ions are in a similar crystal site. In the  $\text{LaF}_3$  and  $\text{LaVO}_4$  nanoparticles the peak is however broader than in the  $\text{LaPO}_4$  nanoparticles, which could indicate more disorder.

**${}^5\text{D}_1$  emission.** The  $\text{LaF}_3$  nanoparticles clearly showed emission from the  ${}^5\text{D}_1$  level indicating the low phonon energies of the  $\text{LaF}_3$  nanoparticles host. In the other two nanoparticles the  ${}^5\text{D}_1$  emission could be observed, but due to multi-phonon relaxation the emissions were very weak. The appearance of  ${}^5\text{D}_1$  emission in the  $\text{LaF}_3$  nanoparticles is comparable to the bulk material and is not often observed in organic environment.<sup>19</sup> This indicates that the shielding from the organic environment is good and that emission properties of the bulk material are also found in the nanoparticles. The separation between the  ${}^5\text{D}_1$  and  ${}^5\text{D}_0$  level is only  $1750 \text{ cm}^{-1}$  and like in bulk  $\text{LaF}_3$  this gap cannot be bridged by multi-phonon emission. The emission of the  ${}^5\text{D}_1$  level is however strongly concentration dependent. A cross-relaxation process as described in chapter 2 is responsible for quenching of the  ${}^5\text{D}_1$  emission at higher concentrations of  $\text{Eu}^{3+}$ . Figure 3.5 shows the emission spectrum of the  ${}^5\text{D}_1$  emission of  $\text{LaF}_3:\text{Eu}$  at different  $\text{Eu}^{3+}$  concentrations, with the spectra normalized to the  ${}^5\text{D}_0 \rightarrow {}^7\text{F}_1$  emission peak at 591 nm.

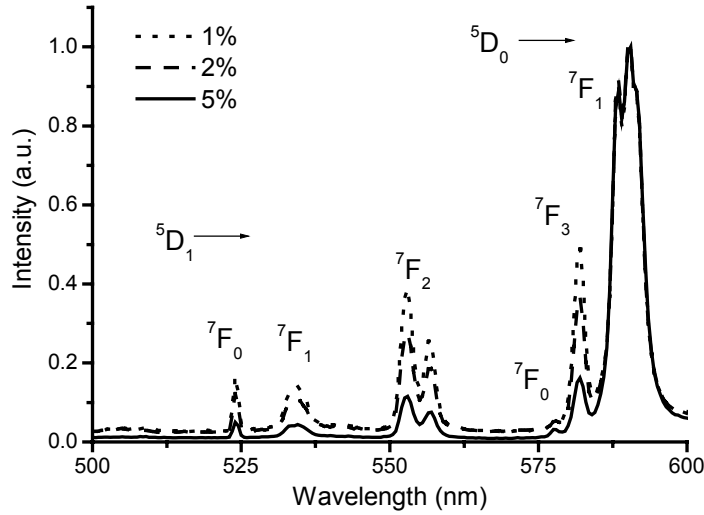


Figure 3.5: Emission spectra of  $\text{LaF}_3:\text{Eu}$  nanoparticles with different concentrations of  $\text{Eu}^{3+}$ , normalized to the  ${}^5\text{D}_0 \rightarrow {}^7\text{F}_1$  emission peak at 591 nm.

A concentration dependence of the  ${}^5\text{D}_1$  emission is indicative of a cross-relaxation process, similar to what is seen for the bulk material. Emissions from the  ${}^5\text{D}_2$  and  ${}^5\text{D}_3$  level are observed in the bulk crystal for the 1 % doped sample, but this is not the case for the nanoparticles. This indicates that quenching of these levels still occurs in the nanoparticles. In bulk  $\text{LaF}_3$ , emission from these levels shows a strong dependence on the concentration and the temperature. The relative emission from the  ${}^5\text{D}_0$  level strongly increases with increasing temperature and increasing doping concentration. No emission from these levels is observed after lowering the concentration in the nanoparticles, but a reduction of the temperature might be of influence.

**Luminescence lifetime.** The luminescence lifetime is an important parameter indicative of the efficiency of the luminescence of the lanthanide ion. The luminescence lifetime is directly related to the quantum yield of emission by Equation 3.1,

$$\phi_{\text{lum}} = \frac{\tau_{\text{obs}}}{\tau_{\text{rad}}} \quad (\text{Eq. 3.1})$$

in which,  $\phi_{\text{lum}}$  is the luminescence quantum yield,  $\tau_{\text{obs}}$  the measured quantum yield, and  $\tau_{\text{rad}}$  the radiative lifetime of the lanthanide ion. The observed luminescence lifetime is the same as the radiative lifetime when quenching does not play a role.

Figure 3.6 shows the luminescence decays of the  ${}^5\text{D}_0$  level of the  $\text{Eu}^{3+}$  ion doped in the three nanoparticles.

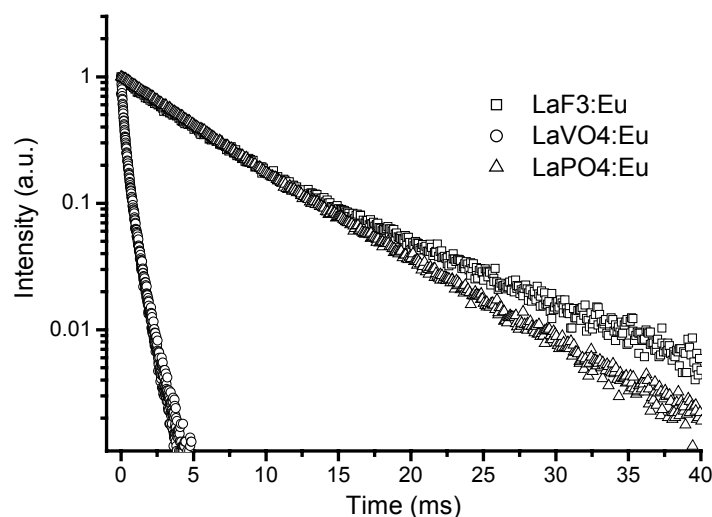


Figure 3.6: Luminescence decays of the  $\text{Eu}^{3+} \ ^5D_0$  level in the three nanoparticles ( $\lambda_{em}$ . 591 nm for  $\text{LaF}_3$  and 613 nm for  $\text{LaVO}_4$  and  $\text{LaPO}_4$ ).

The decays of all three nanoparticles are not mono-exponential, because the decay does not form a straight line in the log plot. A multi-exponential decay is caused by a difference in quenching for different  $\text{Eu}^{3+}$  ions or a difference in radiative lifetime of the  $\text{Eu}^{3+}$  ions caused by different symmetry sites. The influence of the nanoparticles surface, which always has a large impact on nanoparticle properties, is probably the main cause for the existence of a non-mono-exponential decay. In the next chapter a model will be described to fit the luminescence decay of the lanthanide ions in these nanoparticles by taking into account surface effects. Another possibility is to fit the decays using a multi-exponential decay. Although there is no physical reason to do this,<sup>20</sup> it does return average values of the main components of the luminescence decay that can be compared to the lifetimes obtained for bulk materials and lifetimes obtained from organic complexes. When comparing the lifetimes, the influence of the refractive index and the symmetry of the  $\text{Eu}^{3+}$  site on the radiative lifetime of the  $\text{Eu}^{3+}$  ion have to be taken into account. The comparison with lifetimes obtained for organic complexes is a good measure for the shielding of the lanthanide ion from the organic environment. The luminescence lifetimes were fitted using a bi-exponential decay.  $\text{LaF}_3:\text{Eu}$  nanoparticles in dichloromethane have a lifetime of 7.7 ms responsible for 74 % of the luminescence and 2.9 ms responsible for 26 % of the luminescence. For  $\text{LaVO}_4:\text{Eu}$ , the lifetimes are 0.67 ms (59 %) and 0.19 ms (41 %) in dichloromethane and for  $\text{LaPO}_4:\text{Eu}$  nanoparticles in methanol, the lifetimes are 7.1 ms (56 %) and 3.9 ms (44 %). The luminescence lifetime of the  $\text{Eu}^{3+}$  ion in  $\text{LaVO}_4$  is clearly much shorter

than in the other matrices. In the  $\text{LaVO}_4$  nanoparticles the  $\text{Eu}^{3+}$  ion is in a crystal site that has no inversion symmetry as was concluded from the emission spectrum. As a result the radiative lifetime of the  $\text{Eu}^{3+}$  ion in this matrix is much shorter than in the other two matrices. The radiative lifetime of the  $\text{Eu}^{3+}$  ion is strongly dependent on the symmetry of the crystal site and Werts *et al.* have proposed an equation from which the radiative lifetime of the  $\text{Eu}^{3+}$  ion can be calculated from the shape of emission spectrum (Equation 2.1).<sup>21</sup> Using Equation 2.1, radiative lifetimes for  $\text{LaF}_3:\text{Eu}$ ,  $\text{LaVO}_4:\text{Eu}$ , and  $\text{LaPO}_4:\text{Eu}$  of 6.3, 0.8, and 4.8 ms, respectively, were calculated. The long components of the measured lifetimes were even longer than the calculated radiative lifetimes for  $\text{LaF}_3$  and  $\text{LaPO}_4$  nanoparticles, leading to calculated quantum yields above 100 %. These impossible calculated quantum yields could be a result of the influence of the refractive index of the solvent on the measured luminescence lifetime. In the calculation, the refractive indices of 1.59, 1.99, and 1.53 of the host materials were used, but due to the close proximity of the solvent to the lanthanide ion, the refractive index of the solvent cannot be ignored. A relation between the luminescence lifetime of  $\text{Y}_2\text{O}_3:\text{Eu}$  nanoparticles and the refractive index of the surrounding medium was reported before.<sup>22</sup> The obtained lifetimes are also longer than the lifetimes measured for bulk materials<sup>19,23,24</sup> These measured lifetimes were 6.7 ms, 0.35 ms, and 3.2 ms for  $\text{LaF}_3$ ,  $\text{YVO}_4$ , and  $\text{LaPO}_4$ , respectively. Comparison with the lifetimes of the bulk materials indicates a high quantum yield for the nanoparticles and therefore a good shielding of the lanthanide ion from the organic environment.

### 3.2.2 Strongly visible-emitting ions $\text{Tb}^{3+}$ , $\text{Dy}^{3+}$ , and $\text{Sm}^{3+}$

Other lanthanide ions that generally show strong emission in the visible are  $\text{Tb}^{3+}$ ,  $\text{Dy}^{3+}$ , and  $\text{Sm}^{3+}$ . The emission and excitation spectra of nanoparticles doped with these ions are shown in Figure 3.7. Emission spectra recorded for  $\text{LaVO}_4$  nanoparticles are all taken by excitation in the  $\text{VO}_4$  charge transfer band at a low nanoparticle concentration. The excitation spectra all show the broad vanadate absorption band and due to the low concentration the absorption peaks of the lanthanide ions were not observed.

The  $\text{Tb}^{3+}$  ion does not show emission in the  $\text{LaVO}_4$  nanoparticles. The excitation occurs through the charge transfer band of the  $\text{VO}_4$  groups, but due to the low oxidation potential of  $\text{Tb}^{3+}$ , the ion can be oxidized to  $\text{Tb}^{4+}$ , which does not show emission.<sup>25</sup> In the emission spectra very little differences can be observed between the other two nanoparticles of  $\text{LaF}_3$  and  $\text{LaPO}_4$ . Four emission peaks are observed of the  $^5\text{D}_4 \rightarrow ^7\text{F}_J$  ( $J = 3 - 6$ ) transitions after excitation at 380 nm. The positions of the major peaks are the same, because of the good shielding of the  $4f$

electrons from the environment. Small differences can occur in the peak splitting and the intensity ratio between the peaks.

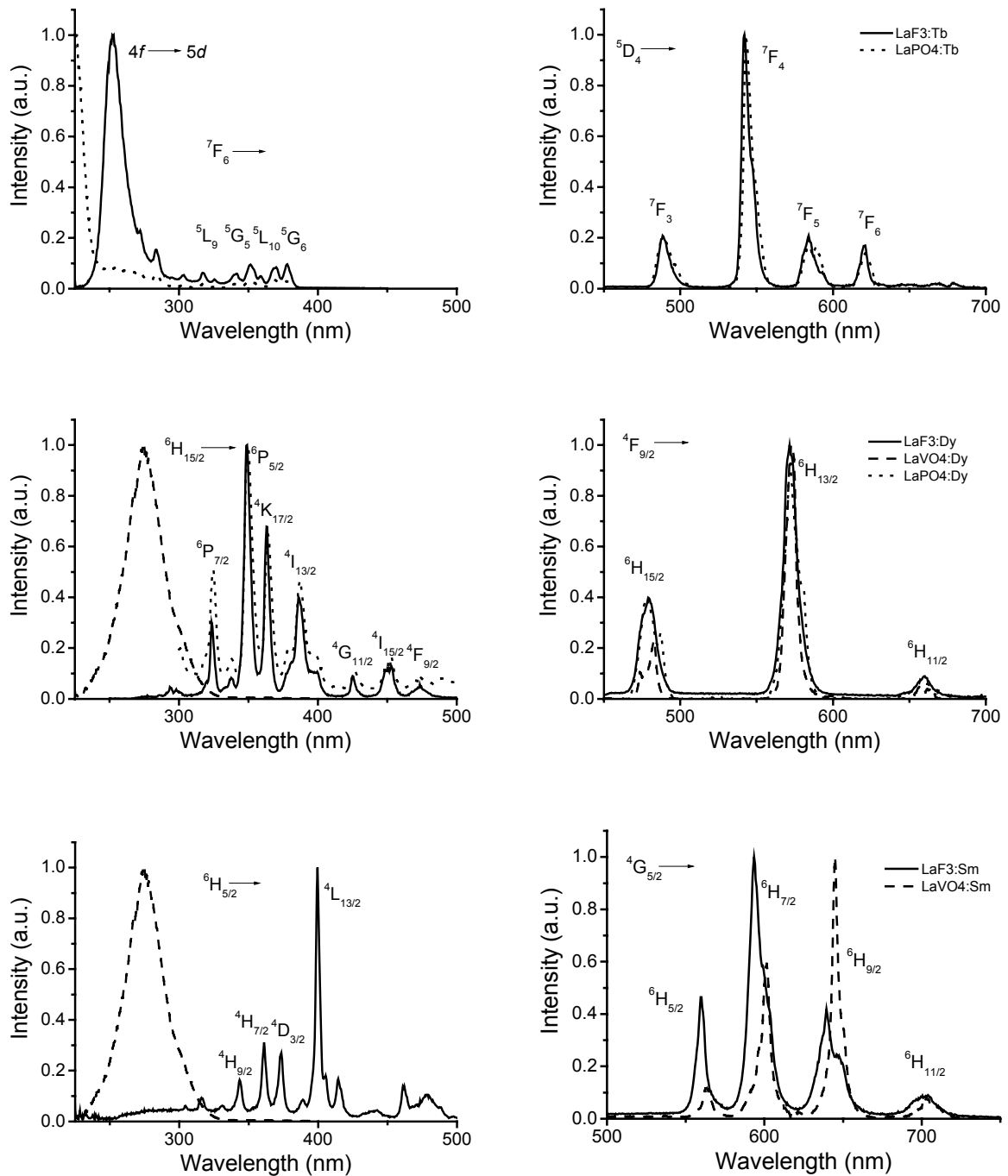


Figure 3.7: Excitation (left) and emission (right) spectra of Tb<sup>3+</sup> (top), Dy<sup>3+</sup> (middle), and Sm<sup>3+</sup> (down) in the three nanoparticle hosts. The LaF<sub>3</sub> and LaVO<sub>4</sub> nanoparticles were in dichloromethane solution and the LaPO<sub>4</sub> nanoparticles in methanol.

These small differences are a result of the difference in symmetry of the doping site. In the excitation spectrum monitoring the emission at 545 nm, the 4f absorption bands are clearly

visible, together with the allowed  $4f-5d$  absorption. In both host materials the  $4f-5d$  absorption band is visible, but in the  $\text{LaF}_3$  nanoparticles it is found at lower energy.  $\text{Dy}^{3+}$  shows three emission bands in the visible from the  $^4\text{F}_{9/2}$  level to the  $^6\text{H}_{15/2}$  (475 nm),  $^6\text{H}_{13/2}$  (570 nm), and the  $^6\text{H}_{11/2}$  (655 nm) levels, after excitation at 352 nm. In the  $\text{LaVO}_4$  nanoparticles the emissions at 475 and 655 nm are less strong than in the other two nanoparticles, due to the lack of inversion symmetry in this host material. The emission spectra in the  $\text{LaF}_3$  and  $\text{LaPO}_4$  host are very similar. The excitation spectra of the doped  $\text{LaF}_3$  and  $\text{LaPO}_4$  nanoparticles show the typical  $4f$  absorption bands of the  $\text{Dy}^{3+}$  ion, monitoring the emission at 572 nm. The charge transfer band of the  $\text{VO}_4$  group is observed in the excitation spectrum for the  $\text{LaVO}_4$  nanoparticles.

$\text{Sm}^{3+}$ -doped nanoparticles of  $\text{LaF}_3$  and  $\text{LaVO}_4$  show the typical emission from the  $^4\text{G}_{5/2}$  level to the  $^6\text{H}_{5/2}$  (560 nm),  $^6\text{H}_{7/2}$  (590 nm),  $^6\text{H}_{9/2}$  (640 nm), and  $^6\text{H}_{11/2}$  (700 nm) after excitation at 400 nm and 280 nm respectively. The difference in symmetry of the doping ion is clearly visible again because the strongest emission band is different for the two materials. The excitation spectrum of  $\text{LaF}_3:\text{Sm}$  nanoparticles is similar to the absorption spectrum of the  $\text{Sm}^{3+}$  ion and for the  $\text{LaVO}_4$  nanoparticles the charge transfer band of the  $\text{VO}_4$  groups is observed. Results for the  $\text{LaPO}_4$  nanoparticles are not shown, because no hydrated  $\text{SmCl}_3$  was available and the anhydrous  $\text{SmCl}_3$  reacts with methanol to form insoluble products. It is, however, likely that  $\text{LaPO}_4:\text{Sm}$  nanoparticles can be formed and that the luminescence is very similar to the luminescence of the  $\text{LaF}_3:\text{Sm}$  nanoparticles.

### 3.2.3 Weakly visible-emitting ions $\text{Pr}^{3+}$ , $\text{Tm}^{3+}$ , and $\text{Ho}^{3+}$

Lanthanide ions that generally show weak emission (if emission is observed at all) in the visible are  $\text{Pr}^{3+}$ ,  $\text{Tm}^{3+}$ , and  $\text{Ho}^{3+}$ . The emission and excitation spectra of nanoparticles doped with these ions are shown in Figure 3.8.

A few reports on the luminescence of  $\text{Pr}^{3+}$  in the visible from organic complexes have appeared.<sup>26</sup> Visible luminescence of the  $\text{Pr}^{3+}$  ion is observed from all three nanoparticles after excitation at 443 nm for the  $\text{LaF}_3$  and  $\text{LaPO}_4$  nanoparticles and at 280 nm for the  $\text{LaVO}_4$  nanoparticles. The luminescence is attributed to emission from the  $^3\text{P}_0$  and  $^1\text{D}_2$  level.

$\text{Tm}^{3+}$  luminescence has been reported for a number of organic complexes.<sup>27</sup>  $\text{Tm}^{3+}$  emission was only observed in the doped  $\text{LaVO}_4$  nanoparticles, probably because the excitation in the other two host materials is not effective. The  $\text{Tm}^{3+}$  ion does have a weak absorption band around 350 nm, but after excitation in this band no luminescence was observed for the doped  $\text{LaF}_3$  and  $\text{LaPO}_4$  nanoparticles. Luminescence occurs from the  $^1\text{G}_4$  level at 475 nm, and 650 nm from transitions to the  $^3\text{H}_6$ ,  $^3\text{H}_4$  levels, respectively and from the  $^3\text{F}_4 \rightarrow ^3\text{H}_6$  transition at 790 nm, after

excitation in the broad absorption band of the LaVO<sub>4</sub>:Tm nanoparticles. Recently, the up-converted emission of Tm<sup>3+</sup>-doped nanoparticles of LuPO<sub>4</sub> co-doped with Yb<sup>3+</sup> was reported.<sup>28</sup> In these nanoparticles the excitation was done through the strong absorption peak of the Yb<sup>3+</sup> ion at 980 nm and with an up-conversion scheme, emission of Tm<sup>3+</sup> was observed in the visible.

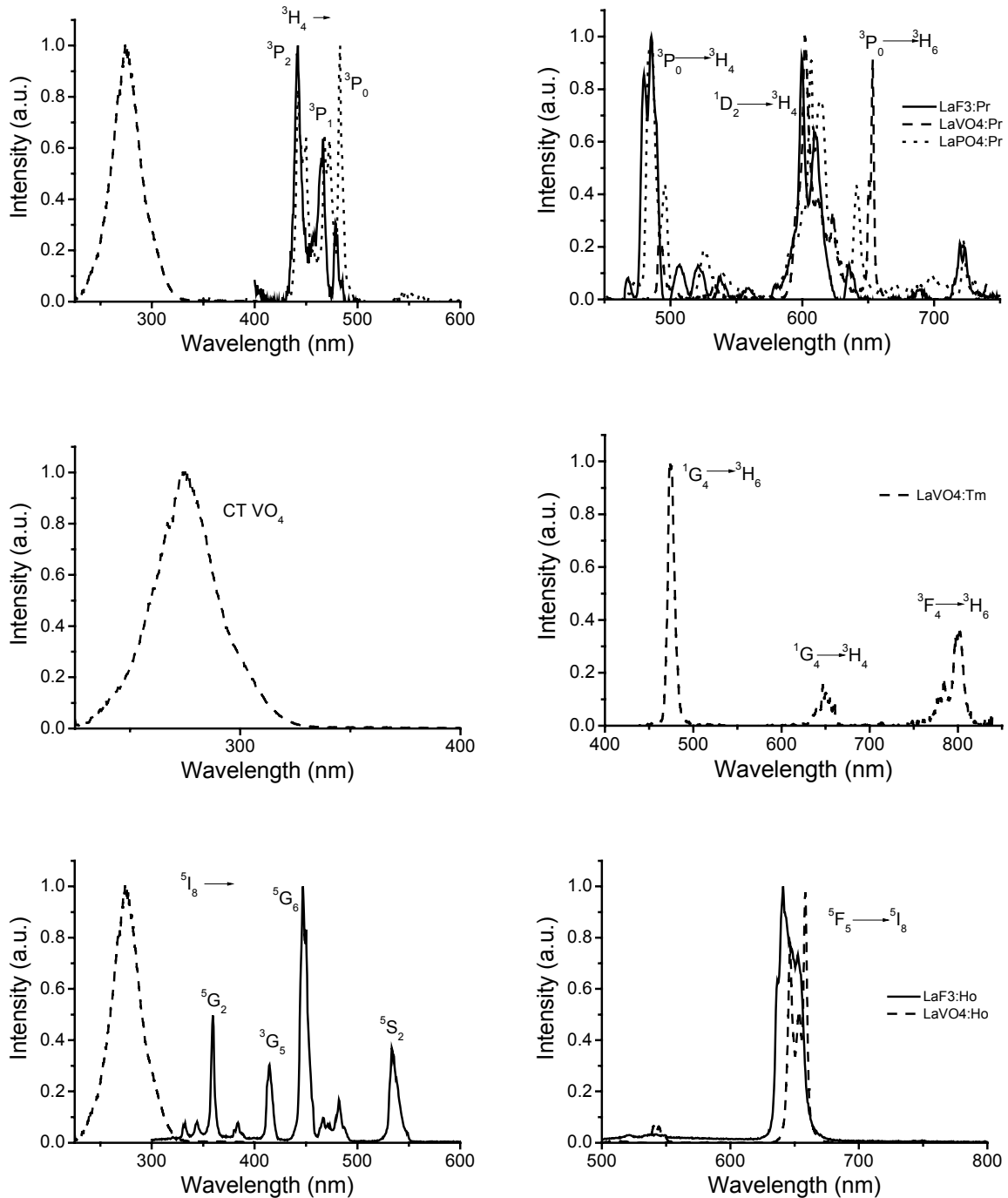


Figure 3.8: Excitation (left) and emission (right) spectra of Pr<sup>3+</sup> (top), Tm<sup>3+</sup> (middle), and Ho<sup>3+</sup> (bottom) in the nanoparticles.

This result shows that with an effective excitation it is probably also possible to observe luminescence from the LaF<sub>3</sub> and LaPO<sub>4</sub> nanoparticles doped with Tm<sup>3+</sup>. Ho<sup>3+</sup> luminescence has not been reported in organic environment. In glasses emission can be observed from different levels and in the visible the emission of the <sup>5</sup>S<sub>2</sub>→<sup>5</sup>I<sub>8</sub> transition usually dominates.<sup>29</sup> Ho<sup>3+</sup> luminescence was observed from the <sup>5</sup>F<sub>5</sub>→<sup>5</sup>I<sub>8</sub> transition at 640 nm in our nanoparticles of LaF<sub>3</sub> and LaVO<sub>4</sub>. Only very weak emission from the <sup>5</sup>S<sub>2</sub> level was observed. The gap between the <sup>5</sup>S<sub>2</sub> level and the <sup>5</sup>F<sub>5</sub> level is only 3000 cm<sup>-1</sup>, which is resonant with the vibrational energy of a CH bond. The presence of CH bonds at the outside of the nanoparticles might lead to an effective non-radiative decay of the <sup>5</sup>S<sub>2</sub> level to the <sup>5</sup>F<sub>5</sub> level leading to a dominating luminescence of the <sup>5</sup>F<sub>5</sub> level. The effective shielding of the luminescent lanthanide ion is, however, demonstrated, because for the first time Ho<sup>3+</sup> luminescence is reported in organic media.

#### 3.2.4 Determination of the quantum yield

Quantum yields of luminescent materials in solution are generally determined by comparing the emission intensity of the solution with the emission intensity of a dye with a known quantum yield. For these quantum yield determinations the absorption of the solution has to be known precisely to correct for the amount of photons absorbed. Due to the low absorption coefficients of the 4f bands of the lanthanide ions a precise measurement of the absorption is virtually impossible. The absorption can be measured accurately when the excitation can be done indirectly using a sensitizer with a high absorption coefficient. The Ce<sup>3+</sup>, Tb<sup>3+</sup> lanthanide couple offers the possibility to determine a quantum yield of the nanoparticles. Ce<sup>3+</sup> has a strong absorption band in the UV of an allowed 4f-5d transition and the Ce<sup>3+</sup> ion can transfer its energy efficiently to the Tb<sup>3+</sup> ion leading to emission in the green. La<sub>0.4</sub>PO<sub>4</sub>:Ce<sub>0.45</sub>,Tb<sub>0.15</sub> is a well known phosphor, that is being applied in fluorescent lamps.<sup>30</sup> From solutions of LaPO<sub>4</sub>:Ce,Tb and LaF<sub>3</sub>:Ce,Tb nanoparticles, with the same lanthanide ion distribution, it is possible to determine the quantum yield by comparing the emission intensity with the emission intensity of quinine bisulfate in 1M H<sub>2</sub>SO<sub>4</sub>. The measured quantum yields were 12 % and 25 % for the LaPO<sub>4</sub> and LaF<sub>3</sub> nanoparticles respectively, including the emission of Ce<sup>3+</sup>. The value found for the LaPO<sub>4</sub> nanoparticles is lower than the value found by Haase *et al.*<sup>7</sup> This can for a part be explained because we used a different dye for comparison. Haase *et al.* used Rhodamine 6G in ethanol for comparison, but this dye is not well suited for excitation in the UV, because it has a very low absorption coefficient in the UV.<sup>31</sup> The quantum yield of the LaF<sub>3</sub>:Ce,Tb can be increased by the addition of a few drops of D<sub>2</sub>O to the dichloromethane solution. The quantum yield increased to



48 % proving that the coordination of a small amount of water to the surface of the nanoparticles plays a role in deactivation of the excited state of the lanthanide ion. The addition of D<sub>2</sub>O to the solution replaces the OH bonds of the coordinating water with OD bonds. OH bonds are stronger quenchers of lanthanide luminescence than OD bonds, so the addition of D<sub>2</sub>O leads to an increase in quantum yield.

The LaVO<sub>4</sub> nanoparticles show a strong absorption band of the VO<sub>4</sub> group and thus quantum yields of these lanthanide-doped nanoparticles could be determined. The quantum yield of these nanoparticles was determined for the Eu<sup>3+</sup> ion with different doping concentrations.

*Table 3.2: Quantum yield of LaVO<sub>4</sub>:Eu nanoparticles with different concentrations of Eu<sup>3+</sup>.*

Eu <sup>3+</sup> content (%)	Q.Y. (%)
5	3.4
10	5.6
15	7.0

The quantum yield shows an increase from 3.4 % for the 5 % doped nanoparticles to 7.0 % for the 15 % doped nanoparticles. The optimum Eu<sup>3+</sup> concentration for bulk YVO<sub>4</sub> is 5 %. An optimum in the doping concentration is observed in this material, because at increasing Eu<sup>3+</sup> concentration more and more excitation energy from the vanadate groups is captured leading to an increased quantum yield for Eu<sup>3+</sup>. This effect is countered by concentration quenching of the Eu<sup>3+</sup> luminescence, leading to an optimum doping concentration. In our LaVO<sub>4</sub> nanoparticles the optimum Eu<sup>3+</sup> content is higher than 5 %, which is likely a result of increased quenching of the vanadate groups at the surface.<sup>32</sup> For YVO<sub>4</sub> nanoparticles in water, it was shown that a surface modification not only decreases quenching of the Eu<sup>3+</sup> luminescence, but also decreases the optimum doping concentration from 15 to 5 %. Quenching at the surface can occur because of the coordination of water to the nanoparticles surface or because of the existence of V-OH bonds. The other lanthanide ions doped in the LaVO<sub>4</sub> host have quantum yields well below 1 %.

### 3.2.5 Near-infrared emitting ions

The nanoparticles of LaF<sub>3</sub>, LaVO<sub>4</sub>, and LaPO<sub>4</sub> were also doped with the NIR-emitting ions Nd<sup>3+</sup> and Er<sup>3+</sup>. Luminescence spectra of these ions are shown in Figure 3.9. The luminescence spectra of Nd<sup>3+</sup> in the three nanoparticles show the typical emission at 880, 1060, and 1330 of the <sup>4</sup>F<sub>3/2</sub>→<sup>4</sup>I<sub>13/2</sub>, <sup>4</sup>F<sub>3/2</sub>→<sup>4</sup>I<sub>11/2</sub> and <sup>4</sup>F<sub>3/2</sub>→<sup>4</sup>I<sub>9/2</sub> transitions, respectively. The emission spectrum

measured for LaF<sub>3</sub>:Nd looks very similar to the spectrum measured in a Nd<sup>3+</sup>-doped LaF<sub>3</sub> thin film.<sup>33</sup> The emissions are almost the same for the three nanoparticles, showing only slightly different splittings of the emission peaks, indicative of a different symmetry around the luminescent ion, like found for the Eu<sup>3+</sup> ion. However, the differences in the luminescence spectra are smaller than for Eu<sup>3+</sup>, because Eu<sup>3+</sup> is much more sensitive to the symmetry of the crystal site than the other lanthanide ions.<sup>34</sup> The excitation spectra of the LaF<sub>3</sub> and LaPO<sub>4</sub> nanoparticles also look very similar and are comparable with the absorption lines of the Nd<sup>3+</sup> ion in solution.<sup>35</sup> The wavelength positions of the peaks do not change; only the peak splitting and the ratio between peak intensities differ. The excitation spectrum of the LaVO<sub>4</sub> nanoparticles shows the broad absorption band of the VO<sub>4</sub> charge transfer.

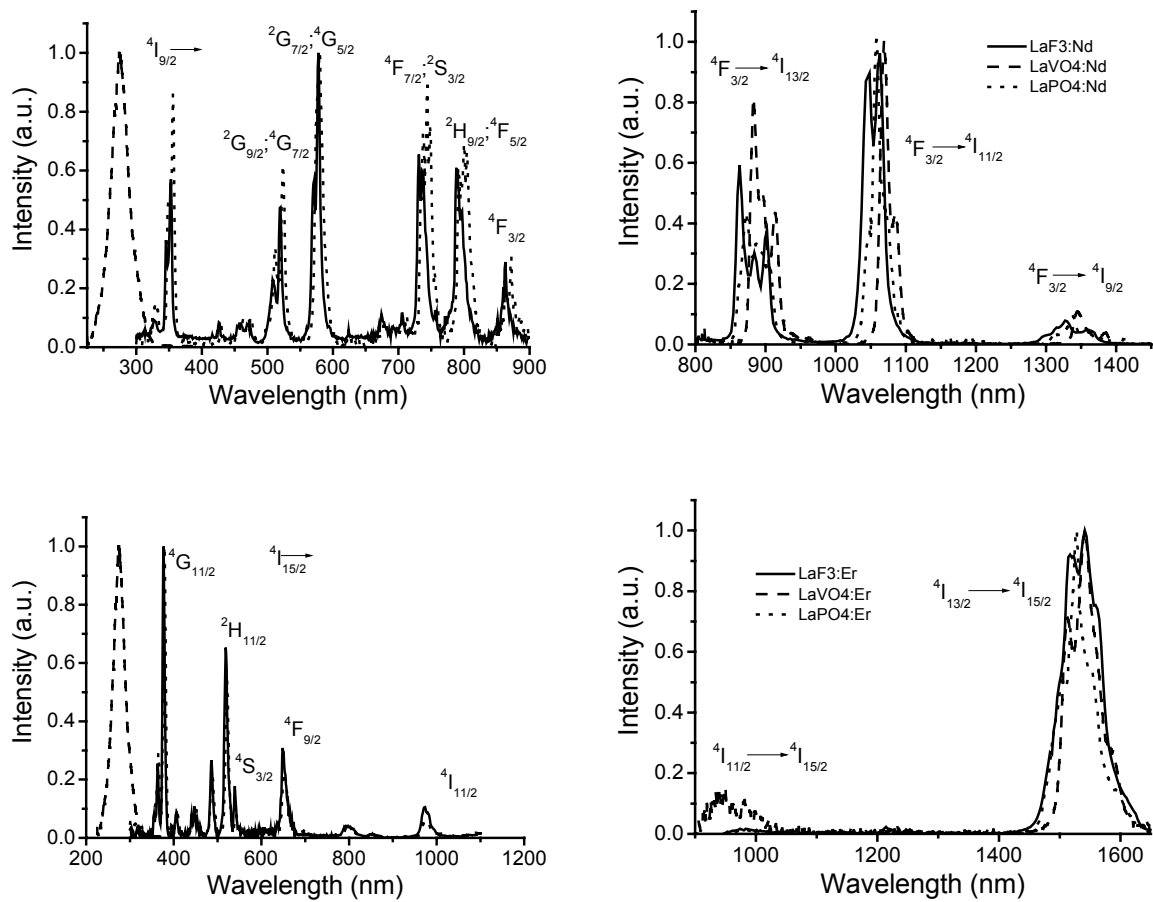


Figure 3.9: Near-infrared excitation (left) and emission (right) spectra of Nd<sup>3+</sup>- and Er<sup>3+</sup>-doped nanoparticles.

Er<sup>3+</sup>-doped materials show typical luminescence at 1530 nm of the  $4I_{13/2} \rightarrow 4I_{15/2}$  transition in the three nanoparticles with a small difference in the shape and the width of the emission peak

caused by a difference in crystal symmetry. The emission of the LaF<sub>3</sub>:Er nanoparticles again looks very similar to the emission spectrum of an Er<sup>3+</sup>-doped LaF<sub>3</sub> thin film.<sup>36</sup> A small emission is observed at 980 nm in the LaVO<sub>4</sub> and LaPO<sub>4</sub> hosts of the <sup>4</sup>I<sub>11/2</sub>→<sup>4</sup>I<sub>15/2</sub> transition, which is not visible in the LaF<sub>3</sub> host, probably because of symmetry reasons. The excitation spectra are very similar again for the LaF<sub>3</sub> and LaPO<sub>4</sub> nanoparticles, showing small differences in peak intensities caused by symmetry differences. The excitation spectrum of the LaVO<sub>4</sub> nanoparticles shows the charge transfer band of the VO<sub>4</sub> groups. The emission spectra of both these ions are very similar to the bulk material, showing the similar symmetry around the lanthanide ions in these materials.

Pr<sup>3+</sup> and Ho<sup>3+</sup> ions are also known to emit in the NIR in bulk materials. Nanoparticles doped with these lanthanide ions were prepared and the emission and excitation spectra are shown in Figure 3.10. Luminescence of the Pr<sup>3+</sup> ion can originate from different levels depending on the crystal field and on the quenching mechanisms.<sup>37</sup>

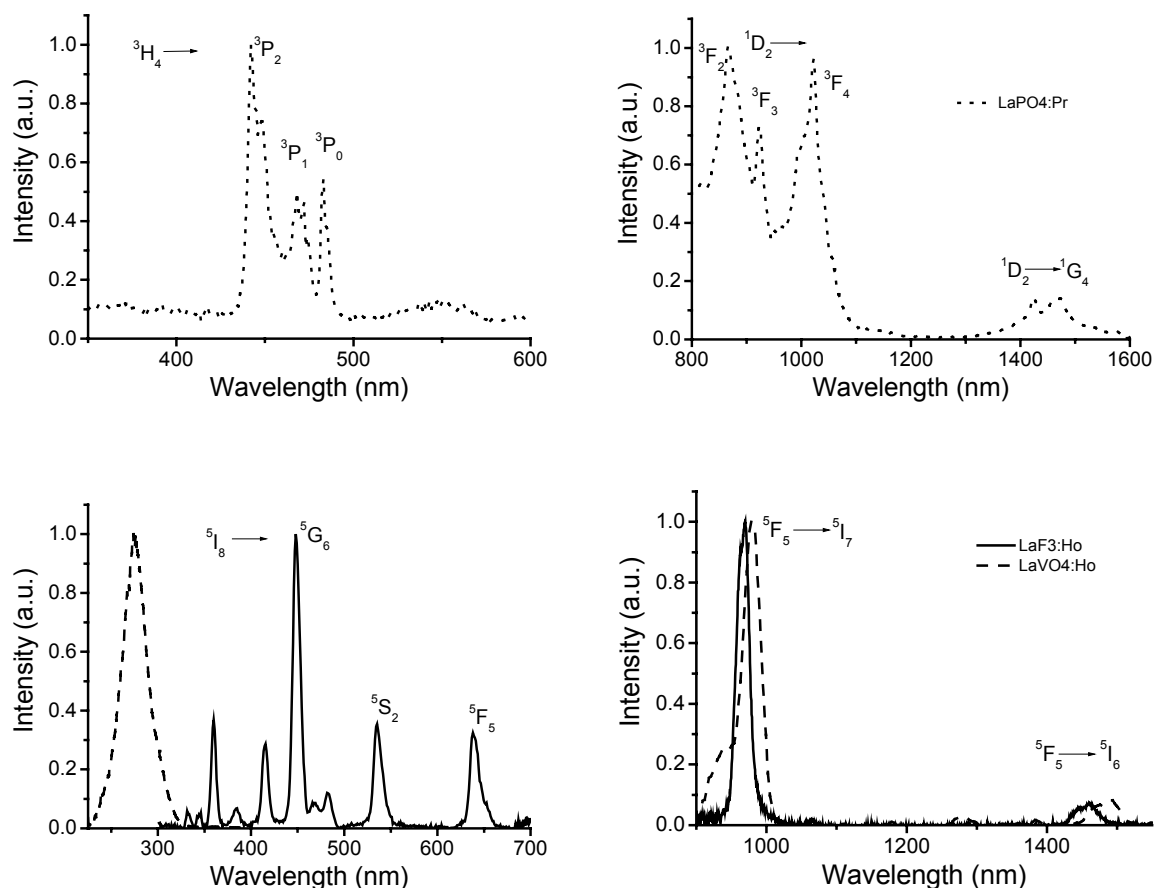


Figure 3.10: Near-infrared excitation (left) and emission (right) spectra of Pr<sup>3+</sup>- ( $\lambda_{em}$ . 1030 nm,  $\lambda_{ex}$ . 476 nm) and Ho<sup>3+</sup>- ( $\lambda_{em}$ . 966 nm,  $\lambda_{ex}$ . 450 nm) doped nanoparticles.

Luminescence originating from the  $^1D_2$  level was observed in  $\text{LaPO}_4:\text{Pr}$  nanoparticles by excitation with the 476 nm line of an  $\text{Ar}^+$  laser. The absence of emission from the  $^1G_4 \rightarrow ^3H_5$  transition at 1300 nm indicates that non-radiative processes dominate for this level, similar to the electroluminescence that was observed of an organic complex.<sup>38</sup> When the  $\text{LaF}_3:\text{Pr}$  nanoparticles were excited using the same laser line, no emission was observed, although it is known that the  $\text{Pr}^{3+}$  ion can emit very efficiently in this host matrix.<sup>39</sup> It is possible that  $\text{Pr}^{3+}$  does not absorb at this wavelength in the  $\text{LaF}_3$  host or that the  $\text{Pr}^{3+}$  ion is very sensitive to the small amount of water present at the surface of the  $\text{LaF}_3$ . Under excitation with an Xe arc lamp at 443 nm, the emission of  $\text{LaPO}_4:\text{Pr}$  could also be detected, but only weak emission was observed for  $\text{LaF}_3:\text{Pr}$  nanoparticles.

Emission of the  $\text{Ho}^{3+}$  ion could be detected in the  $\text{LaF}_3:\text{Ho}$  and  $\text{LaVO}_4:\text{Ho}$  nanoparticles at 960 and 1460 nm from the  $^5F_5 \rightarrow ^5I_7$  and  $^5F_5 \rightarrow ^5I_6$  transitions. The emission of the  $\text{LaVO}_4:\text{Ho}$  nanoparticles was substantially weaker than for the  $\text{LaF}_3:\text{Ho}$  nanoparticles, which could be a result of the higher phonon energies of the host material. The  $\text{LaPO}_4:\text{Ho}$  nanoparticles did not show any luminescence at all, probably due to the high phonon energies.  $\text{Ho}^{3+}$  emission was also not detected in bulk  $\text{YPO}_4$  indicating that the high-energy phonons of the lattice prevent emission in this host material.<sup>40</sup> NIR emission of  $\text{Ho}^{3+}$  in an organic environment has not been reported till now and for  $\text{Pr}^{3+}$  the reports are limited, proving the good shielding against the organic groups when they are doped in the nanoparticles. The spectral window between 1300-1600 nm, which is of interest to telecommunication purposes, can be covered completely with the emissions of these NIR-emitting lanthanide ions.

**Yb<sup>3+</sup> co-doping.** The  $\text{Yb}^{3+}$  ion is often used as a sensitizer for  $\text{Er}^{3+}$  emission, because of a higher absorption coefficient and an efficient energy transfer to the  $\text{Er}^{3+}$  ion. The  $\text{Yb}^{3+}$  ion has only one excited state  $4f$  level and it can be excited over a broad range from 940-1000 nm with a peak at 980 nm. The  $\text{LaVO}_4$  nanoparticles offer the possibility for excitation in the UV because of the charge transfer band of the  $\text{VO}_4$  group, but also the  $\text{LaPO}_4$  nanoparticles offer the possibility to excite the  $\text{Yb}^{3+}$  ion in the UV. The  $\text{Yb}^{3+}$  ion has a low reduction potential similar to the  $\text{Eu}^{3+}$  ion and in the  $\text{LaPO}_4$  nanoparticles this gives rise to a charge transfer band peaking at 250 nm. The emission and excitation spectra of  $\text{LaPO}_4:\text{Yb}$  nanoparticles in methanol- $d_4$  are shown in Figure 3.11.

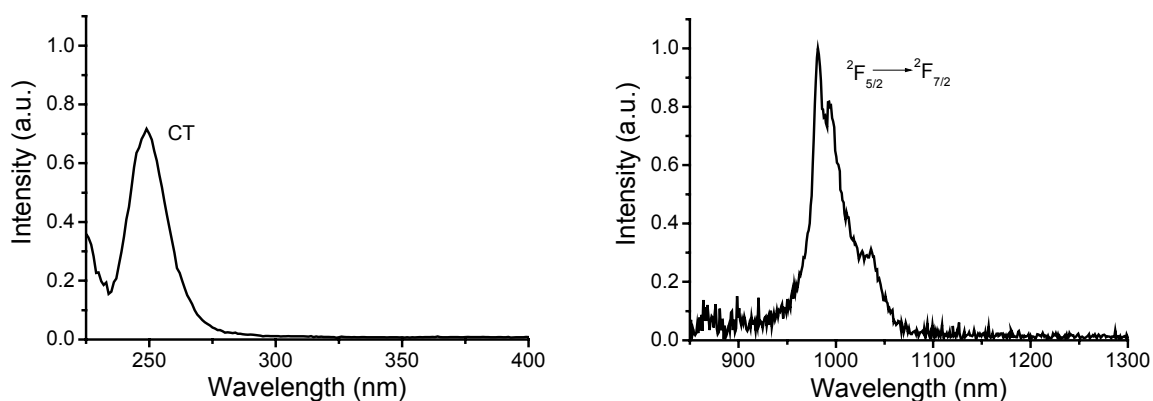


Figure 3.11: Excitation (left) and emission (right) spectra of LaPO<sub>4</sub>:Yb nanoparticles in methanol-d<sub>4</sub>.

The charge transfer band of Yb<sup>3+</sup> is somewhat blue shifted compared to the charge transfer band of Eu<sup>3+</sup> in LaPO<sub>4</sub>, reflecting the higher reduction potential of Yb<sup>3+</sup>.<sup>40</sup> In the emission spectrum the typical emission of the <sup>2</sup>F<sub>5/2</sub>→<sup>2</sup>F<sub>7/2</sub> transition peaking at 980 nm is observed. Yb<sup>3+</sup> can be used as a sensitizer for Er<sup>3+</sup> emission, increasing the effective absorption of Er<sup>3+</sup>. Energy transfer between Yb<sup>3+</sup> and Er<sup>3+</sup> is also observed in the nanoparticles. The emission and excitation spectra of LaPO<sub>4</sub> nanoparticles co-doped with Yb<sup>3+</sup> and Er<sup>3+</sup> both at 5 % are shown in Figure 3.12. The absorption lines of Er<sup>3+</sup> and a broad band with a maximum at 250 nm are visible in the excitation spectrum, when monitoring the Er<sup>3+</sup> emission at 1530 nm. The presence of this broad band is caused by charge transfer excitation of Yb<sup>3+</sup> followed by energy transfer to Er<sup>3+</sup>. When the sample was excited in the broad band at 250 nm, emission at 980 nm from Yb<sup>3+</sup> and at 1530 nm from Er<sup>3+</sup> was observed. The appearance of Yb<sup>3+</sup> emission means that energy transfer is not complete. The direct excitation of Er<sup>3+</sup> at 378 nm leads to Er<sup>3+</sup> emission at 1530 nm as expected, but also Yb<sup>3+</sup> emission at 980 nm is observed, showing that energy transfer from Er<sup>3+</sup> to Yb<sup>3+</sup> also occurs. This reverse process needs phonon energy from the surroundings because the <sup>4</sup>I<sub>11/2</sub> energy level of Er<sup>3+</sup> is slightly lower in energy than the <sup>2</sup>F<sub>5/2</sub> level of Yb<sup>3+</sup>. In LaF<sub>3</sub> nanoparticles energy transfer between Yb<sup>3+</sup> and Er<sup>3+</sup> is also observed after direct excitation of Yb<sup>3+</sup> into the <sup>2</sup>F<sub>5/2</sub> level around 980 nm. In this matrix no charge transfer band is observed, for the same reason as for the Eu<sup>3+</sup> ion. Nanoparticles of LaF<sub>3</sub> co-doped with various amounts of Yb<sup>3+</sup> and 5 % Er<sup>3+</sup> were synthesized and the luminescence properties were determined in order to optimize the energy transfer.

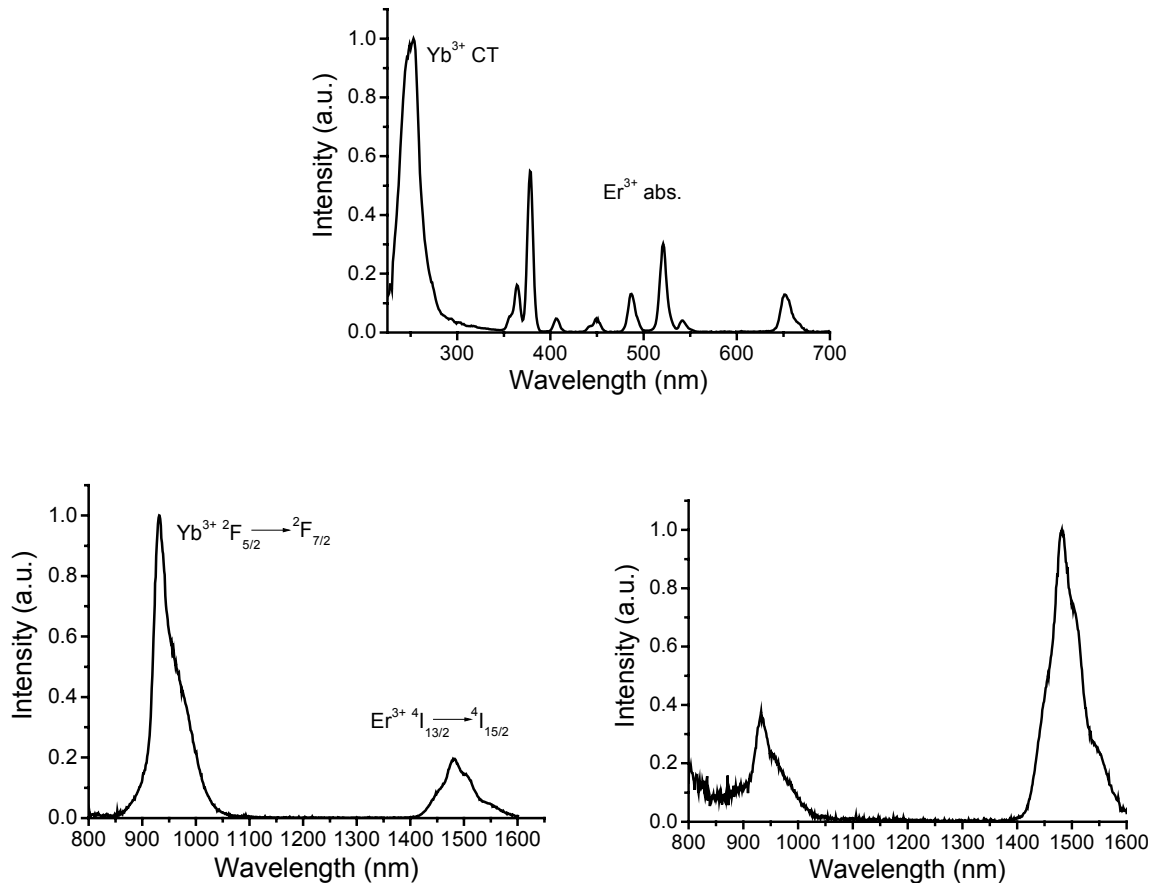


Figure 3.12: Excitation (up:  $\lambda_{em}$  1530 nm) and emission (left:  $\lambda_{ex}$  250 nm, right:  $\lambda_{ex}$  378 nm) spectra of  $\text{LaPO}_4:\text{Yb, Er}$  in methanol.

The emission spectra of  $\text{LaF}_3$  nanoparticles doped with a varying concentration of  $\text{Yb}^{3+}$  and 5 %  $\text{Er}^{3+}$  excited at 940 nm are shown in Figure 3.13. The emission spectra are normalized to the  $\text{Yb}^{3+}$  emission. Excitation at 940 nm was chosen because  $\text{Er}^{3+}$  has no absorption at this wavelength, so all emission from  $\text{Er}^{3+}$  is formed through sensitized emission by  $\text{Yb}^{3+}$ .  $\text{Er}^{3+}$  emission is clearly observed at 1530 nm, proving the energy transfer between the ions. The  $\text{Yb}^{3+}$  emission at 980 nm is still dominating, so energy transfer is not complete. By increasing the concentration of  $\text{Yb}^{3+}$  the relative  $\text{Er}^{3+}$  emission increases, so the energy transfer becomes more efficient up to a doping concentration of 20 %  $\text{Yb}^{3+}$  where the maximum energy transfer is reached. Increasing the concentration of  $\text{Yb}^{3+}$  above 25 % does not increase the energy transfer further.

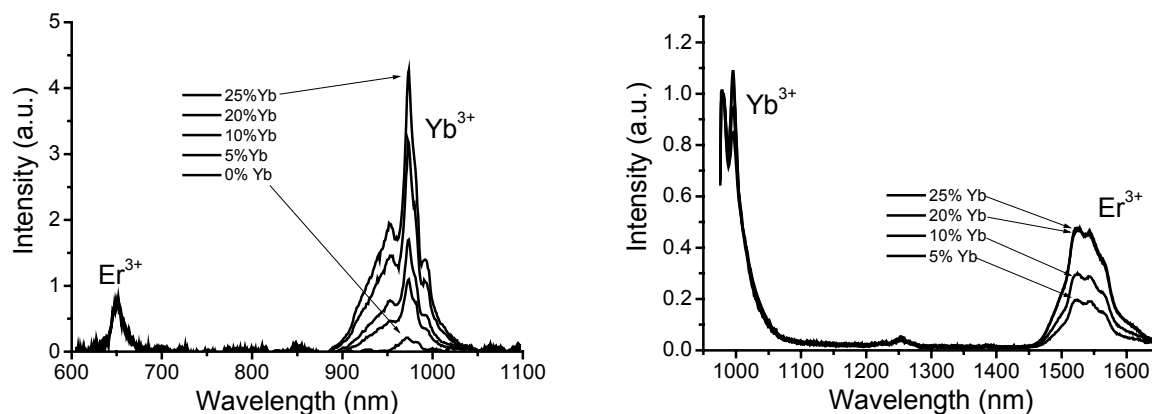


Figure 3.13: Excitation (left) and emission (right) spectra of  $\text{LaF}_3:\text{Yb}, \text{Er}$  with varying concentrations of  $\text{Yb}^{3+}$ . The excitation spectra are scaled to the  $\text{Er}^{3+}$  absorption band at 650 nm and the emission spectra to the  $\text{Yb}^{3+}$  emission at 980 nm.

At increasing  $\text{Yb}^{3+}$  concentration the energy transfer becomes more efficient because the average distance between the ions decreases. It levels off when all the  $\text{Er}^{3+}$  ions have at least one  $\text{Yb}^{3+}$  ion as the nearest neighbor.<sup>41</sup> The excitation spectra of  $\text{Er}^{3+}$  luminescence at 1530 nm for samples doped with different concentrations of  $\text{Yb}^{3+}$  are also shown in Figure 3.13. The excitation spectra are scaled to the  $\text{Er}^{3+}$  absorption peak at 650 nm, because the concentration of  $\text{Er}^{3+}$  in the sample is constant. It can be seen that the excitation peak of  $\text{Er}^{3+}$  in the sample *without*  $\text{Yb}^{3+}$  around 980 nm is very low and that co-doping with  $\text{Yb}^{3+}$  increases it. Increasing the concentration of  $\text{Yb}^{3+}$  leads to a linear increase of the  $\text{Yb}^{3+}$  peak compared to the  $\text{Er}^{3+}$  peak, because more energy is absorbed by  $\text{Yb}^{3+}$  ions. It was reported in the literature that energy transfer from  $\text{Yb}^{3+}$  to  $\text{Er}^{3+}$  in  $\text{Y}_2\text{O}_2\text{S}$  nanoparticles is less efficient than in bulk material, because of the absence of low energy phonons.<sup>42</sup> These low energy phonons are required to take up the small energy released when the excitation energy is transferred from  $\text{Yb}^{3+}$  to  $\text{Er}^{3+}$ . In the present case, in which the nanoparticles are capped with organic molecules these low energy phonons are present in the form of vibrational and rotational energies, thus facilitating a more efficient energy transfer. The amount of energy that is actually transferred from  $\text{Yb}^{3+}$  to  $\text{Er}^{3+}$  is difficult to estimate from the emission spectrum, because the intrinsic quantum yields of both ions are different and difficult to estimate.

**Luminescence lifetimes of NIR-emitting ions.** Decays of the NIR-emitting ions were fitted using a bi-exponential decay or in one case a mono-exponential decay. The results of the  $\text{LaF}_3$  and  $\text{LaPO}_4$  nanoparticles are summarized in Table 3.3.

Table 3.3: Luminescence lifetimes of  $\text{Nd}^{3+}$ ,  $\text{Er}^{3+}$ ,  $\text{Ho}^{3+}$ , and  $\text{Pr}^{3+}$  in  $\text{LaF}_3$  and  $\text{LaPO}_4$  nanoparticles.

Host material	Ion <sup>a</sup>	$\tau_1$ ( $\mu\text{s}$ )	$\tau_2$ ( $\mu\text{s}$ )	$\lambda_{\text{ex}}/\lambda_{\text{em}}$
$\text{LaF}_3$	$\text{Nd}^{3+}$	240 (77 %)	40 (23 %)	514/880
	$\text{Er}^{3+}$ b	220		488/1536
	$\text{Ho}^{3+}$	340 (6 %)	30 (94 %)	488/966
$\text{LaPO}_4$	$\text{Nd}^{3+}$	81 (21 %)	15 (79 %)	514/880
	$\text{Er}^{3+}$	1280 (12 %)	260 (88 %)	488/1536
	$\text{Pr}^{3+}$	5.4 (29 %)	0.5 (72 %)	476/868

a)  $\text{LaF}_3$  nanoparticles were dissolved in dichloromethane and the  $\text{LaPO}_4$  nanoparticles in methanol, except the  $\text{LaPO}_4:\text{Pr}$  nanoparticles which were dissolved in methanol- $d_4$

b) Mono-exponential fit

All but one of the decays were fitted bi-exponentially, only the decay of  $\text{Er}^{3+}$  in  $\text{LaF}_3$  could be fitted with a single exponential. This might indicate a different distribution of the luminescent ion, but also that different quenching mechanisms play a role. Compared to the lifetimes obtained in organic complexes for  $\text{Nd}^{3+}$  and  $\text{Er}^{3+}$ , the luminescence lifetimes have increased substantially. In organic complexes the lifetimes of  $\text{Nd}^{3+}$  do not exceed 6  $\mu\text{s}$  for a fully deuterated or fluorinated complex.<sup>43</sup> The longest lifetime reported for  $\text{Nd}^{3+}$  in organic environment is 9  $\mu\text{s}$  for  $\text{Nd}(\text{NO}_3)_3$  in  $\text{DMSO}-d_6$ .<sup>44</sup> An increase of more than an order of magnitude is observed, indicative of the good shielding of the lanthanide ion from the quenching organic environment. The measured lifetimes for  $\text{Nd}^{3+}$  are longer in  $\text{LaF}_3$  than in  $\text{LaPO}_4$  in line with the lower phonon energy of the  $\text{LaF}_3$  host lattice. For  $\text{Er}^{3+}$ , differences in the luminescence lifetimes of both materials are less pronounced and the lifetime in  $\text{LaPO}_4$  is even slightly longer. The decay of  $\text{LaF}_3:\text{Er}$  could be fitted using a single exponential indicating that other quenching pathways are important in this material. Nevertheless, the lifetimes are two orders of magnitude longer than the lifetimes measured for  $\text{Er}^{3+}$  in organic complexes, which are in the order of several microseconds.<sup>4c</sup> A comparison with the luminescence lifetimes of  $\text{Nd}^{3+}$  and  $\text{Er}^{3+}$  in the corresponding bulk materials, leads to the conclusion that the quantum yield of  $\text{Nd}^{3+}$  is probably very high. A luminescence lifetime of  $\text{Nd}^{3+}$  in  $\text{LaF}_3$  around 600  $\mu\text{s}$  was reported in the literature.<sup>45</sup> Not taking into account the influence of the refractive index, the quantum yield of the  $\text{LaF}_3:\text{Nd}$  nanoparticles is around 30-40 %. For  $\text{Er}^{3+}$ , the lifetime of the  $^4\text{I}_{13/2}$  level of 12 ms was reported in  $\text{LaF}_3$ .<sup>46</sup> This indicates that the quantum yield of  $\text{Er}^{3+}$  in the  $\text{LaF}_3$  nanoparticles is about 2 %, substantially lower than for the  $\text{Nd}^{3+}$  ion. One reason for the lowered lifetime is



probably concentration quenching, because the  $\text{Er}^{3+}$  luminescence lifetime is strongly concentration dependent, so a decrease of the  $\text{Er}^{3+}$  concentration should lead to a substantial increase in the luminescence lifetime.

For the other two ions no data on the luminescence lifetime in organic media are available, so no comparison can be made. For bulk  $\text{LaF}_3\text{:Ho}$  a luminescence lifetime of the  $^5\text{F}_5$  level of 300  $\mu\text{s}$  was reported.<sup>47</sup> This would indicate a quantum yield for the  $\text{LaF}_3\text{:Ho}$  nanoparticles of around 10 %. For  $\text{LaPO}_4$  doped with  $\text{Pr}^{3+}$  no data could be found. Most research efforts of  $\text{Pr}^{3+}$ -doped materials focus on the  $^1\text{G}_4 \rightarrow ^3\text{H}_5$  transition of  $\text{Pr}^{3+}$  around 1300 nm. This transition requires a material with a low phonon energy, so  $\text{LaPO}_4$  is not of interest. However, in our case,  $\text{Pr}^{3+}$  shows luminescence in a high phonon lattice around 1450 nm, which could also be of interest to telecommunication purposes.

### 3.3 Conclusions

Nanoparticles of  $\text{LaF}_3$ ,  $\text{LaVO}_4$ , and  $\text{LaPO}_4$  doped with lanthanide ions show luminescence properties that are very similar to the corresponding bulk materials. Quenching of the lanthanide ions in these nanoparticles is strongly reduced compared to the same ions in organic complexes. The luminescence decay of the ions is not mono-exponential, so not all ions in the nanoparticles have the same probability of decay.

### 3.4 Experimental section

#### General

TEM images were collected on a Philips CM 30 Twin FTEM, operating at 300 kV. Samples were prepared by evaporating a drop of a diluted nanoparticle dispersion, in methanol in the case of  $\text{LaPO}_4$  and dichloromethane in the case of  $\text{LaF}_3$  and  $\text{LaVO}_4$  nanoparticles, on a carbon coated 200 mesh copper grid. Size distributions were determined by measuring the sizes of at least 100 nanoparticles from different places on the grid. Melting points were determined with a Reichert melting point apparatus and are uncorrected. Mass spectra were recorded on a Finnigan MAT 90 spectrometer using m-NBA (nitrobenzyl alcohol) as a matrix or on a Perkin Elmer/Perspective biosystems Voyager-DE-RP MALDI-TOF mass spectrometer. IR spectra were recorded with a Perkin Elmer Spectrum BX FT-IR System using KBr pellets as matrix.  $^1\text{H}$  NMR spectra were recorded with a Varian-300 spectrometer using  $\text{CDCl}_3$  as the solvent unless stated otherwise, using residual  $\text{CHCl}_3$  ( $\delta = 7.26$  ppm) as the internal standard. X-ray fluorescence was carried out on a Philips PW 1489 spectrometer using  $\text{LaF}_3$ ,  $\text{Li}_3\text{PO}_4$ ,  $\text{Eu}_2\text{O}_3$ ,  $\text{Nd}_2\text{O}_3$ ,

Er<sub>2</sub>O<sub>3</sub>, Pr<sub>6</sub>O<sub>11</sub>, and Ho<sub>2</sub>O<sub>3</sub> as the standards. Elemental analyses were performed on a Carlo Erba EA 1106 apparatus. The lanthanide salts were purchased from Aldrich or Acros in the highest purity available (at least 99.9 %). Octadecanol (99 %), Sodium fluoride (99 %), and tris(ethylhexyl)phosphate (98 %) were purchased from Fluka, phosphorous pentasulfide (99 %) from Aldrich and trioctylamine (98 %) from Acros. All chemicals were used as received without further purification. CH<sub>2</sub>Cl<sub>2</sub> and hexane were distilled from CaCl<sub>2</sub>, ethyl acetate was distilled from K<sub>2</sub>CO<sub>3</sub>.

### Compound 1

19 g (0.07 mol) Octadecanol and 4.44 g (0.02 mol) P<sub>2</sub>S<sub>5</sub> were heated at 75°C for 3 hours. The suspension was cooled to room temperature followed by the addition of 50 ml of dichloromethane. To remove inorganic salts the solution was filtered followed by evaporation of the solvent. The remaining residue was taken up in 50 ml of hexane and ammonia was bubbled through the solution. The precipitate was separated by filtration, washed with hexane, and dried; yield 13.3 g, 60 %, m.p. 103-106 °C. <sup>1</sup>H NMR (DMSO-*d*<sub>6</sub>): δ 7.2-6.9 (broad, 4H), 3.7 (dt, *J* = 8.1, 6.6 Hz, 4H), 1.5-1.4 (m, 4H), 1.35-1.1 (m, 60H), 0.84 (t, *J* = 6.2 Hz, 6H); MS (MALDI-TOF) *m/z* = 634.0 [(M-NH<sup>4+</sup>)<sup>-</sup>], calcd. for C<sub>36</sub>H<sub>74</sub>O<sub>2</sub>PS<sub>2</sub>: 633.5; Anal calcd. for C<sub>36</sub>H<sub>78</sub>NO<sub>2</sub>PS<sub>2</sub>: C, 66.31, H, 12.06, N, 2.15, S, 9.83. Found C, 66.50, H, 12.24, N, 2.27, S, 9.56.

### Compound 2

20 g (0.079 mol) Bromoundecanol, 9.6 g (0.1 mol) phenol, and 4.5 g (0.1mol) K<sub>2</sub>CO<sub>3</sub> were refluxed in 100 ml acetonitril overnight under an argon atmosphere. The reaction mixture was cooled to room temperature and 300 ml of ethylacetate was added. The organic phase was washed three times with 1 N NaOH and dried over MgSO<sub>4</sub>. The solvent was evaporated and the residue dried.

19.58 g (0.074 mol) of the alcohol obtained in the first step and 4.7 g (0.021 mol) P<sub>2</sub>S<sub>5</sub> were heated at 75 °C for 3 hours. The suspension was cooled to room temperature followed by the addition of 50 ml of dichloromethane. To remove inorganic salts the solution was filtered and the solvent evaporated. The remaining residue was taken up in 50 ml of hexane and ammonia was bubbled through the solution. The precipitate was separated by filtration, washed with hexane, and dried; yield 19.8 g, 78 % m.p. 80-82 °C. <sup>1</sup>H NMR (Acetone *d*<sub>6</sub>): δ 7.8-7.5 (broad, 4H), 7.3 (m, 4H), 6.9 (m, 6H), 4.0 (t, *J* = 6.6 Hz, 4 H), 3.9 (dt, *J* = 8.1, 6.6 Hz, 4H), 1.8 (m, 4H), 1.6 (m, 32H); MS (FAB) *m/z* = 621.1 [(M-NH<sub>4</sub><sup>+</sup>)<sup>-</sup>], calcd. for C<sub>34</sub>H<sub>54</sub>O<sub>4</sub>PS<sub>2</sub>: 621.3; Anal calcd. for C<sub>34</sub>H<sub>58</sub>NO<sub>4</sub>PS<sub>2</sub>: C, 63.81, H, 9.14, N, 2.19, S, 10.02. Found C, 63.87, H, 9.04, N, 2.23, S, 10.07.

### LaPO<sub>4</sub> nanoparticles

1 Mmol of the hydrated LnCl<sub>3</sub> (Ln = La<sup>3+</sup>, Eu<sup>3+</sup>, Nd<sup>3+</sup>, Er<sup>3+</sup> or Pr<sup>3+</sup>) was first dissolved in 10 ml of methanol followed by the addition of 6 ml of tris(ethylhexyl)phosphate and evaporation of the methanol under vacuum. The solution was heated to 70°C under vacuum to remove water and methanol. A solution

of 1 mmol orthophosphoric acid and 3 mmol trioctylamine in 3 ml of tris(ethylhexyl)phosphate was added and the reaction mixture was heated at 200°C under argon. After 40 hours the solution was cooled to room temperature and methanol was added to precipitate the nanoparticles. The nanoparticles were separated by centrifugation and washed two times with methanol. The nanoparticles were soluble in methanol by the addition of tetramethylammonium hydroxide. The nanoparticles can be precipitated by the addition of ethyl acetate and separated by centrifugation.

### **LaF<sub>3</sub> nanoparticles**

The LaF<sub>3</sub> nanoparticles were prepared by heating a solution of 0.95 mmol of compound **1** (618 mg) or compound **2** (608 mg) and 126 mg (1 mmol) NaF in 35 ml ethanol/water at 75°C. A solution of La(NO<sub>3</sub>)<sub>3</sub>·6H<sub>2</sub>O and Eu(NO<sub>3</sub>)<sub>3</sub>·6H<sub>2</sub>O (1.33 mmol total) in 2 ml of water was added dropwise and the solution was stirred at 75°C for 2 hours and then cooled to room temperature. The precipitate was separated by centrifugation and was washed subsequently with water and ethanol. The nanoparticles were further purified by dispersing in dichloromethane and precipitation by the addition of ethanol. After separation by centrifugation the nanoparticles were dried in vacuum over P<sub>2</sub>O<sub>5</sub> for two days. After drying the nanoparticles, they are soluble in apolar solvents like chloroform, dichloromethane, and toluene.

### **LaVO<sub>4</sub> nanoparticles**

These nanoparticles were synthesized as the LaF<sub>3</sub> nanoparticles but instead of NaF, Na<sub>3</sub>VO<sub>4</sub> was used.

### **Photophysical measurements**

Photoluminescence measurements in the visible were done with an Edinburgh Instruments FS/FL instrument with a 450 W Xe arc lamp for steady state measurements and for the time-resolved measurements a micro-flashlamp as the excitation source. The excitation light was fed to a monochromator (single grating, 1800 lines/mm) and focused on a square quartz cuvet (1x1 cm) containing the nanoparticle solution. The emitted visible light was fed to a second monochromator (1800 lines/mm grating) and collected on a red sensitive Peltier element cooled Hamamatsu R955 PMT. The emission spectra were corrected for the detector response and the excitation spectra were corrected for the lamp intensity. The NIR spectrum of Ho<sup>3+</sup> was measured with the same instrument using a liquid nitrogen cooled Ge detector and a monochromator equipped with a 600 lines/mm grating. The other NIR spectra were measured by exciting the samples with a CW Ar<sup>+</sup> ion laser operating at 488 nm (Er<sup>3+</sup>), 476 nm (Pr<sup>3+</sup>), and 514 nm (Nd<sup>3+</sup>). The continuous light was modulated with an acousto-optic modulator and focused on the sample in 1x1 cm quartz cuvettes. The signal was focused with a 20 cm lens on a monochromator and detected at the monochromator exit with a liquid nitrogen cooled Ge detector (Northcoast) or a PMT (AgOCS) for the spectral region between 700-1000 nm. The signal of the detector was fed to a lock-in amplifier. The spectra of the near-infrared emitting ions were measured with a resolution of 6 nm and of the visible emitting ions with a resolution of 0.9 nm. The concentration of the

nanoparticles was 50-100 mg/ml for the LaF<sub>3</sub> and LaPO<sub>4</sub> and for LaVO<sub>4</sub> the absorption was kept below 0.6 at 280 nm (~ μg/ml). The LaF<sub>3</sub> and LaVO<sub>4</sub> nanoparticles were dissolved in dichloromethane and the LaPO<sub>4</sub> nanoparticles in methanol, unless stated otherwise.

Luminescence quantum yields were determined by comparing the luminescence intensity of a nanoparticle solution with a solution of quinine bisulfate in 1M H<sub>2</sub>SO<sub>4</sub> with approximately the same absorption at the excitation wavelength. The quantum yield was calculated from Equation 3.2.

$$\phi_{\text{sample}} = \frac{n_{\text{sample}}^2 I_{\text{sample}} A_{\text{ref}}}{n_{\text{ref}}^2 I_{\text{ref}} A_{\text{sample}}} \phi_{\text{ref}} \quad (\text{Eq. 3.2})$$

in which n is the refractive index, A the absorption, and I the emission intensity and taking the quantum yield of quinine bisulfate as 54.4 %.<sup>48</sup>

### 3.5 References and notes

- <sup>1</sup> Blasse, G.; Grabmeier, B. C. *Luminescent materials*; Springer: Berlin, 1994.
- <sup>2</sup> Becker, P. C.; Olsson, N. A.; Simpson, J. R. *Erbium Doped Amplifiers: Fundamentals and Technology*; Academic Press: San Diego, 1999.
- <sup>3</sup> Reisfeld, R.; Jorgensen, C. K. *Lasers and excited states of rare earths*; Springer: Berlin, 1977.
- <sup>4</sup> A number of reports dealing with lanthanide luminescence in organic solution have been published using organic complexes. In this case the organic ligand is still close to the lanthanide ion leading to very efficient quenching by the ligand. See for example (a) Yanagida, S.; Hasegawa, Y.; Murakoshi, K.; Wada, Y.; Nakashima, N.; Yamanaka, T. *Coord. Chem. Rev.* **1998**, *171*, 461; (b) Brown, W. R.; Vos, J. G. *Coord. Chem. Rev.* **2001**, *219-221*, 761; (c) Hebbink, G. A.; Reinhoudt, D. N.; van Veggel, F. C. J. M. *Eur. J. Org. Chem.* **2001**, *21*, 4101.
- <sup>5</sup> Wakefield, G.; Holland, E.; Dobson, P. J.; Hutchison, J. L. *Adv. Mater.* **2001**, *13*, 1557.
- <sup>6</sup> Riwozki, K.; Meyssamy, H.; Kornowski, A.; Haase, M. *J. Phys. Chem. B* **2001**, *104*, 2824.
- <sup>7</sup> Riwozki, K.; Meyssamy, H.; Schnablegger, H.; Kornowski, A.; Haase, M. *Angew. Chem. Int. Ed.* **2001**, *40*, 573.
- <sup>8</sup> In current OH-free optical fibers the overtone absorption of the OH chemical bonds at 1400 nm is not present, making the entire window from 1300-1600 nm a low loss window. See for example the Allwave™ single mode-optical fiber produced by Lucent Technologies at [www.lucnet.com](http://www.lucnet.com).
- <sup>9</sup> Barber, D. B.; Pollock, C. R.; Becroft, L. L.; Ober, C. K. *Opt. Lett.* **1997**, *22*, 1247.
- <sup>10</sup> Zhou, J.; Wu, Z.; Zhang, Z.; Liu, W.; Dang, H. *Wear* **2001**, *249*, 333.

11 The ligand was changed from pyridinium di-n-tetradecylthiophosphate to ligands **1** or **2**, because  
nanoparticles stabilized with these ligands show higher solubility after drying.

12 When the stronger coordinating dialkyl phosphate ligand was used no nanoparticles were formed,  
but only the complex of the lanthanide ion with the ligand, as could be seen from the luminescence  
spectrum and the luminescence lifetime. The coordination of this ligand is apparently too strong to  
allow nanoparticle growth.

13 Scattering is dependent on the nanoparticle size and the difference in refractive index between the  
nanoparticles and the polymer. For a nanoparticle size of 10 nm, large differences in refractive  
index can be used and still scattering will be negligible.

14 Payne, S. A.; Chase, L. L.; Smith, L. K.; Kway, W. L.; Krupke, W. F. *IEEE J. Quant. Electron.*  
**1992**, *28*, 2619.

15 Weber, M. J. *Phys. Rev. B* **1967**, *10*, 2837.

16 Carnall, W. T.; Goodman, G. L.; Rajnak, K.; Rana, R. S. *J. Chem. Phys.* **1989**, *90*, 3443.

17 Riwoitzky, K.; Haase, M. *J. Phys. Chem. B* **1998**, *102*, 10129.

18 Ropp, R. C. *J. Electrochem. Soc.* **1968**, *115*, 841.

19 Crosswhite, H. M.; Moos, H. W. *Optical properties of ions in crystals*; Interscience Publishers:  
New York, 1967, p 467.

20 Fitting the luminescence decay using two exponentials assumes that there are two different sets of  
Eu<sup>3+</sup> ions present in the sample. Assuming a random distribution of the ions over the nanoparticles  
there is a gradual change in lifetime going from the surface to the core of the nanoparticle.

21 Werts, M. H. V.; Jukes, R. T. F.; Verhoeven, J. W. *Phys. Chem. Chem. Phys.* **2002**, *4*, 1542.

22 Tissue, B. M. *Chem. Mater.* **1998**, *10*, 2837.

23 Hsu, C.; Powell, R. C. *J. Lumin.* **1975**, *10*, 273.

24 Dexpert-Ghys, J.; Mauricot, R.; Faucher, M. D. *J. Lumin.* **1996**, *69*, 203.

25 Blasse, G. *Prog. Solid St. Chem.* **1988**, *18*, 79.

26 (a) Oude Wolbers, M. P.; van Veggel, F. C. J. M.; Snellink Ruël, B. H. M.; Hofstraat, J. W.;  
Geurts, F. A. J.; Reinhoudt, D. N. *J. Chem. Soc., Perkin Trans. 2* **1998**, *10*, 2141; (b) Voloshin, A.  
I.; Shavaleev, N. M.; Kazakov, V. P. *J. Lumin.* **2001**, *93*, 199; (c) Macalik, L.; Hanuza, J.;  
Hermanowicz, K.; Oganowski, W.; Ban-Oganowski, H. *J. Alloy. Comp.* **2000**, *300-301*, 383.

27 (a) Sharma, P. K.; van Doorn, A. R.; Staring, A. G. J. *J. Lumin.* **1994**, *62*, 219; (b) Serra, O. A.;  
Nassar, E. J.; Calefi, P. S.; Rosa, I. L. V. *J. Alloy. Comp.* **1998**, *277*, 838; (c) Hong, Z. R.; Li, W.  
L.; Zhao, D. X.; Liang, C. J.; Liu, X. Y.; Peng, J. B.; Zhao, D. *Synth. Met.* **1999**, *104*, 165.

28 Heer, S.; Lehmann, O.; Haase, M.; Güdel, H. U. *Angew. Chem. Int. Ed.* **2003**, *42*, 3179.

- <sup>29</sup> (a) Reddy, B. R.; Nash-Stevenson, S.; Venkateswarlu, P. *J. Opt. Soc. Am. B* **1994**, *11*, 923; (b) Malinowski, M.; Frukacz, Z.; Szuflińska, M.; Wnuk, A.; Kaczkan, M. *J. Alloy. Comp.* **2000**, *300-301*, 389.
- <sup>30</sup> Maestro, P.; Huguenin, D. *J. Alloy. Comp.* **1995**, *225*, 520.
- <sup>31</sup> Demas, J. N.; Crosby, G. A. *J. Phys. Chem.* **1971**, *75*, 991.
- <sup>32</sup> Huignard, A.; Buisette, V.; Franville, A. C.; Gacoin, T.; Boilot, J. P. *J. Phys. Chem. B* **2003**, *107*, 6754.
- <sup>33</sup> Bhutta, T.; Chardon, A. M.; Shepherd, D. P.; Daran, C.; Serrano, C.; Munoz-Yague, A. *IEEE J. Quant. Elec.* **2001**, *37*, 1469.
- <sup>34</sup> Kirby, A. F.; Richardson, F. S. *J. Phys. Chem.* **1983**, *87*, 2544.
- <sup>35</sup> Heller, A. *J. Am. Chem. Soc.* **1967**, *89*, 167.
- <sup>36</sup> Buchal, C.; Siegrist, T.; Jacobson, D. C.; Poate, J. M. *Appl. Phys. Lett.* **1996**, *68*, 438.
- <sup>37</sup> Nishida, Y.; Yamada, M.; Kanamori, T.; Kobayashi, K.; Temmyo, J.; Sudo, S.; Ohishi, Y. *IEEE J. Quantum Elec.* **1998**, *34*, 1332.
- <sup>38</sup> Hong, Z.; Liang, C.; Li, R.; Zang, F.; Fan, D.; Li, W.; Hung, L. S.; Lee, S. T. *Appl. Phys. Lett.* **2001**, *79*, 13.
- <sup>39</sup> Hegarty, J.; Huber, D. L.; Yen, W. M. *Phys. Rev. B* **1982**, *25*, 5638.
- <sup>40</sup> Nakazawa, E.; *J. Lum.* **2002**, *100*, 89.
- <sup>41</sup> Manssmann, M. *Z. Kristall.* **1965**, *122*, 375.
- <sup>42</sup> Liu, G. K.; Zhuang, H. Z.; Chen, X. Y. *Nano Lett.* **2002**, *2*, 535.
- <sup>43</sup> Yanagida, S.; Hasegawa, Y.; Murakoshi, K.; Wada, Y.; Nakashima, N.; Yamanka, T. *Coord. Chem. Rev.* **1998**, *171*, 461.
- <sup>44</sup> Beeby, A.; Faulkner, S. *Chem. Phys. Lett.* **1997**, *266*, 116.
- <sup>45</sup> Lahoz, F.; Daran, E.; Zhang, X.; Muñoz-Yagüe, A.; Cases, R.; Alcalá, R. *J. Appl. Phys.* **1999**, *86*, 3699.
- <sup>46</sup> Buchal, C.; Siegrist, T.; Jacobson, D. C.; Poate, J. M. *Appl. Phys. Lett.* **1996**, *68*, 438.
- <sup>47</sup> Zhang, X.; Liu, X.; Jouart, J. P.; Mary, G. *J. Lumin.* **1998**, *78*, 289.
- <sup>48</sup> Eaton, D. F. *Pure Appl. Chem.* **1988**, *60*, 1107.

# CHAPTER 4

## *Surface effects on the luminescence of lanthanide(III)-doped nanoparticles*<sup>\*</sup>

*Nanoparticles consist for a large part of surface atoms. Luminescence of lanthanide-doped nanoparticles is therefore always influenced by the way the surface is terminated. In this chapter, the influence of the surroundings on the luminescence lifetime of lanthanide ions doped in nanoparticles is investigated. The influences of the quenching strength of the solvent and the refractive index of the solvent on the luminescence lifetime were studied. Concentration quenching was investigated by changing the doping concentration of the luminescent ion. The high-energy vibrations of molecules outside the nanoparticles are the most important quenchers and a model is proposed to fit the non-mono-exponential luminescence decay taking into account quenching from the surface.*

---

<sup>\*</sup> The major part of the work in this chapter was published: Stouwdam, J. W.; van Veggel, F. C. J. M. *Nano Lett.* **2002**, 2, 733; Hebbink, G. A.; Stouwdam, J. W.; Reinhoudt, D. N.; van Veggel, F. C. J. M. *Adv. Mater.* **2002**, 14, 1147; Stouwdam, J. W.; Hebbink, G. A.; Huskens, J.; van Veggel, F. C. J. M. *Chem. Mater.* **2003**, 15, 4604.

## 4.1 Introduction

The spectra of lanthanide or transition metal ion doped nanoparticles usually do not differ much from the spectra of the same bulk material.<sup>1</sup> In a bulk crystals, the sites that are close to the surface do not contribute significantly to the overall properties of the material. However, in nanocrystals, the surface sites cannot be neglected, because they provide a major contribution to the total. The ratio of surface site, to bulk site, in the nanoparticles is strongly dependent on the size of the nanoparticles. The coordination of water and other organic molecules to the surface of the nanoparticles can lead to quenching of the excited state of the lanthanide ion by the high-energy vibrations of the bonds. Krebs *et al.* found that the main source of quenching of Yb<sup>3+</sup>-doped in  $\gamma$ -Al<sub>2</sub>O<sub>3</sub> nanoparticles was the coordination of water to the surface of the nanoparticles.<sup>2</sup> The surface quenching leads to a non-mono-exponential decay of the luminescence of the Yb<sup>3+</sup> ion. Deviations from exponential decay were found more often for example in YVO<sub>4</sub>:Eu nanoparticles. Different symmetry sites were found by site-selective excitation.<sup>3</sup> Eu<sup>3+</sup> ions in different symmetry sites have different radiative lifetimes leading to a multi-exponential decay of the Eu<sup>3+</sup> luminescence. The refractive index surrounding the nanoparticles can have a significant effect as well on the luminescence lifetime of Eu<sup>3+</sup> ions doped in Y<sub>2</sub>O<sub>3</sub> nanoparticles.<sup>4</sup> The measured luminescence lifetime can differ by a factor of three when the nanoparticles are dispersed in carbon disulfide or in air, with the longest lifetime for a medium with the lowest refractive index. The influence of the refractive index on the spontaneous emission rate has also been studied for a Eu<sup>3+</sup> complex in solution.<sup>5</sup> The coordination of the ligand around the Eu<sup>3+</sup> ion can change when the complex is dissolved in different solvents, leading to a significant effect on the radiative lifetime of the Eu<sup>3+</sup> ion.<sup>6</sup> These differences in coordination overshadow the influence of the refractive index. The coordination around the Eu<sup>3+</sup> ion in nanoparticles is fixed, making them ideal for the study of the refractive index on the radiative lifetimes of the doping ions.

The Tb<sup>3+</sup> luminescence of CePO<sub>4</sub>:Tb nanoparticles synthesized by Haase *et al.* did not show a mono-exponential decay. A model, taking into account randomly distributed quenchers, was used to fit the decay.<sup>7</sup> This model has been used for bulk crystals when randomly distributed quenchers were incorporated in the crystal lattice. A strong solvent effect was also reported in the case of these nanoparticles, indicating that quenching from outside the nanoparticles plays an important role. Quenchers outside the nanoparticles are not randomly distributed, but are at the surface and in the solvent surrounding the nanoparticles, so this model cannot be used to describe a multi-exponential decay, when surface quenching is important.



In the previous chapter, luminescence decays of lanthanide-doped nanoparticles that are soluble in organic solvents were described. These nanoparticles do not show a mono-exponential decay of the lanthanide luminescence. In this chapter more insight is given in the luminescence decay of these nanoparticles. Solvent quenching, concentration quenching, and the influence of the refractive index of the solvent on the luminescence lifetime have been studied. A model was developed to fit the luminescence decays. The model explains why the luminescence decay is not mono-exponential by taking into account quenching from outside the nanoparticles.

## 4.2 Results and discussion

### 4.2.1 Quenching by solvents

Quenching by the solvent in which the nanoparticles are dissolved can easily be varied and the influence this has on the luminescence lifetime of the lanthanide ions can be studied. LaPO<sub>4</sub> nanoparticles doped with different lanthanide ions are soluble in water and methanol. The quenching strength of these solvents can be altered by using deuterated solvents, replacing the OH and CH bonds for OD and CD bonds.<sup>8</sup> The lower vibrational frequency of a deuterated bond compared to the hydrated bond leads to a reduced quenching of the lanthanide ion. The luminescence lifetimes obtained in deuterated and non-deuterated solvents, after fitting with a bi-exponential decay, are shown in Table 4.1.

Table 4.1: Luminescence lifetimes of LaPO<sub>4</sub>:Eu in different solvents.

Solvent	$\tau_1$ (ms) <sup>a,b</sup>	$\tau_2$ (ms)
H <sub>2</sub> O	5.7 (71 %)	2.6 (29 %)
D <sub>2</sub> O	7.6 (44 %)	4.9 (56 %)
CH <sub>3</sub> OH	6.4 (57 %)	3.4 (43 %)
CD <sub>3</sub> OD	7.6 (41 %)	4.9 (59 %)

a) The percentages reflect the amount of the component contributing to the total lifetime.

b) The absolute errors in the fit are 0.2 ms in the lifetime and 5 % in the component contributing to the total lifetime.

In the strongest quenching solvent, water, the luminescence lifetimes were the shortest. When the OH bonds were replaced by OD bonds, that quench less, a substantial increase in the luminescence lifetimes was observed. This was accompanied by a change in the ratio of the long

and short lifetime. The change in the ratio of the two lifetimes indicates that the non-mono-exponential behavior is strongly influenced by the solvent and that quenching from outside the nanoparticle has an influence on the shape of the decay curve. A similar effect on the luminescence lifetime was observed when the luminescence lifetime was measured in the solvents methanol and methanol- $d_4$ .

LaF<sub>3</sub>:Eu nanoparticles were not soluble in water or methanol, but also with these nanoparticles OH bonds are important quenchers of the Eu<sup>3+</sup> luminescence. When the nanoparticles were synthesized in a mixture of D<sub>2</sub>O/EtOD, the lifetimes increased to 9.0 ms, contributing to 65 % of the total luminescence and 4.0 ms, contributing to 35 % of the total luminescence. Compared to the lifetimes obtained for nanoparticles synthesized in non-deuterated solvents of 7.7 ms contributing to 74 % of the total luminescence and 2.9 ms contributing to 26 % of the total luminescence, an increase in the lifetime as well as a shift in the ratios of the two components was observed. The difference in luminescence lifetime is caused by the coordination of water to the surface, because stirring of the nanoparticles, synthesized in deuterated solvents, in a mixture of EtOH/H<sub>2</sub>O leads to a decrease of the lifetime to the values of nanoparticles synthesized in non-deuterated solvent. The decrease of the luminescence lifetime proves that the quenching groups are accessible to the solvent and are therefore located at the surface of the nanoparticles and not in the core.

#### 4.2.2 Influence of the refractive index

The influence of the refractive index on the luminescence lifetime of Eu<sup>3+</sup>-doped nanoparticles was investigated by dissolving the nanoparticles in different solvents. The solvents used have a refractive index ranging from 1.352 for ethylether to 1.525 for chlorobenzene. A gradual change in the luminescence lifetime of the <sup>5</sup>D<sub>0</sub> level of Eu<sup>3+</sup> was found. The decays had to be fitted with a bi-exponential decay and the luminescence lifetimes are summarized in Table 4.2. When the refractive index of the solution is increased, a gradual increase in the luminescence lifetime is observed. This effect is most pronounced on the long component of the lifetime. The differences on the short component are within the experimental error of the fit. This constant value of the short component of the luminescence lifetime indicates that the short component is not influenced primarily by the refractive index, but that quenching is more important. The solvents that were used have approximately the same quenching strength, because all solvents have CH bonds as bonds with the highest vibrational energy and no OH bonds. Probably, the strongest quencher is the coordinated water and the ligand, which forms a densely packed monolayer around the nanoparticles, and not the solvent. The emission spectra of

Eu<sup>3+</sup> were the same in the different solvents, so a change in coordination around the lanthanide ion is not responsible for the change in luminescence lifetime.

Table 4.2: Luminescent lifetimes of LaF<sub>3</sub>:Eu nanoparticles in different solvents<sup>a,b</sup>

Solvent	n <sup>D</sup>	τ <sub>1</sub> (ms)	τ <sub>2</sub> (ms)
Ethylether	1.352	9.5 (67 %)	3.6 (33 %)
Pentane	1.357	8.4 (77 %)	2.9 (23 %)
Hexane	1.375	8.2 (76 %)	2.9 (24 %)
THF	1.407	8.1 (73 %)	3.0 (27 %)
Dichloromethane	1.424	7.7 (74 %)	2.9 (26 %)
Chloroform	1.446	7.4 (75 %)	2.8 (25 %)
Toluene	1.497	6.8 (75 %)	2.7 (25 %)
Chlorobenzene	1.525	6.8 (72 %)	2.8 (28 %)

a) The percentages reflect the amount of the component contributing to the total lifetime

b) The absolute errors in the fit are 0.2 ms in the lifetime and 5 % (absolute) in the component contributing to the total lifetime.

#### 4.2.3 Concentration quenching

There are different quenching mechanisms for lanthanide ion-doped nanoparticles. Quenching does not only take place by interaction with high-energy vibrations of the host matrix and impurities, but also the interactions between lanthanide ions can play an important role. Variation of the doping concentration of the luminescent ion can change the interactions between lanthanide ions. In the previous chapter it was shown that the concentration of Eu<sup>3+</sup> ions in the LaF<sub>3</sub> nanoparticles has an influence on the cross-relaxation quenching of the <sup>5</sup>D<sub>1</sub> emission. A concentration effect was also found on the luminescence lifetime of the <sup>5</sup>D<sub>0</sub> level of Eu<sup>3+</sup> ions in LaF<sub>3</sub> and LaPO<sub>4</sub> nanoparticles. The luminescence lifetimes of LaF<sub>3</sub>:Eu and LaPO<sub>4</sub>:Eu nanoparticles with a different doping concentration are shown in Table 4.3. An increase in the average luminescence lifetime is observed, for both nanoparticles, but for LaPO<sub>4</sub> these differences are less pronounced. A shift in the ratios of the two components is also observed for the LaF<sub>3</sub> nanoparticles. For a lower Eu<sup>3+</sup> content the amount of the short component decreases, consistent with reduced Eu<sup>3+</sup>-Eu<sup>3+</sup> interaction. Due to the lower concentration the rate of migration of excitation energy through the nanoparticle is lowered and the amount of Eu<sup>3+</sup> ions in contact with the surface is decreased. As a result the amount of the short component in the luminescence decay decreases. Although there is a clear influence of the concentration on the

ratios of the two components in the luminescence lifetime, at low concentration the decay is also not mono-exponential. The concentration of the lanthanide ion is therefore not the cause of the deviation from mono-exponential behavior.

*Table 4.3: Luminescent lifetimes of the  $^5D_0$  level of  $Eu^{3+}$  in  $LaF_3$  nanoparticles at different concentrations of  $Eu^{3+}$ .<sup>a,b</sup>*

Nanoparticle	$Eu^{3+}$ conc.	$\tau_1$ (ms)	$\tau_2$ (ms)	$\tau_{av}$ (ms)
$LaF_3$	1 %	9.1 (87 %)	2.8 (13 %)	8.8
	2 %	8.5 (83 %)	2.7 (17 %)	8.1
	5 %	7.7 (74 %)	2.9 (26 %)	7.1
$LaPO_4$	1 %	7.3 (65 %)	4.0 (35 %)	6.5
	2 %	7.6 (57 %)	4.3(43 %)	6.6
	5 %	6.4 (57 %)	3.4 (43 %)	5.5

- a) The percentages reflect the amount of the component contributing to the total lifetime  
b) The absolute errors in the fit are 0.2 ms in the lifetime and 5 % (absolute) in the component contributing to the total lifetime.

#### 4.2.4 Modeling of the luminescence lifetime

From the previous results it can be concluded that quenching from outside the nanoparticle causes the deviation from mono-exponential behavior. This quenching from outside the nanoparticles leads to shorter luminescence lifetimes of ions close to the surface of the nanoparticles and longer luminescence lifetimes for ions in the core of the nanoparticles. This decrease in the luminescence lifetime towards the surface of the nanoparticles is a gradual change and not one of two distinct populations as assumed in a bi-exponential fit. With this in mind, a model is proposed to fit the luminescence decay, which incorporates quenching from outside the nanoparticle. The different  $Ln^{3+}$  luminescent centers are related to each other with a radiative lifetime that is the same for all lanthanide ions and a quenching factor that is related to the distance to the surface. When the nanoparticle is divided in a number of shells, the luminescence decay can be described using Equation 4.1

$$I_t = I_0 \sum_{i=1}^n \frac{1}{n} e^{-k_i t}; k_i = \frac{1}{\tau_i} = k_R + C \times f_{q,i} \quad (Eq. 4.1)$$

in which  $I_t$  is the intensity of light at time  $t$ ,  $I_0$  the intensity at  $t = 0$ ,  $k_i = 1/\tau_i$  is the rate constant in shell  $i$ ,  $k_R = 1/\tau_R$  the rate constant in absence of surface quenching,  $C$  a quenching constant, and  $f_{q,i}$  the quenching factor of shell  $i$ , that takes into account the integrated distance of the shell to the surface with a distance dependence of the quenching of  $r^{-6}$ . For more information on the model see the appendix. The model assumes that all the luminescent ions are in the same crystal site, with the same refractive index, that they are randomly distributed over the nanoparticle, and that surface quenching is the cause of deviation from exponential behavior. The observation of one emission peak for the  ${}^5D_0 \rightarrow {}^7F_0$  transition in the  $\text{Eu}^{3+}$ -doped nanoparticles was a strong indication that the ions are all doped in a crystal site with the same environment. More evidence can be found in the time-resolved emission spectrum.  $\text{Eu}^{3+}$  ions in different crystal sites with a different symmetry have a different radiative lifetime. In a time-resolved emission spectrum, the emission shortly after the excitation pulse is dominated by the emission centers with the shortest lifetime and the emission at the end of the decay is dominated by emission centers with the longest lifetimes.

Figure 4.1 shows the time-resolved emission spectra of  $\text{LaVO}_4:\text{Eu}$  and  $\text{LaPO}_4:\text{Eu}$  nanoparticles. When the normalized emission spectra taken shortly after an emission pulse and at the end of the decay are compared, the differences observed are not large, indicating that the luminescent centers emitting at the end of the decay and the emission centers emitting shortly after excitation are in a crystal site with the same symmetry. For  $\text{LaF}_3:\text{Eu}$  nanoparticles the absorption is too low to measure an emission spectrum with enough intensity and high enough resolution to make a good comparison. The emission spectrum of  $\text{LaF}_3:\text{Eu}$  nanoparticles shows differences in time, because of the overlap of the emission from the  ${}^5D_1$  and  ${}^5D_0$  level, which have a different lifetime.

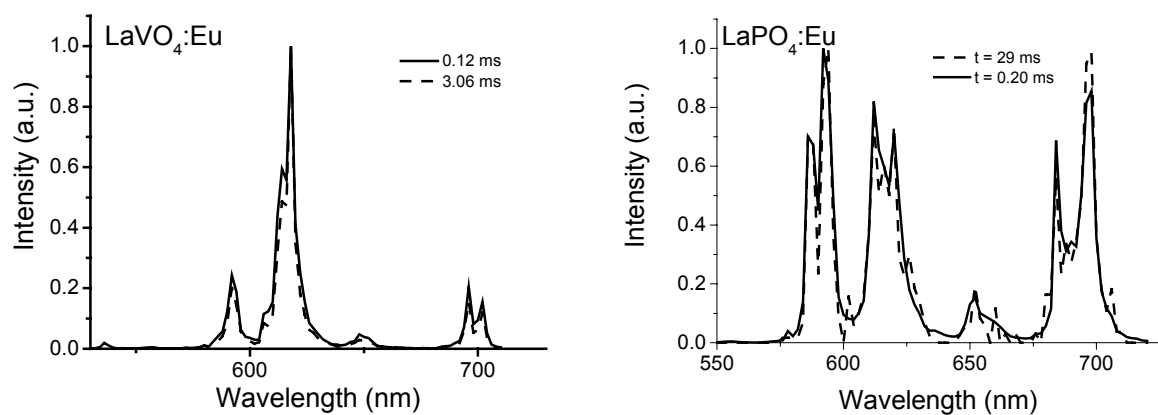


Figure 4.1: Time-resolved emission spectra of  $\text{Eu}^{3+}$ -doped nanoparticles of (left)  $\text{LaVO}_4$  and (right)  $\text{LaPO}_4$ .

The result for the other two nanoparticles make it safe to assume that for LaF<sub>3</sub> nanoparticles the ions are also in crystal sites with the same symmetry. The luminescence decays of the Eu<sup>3+</sup>-doped nanoparticles and the fits using Equation 4.1, are shown in Figure 4.2.

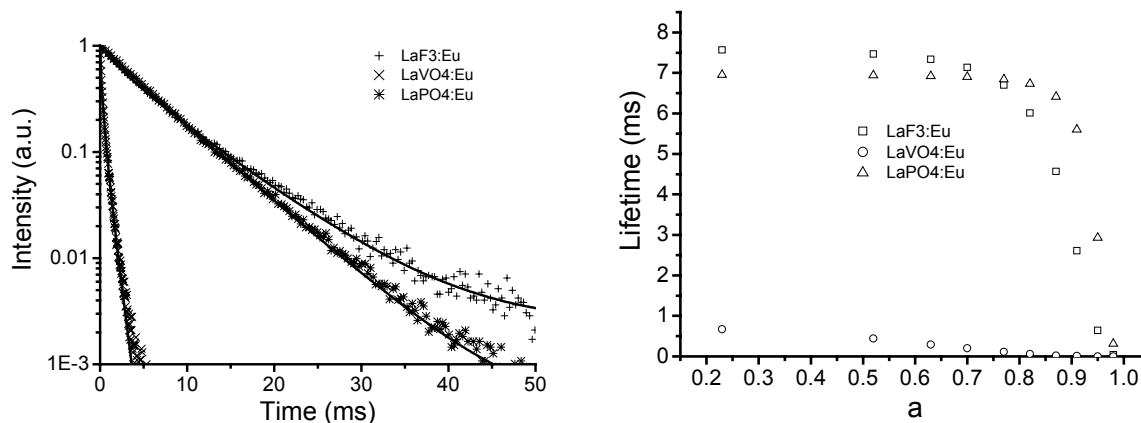


Figure 4.2: Luminescence decays and fits for Eu<sup>3+</sup>-doped nanoparticles of LaF<sub>3</sub>, LaVO<sub>4</sub>, and LaPO<sub>4</sub> (left) and the lifetime distributions in the nanoparticles (right). The LaF<sub>3</sub> and LaVO<sub>4</sub> nanoparticles were dissolved in dichloromethane and the LaPO<sub>4</sub> nanoparticles in methanol.

Equation 4.1 is able to fit the luminescence decay of the Eu<sup>3+</sup> luminescence very accurately. The values obtained for the luminescence lifetimes, the quenching constants, and the average lifetimes of the ten shells are shown in Table 4.4.

Table 4.4: Luminescence lifetimes, quenching constants, and average lifetimes obtained by fitting the luminescence decays of Eu<sup>3+</sup>-doped LaF<sub>3</sub>, LaVO<sub>4</sub>, and LaPO<sub>4</sub> nanoparticles with the model described in the appendix.

Nanoparticles	$\tau_R$ (ms)	C	$\tau_{av}$ (ms)
LaF <sub>3</sub>	7.7	$2.94 \cdot 10^{-1}$	6.5
LaVO <sub>4</sub>	1.4	$1.48 \cdot 10^2$	0.45
LaPO <sub>4</sub>	7.0	$4.06 \cdot 10^{-2}$	6.5

The apparent radiative lifetimes show that in absence of surface quenching the lifetime in LaF<sub>3</sub> nanoparticles is the longest, then the lifetime of the LaPO<sub>4</sub> nanoparticles, and then the LaVO<sub>4</sub> lifetime. The same dependence of the Eu<sup>3+</sup> lifetime on the host material was found for bulk materials.<sup>9</sup> The size and size distribution are incorporated in the C constant, so the C constants cannot be compared directly. Quenching in the LaF<sub>3</sub> nanoparticles must be stronger

than in the  $\text{LaPO}_4$  nanoparticles, because the average lifetimes of the shells are the same for both nanoparticles. Luminescence lifetimes for all ten shells are obtained and the lifetimes of these shells are plotted in Figure 4.2 as well. It can be seen that the quenching in the core of the nanoparticles is minimal and that going to the outside of the nanoparticles the lifetime decreases. For the  $\text{LaF}_3$  and  $\text{LaVO}_4$  nanoparticles the quenching seems to have a longer range, going deeper into the nanoparticle. All shells are under the influence of quenching for the  $\text{LaVO}_4$  nanoparticles, because the first shell in the core of the nanoparticle has a lifetime that is substantially lower than the radiative lifetime. About half of the shells are not quenched for  $\text{LaF}_3$  and for the other five shells quenching increases going to the surface of the nanoparticle. For the  $\text{LaPO}_4$  nanoparticles about 7 shells are not quenched. Quenching from the surface is stronger in the  $\text{LaF}_3$  and  $\text{LaVO}_4$  nanoparticles than in the  $\text{LaPO}_4$  nanoparticles, because in the  $\text{LaF}_3$  and  $\text{LaVO}_4$  nanoparticles, more shells are influenced by surface quenching.

Luminescence decays of NIR emitting ions could also be fitted using Equation 4.1. The decays of  $\text{Nd}^{3+}$  and  $\text{Er}^{3+}$  in  $\text{LaF}_3$  and  $\text{LaPO}_4$  nanoparticles with the corresponding fits are shown in Figure 4.3 and Table 4.5 gives the values of the fit constants  $\tau_R$  and  $C$ .

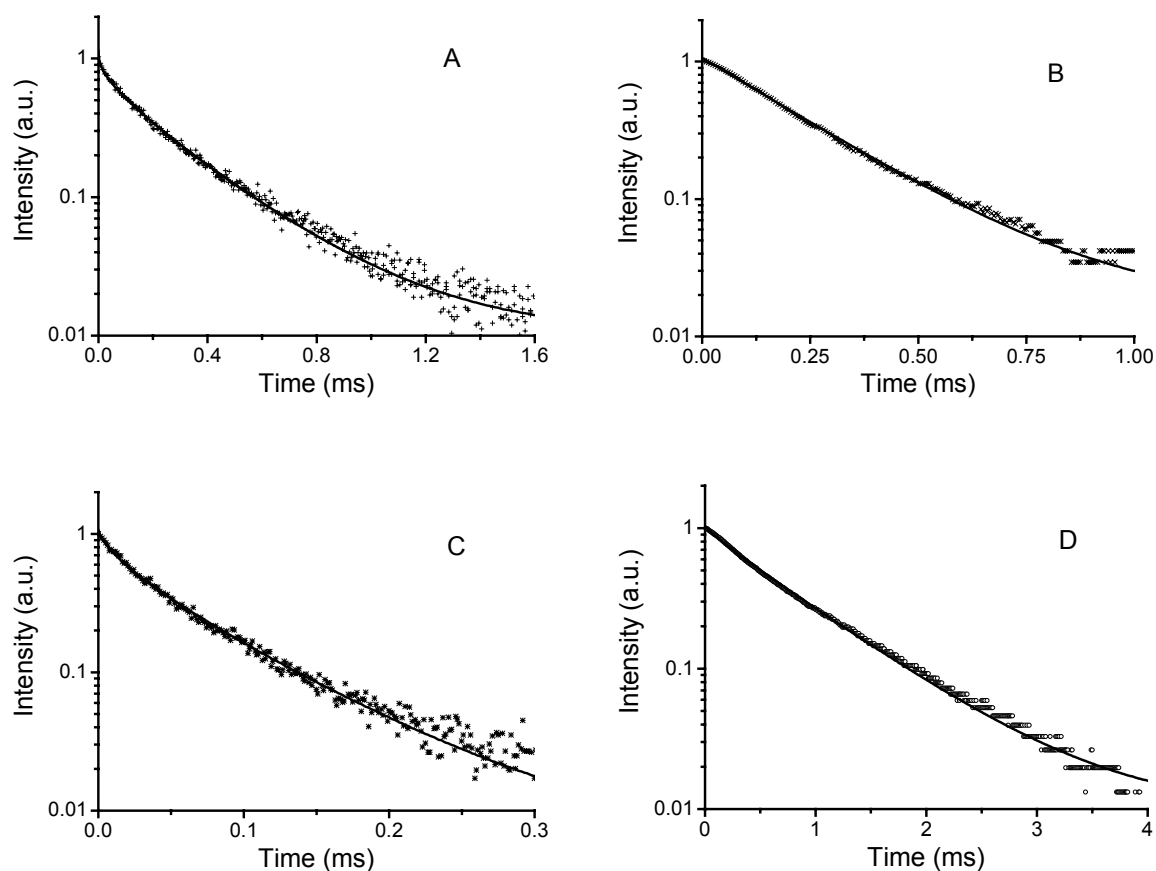


Figure 4.3: Luminescence decays of (A)  $\text{LaF}_3:\text{Nd}$ , (B)  $\text{LaF}_3:\text{Er}$ , (C)  $\text{LaPO}_4:\text{Nd}$ , and (D)  $\text{LaPO}_4:\text{Er}$ .

The average luminescence lifetimes for  $\text{Er}^{3+}$  and  $\text{Nd}^{3+}$  show the same trend as when the decay was fitted using a bi-exponential decay. An increase by a factor 10-1000 in the luminescence lifetime is observed compared to the lifetimes of organic complexes, containing  $\text{Nd}^{3+}$  or  $\text{Er}^{3+}$ . For  $\text{Nd}^{3+}$  the values of the average lifetime and  $\tau_R$  are higher for  $\text{LaF}_3$  than for  $\text{LaPO}_4$  reflecting the difference in the phonon energies of the matrices. This is the other way around for  $\text{Er}^{3+}$ , the value of  $\tau_R$  and the average lifetime are lower for the  $\text{LaF}_3:\text{Er}$  nanoparticles compared to the  $\text{LaPO}_4:\text{Er}$  nanoparticles.

Table 4.5: Luminescence lifetimes of the NIR-emitting ions in the two different nanoparticles.<sup>a</sup>

Nanoparticle	Solvent	$\tau_R$ ( $\mu\text{s}$ )	$C(\text{s}^{-1})$	$\tau_{\text{av}}$ ( $\mu\text{s}$ )
$\text{LaPO}_4:\text{Nd}$	$\text{CD}_3\text{OD}$	90	107	68
$\text{LaF}_3:\text{Nd}$	$\text{CH}_2\text{Cl}_2$	347	23.5	265
$\text{LaPO}_4:\text{Er}$	$\text{CD}_3\text{OD}$	315	4.66	304
$\text{LaF}_3:\text{Er}$	$\text{CH}_2\text{Cl}_2$	236	3.29	226
$\text{LaPO}_4:\text{Pr}$	$\text{CD}_3\text{OD}$	4.0	57.3	3.7
$\text{LaF}_3:\text{Ho}$	$\text{CH}_2\text{Cl}_2$	35	27	31

a) All doping concentrations were 5 %. The errors in  $\tau_R$  are  $\approx 3$  % and in  $C \approx 10$  % determined from duplicate measurements.

Not only the quenching is stronger, but also the lower  $\tau_R$  indicates that there are more quenching possibilities for  $\text{Er}^{3+}$  inside the nanoparticles. Quenching by cross-relaxation, or concentration quenching could be more important in the  $\text{LaF}_3$  nanoparticles, compared to the  $\text{LaPO}_4$  nanoparticles as a result of different average distances between the luminescent ions. The average lifetimes of  $\text{Pr}^{3+}$  and  $\text{Ho}^{3+}$  are in the  $\mu\text{s}$  range reflecting the shorter radiative lifetimes of these ions. A lifetime of 70  $\mu\text{s}$  for the  $^1\text{D}_2$  level was reported for  $\text{Pr}^{3+}$  in a phosphate host<sup>10</sup> and for  $\text{Ho}^{3+}$  in  $\text{LaF}_3$ , a lifetime of the  $^5\text{F}_5$  level of 780  $\mu\text{s}$  was calculated.<sup>11</sup>

Using Equation 4.1, different factors influencing the luminescence lifetimes of these nanoparticles were investigated.  $\text{Er}^{3+}$  usually shows a large dependence on the doping concentration and when the nanoparticles are doped with different concentrations of  $\text{Er}^{3+}$  this is indeed reflected in the values of  $\tau_R$  and  $C$  (Table 4.6). A decrease in  $\text{Er}^{3+}$  concentration should not change the quenching constant  $C$  because the  $\text{Er}^{3+}$  ions are still in the same crystal site and at the same average distance to the surface.  $\tau_R$  should increase with a decreasing doping concentration because quenching processes like cross-relaxation and up-conversion become less



important.<sup>12</sup> This is clearly observed in the values for LaF<sub>3</sub>:Er with different Er<sup>3+</sup> concentrations. A pronounced increase in  $\tau_R$  is observed when the concentration is lowered, while C remains about the same for the concentrations used.

Table 4.6: Luminescence lifetimes of LaF<sub>3</sub>:Er and LaPO<sub>4</sub>:Er at different doping concentrations.<sup>a</sup>

Concentration	LaF <sub>3</sub> :Er		LaPO <sub>4</sub> :Er	
	$\tau_R(\mu\text{s})$	$C(\text{s}^{-1})$	$\tau_R(\mu\text{s})$	$C(\text{s}^{-1})$
5 %	236	3.29	315	4.66
2 %	332	3.73	758	4.27
1 %	465	3.54	1070	2.92

a) The errors in  $\tau_R$  are  $\approx 3\%$  and in C  $\approx 10\%$  determined from duplicate measurements.

The constant C does change for the LaPO<sub>4</sub>:Er nanoparticles and becomes lower at a lower doping concentration. The different surface termination of the nanoparticles could play a role here. One quenching path is the transfer of the excitation energy of ions in the core of the nanoparticles to ions closer to the surface followed by quenching. This process is dependent on the concentration of the doping ion, because energy transfer becomes more efficient at higher doping concentrations, but also on the surface termination. In the LaF<sub>3</sub> nanoparticles the lanthanide ions are coordinated directly to the ligand and other possible quenchers, but in the case of the LaPO<sub>4</sub> nanoparticles PO<sub>4</sub> groups are at the surface.

In addition, quenching by solvents with a different quenching strength can be described using Equation 4.1. The luminescence lifetimes of LaPO<sub>4</sub>:Nd and LaPO<sub>4</sub>:Eu in methanol with a different degree of deuteration are given in Table 4.7.

Table 4.7: Luminescence lifetimes of LaPO<sub>4</sub>:Nd and LaPO<sub>4</sub>:Eu in methanol with different degrees of deuteration.<sup>a</sup>

Solvent	Nd <sup>3+</sup>		Eu <sup>3+</sup>	
	$\tau_R(\mu\text{s})$	$C(\text{s}^{-1})$	$\tau_R(\text{ms})$	$C(\text{s}^{-1})$
CH <sub>3</sub> OH	87	733	7.0	$4.06 \cdot 10^{-2}$
CH <sub>3</sub> OD	91	214	6.9	$1.18 \cdot 10^{-2}$
CD <sub>3</sub> OD	90	107	6.9	$1.31 \cdot 10^{-2}$

a) The errors in  $\tau_R$  are  $\approx 3\%$  and in C  $\approx 10\%$  determined from duplicate measurements.

The same  $\tau_R$  is found for all three solvents in agreement with the fact that the nanoparticle itself does not change. The C constants are different, because the quenching of the solvent is varied. A small quenching constant is found for the  $\text{Eu}^{3+}$  ions, because the energy gap of  $\text{Eu}^{3+}$  is relatively large and it is therefore less sensitive to quenching. In non-deuterated methanol the strongest quencher is the OH group and replacing this with an OD group leads to a large decrease in C. Replacement of the CH group by CD leads to another small decrease in quenching in the case of  $\text{Nd}^{3+}$ , but in the case of  $\text{Eu}^{3+}$  the effect is negligible consistent with the larger energy gap between the excited state and the ground state of the  $\text{Eu}^{3+}$  ion.

The model does not include the influence of the refractive index on the luminescence lifetime. Lanthanide ions in the core of the nanoparticles experience a different refractive index than nanoparticles close to the surface of the nanoparticles. The luminescence lifetimes of  $\text{LaF}_3:\text{Eu}$  nanoparticles in different solvents showed that the refractive index mainly influences the long component of the decay (Table 4.2). The lifetime of  $\text{Eu}^{3+}$  ions doped in the core of the nanoparticles is strongly influenced by a change in refractive index of the solvent, which is at a distance of approximately 4 nm. The spontaneous emission rate of  $\text{Er}^{3+}$  near surfaces of different refractive indices changes even when the  $\text{Er}^{3+}$  ions are 150 nm away from the interface.<sup>13</sup> It is therefore safe to assume that the distance dependence of the luminescence lifetime on the refractive index in the nanoparticles is much smaller than the distance dependence of quenching.

The model also assumes that the excited state stays in one place, although a known quenching mechanism for lanthanide ions is the transfer of the lanthanide ions, until a quenching site is met.<sup>14</sup> This quenching mechanism also occurs in the nanoparticles, which can be seen from the luminescence lifetimes of  $\text{LaF}_3:\text{Eu}$  nanoparticles with a varying  $\text{Eu}^{3+}$  concentration (Table 4.3). The decrease of the ratio of the short luminescence lifetime at a low  $\text{Eu}^{3+}$  concentration indicates that quenching is more confined to the surface, which could be caused by a decreased energy migration.

The size and size distribution of the nanoparticles is currently in the constant C of the model. In order to get the size and size distribution separated it is necessary to synthesize nanoparticles with different sizes and with a small size distribution.

#### 4.2.5 Nanoparticles with different sizes

Several techniques have been developed to influence the size and size distribution of nanoparticles during or after the synthesis. During the synthesis it is often a ligand that controls the growth of the nanoparticles and changing the concentration of ligand can have an influence on the nanoparticle size.<sup>15</sup>

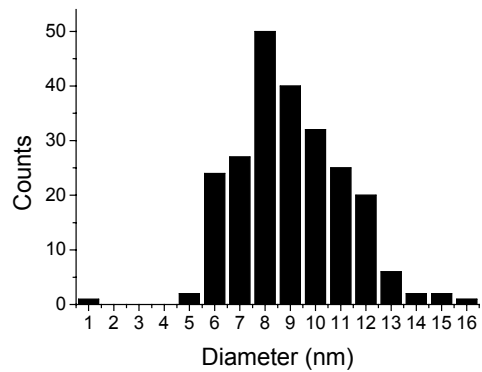
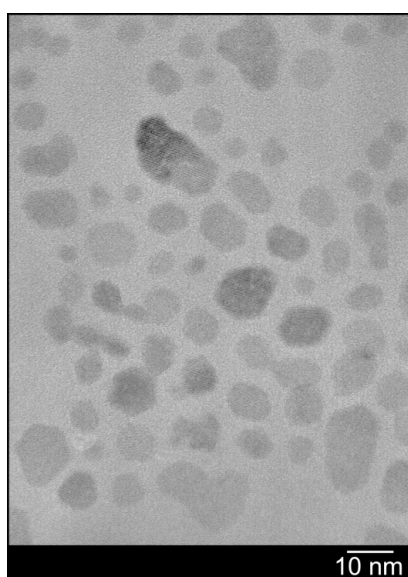
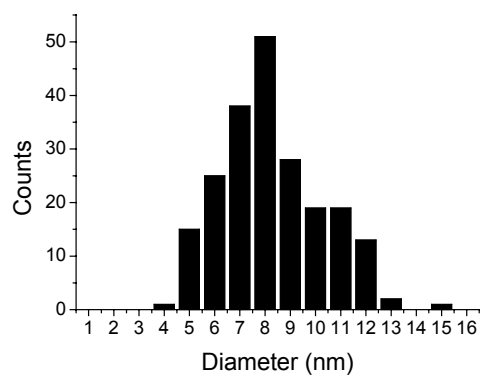
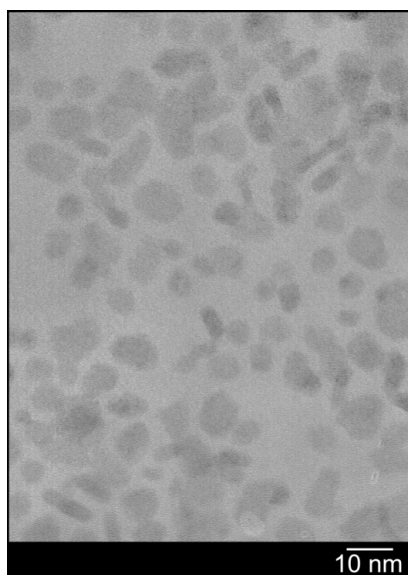
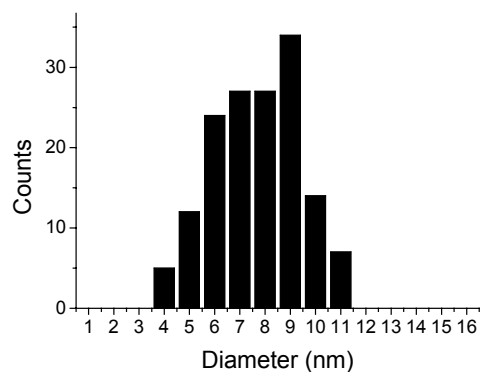
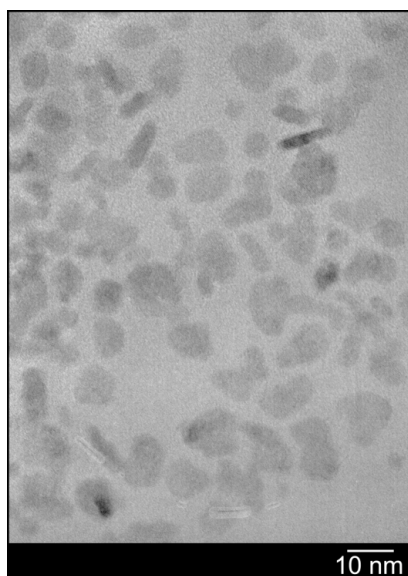


Figure 4.4: TEM pictures with the corresponding size distributions for LaF<sub>3</sub>:Eu nanoparticles synthesized with different ligand ratios; (top) ligand / NaF 2/3, (middle) 1/3, (bottom) 1/6.

When more ligand is present, there is more overall interaction between the monomer and ligand, slowing down the reaction rate. This allows for more nucleation and a decrease in nanoparticle size. The effect of the ligand ratio on the size distribution is usually small. The ratio of ligand to lanthanide/NaF was changed for the reaction of LaF<sub>3</sub>:Eu nanoparticles. The influence on the size of the nanoparticles was studied with TEM. Typical TEM pictures with the corresponding size distribution histograms are shown in Figure 4.4. The average sizes of the nanoparticles varied between 7.1 nm, 7.7 nm, and 8.4 nm for the nanoparticles synthesized with a 2/3, 1/3, and 1/6 ligand/F ratio, respectively. When the concentration of ligand was lowered, an increase in the nanoparticles size was observed. The size distributions of the nanoparticles were also increased slightly from 23.7 %, 25.6 %, and 28.2 %, respectively. An effect on the luminescence decay was found for nanoparticles with different sizes. The decays of the <sup>5</sup>D<sub>0</sub> level are shown in Figure 4.5.

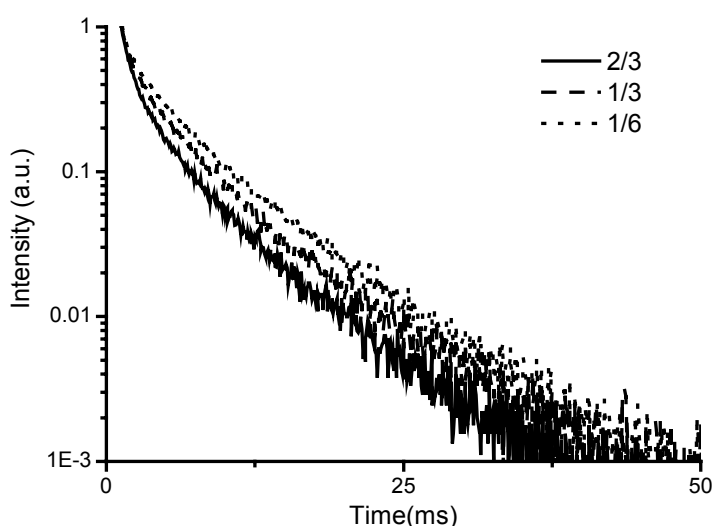


Figure 4.5: Decays of the Eu<sup>3+</sup> luminescence for the differently sized nanoparticles by changing the ligand to NaF ratio. The nanoparticles were dissolved in toluene.

The main difference between the decays is observed shortly after the excitation pulse, where a shorter component in the luminescence lifetime is observed for the smallest nanoparticles. This is a strong indication that the surface plays an important role in the quenching of the lanthanide ion, because the smaller nanoparticles have a larger surface to core ratio. About 15-20 ms after the excitation pulse the decays are almost parallel indicating the ions with a long luminescent lifetime are not much influenced by the size of the nanoparticles. The influence of surface quenching does not reach to the core of the nanoparticles, so ions in the core

of the small nanoparticles show the same luminescence lifetime as ions in the core of the larger nanoparticles. The luminescence lifetimes obtained after fitting with a bi-exponential decay are shown in Table 4.8. When the nanoparticle size is decreased, a clear decrease in luminescence lifetime of both components is observed. The relative amounts of the two components did not change as would be expected for a size increase.

*Table 4.8: Luminescence lifetimes of different sized LaF<sub>3</sub>:Eu nanoparticles in toluene after changing the ligand ratio.<sup>a,b</sup>*

Average batch size (nm)	$\tau_1$ (ms)	$\tau_2$ (ms)
8.4	7.4 (71 %)	2.6 (29 %)
7.7	6.8 (68 %)	2.2 (32 %)
7.1	6.5 (68 %)	1.8 (32 %)

a) The percentages reflect the amount of the component contributing to the total lifetime.

b) The absolute errors are 0.2 in the lifetime and 5 % in the relative amount.

Another technique to decrease the size distribution of the nanoparticles is applied after the synthesis. Size-selective precipitation has been widely applied to decrease the size distribution of a nanoparticle solution and to select nanoparticles of different sizes.<sup>16</sup> To a solution of the nanoparticles a non-solvent is slowly added, until a precipitate starts to form. This precipitate is enriched with the largest nanoparticles in solution, because these have the largest surface area. Nanoparticles with different sizes can be obtained by separating the precipitate and repeating the procedure with the residue. Typical TEM pictures of the size-selected nanoparticles are shown in Figure 4.6. The nanoparticles are more clustered than directly after the synthesis, which might be a result of the prolonged stirring in the precipitated form. It is therefore more difficult to measure an accurate nanoparticle distribution. A clear difference in size could be observed for the different batches ranging from 7.2, 6.8, and 5.3 nm, respectively. The size distribution was not narrowed and was 18.1, 23.4, and 21.5 % for the different batches. The luminescence lifetime of the <sup>5</sup>D<sub>0</sub> level of Eu<sup>3+</sup> was also influenced.

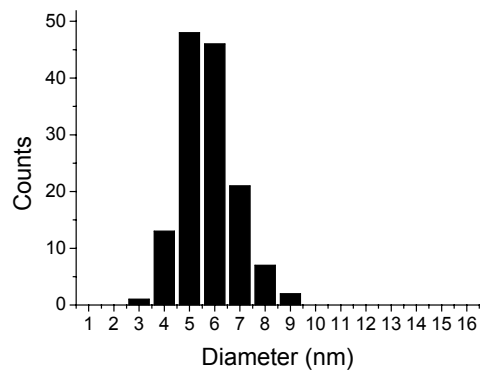
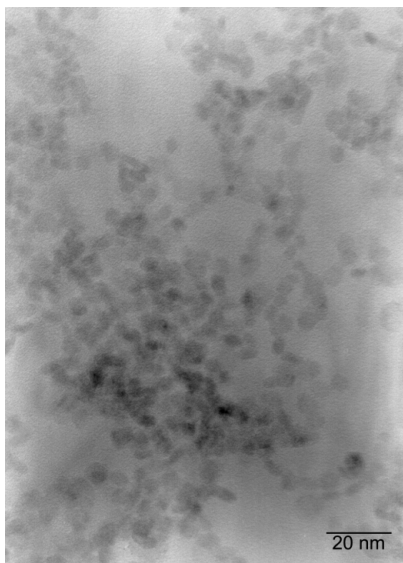
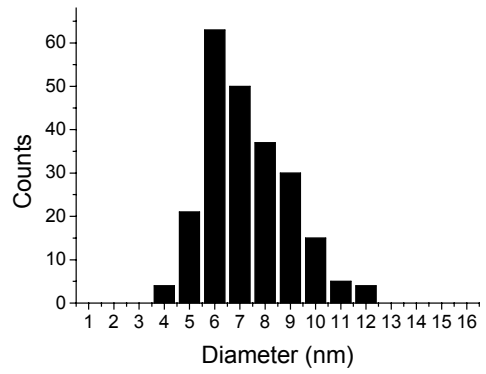
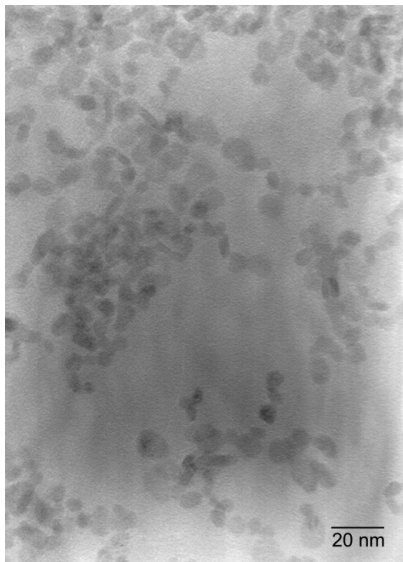
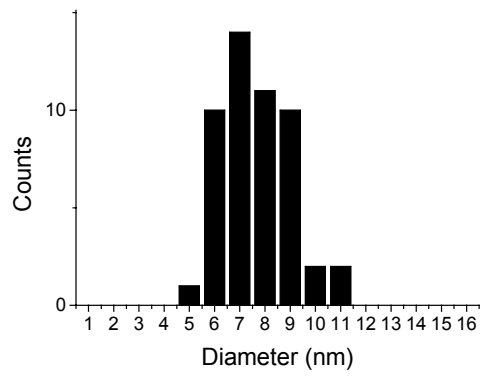
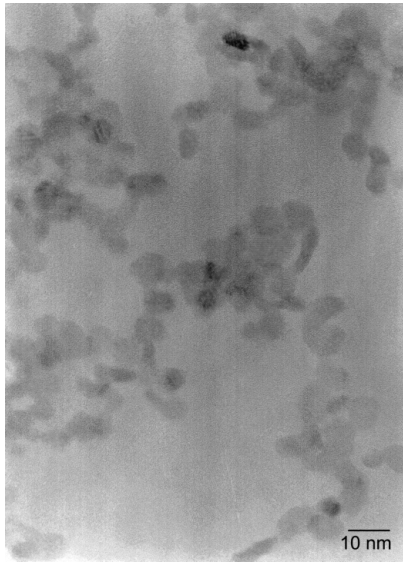


Figure 4.6: TEM pictures of size selected nanoparticles of  $\text{LaF}_3:\text{Eu}$ .

The luminescence decays are shown in Figure 4.7. The differences in the luminescence decay are less pronounced than in Figure 4.5 for nanoparticles synthesized with different concentrations of ligand. The inset of Figure 4.7 shows an enlargement of the decay between 22 and 24 ms. This shows that the decay of the smallest nanoparticles is indeed below the decay of the larger nanoparticles. The values obtained after fitting with a bi-exponential decay also show that the luminescence lifetime is the longest for the nanoparticles with the largest size as summarized in Table 4.9. From the fit a relevant difference in the luminescence lifetimes was obtained.

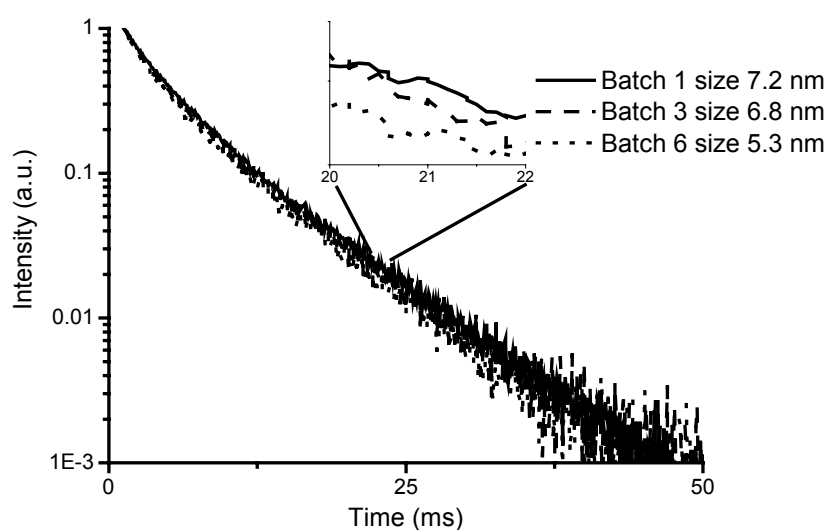


Figure 4.7: Normalized luminescence decays of size-selected nanoparticles of  $\text{LaF}_3:\text{Eu}$  in dichloromethane. The inset shows an enlargement of the decays at a time interval between 20 and 22 ms.

Table 4.9: Luminescence lifetimes of differently sized  $\text{LaF}_3:\text{Eu}$  nanoparticles after size selective precipitation.<sup>a,b</sup>

Batch size (nm)	$\tau_1$ (ms)	$\tau_2$ (ms)
7.2	7.6 (63 %)	2.9 (37 %)
6.8	7.3 (68 %)	2.6 (32 %)
5.3	7.1 (67 %)	2.5 (33 %)

a) The percentages reflect the amount of the component contributing to the total lifetime.

b) The absolute errors are 0.2 in the lifetime and 5 % in the relative amount.

### 4.3 Conclusions

The shape of the luminescence decay of lanthanide ions doped in the nanoparticles is strongly dependent on the surroundings of the nanoparticles. The quenching strength of the solvent has a large influence on the shape of the decay curve, leading to the conclusion that the deviation from mono-exponential behavior is caused by surface quenching. The luminescence decays can be fitted with a model that takes into account quenching from outside the nanoparticles.

### 4.4 Experimental section

**Nanoparticle synthesis.** The nanoparticles were synthesized as described in chapter 3. For the nanoparticles with a different concentration of lanthanide ions, the total amount of lanthanide salts was constant. For the LaF<sub>3</sub>:Eu nanoparticles with the different ligand ratios, the amount of NaF, lanthanide salts and solvent were kept constant and only the concentration of ligand was varied.

**Size selective precipitation.** Methanol was added dropwise to a solution of LaF<sub>3</sub>:Eu in toluene (1g/50 ml). The solution became cloudy after the addition of about 45 ml of methanol. This cloudy solution was stirred overnight and the precipitate separated by centrifugation. A few drops of methanol were added to the supernatant until the solution was cloudy again and this was stirred overnight again. The procedure was repeated 7 times until no precipitate was formed anymore after addition of methanol.

Photophysical measurements were performed using the setup described in chapter 3.

### 4.5 References and notes

- <sup>1</sup> Meltzer, R. S.; Yen, W. M.; Zheng, H.; Feofilov, S. P.; Dejneka, M. J. *Phys. Rev. B* **2001**, *64*, 100201.
- <sup>2</sup> Krebs, J. K.; Feofilov, S. P.; Kaplyanskii, A. A.; Zakharchenya, R. I.; Happek, U. *J. Lumin.* **1999**, *83-84*, 209.
- <sup>3</sup> Yan, C. H.; Sun, L. D.; Liao, C. S.; Zhang, Y. X.; Lu, Y. Q.; Huang, S. H.; Lü, S. Z. *Appl. Phys. Lett.* **2003**, *82*, 3511.
- <sup>4</sup> Meltzer, R. S.; Yen, W. M.; Zheng, H.; Feofilov, S. P.; Dejneka, M. J.; Tissue, B.; Yuan, H. B. *J. Lumin.* **2001**, *94-95*, 217.
- <sup>5</sup> Schuurmans, F. J. P.; de Lang, D. T. N.; Wegdam, G. H.; Sprik, R.; Lagendijk, A. *Phys. Rev. Lett.* **1998**, *80*, 5077.
- <sup>6</sup> Schuurmans, F. J. P.; Lagendijk, A. *J. Chem. Phys.* **2000**, *113*, 3310.
- <sup>7</sup> Riwotsky, K.; Meysamy, H.; Kornowski, A.; Haase, M. *J. Phys. Chem. B* **2001**, *104*, 2824.
- <sup>8</sup> Browne, W. R.; Vos, J. G. *Coord. Chem. Rev.* **2001**, *219-221*, 761.



- <sup>9</sup> (a) Crosswhite, H. M.; Moos, H. W. *Optical properties of ions in crystals*; Interscience Publishers: New York, 1967, p 467; (b) Hsu, C.; Powell, R. C. *J. Lumin.* **1975**, *10*, 273; (c) Dexpert-Ghys, J.; Mauricot, R.; Faucher, M. D. *J. Lumin.* **1996**, *69*, 203.
- <sup>10</sup> Lian, R.; Yin, M.; Zhang, W.; Lou, L; Krupa, J. C. *J. Alloy. Compd.* **2000**, *311*, 97.
- <sup>11</sup> Weber, M. J.; Matsinger, B. H.; Donlan, V. L.; Surrat, G. T. *J. Phys. Chem.* **1972**, *57*, 562.
- <sup>12</sup> In cross-relaxation processes the energy of a highly excited state of an ion is transferred to a neighbouring ion in the ground state promoting it to an excited state. This process can be positive leading to two ions in the right excited state or negative leading to two ions in the wrong levels. In up-conversion two ions in the excited state couple in a way that when one ion decays to the ground state it transfers its energy to the other ion promoting it to a higher excited level. This can lead to the emission of a photon of higher energy or to non-radiative decay to the first excited level.
- <sup>13</sup> Snoeks, E.; Lagendijk, A.; Polman, A. *Phys. Rev. Lett.* **1995**, *74*, 2459.
- <sup>14</sup> Blasse, G.; Grabmeier, B. C. *Luminescent materials*; Springer: Berlin, 1994.
- <sup>15</sup> Hostetler, M. J.; Wingate, J. E.; Zhong, C. J.; Harris, J. E.; Vachet, R. W.; Clark, M. R.; Londono, J. D.; Green, S. J.; Stokes, J. J.; Wignall, G. D.; Glish, G. L.; Porter, M. D.; Evans, N. D.; Murray, R. W. *Langmuir* **1998**, *14*, 17.
- <sup>16</sup> Murray, C. B.; Norris, D. J.; Bawendi, M. G. *J. Am. Chem. Soc.* **1993**, *115*, 8706.

#### 4.A.1 Modeling the luminescence decay

When it is assumed that most of the quenching of the excited state is located close to the surface, a model can be designed taking into account these surface effects. Ions in the core of the particles will have the longest lifetime and going to the outside the lifetime will decrease. When a particle is divided into a number of shells, the lifetime of one shell can be related to the lifetime in another shell by an effective radiative lifetime and a quenching factor that is dependent on the distance to the surface. The luminescence decay can thus be described using Equation 4.A.1.

$$\frac{I_t}{I_0} = \sum_{i=1}^n \frac{1}{n} e^{-k_i t}; k_i = \frac{1}{\tau_i} = k_R + C \times f_{q,i} \quad (\text{Eq. 4.A.1})$$

In this equation  $I_t$  is the luminescence intensity at time  $t$ ,  $I_0$  the intensity at  $t = 0$ ,  $n$  the number of shells,  $k_i = 1/\tau_i$  the rate constant in shell  $i$ , with  $\tau_i$  the luminescent lifetime of this shell,  $t$  the time,  $k_R$  a rate constant in the absence of quenching from outside the particle so it is an apparent radiative decay rate, and  $C$  the quenching constant. This constant is a fit parameter that is dependent on the individual ion, the size and size distribution of the particles, and on the strength of the quenching. The relative quenching factor  $f_{q,i}$  takes into account the distance of a shell to the surface and the distance dependence of the quenching. When quenching is assumed to take place via a dipole-dipole mechanism, the quenching has a distance dependence of  $r^{-6}$ .<sup>1</sup> The total quenching then has to be integrated over the total volume outside the nanoparticle. Integration over the total volume gives the total quenching factor  $f_{q,i}$  (Equation 4.A.2).

$$f_{q,i}(a_i) = \int_V r^{-6} dV \quad (\text{Eq. 4.A.2})$$

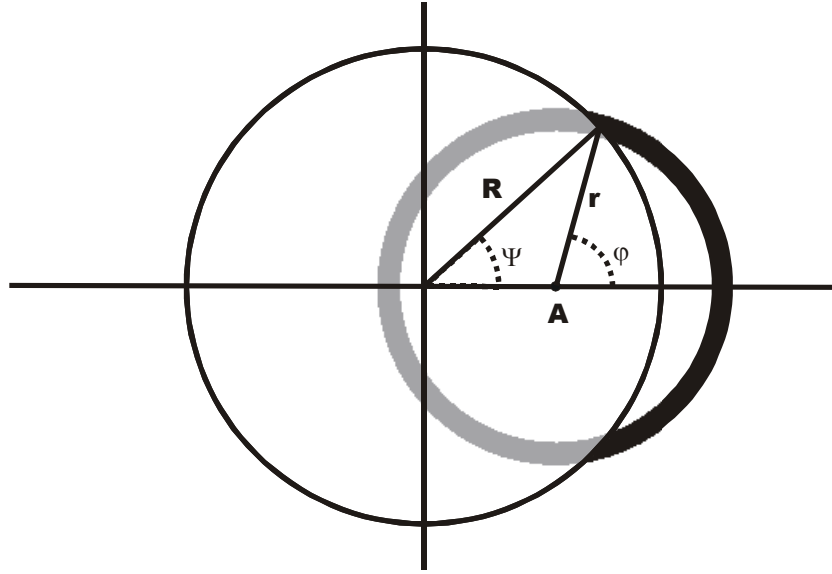


Figure 4.A.1: Definition of symbols used in the text.

This equation was solved for a particle shell  $i$ , with  $a_i = A_i/R_i$  as the center of each shell, by varying the radius  $r$  (Figure 4.A.1). Three domains can be defined. The first domain is totally inside the particle ranging from  $r = 0$  to  $r = (R-A)$ , so for this domain no quenching is taken into account. In the second domain the volume fraction  $d[V(r,\varphi)]$  is dependent on both the radius and the angle  $\varphi$  (part of the shell is inside the particle with no quenching and part is outside the shell, but with quenching). This domain ranges from  $r = (R-A)$  to  $r = (R+A)$  (Figure 4.A.1). The third domain lies totally out of the particle and is from  $r = (R+A)$  to  $\infty$ . The fraction of a shell in the second domain that is outside the particle equals  $2\pi r^2 (1-\cos\varphi)dr$ . The volume fraction  $dV$  of a shell in the third domain is  $4\pi r^2 dr$ . Multiplying this with  $r^{-6}$  results in Equation 4.A.3, that was numerically solved for a particle consisting of 10 shells of equal volume.<sup>2</sup> Assuming that the ions are randomly distributed in the particle it will give all ions the same weight in the fit.

$$f_{q,i}(A,\varphi) = \int_V r^{-6} dV = \int_{R-A}^{R+A} \frac{1}{r^6} 2\pi r^2 (1-\cos\varphi) dr + \int_{R+A}^{\infty} \frac{1}{r^6} 4\pi r^2 dr \quad (\text{Eq. 4.A.3})$$

This results in relative quenching factors for the different shells as shown in Table 4.A.1.

Table 4.A.1: Quenching factor for the ten shells.

Shell i	$a_i$	$f_{q,i}(a_i)$
1	0.23	4.9
2	0.52	11
3	0.63	19
4	0.70	32
5	0.77	63
6	0.82	121
7	0.87	$3.0 \cdot 10^2$
8	0.91	$8.6 \cdot 10^2$
9	0.95	$4.9 \cdot 10^3$
10	0.98	$7.7 \cdot 10^4$

Using this model a radiative lifetime and a quenching constant is obtained. For all of the ten shells a luminescence lifetime is calculated and an average lifetime of these ten values can be calculated using Equation 4.A.4.<sup>3</sup>

$$\tau_{av} = \frac{\sum A_i \tau_i^2}{\sum A_i \tau_i} \quad (Eq. 4.A.4)$$

In this equation,  $\tau_i$  is the lifetime of each shell and  $A_i$  the weight of each shell. The weight of each shell is the same i.e. 0.1 for 10 shells, so it can be taken out of the equation. This intensity-average lifetime is equal to the average time a fluorophore spends in the excited state.

#### 4.A.2 References and notes

- <sup>1</sup> Ermolaev, V. L.; Sveshnikov, E. B. *Russ. Chem. Rev.* **1994**, *63*, 905.
- <sup>2</sup> The choice to take ten shells is an arbitrary choice. Fitting with 6 shells gave the same results, but more shells could increase the accuracy of the fit.
- <sup>3</sup> Sillen, A.; Engelborghs, Y. *Photochem. Photobiol.* **1998**, *67*, 475.

# CHAPTER 5

## *Surface modification of lanthanide(III)-doped nanoparticles*

*Lanthanide-doped luminescent nanoparticles can be used as functional materials in polymer-based optics. The solubility of the nanoparticles is determined by the surface and the surface also has a major influence on the optical properties of the lanthanide ions. Control over the solubility can be obtained by coordinating various functionalized ligands to the surface of the nanoparticles. In this chapter the exchange of ligands used in the synthesis of the nanoparticles is discussed together with the reaction of functionalized ligands with the nanoparticle surface. The growth of an inorganic shell around the nanoparticles is also discussed. With this inorganic shell the luminescence properties of the lanthanide ions in the nanoparticles can be improved significantly. This improvement is demonstrated by an increase in the luminescence quantum yield and an increase in the luminescence lifetime of the lanthanide ions.*

## 5.1 Introduction

Particles on the nanometer scale consist for a large part of surface atoms. Control over the surface of these nanoparticles is important to obtain control over the physical properties of the nanoparticles.<sup>1</sup> Nanoparticles that are soluble in organic solvents usually have organic ligands coordinated to the surface. This ligand is present to control the nanoparticle growth and to keep the nanoparticles from aggregating after the synthesis. Using ligands with functional groups could change the solubility of the nanoparticles. The synthesis of nanoparticles in organic solvents usually involves ligands with straight alkyl chains, making the nanoparticles soluble in apolar organic solvents.<sup>2</sup> The use of ligands functionalized with for instance hydroxyl groups would yield nanoparticles that are soluble in short chain alcohols.<sup>3</sup> The introduction of functionalized ligands has been used to induce a phase transfer of nanoparticles synthesized in water to make them soluble in organic solvents.<sup>4</sup> The introduction of functionalized ligands is also used to induce ordering in nanoparticle systems. DNA strands on the surface of gold and CdSe nanoparticles have been used to make ordered structures, by the complementary binding of the DNA strands.<sup>5</sup> Complementary groups like amines and carboxylic acids have also been used to induce aggregation of binary nanoparticle systems.<sup>6</sup> The functional groups can be introduced by an exchange reaction, in which the ligand used in the synthesis of the nanoparticles is partially or completely substituted for the ligand bearing the functional group.<sup>7</sup> In some cases it is also possible to perform the synthesis with ligands bearing the functional group, but in this case the functional group should of course not be interfering in the reaction.<sup>8</sup> Control over coordinated ligands is very important, for the control over the processability and the assembly behavior of nanoparticle systems. The use of nanoparticles in polymer systems requires the optimization of several steps, including the solvent and solubility of the nanoparticles when spin-coating is being used.

Quenching of the luminescent nanoparticles mainly occurs from the surface, where the high-energy vibrations of the surrounding molecules are located. Coordinating ligands can help to prevent the quenching of the excited state, but an inorganic surface coating has proved to be more successful.<sup>9</sup> In these so called core-shell nanoparticles the original luminescent core is coated with an inorganic shell that protects the original core from the environment. This process has proven to be very efficient in enhancing the optical properties of luminescent semiconductor nanoparticles. The quantum yield of CdSe can be increased from a few percent to more than 50 % by the overcoating with a CdS shell.<sup>9</sup> The CdS overcoating confines the hole of the exciton to

the core of the nanoparticle, leading to increased photostability and increased quantum yield. Surface modification has also been applied to mask the toxic properties of semiconductor nanoparticles, to make them applicable in biological systems.<sup>10</sup> One known pathway for the quenching of lanthanide luminescence is the energy transfer over neighbouring lanthanide ions, until a quenching site is met.<sup>11</sup> It is likely that this quenching site is located at the surface of the nanoparticles, because here, the high-energy vibrations of chemical bonds are located, in the form of ligands, water, or other solvents. In nanoparticles, the distance to the surface is always small and quenching at surface sites can play a major role. A core-shell structure, in which the core is doped with the lanthanide ion and the shell is not doped, could confine the excited state well away from the surface and in this way reduce surface quenching. Haase *et al.* reported the influence of different solvents on the luminescence quantum yield of lanthanide-doped LaPO<sub>4</sub> nanoparticles and suggested that surface modification might increase the quantum yield of these nanoparticles.<sup>12,13</sup>

In this chapter, the surface modification of LaF<sub>3</sub> and LaPO<sub>4</sub> nanoparticles is discussed. First, the organic molecules bound to the surface of the nanoparticles are varied to alter the solubility properties of the nanoparticles. In the second part, the synthesis of core-shell nanoparticles is discussed. The luminescent nanoparticles are also coated with an inorganic shell to enhance the luminescent properties of the nanoparticles.

## 5.2 Results and discussion

### 5.2.1 Surface modification of LaF<sub>3</sub> and LaPO<sub>4</sub> nanoparticles

**Surface modification of LaF<sub>3</sub> nanoparticles.** One way of substituting a ligand for another ligand is by an exchange reaction.<sup>7</sup> The LaF<sub>3</sub> nanoparticles were synthesized with ligands **1** and **2** (Figure 5.1) as described in chapter 3. These ligands have a dithiophosphate headgroup, which binds weakly to the nanoparticle surface, to allow the growth of the nanoparticles, but coordinates strongly enough to prevent aggregation of the nanoparticles. Oxygen bearing coordinating groups have a higher binding affinity towards lanthanide ions and examples of such ligands would be dioctadecyl phosphate and oleic acid (ligands **3** and **4**) in Figure 5.1, with a phosphate group or a carboxylic acid group, respectively.

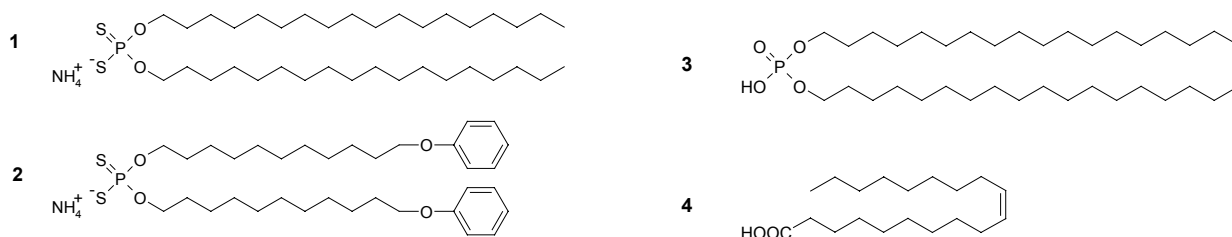


Figure 5.1: Ligands used in the synthesis and for the exchange of  $\text{LaF}_3$  nanoparticles.

The ligands used in the synthesis were exchanged by stirring a nanoparticle solution with ligand **3** or **4** and a small amount of base to ensure the deprotonation of the coordinating group. The exchange reactions of these ligands on the nanoparticles were monitored using  $^1\text{H}$  NMR spectroscopy. Figure 5.2 shows the result of nanoparticles synthesized with ligand **2** and exchanged with the phosphate ligand **3**.

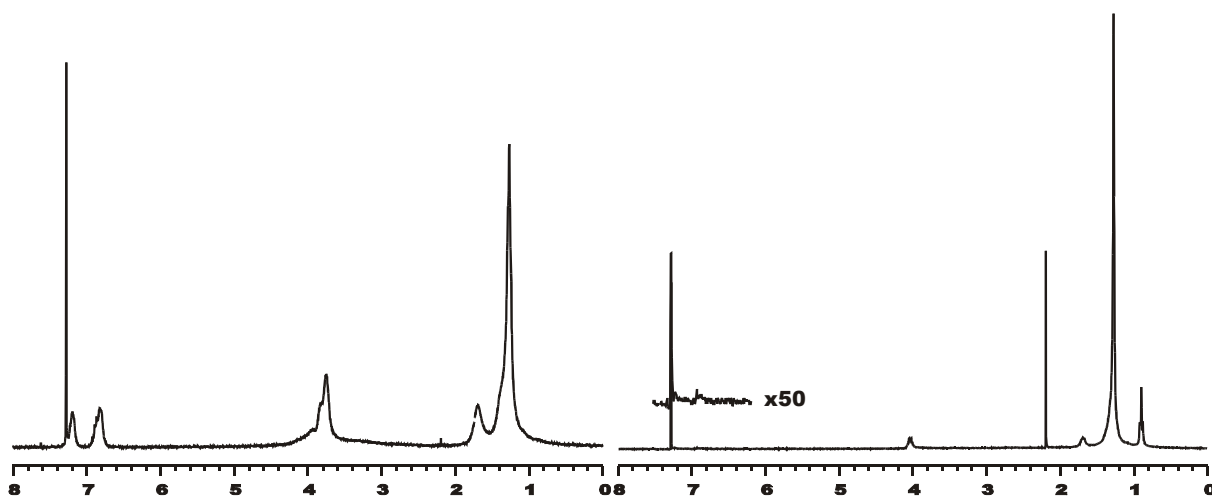


Figure 5.2:  $^1\text{H}$  NMR spectra of  $\text{LaF}_3$  nanoparticles synthesized with ligand **2** (left) and after exchange with ligand **3** (right).

The  $^1\text{H}$  NMR spectrum of the nanoparticles obtained after the synthesis shows broadened signals of the ligand due to coordination of the ligand to the nanoparticle surface. This broadening of the NMR signals of nanoparticle bound ligands can be ascribed to the inhomogeneous distribution of the magnetic environment around the nanoparticle and a reduction in rotational freedom of the ligand.<sup>14,15</sup> No free ligand is present, because no sharp signals are observed for unbound ligand in solution. A complete exchange of the dithiophosphate ligand was accomplished as can be seen in the  $^1\text{H}$  NMR spectrum of the exchanged product. The aromatic proton signals at 6.8 and 7.2 ppm of the dithiophosphate ligand have disappeared and the triplet of the  $\text{CH}_3$  endgroup of the phosphate ligand is present at 0.9 ppm. The ligand exchange is accompanied by a small change in solubility. Before the exchange the nanoparticles



were not soluble in apolar aliphatic solvents like hexane or pentane, but after the exchange they were. This is a confirmation that before the exchange the surface of the nanoparticles consists of the aromatic groups of the ligand making the nanoparticles soluble in aromatic solvents like toluene. After the exchange the surface of the nanoparticles consists of the CH<sub>3</sub> endgroups making the nanoparticles also soluble in hexane and pentane. Figure 5.3 shows the <sup>1</sup>H NMR spectrum of LaF<sub>3</sub> nanoparticles synthesized with ligand **1**, before and after the exchange with an excess of oleic acid. The ligands all contain long alkyl chains and in the proton spectrum these are mainly located between 0.9 and 2 ppm. It is difficult to observe changes in this region of the spectrum except for changes in the intensities. The <sup>1</sup>H NMR signals of the protons next to the functional groups are shifted downfield and were used to monitor the exchange reaction.

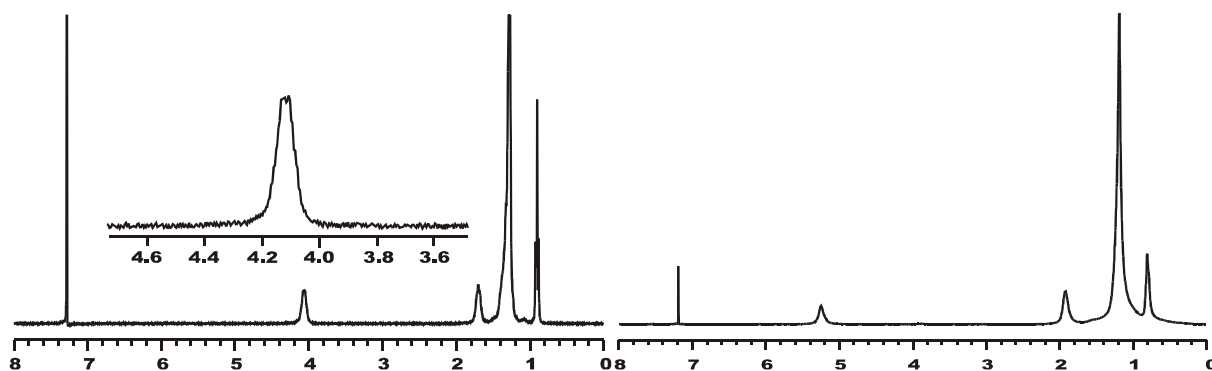
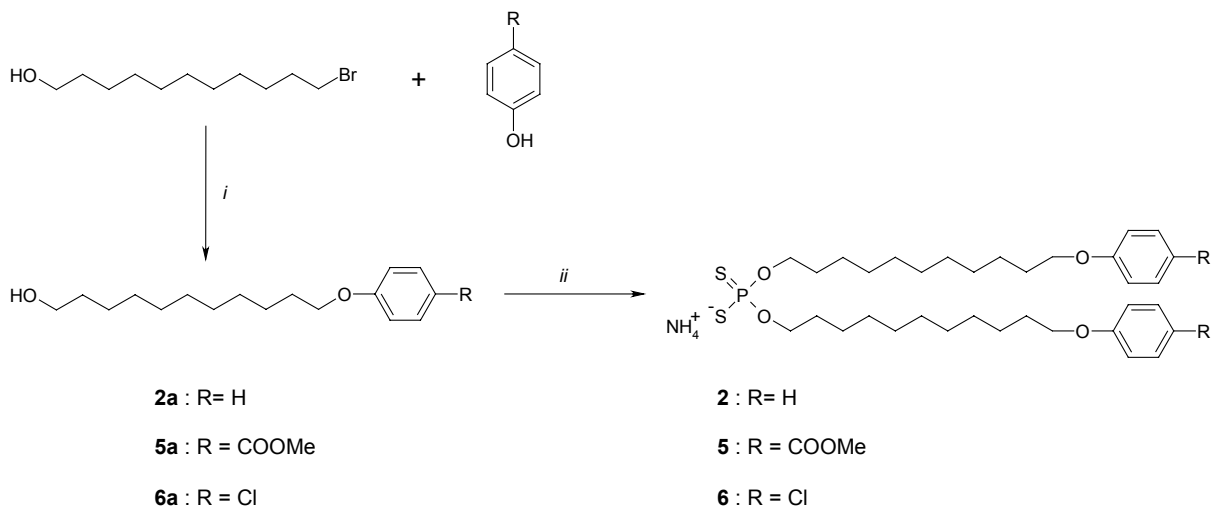


Figure 5.3: <sup>1</sup>H NMR spectrum of LaF<sub>3</sub> nanoparticles synthesized with ligand **1** before (left) and after (right) the exchange with oleic acid. The left picture shows an enlargement of the broad peak of the protons next to the dithiophosphate group.

The left spectrum in Figure 5.3 shows the nanoparticles with ligand **1**. The spectrum of the free ligand has a characteristic double triplet at 4.1 ppm of the protons next to the phosphorous atom (not shown), but on the nanoparticles the signal is broadened and only a single broad peak is observed. The spectrum on the right shows the broadened signals of the oleate ligand coordinated to the surface of the nanoparticles after the exchange reaction. The exchange is complete, because the signal of ligand **1** at 4.1 ppm is absent and a peak of oleate at 5.2 ppm of the protons on the double bond is observed. These results confirm that the ligand used in the synthesis of LaF<sub>3</sub> nanoparticles can be exchanged completely for another ligand with a more strongly coordinating group. This provides a straightforward method for the introduction of functional groups at the surface of the nanoparticles. The stability of the nanoparticles was not much influenced. Apparently, the coordination of the ligand to the nanoparticle surface is not the limiting factor for the stability, but the size of the hydrocarbon tails most likely is.

Another possibility to functionalize the surface of the LaF<sub>3</sub> nanoparticles is to carry out the synthesis with ligands that already have functional groups. This is probably the most straightforward way to tune the solubility of the nanoparticles in different solvents. A synthesis route to obtain functionalized dithio ligands is shown Scheme 5.1.



*Scheme 5.1: Synthesis route for functional dithio-phosphate ligands: i: K<sub>2</sub>CO<sub>3</sub>, acetonitril, reflux, yield: 99 %; ii: P<sub>2</sub>S<sub>5</sub>, NH<sub>3</sub>, yield: 60 %.*

The synthesis of these ligands is similar to the synthesis of ligand **2**, using a functionalized phenol instead of phenol. Every functionality that does not interfere in the second step of the reaction can be used, making this a versatile method to functionalize the surface of the LaF<sub>3</sub> nanoparticles. Nanoparticles synthesized with these ligands do show different solubilities. Nanoparticles synthesized with ligand **2** are soluble in apolar solvents like, toluene, dichloromethane, and chloroform. Nanoparticles synthesized with ligand **5** are soluble in solvents containing ester and ketone groups like, ethylacetate, cyclopentanone, and  $\gamma$ -butyrolactone. The last two solvents are commonly used for the spin-coating of polymer solutions. The optical properties of the nanoparticles are independent of the functionalities of the ligand, so the functionalities do not interfere in the formation of the inorganic core of the nanoparticles. The same luminescence spectrum and luminescence lifetime were measured and no change in the nanoparticle cores was observed with TEM.

**Surface modification of LaPO<sub>4</sub> nanoparticles.** The surface of LaPO<sub>4</sub> nanoparticles consists of phosphate groups and some coordinated diphosphate ligands originating from the decomposition of the solvent. The surface of the nanoparticles is covered with OH groups of the phosphate groups, which provide the opportunity to bind molecules covalently to the surface.

The presence of the OH groups was proven by solubility experiments. Directly after the synthesis, the nanoparticles were soluble in polar aprotic solvents, like DMF and DMSO. This means that the surface has a polar nature, which is inconsistent with a full coverage with ethylhexyl chains of the coordinating solvent. A full coverage with these apolar ligands should make the nanoparticles soluble in apolar solvents, like hexane, toluene, and dichloromethane. The nanoparticles can be solubilized in alcohols, such as methanol and iso-propanol by the addition of tetraalkylammonium hydroxides. The addition of tetraalkylammonium bromides does not lead to solubility in the alcohols, proving that the base is necessary to deprotonate surface OH groups. Deprotonation of the surface OH groups leads to a negatively charged surface, that makes the coordination of the positively charged ammonium ions possible. Surface functionalization could involve the reaction of the surface OH groups with alcohols, to form phosphate esters. The OH groups of the surface phosphate groups were converted into chlorides by a reaction with phosphorus oxychloride. The surface of the nanoparticles could subsequently be functionalized by a reaction with an excess of dodecanol. The  $^1\text{H}$  NMR of this product is shown in Figure 5.4.

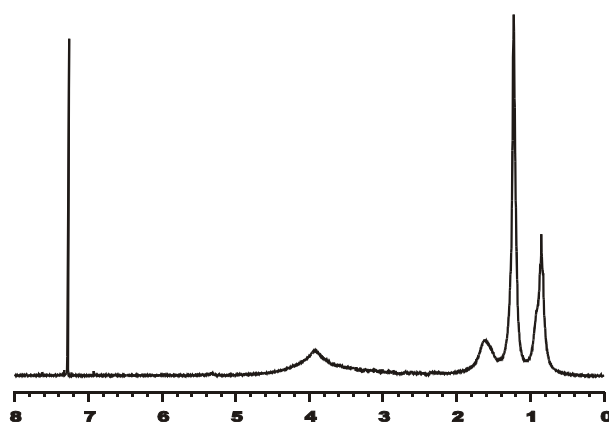


Figure 5.4:  $^1\text{H}$  NMR of  $\text{LaPO}_4$ , surface modified by a reaction with dodecanol.

The  $^1\text{H}$  NMR signals of the dodecane chains are broadened due to the binding to the nanoparticles surface. The  $\text{LaPO}_4$  nanoparticles before surface functionalization were only soluble in polar aprotic solvents like DMSO and DMF, but after the surface modification the nanoparticles are soluble in apolar solvents like toluene, chloroform, and dichloromethane. The reaction of phosphorus oxychloride with the nanoparticles is a rigorous method to introduce the chlorides to the surface of the nanoparticles and they were further characterized. TEM pictures of the reaction product showed that the nanoparticle cores are still intact and that no change in nanoparticle size and size distribution had occurred. Elemental analysis confirmed the presence of about 10 % organic material in the product, which is consistent with a monolayer formation

around 5 nm sized nanoparticles. Luminescence studies also revealed no change in the environment of the  $\text{Eu}^{3+}$  ion when the surface modification was performed on  $\text{Eu}^{3+}$ -doped nanoparticles as shown in Figure 5.5. The luminescence spectra have the same line positions and the same peak splitting showing that the  $\text{Eu}^{3+}$  ion is still in the  $\text{LaPO}_4$  matrix.

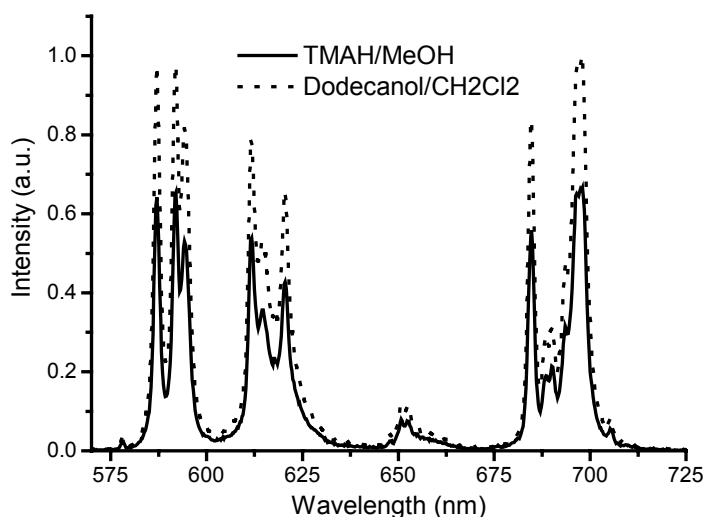


Figure 5.5: Emission spectra of  $\text{LaPO}_4:\text{Eu}$  nanoparticles in methanol with tetramethylammonium hydroxide (TMAH) and after the surface reaction with dodecanol. The difference in intensity is for clarity.

This reaction can thus be used to make the nanoparticles hydrophobic and soluble in apolar solvents. The reaction also offers a way to introduce other functional groups on the surface of the nanoparticles, making the tunability of the solubility properties possible. Haase *et al.* reported the surface modification of  $\text{LaPO}_4$  nanoparticles, by heating them in dodecylamine.<sup>16</sup> These nanoparticles with dodecylamine coordinated to the surface were also soluble in apolar solvents and could be precipitated from solution by the addition of methanol.

### 5.2.2 Synthesis of core-shell nanoparticles of $\text{LaF}_3$

The synthesis of core-shell nanoparticles can be an easy way to enhance the luminescence properties of lanthanide-doped nanoparticles, because interaction with the high-energy vibrations of the surrounding organic environment can be reduced in this way. A schematic representation of such a core-shell nanoparticle is shown in Figure 5.6. All the lanthanide ions involved in the luminescence of the nanoparticle are doped in the core and therefore have no direct interaction with the surface of the nanoparticle.

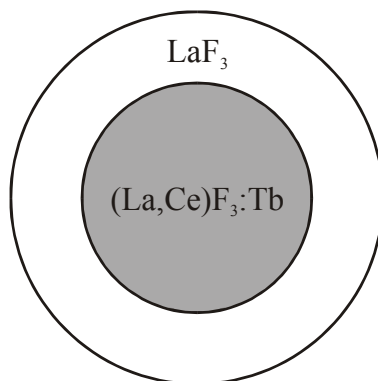


Figure 5.6: Schematic representation of a core-shell nanoparticle, with a  $(\text{La,Ce})\text{F}_3:\text{Tb}$  core and a  $\text{LaF}_3$  shell.

In the previous chapter it was shown that the sizes of  $\text{LaF}_3$  nanoparticles could be manipulated by changing the ratio of the ligand and reagents that form the core. This is a strong indication that the nanoparticles form after an initial nucleation followed by growth after the addition of more reagent. This mechanism allows the growth of a core-shell structure in a one-pot synthesis, by a stepwise addition of reagents. In the core-shell experiments, ammonium fluoride was used instead of sodium fluoride as the fluoride precursor, because this salt shows a higher solubility in water, making it possible to add fluoride precursor, dissolved in a small amount of water, to the reaction mixture. Core-shell nanoparticles with a core of  $\text{La}_{0.4}\text{F}_3\text{Ce}_{0.45}\text{Tb}_{0.15}$  and a shell of  $\text{LaF}_3$  were synthesized to study the influence of the shell on the quantum yield of the nanoparticles. During the growth of the shell no additional nucleation should occur, because this would result in the formation of un-doped nanoparticles. The size of the nanoparticles is a good indication for this. The size of the nanoparticles should increase, roughly corresponding to an increase in volume that is similar to the amount of shell material added. The nanoparticle sizes before and after the growth of an un-doped shell around a  $(\text{La,Ce})\text{F}_3\text{Tb}$  core were measured using TEM. Figure 5.7 shows typical TEM pictures of core nanoparticles and core-shell nanoparticles, with the corresponding size distribution histograms. A growth of the nanoparticles is clearly observed from 7.0 nm with a size distribution of 28.1 % for the core nanoparticles, to 9.0 nm with a size distribution of 22.7 % for the core-shell nanoparticles, when the same amount of reagent was used for the shell as for the initial core. This increase in size corresponds to an increase in volume by a factor of 2, indicating that all of the added monomer had grown on the existing core nanoparticles and no new nucleation had occurred. This is consistent with the finding in the previous chapter, in which nanoparticles with different sizes were synthesized by changing the amount of ligand. The size distribution is the

same in absolute value but because of the increased size it appears like it has narrowed. In this case the effective ligand ratio is also lowered after the addition of the shell monomer, making it possible to form larger nanoparticles.

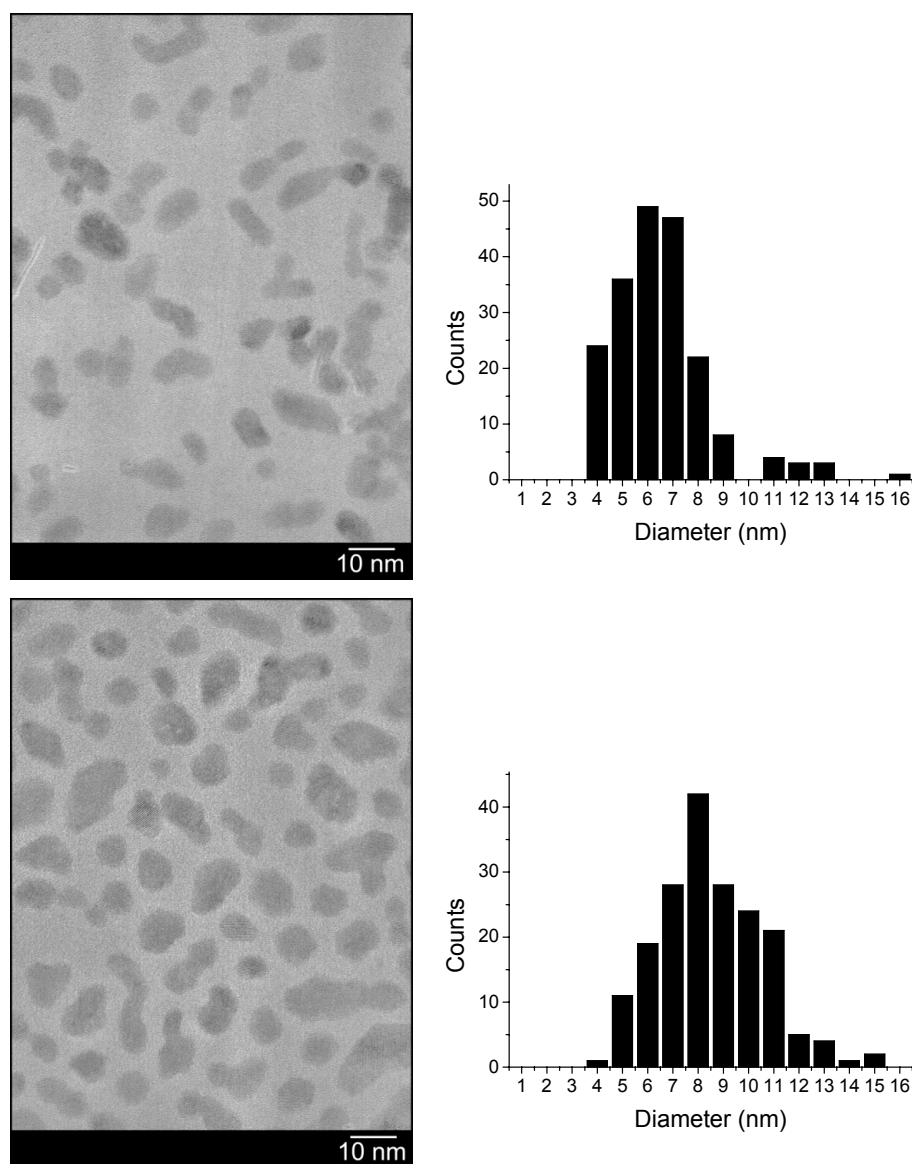


Figure 5.7: TEM pictures of  $\text{LaCeF}_3\text{Tb}$  nanoparticles with the corresponding size distribution histograms, core (top) and core-shell (down)

To determine the effect of the un-doped core around the nanoparticles, the quantum yields of  $\text{Ce}^{3+}$ - and  $\text{Tb}^{3+}$ -doped nanoparticles were determined by comparing the emission intensity with the emission intensity of quinine bisulfate. Upon excitation of the  $\text{Ce}^{3+}$  absorption band at 282 nm, one emission band of  $\text{Ce}^{3+}$  at 350 nm and four emission peaks of  $\text{Tb}^{3+}$  at 489, 543, 584, and 621 nm of the  $^5\text{D}_4 \rightarrow ^7\text{F}_J$  ( $J = 3-6$ ) were observed. The quantum yield of the emission was determined by measuring both the emission of  $\text{Ce}^{3+}$  and  $\text{Tb}^{3+}$ . Three methods were used to grow

a shell of LaF<sub>3</sub> around the core nanoparticles, which are described in the experimental section and differ only in the way the shell reagents were added to the reaction mixture.

*Table 5.1: Luminescence quantum yield of LaCeF<sub>3</sub>:Tb core shell nanoparticles.*

Nanoparticles	Quantum Yield (%)
No shell	24.4
Method 1	42.7
Method 2	41.7
Method 3	54.2
Reference <sup>a</sup>	27

a) In the reference experiment the nanoparticles have the same size as the core-shell nanoparticles, but they lack the core-shell structure

The quantum yields of the core nanoparticles were very similar to the quantum yields of the nanoparticles synthesized with NaF as the fluoride reagent, determined in chapter 3, as an indication that the source of the fluoride ion has no influence on the optical properties of the nanoparticles. All methods to synthesize shell material were successful according to the quantum yield measurements. The best method was to grow the shell material around the core by the alternate addition of small portions of the shell reagents. The quantum yield of nanoparticles coated in this way more than doubled. As a reference experiment, nanoparticles of the same size as the core-shell nanoparticles were synthesized, but lacking the core-shell structure, to check if the increase in quantum yield is not caused by the dilution of the luminescent ions. Nanoparticles synthesized in this way had a quantum yield of 27 %, only a little higher than the core nanoparticles, but clearly much lower than the core-shell nanoparticles. The higher quantum yield compared to the core nanoparticles could be a result of the increased size, reducing the overall surface quenching. The Ce<sup>3+</sup> emission in these diluted nanoparticles was stronger compared to the core and the core-shell nanoparticles indicating that energy transfer from Ce<sup>3+</sup> to Tb<sup>3+</sup> is less efficient due to an increase in the average distance between the Ce<sup>3+</sup> and Tb<sup>3+</sup> ions. From this experiment, it can be concluded that the increase in quantum yield is a result of the core-shell structure and not of nanoparticle size or a different distribution of the lanthanide ions in the nanoparticles.

Figure 5.8 shows the luminescence decay curves of both luminescent levels of the Eu<sup>3+</sup> ion in LaF<sub>3</sub> nanoparticles, with different equivalents of LaF<sub>3</sub> grown as a shell over the original core. The non-exponential decay of the <sup>5</sup>D<sub>0</sub> level is clearly observed and when one equivalent of shell

reagent was grown on the nanoparticles, a large change in the decay was observed. The decay becomes almost single exponential and an increase in the luminescence lifetime was observed. The luminescence lifetimes obtained by fitting with a bi-exponential decay are shown in Table 5.2. The increase in the luminescence lifetimes shows the increased shielding from quenching groups at the surface and the shift in the ratio of the two components of the luminescence lifetime shows that the decay was almost mono-exponential after the growth of a shell around the core.

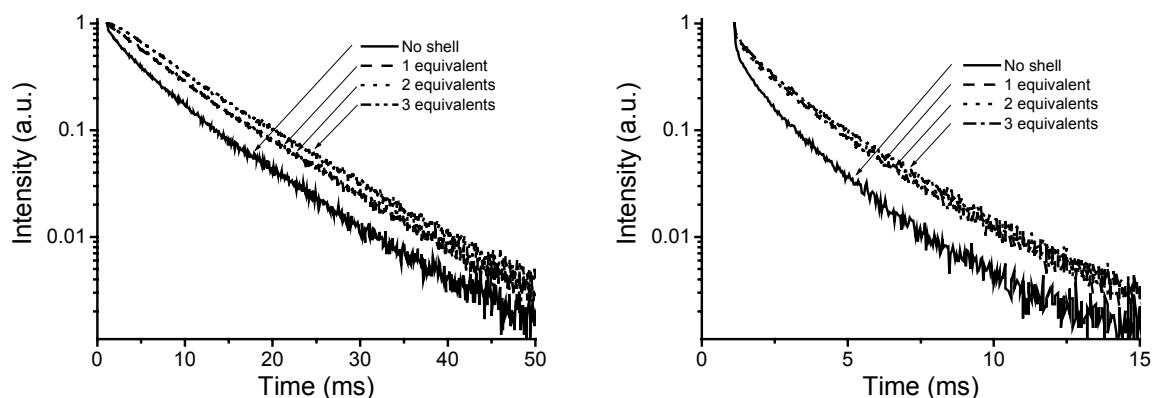


Figure 5.8: Luminescence decay curves of the  ${}^5D_0$  (left) and  ${}^5D_1$  (right) level of  $\text{Eu}^{3+}$  in  $\text{LaF}_3$  nanoparticles with a different amount of shell material in toluene.

Table 5.2: Luminescence lifetimes of the  ${}^5D_0$  and  ${}^5D_1$  level of  $\text{LaF}_3:\text{Eu}$  nanoparticles with different amount of  $\text{LaF}_3$  grown over the original core, in toluene.<sup>a,b</sup>

	${}^5D_0$		${}^5D_1$	
	$\tau_1$ (ms)	$\tau_2$ (ms)	$\tau_1$ (ms)	$\tau_2$ (ms)
no shell	7.9 (74 %)	3.1 (26 %)	2.0 (73 %)	0.65 (27 %)
1 equivalent	9.7 (5.8 %)	5.3 (42 %)	2.3 (83 %)	0.72 (17 %)
2 equivalents	9.9 (54 %)	5.6 (46 %)	2.4 (81 %)	0.78 (19 %)
3 equivalents	9.5 (69 %)	5.4 (31 %)	2.5 (82 %)	0.80 (18 %)

a) The percentages reflect the amount of the component contributing to the total lifetime.

b) The absolute errors in the fit are 0.2 ms in the lifetime and 5 % in the component contributing to the total lifetime.

The biggest change in the decay is observed after the addition of one equivalent of the shell material. The growth of more shell material has a smaller influence on the decay curve, but with the growth of three equivalents of  $\text{LaF}_3$  over the core, a small rise in the decay curve of the  ${}^5D_0$



level is observed. Due to the reduced quenching of the higher  $\text{Eu}^{3+}$  levels like the  $^5\text{D}_1$ ,  $^5\text{D}_2$ , and  $^5\text{D}_3$  levels the  $^5\text{D}_0$  level is populated more slowly in the core-shell nanoparticles, giving rise to a build-up in the luminescence from this level. Due to the rise in the decay the fitting of the decay curve was started 5 ms after the excitation pulse. As a result the values of the luminescence lifetimes for three equivalents of  $\text{LaF}_3$  are lower than for two equivalents of  $\text{LaF}_3$ . The effect of the shell on the luminescence lifetime of the  $^5\text{D}_1$  decay is also shown in Figure 5.8 and the corresponding lifetimes obtained after fitting with a bi-exponential decay are given in Table 5.2. The effect is similar to what was observed for the  $^5\text{D}_0$  level. The growth of one equivalent of  $\text{LaF}_3$  is enough to increase the luminescence lifetime substantially and a thicker shell only has a small influence on the luminescence lifetime. Emission of  $\text{Eu}^{3+}$  from the  $^5\text{D}_2$  level is located between 460 and 520 nm. The  $\text{LaF}_3:\text{Eu}$  core nanoparticles do not show emission from this level, but in the core-shell nanoparticles emission peaks from this level were visible, due to the reduced quenching. The emission spectra are shown in Figure 5.9.

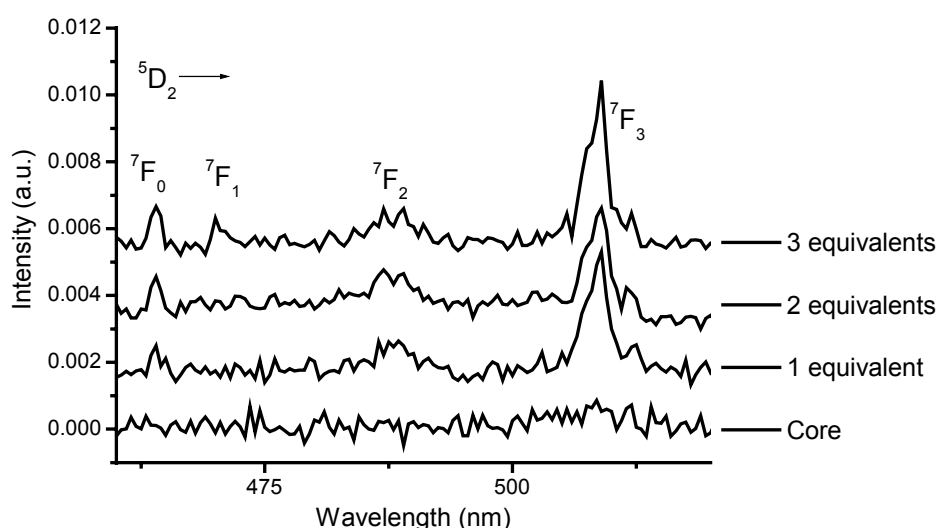


Figure 5.9: Emission of the  $^5\text{D}_2$  level of  $\text{Eu}^{3+}$  in core-shell nanoparticles. The spectra are normalized to the emission of the  $^5\text{D}_0 \rightarrow ^7\text{F}_1$  emission peak. The offset is for clarity.

After the growth of  $\text{LaF}_3$  shell material emission lines start to appear at 464, 472, 489, and 509 nm of the  $^5\text{D}_2 \rightarrow ^7\text{F}_J$  ( $J = 0-3$ ) transitions, respectively. These lines become more intense after the growth of more shell material, indicating reduced quenching of the  $^5\text{D}_2$  level. Emission from the  $^5\text{D}_2$  level is also observed in the bulk material at this  $\text{Eu}^{3+}$  concentration, at room temperature.<sup>17</sup>

### 5.3 Conclusions

The solubility of LaF<sub>3</sub> and LaPO<sub>4</sub> nanoparticles can be varied by changing the ligands that are coordinated to the surface of the nanoparticles. Surface quenching of lanthanide-doped nanoparticles was reduced by the synthesis of core-shell nanoparticles. The synthesis of an un-doped shell around the nanoparticles reduces the quenching of lanthanide ions that are doped in the core of the nanoparticles.

### 5.4 Experimental section

Oleic acid and octadecanol were purchased from Fluka. Phosphorus oxychloride was purchased from Acros. THF was freshly distilled from Na/benzophenon. <sup>1</sup>H NMR measurements on nanoparticles were performed on un-doped nanoparticles to exclude the influence of the paramagnetic nature of some of the luminescent lanthanide ions.

**Ligand 3.** A solution of 5 g (18.5 mmol) of octadecanol in 20 ml of anhydrous THF was slowly dropped into 1.42 g (9.2 mmol) of OPCl<sub>3</sub> at -15 °C under Ar. The solution was slowly allowed to warm to room temperature and stirred for two hours. After the addition of 1 ml of water, the solution was vigorously stirred for 1 hour, followed by the addition of 100 ml of ethyl acetate. The organic phase was separated and washed three times with 1 N HCl. The organic layer was dried over MgSO<sub>4</sub> and evaporated to dryness. The residue was dissolved in 20 ml of hexane and NH<sub>3</sub> was bubbled to the solution. The precipitate was filtered, washed with hexane, and dried. To substitute the ammonium counterion for a proton, the product was taken up in ethyl acetate and washed three times with 1 N HCl. The organic layer was dried over MgSO<sub>4</sub> and evaporated to dryness. A white solid remained, yield 2.9 g, 53 %, m.p. 71-73 °C. <sup>1</sup>H NMR (CDCl<sub>3</sub>): δ 4.1 (dt, *J* = 7.0, 6.6 Hz, 4H), 1.7 (m, 4H), 1.3 (m, 60 H), 0.9 (t, *J* = 6.6 Hz, 6H); MS (FAB) *m/z* = 602.5 [(M<sup>+</sup>), calcd. for C<sub>36</sub>H<sub>75</sub>O<sub>4</sub>P: 603.0]; Anal calcd. for C<sub>36</sub>H<sub>75</sub>O<sub>4</sub>P: C, 71.71; H, 12.54. Found: C, 71.45; H, 12.80.

**Compound 5a** was synthesized by refluxing overnight a mixture of; 10 g (39.3 mmol) bromoundecanol, 7.78 g (51 mmol) of methyl-4-hydroxy benzoate, and 7.06 g (51 mmol) K<sub>2</sub>CO<sub>3</sub> in 100 ml of acetonitril. The mixture was cooled to room temperature and 300 ml of ethylacetate were added. This solution was washed with 1 N NaOH three times and one time with water. The organic layer was dried over MgSO<sub>4</sub>, filtered, and the organic solvent removed under vacuum. A white solid remained, that was recrystallized from ethylacetate, yield 99 %, m. p. 69-71 °C. <sup>1</sup>H NMR (CDCl<sub>3</sub>): δ 8.1 (d, *J* = 8.8 Hz, 2H), 6.9 (d, *J* = 8.8 Hz, 2H), 4.0 (t, *J* = 6.2 Hz, 2H), 3.9 (s, 3H), 3.6 (dt, *J* = 6.6, 4.4 Hz, 2H), 1.8 (m, 2H), 1.6-1.4(m, 16H);

MS (FAB)  $m/z = 323.2 [(M+H)^+]$ , calcd. for  $C_{19}H_{31}O_4$ : 323.2]; Anal calcd. for  $C_{19}H_{30}O_4$ : C, 70.77; H, 9.38. Found: C, 70.88; H, 9.55.

**Ligand 5** was synthesized by heating 9.72 g (30 mmol) of compound **5a** with 1.91 g (8.6 mmol) of  $P_2S_5$  at 80 °C for 3 hours. The workup of this reaction was the same as for ligand **2** in chapter 3. The product was obtained as a white solid, in a yield of 73 %, m. p. 81-83 °C.  $^1H$  NMR (acetone- $d_6$ ):  $\delta$  7.9 (d,  $J = 9.2$  Hz, 4H), 7.0 (d,  $J = 9.2$  Hz, 4H), 4.1 (t,  $J = 6.6$  Hz, 4H), 3.9 (dt,  $J = 8.4, 6.6$  Hz, 4H), 3.8 (s, 6H), 1.8 (m, 4H), 1.5-1.3 (m, 32H); MS (FAB)  $m/z = 737.5 [(M-NH_4)^+]$ , calcd. for  $C_{38}H_{58}O_8PS_2$ : 737.0]; Anal calcd. for  $C_{38}H_{62}O_8PS_2N$ : C, 60.37; H, 8.27; N, 1.85; S, 8.48. Found: C, 59.87; H, 8.72; N, 1.95; S, 8.37.

**Compound 6a** was synthesized by refluxing overnight; 7.06 g (51 mmol) of  $K_2CO_3$ , 6.6 g (51 mmol) of 4-chlorophenol, and 10 g (39.3 mmol) of bromoundecanol in 100 ml of acetonitril. The workup of the reaction mixture was the same as for compound **5a**. The product was obtained as a white solid after recrystallization from hexane, in a yield of 98 %, m. p. 42-43 °C.  $^1H$  NMR ( $CDCl_3$ ):  $\delta$  7.3 (d,  $J = 9.2$  Hz, 2H), 6.8 (d,  $J = 9.2$  Hz, 2H), 3.9 (t,  $J = 6.6$  Hz, 2H), 3.7 (dt,  $J = 6.6, 5.1$  Hz, 2H), 1.8 (m, 2H), 1.6-1.3 (m, 16H); MS (FAB)  $m/z = 298.3 [M^+]$ , calcd. for  $C_{17}H_{27}O_2Cl$ : 298.2; Anal calcd. for  $C_{17}H_{25}O_2Cl$ : C, 68.79; H, 8.49. Found: C, 68.54; H, 8.35.

**Ligand 6** was synthesized by heating 9.7 g (32.5 mmol) of compound **6a** and 2.06 g (9.3 mmol) of  $P_2S_5$  at 80 °C for 3 hours. The workup of this reaction mixture was the same as for Ligand **5**. The product was a white solid obtained in 70 % yield, m. p. 57-60 °C.  $^1H$  NMR ( $CDCl_3$ )  $\delta$  7.2 (d,  $J = 9.2$  Hz, 4H), 6.8 (d,  $J = 8.8$  Hz, 4H), 4.0 (dt,  $J = 8.4, 6.9$  Hz, 4H), 3.9 (t,  $J = 6.6$  Hz, 4H), 1.8-1.7 (m, 8H), 1.4-1.3 (m, 28H); MS (FAB)  $m/z = 689.2 [(M-NH_4)^+]$ , calcd. for  $C_{34}H_{52}O_4PS_2Cl_2$ : 689.2]; Anal calcd. for  $C_{34}H_{56}O_4PS_2NCl_2$ : C, 57.61; H, 7.96; N, 1.98; S, 9.05. Found: C, 57.42; H, 8.05; N, 2.04; S, 9.20.

**Exchange reaction on  $LaF_3$  nanoparticles.** To a solution of 100 mg of  $LaF_3$  nanoparticles in 5 ml dichloromethane was added 100 mg of ligand **3** or **4** and 100  $\mu$ l of triethylamine. This solution was stirred overnight and methanol was added to precipitate the nanoparticles. The precipitate was separated by centrifugation and washed repeatedly with polar solvents like methanol, ethanol, or acetone, until no free ligand was observed in the  $^1H$  NMR spectrum.

**Surface modification of  $LaPO_4$  nanoparticles.** The surface phosphate groups of the nanoparticles were first reacted with phosphorus oxychloride by heating 100 mg of nanoparticles in 5 ml of  $OPCl_3$  for two hours at 120 °C. After two hours the solution was cooled to room temperature and the  $OPCl_3$  was evaporated under vacuum followed by the addition of 5 ml of toluene containing 1 ml of dodecanol. This solution was refluxed for two hours and then cooled to room temperature. To remove excess dodecanol

the nanoparticles were precipitated by the addition of 20 ml of methanol and separated by centrifugation. After washing a few times with methanol the nanoparticles were soluble in apolar solvent like toluene, dichloromethane, and chloroform.

**Core-shell nanoparticles.** LaF<sub>3</sub> core-shell nanoparticles were synthesized similar to the core nanoparticles described in chapter 3. NaF was substituted by NH<sub>4</sub>F because of an increased solubility in water. The core of the nanoparticles was synthesized by the dropwise addition of the lanthanide salts to the NH<sub>4</sub>F and ligand **1** in 35 ml of a water/ethanol mixture at 75 °C. This mixture was stirred for 10 min followed by the shell growth. To determine the best way of growing a shell around a core, several methods were tested.

*method 1.* After the synthesis of the core nanoparticles 3 mmol of NH<sub>4</sub>F was added dropwise followed by the drop-wise addition of 1.33 mmol of La(NO<sub>3</sub>)<sub>3</sub>.

*method 2.* The synthesis of the core nanoparticles was started with 6 mmol of NH<sub>4</sub>F and to this solution was first added the lanthanide salts for the core, followed after 10 min by the addition of La(NO<sub>3</sub>)<sub>3</sub> for the shell.

*method 3.* After the synthesis of the core, 3 mmol of NH<sub>4</sub>F and 1.33 mmol of La(NO<sub>3</sub>)<sub>3</sub> dissolved in 2 ml water were added alternately in 10 portions.

After the addition of the shell material, the solution was stirred for 2 more hours at 75 °C, after which it was cooled down to room temperature. The workup of the nanoparticle product was the same as described in chapter 3.

## 5.5 References and notes

- <sup>1</sup> Spanhel, L.; Haase, M.; Weller, H.; Henglein, A. *J. Am. Chem. Soc.* **1987**, *109*, 5649.
- <sup>2</sup> (a) Murray, C. B.; Norris, D. J.; Bawendi, M. G. *J. Am. Chem. Soc.* **1993**, *115*, 8706; (b) Brust, M.; Walker, M.; Bethell, D.; Schiffrin, D. J.; Whyman, R. *J. Chem. Soc., Chem. Commun.* **1994**, *7*, 801.
- <sup>3</sup> Brust, M.; Fink, J.; Bethell, D.; Schiffrin, D. J.; Kiely, C. *J. Chem. Soc., Chem. Commun.* **1995**, *16*, 1655.
- <sup>4</sup> Gaponik, N.; Talapin, D. V.; Rogach, A. L.; Eychmüller, A.; Weller, H. *Nano Lett.* **2002**, *2*, 803.
- <sup>5</sup> Mitchell, G. P.; Mirkin, C. A.; Letsinger, R. L. *J. Am. Chem. Soc.* **1999**, *121*, 8122.
- <sup>6</sup> Galow, T. H.; Boal, A. K.; Rotello, V. M. *Adv. Mater.* **2000**, *12*, 577.
- <sup>7</sup> Hostetler, M. J.; Templeton, A. C.; Murray, R. W. *Langmuir* **1999**, *15*, 3782.
- <sup>8</sup> Johnson, S. R.; Evans, S. D.; Brydson, R. *Langmuir* **1998**, *14*, 6639.
- <sup>9</sup> Peng, X.; Schlamp, M. C.; Kadavanich, A. V.; Alivisatos, A. P. *J. Am. Chem. Soc.* **1997**, *119*, 7019.

- <sup>10</sup> (a) Gerion, D.; Pinaud, F.; Williams, S. C.; Parak, W. J.; Zanchet, D.; Weiss, S.; Alivisatos, A. P. *J. Phys. Chem. B* **2001**, *105*, 8861; (b) Parak, W. J.; Gerion, D.; Zanchet, D.; Woerz, A. S.; Pellegrino, T.; Micheel, C.; Williams, S. C.; Seitz, M.; Bruehl, R. E.; Bryant, Z.; Bustamente, C.; Bertozzi, C. R.; Alivisatos, A. P. *Chem. Mater.* **2002**, *14*, 2113; (c) Schroedter, A.; Weller, H.; Eritja, R.; Ford, W. E.; Wessels, J. M. *Nano Lett.* **2002**, *2*, 1363.
- <sup>11</sup> Blasse, G.; Grabmeier, B. C. *Luminescent materials*; Springer: Berlin, 1994.
- <sup>12</sup> Riwozki, K.; Meyssamy, H.; Kornowski, A.; Haase, M. *J. Phys. Chem. B* **2000**, *104*, 2824.
- <sup>13</sup> Riwozki, K.; Meyssamy, H.; Schnablegger, H.; Kornowski, A.; Haase, M. *Angew. Chem. Int. Ed.* **2001**, *40*, 573.
- <sup>14</sup> Kuno, M.; Lee, J. K.; Dabbousi, B. O.; Mikulec, F. V.; Bawendi, M. G. *J. Chem. Phys.* **1997**, *106*, 9869.
- <sup>15</sup> Sachleben, J. R.; Wooten, E. W.; Emsley, L.; Pines, A.; Colvin, V. L.; Alivisatos, A. P. *Chem. Phys. Lett.* **1992**, *198*, 431.
- <sup>16</sup> Lehmann, O.; Meyssamy, H.; Kömpe, K.; Schnablegger, H.; Haase, M. *J. Phys. Chem. B* **2003**, *107*, 7449.
- <sup>17</sup> Weber, M. J. In *Optical properties of ions in crystals*; Crosswhite, H. M., Moose, H. W. Eds.; Interscience: New York, 1967, p 467.



# CHAPTER 6

## *Synthesis of lanthanide(III)-doped semiconductor nanoparticles*

*In the previous chapters the doping of lanthanide ions in nanoparticles was described as a way to enhance the optical properties of the lanthanide ions in organic media. The host materials of these nanoparticles prevent quenching of the luminescence, but the contribution to an effective excitation of the lanthanide ions is limited. In this chapter the synthesis of semiconductor nanoparticles doped with lanthanide ions is described. Semiconductor materials can be excited by photo-excitation or electro-excitation and have the possibility to transfer the excitation energy to dopant ions. The doping of semiconductor nanoparticles with lanthanide ions could provide alternative excitation routes of the lanthanide ions. This chapter describes the successful doping of TiO<sub>2</sub> nanoparticles that are soluble in organic solvents with a variety of lanthanide ions, that emit in the visible and in the near-infrared (NIR).*

## 6.1 Introduction

The luminescence properties of lanthanide ions in organic media can be enhanced by doping the lanthanide ions in inorganic nanoparticles that are soluble in organic solvents, as was shown in the previous chapters. The host material is not active in the excitation of the lanthanide ions in LaF<sub>3</sub> nanoparticles and for the LaPO<sub>4</sub> nanoparticles only through a charge transfer band to Eu<sup>3+</sup> or Yb<sup>3+</sup>. In the LaVO<sub>4</sub> host, the ions can be excited by using the charge transfer band of the VO<sub>4</sub> group, giving rise to a high absorption band in the UV.<sup>1</sup> Another possibility to involve the host material in the excitation of lanthanide ions, is by the use of energy transfer from a semiconductor host. Doping of lanthanide ions in semiconductor hosts can lead to efficient photo- and electro-excitation of the lanthanide ion, which has been shown with bulk semiconductors.<sup>2</sup> Semiconductor nanoparticles of various materials, like CdS, CdSe, CdTe, HgTe, PbSe etc., have been prepared.<sup>3</sup> These nanoparticles have broad absorption bands ranging from the UV till the NIR, offering the possibility for broadband photo-excitation. Electroluminescence provides alternative ways for the excitation of semiconductor materials. In a light-emitting diode (LED) the active material can be excited by charge carriers generated from electricity, leading to luminescence generated directly from electricity. Several groups, including our own, have investigated the possibility to excite lanthanide ions in polymer-based LEDs by the use of lanthanide complexes.<sup>4</sup> Quenching of the lanthanide luminescence, especially for the NIR-emitting lanthanide ions, is a problem in these devices. The lifetime of the lanthanide ion could be increased by doping in semiconductor nanoparticles and energy transfer from the semiconductor host to the lanthanide ion could offer the possibility for electroluminescence. Polymer light-emitting diodes (LEDs) doped with semiconductor nanoparticles, which emit in the visible have been prepared by Colvin *et al.*<sup>5</sup> and in the NIR by Tessler *et al.*<sup>6</sup> Energy transfer from semiconductor nanoparticles to lanthanide ions is possible and has been shown in glass materials. Energy transfer from silicon nanocrystals to Er<sup>3+</sup> ions is widely studied<sup>7</sup> and energy transfer from CdS to Eu<sup>3+</sup> or SnO<sub>2</sub> to Eu<sup>3+</sup> is also reported.<sup>8,9</sup> In these glasses, the lanthanide ion does not have to be doped in the nanoparticle to have energy transfer.

A number of papers reported on the doping of lanthanide ions in semiconductor nanoparticles of ZnS and CdS, that are soluble in organic solvents.<sup>10</sup> In most of the papers direct proof of the energy transfer of the semiconductor host to the lanthanide ion is not shown, because the excitation spectra of the lanthanide ions are not published. Bol *et al.* tried to reproduce the synthesis of these nanoparticles, but could not find evidence that the lanthanide ion was doped in the nanoparticle and that energy transfer from the nanoparticle to the lanthanide ion



occurred.<sup>11</sup> Raola and Strouse reported the doping of  $\text{Eu}^{3+}$  ions in CdSe nanoparticles, starting with  $\text{Eu}^{2+}$  as the europium source, but luminescence studies to see if energy transfer from the nanoparticle host to the lanthanide ion occurs were not performed.<sup>12</sup> Difficulties in doping most likely arise from the large difference in size between the host cation and the lanthanide ion, the charge mismatch between the cations, and the low affinity of lanthanide ions towards sulfur and selenium. The lanthanide ions do have a high affinity towards oxygen and in this chapter the doping of lanthanide ions in  $\text{TiO}_2$  semiconductor nanoparticles is discussed. The effect of lanthanide doping on the catalytic activity of  $\text{TiO}_2$  has been investigated, but no luminescence studies were performed on these materials.<sup>13</sup> The luminescence of the visible emitting ions  $\text{Eu}^{3+}$  and  $\text{Tb}^{3+}$  doped in  $\text{TiO}_2$  films has been reported by Conde-Gallardo *et al.*<sup>14,15</sup> They observed energy transfer from the  $\text{TiO}_2$  host to the lanthanide ions after photo-excitation, which means that energy transfer from this semiconductor host to the lanthanide ions is possible. The luminescence of  $\text{Er}^{3+}$ -doped  $\text{TiO}_2$  waveguide materials and nanocrystals was also reported, but in these cases the  $\text{Er}^{3+}$  ions were excited directly and not through the semiconductor host.<sup>16,17</sup>

Nanoparticles of  $\text{TiO}_2$  are widely studied for applications in solar cells and as photocatalysts.<sup>18</sup> A general synthesis route of  $\text{TiO}_2$  nanoparticles comprises the decomposition of  $\text{Ti}(\text{OPr}^i)_4$  in water at a low pH.<sup>19</sup> This leads to nanoparticles that are soluble in water, but other synthesis procedures to make nanoparticles that are soluble in organic solvents are described by for instance Wu *et al.* and Trentler *et al.*<sup>20</sup>

The procedure described by Parala *et al.* involves the thermal decomposition of  $\text{Ti}(\text{OPr}^i)_3(\text{dmae})$  ( $\text{dmae}$  = Dimethylaminoethoxide) in TOPO (trioctylphosphine oxide) to form nanoparticles coated with TOPO ligands.<sup>21</sup> We modified this procedure by dissolving lanthanide chloride salts in the TOPO, to obtain lanthanide-doped nanoparticles.

## 6.2 Results and discussion

### 6.2.1 Characterization of $\text{Eu}^{3+}$ -doped nanoparticles

The nanoparticles of  $\text{TiO}_2:\text{Eu}$  were characterized by TEM, by evaporating a drop of a nanoparticle solution on a carbon coated copper grid. A typical picture of nanoparticles obtained by heating the reaction mixture for 30 min is shown in Figure 6.1. The picture shows small particles with low contrast, due to the small size of the nanoparticles and the low atomic weight of the Ti and O atoms. The nanoparticles are between 3-5 nm in size and in some nanoparticles lattice fringes can be seen, indicating that these are crystalline. The inset shows an enlargement

of such a crystalline nanoparticle in which the lattice planes are clearly observed. The size of the nanoparticles is similar to those found for un-doped TiO<sub>2</sub> nanoparticles, synthesized via the same method.<sup>21</sup>

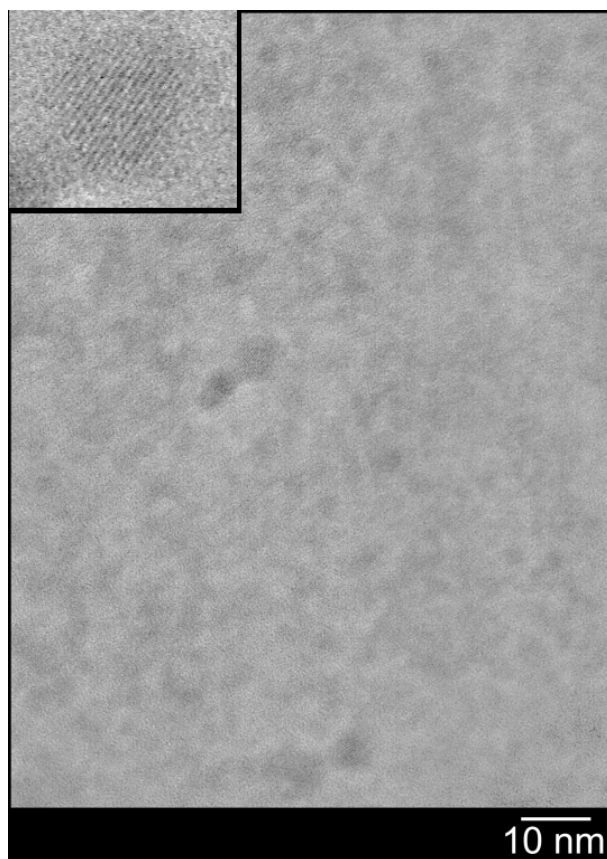


*Figure 6.1: TEM picture of TiO<sub>2</sub>:Eu nanoparticles obtained by heating the reaction mixture for 30 min. The inset shows a magnification of a single nanoparticle with lattice fringes.*

The composition of the nanoparticles was measured by X-ray fluorescence (XRF). For a sample synthesized with a molar ratio of Eu<sup>3+</sup> to Ti<sup>4+</sup> of 1:17.7 and a reaction time of 30 minutes, a weight ratio of Eu<sub>2</sub>O<sub>3</sub>:TiO<sub>2</sub> 10.9:61.6 % was found, corresponding to a molar ratio of 1:12.5 in the nanoparticles. The molar ratio of Eu<sup>3+</sup> in the nanoparticles is higher than applied in the synthesis, which might be the result of incomplete precursor decomposition at this reaction time. The other 27.5 % of the weight consists of the TOPO capping groups around the nanoparticles.

The emission of the Eu<sup>3+</sup> ion was used as a probe for the environment around the lanthanide ion. The sensitivity of the emission lines of Eu<sup>3+</sup> to the symmetry of the surrounding gives valuable information on the site in which the ion is located and it gives the possibility to compare the emission spectrum with emission spectra from the literature of Eu<sup>3+</sup> doped in other TiO<sub>2</sub> materials. The emission, absorption and excitation spectra of TiO<sub>2</sub>:Eu nanoparticles in dichloromethane are shown in Figure 6.2. The emission spectrum shows typical Eu<sup>3+</sup>

luminescence from the  $^5D_0$  level after excitation in the  $TiO_2$  absorption band. The emission spectrum shows a striking similarity to the emission spectra of  $Eu^{3+}$  in a  $TiO_2$  thin film<sup>14</sup> and in mesoporous  $TiO_2$ .<sup>22</sup> The ratios of the different peaks in the emission spectra are the same and also the peak splitting is very similar, which is a strong indication that the environment around the  $Eu^{3+}$  ion is the same. The emission of the  $^5D_0 \rightarrow ^7F_2$  transition is clearly the dominating emission line, indicating the  $Eu^{3+}$  ion is in an environment without inversion symmetry. The peaks of the transitions are not well resolved. Sharp transition lines are observed when the  $Eu^{3+}$  ions are all doped in a limited number of well-defined crystal sites. The broad emission lines found in the emission spectrum of the  $TiO_2:Eu$  nanoparticles could be caused by the doping of  $Eu^{3+}$  in amorphous material, but in the TEM pictures crystalline nanoparticles were found. Another reason for the broadening of the emission lines could be the distortion of the crystal lattice around the  $Eu^{3+}$  ion. The size and charge mismatch between the two cations ( $Eu^{3+}$  0.95 Å,  $Ti^{4+}$  0.69 Å) leads to oxygen vacancies around the  $Eu^{3+}$  ions. This would make the sites of each of the  $Eu^{3+}$  ions slightly different, leading to broadening of the emission lines.

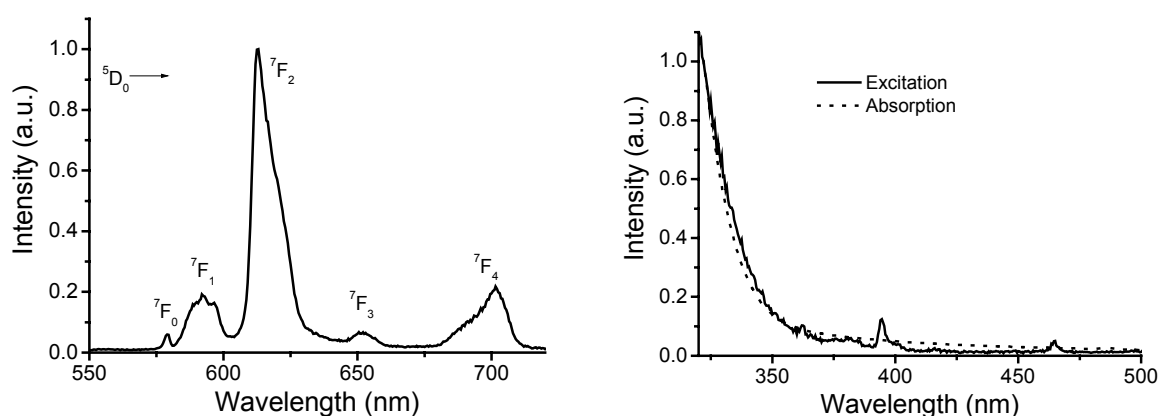


Figure 6.2: Emission spectrum of  $TiO_2:Eu$  nanoparticles in dichloromethane excited at 300 nm (left). Absorption (dotted line) and excitation (straight line,  $\lambda_{em}$  610 nm) spectrum of  $TiO_2:Eu$  nanoparticles in dichloromethane (right).

The absorption spectrum of the doped nanoparticle solution is also shown in Figure 6.2. A strong absorption band of the  $TiO_2$  host is observed starting at 350 nm. The onset of this absorption is the band gap of the  $TiO_2$  host and compared to bulk  $TiO_2$ , which has a band gap of 382 nm, this is blue shifted.<sup>18</sup> The blue shift of the band gap is caused by quantum size effects, due to small size of the nanoparticles. The lanthanide absorption bands are not observed in the absorption spectrum, because of their low absorption coefficients.

The excitation spectrum of the  $\text{Eu}^{3+}$  emission at 610 nm is very similar to the absorption spectrum, except that the absorption peaks of the  $\text{Eu}^{3+}$  ion are observed at 395 and 465 nm. The presence of the  $\text{TiO}_2$  absorption band in the excitation spectrum demonstrates the energy transfer from the semiconductor host to the  $\text{Eu}^{3+}$  ion. The luminescence decay of the  $\text{TiO}_2$  nanoparticles after excitation at 300 nm is shown in Figure 6.3.

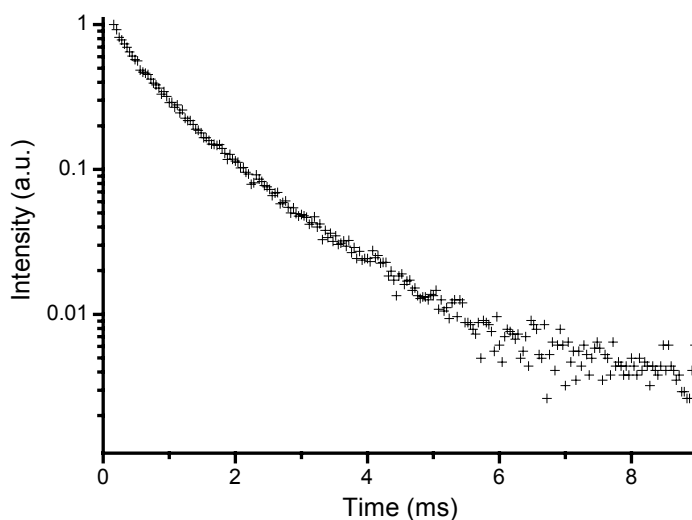


Figure 6.3: Luminescence decay of  $\text{TiO}_2:\text{Eu}$  nanoparticles in dichloromethane ( $\lambda_{\text{ex}}$  300 nm).

Energy transfer from the semiconductor host to the lanthanide ion is faster than the instrument response, because in the decay no build-up in the luminescence is observed. The decay shows a deviation from mono-exponential behavior, just like for the other lanthanide-doped nanoparticles described in chapter 4. Fitting the decay with a bi-exponential decay gave the luminescence lifetimes of the  $\text{Eu}^{3+}$  emission. A long component of 1.2 ms is responsible for 77 % of the luminescence and a short component of 0.4 ms is responsible for 23 % of the luminescence. The equation of Werts *et al.* (see chapter 2, Equation 2.1) was used to calculate the radiative lifetime of the  $\text{Eu}^{3+}$  ion and to estimate the *intrinsic* quantum yield of the  $\text{Eu}^{3+}$  ion.<sup>23</sup> Using the refractive index of dichloromethane, a radiative lifetime of 2.9 ms was calculated from the shape of the emission spectrum. This radiative lifetime implies that the *intrinsic* quantum yield of the  $\text{Eu}^{3+}$  ion is about 40 %. The effective refractive index experienced by the  $\text{Eu}^{3+}$  ions is not exactly known. The ions itself are doped in the  $\text{TiO}_2$  host material with a refractive index of 2.6-2.9 and the nanoparticles are dissolved in dichloromethane with a refractive index of 1.42.<sup>24</sup> It is therefore likely that the refractive index the  $\text{Eu}^{3+}$  ions experience is a bit higher than the refractive index of the solvent and this would lead to a shorter radiative lifetime and as a

consequence a slightly higher intrinsic quantum yield. The luminescence lifetime of the  $\text{Eu}^{3+}$  ion in these nanoparticles is longer than the luminescence lifetime measured for  $\text{Eu}^{3+}$  in mesoporous  $\text{TiO}_2$  of 0.5 ms.<sup>22</sup> This difference can be attributed to the influence of the solvent with the lower refractive index, making the radiative lifetime of the  $\text{Eu}^{3+}$  ion longer.

A quantum yield of the *sensitized* emission of the  $\text{TiO}_2:\text{Eu}$  nanoparticles was determined by comparing the emission intensity with the emission intensity of a solution of ruthenium tris bipyridine in deoxygenated water with the same optical density at the excitation wavelength. The determined quantum yield of the sensitized  $\text{Eu}^{3+}$  emission was only 0.03 %. This very low quantum yield seems in contradiction with the high intrinsic quantum yield of the excited  $\text{Eu}^{3+}$  ion and this will be discussed in the next paragraph.

### 6.2.2 Quenching in lanthanide-doped $\text{TiO}_2$ nanoparticles

The quenching routes of the lanthanide ion in the  $\text{TiO}_2$  nanoparticles were investigated to explain the low quantum yield. Residual OH groups at the surface of the nanoparticles or in the core of the nanoparticles could quench the luminescence of the lanthanide ion.<sup>25</sup> An FT-IR spectrum was measured to see if water or OH groups are present in the product. The nanoparticles were dried over  $\text{P}_2\text{O}_5$  to remove any physisorbed water present on the nanoparticles surface after the synthesis.

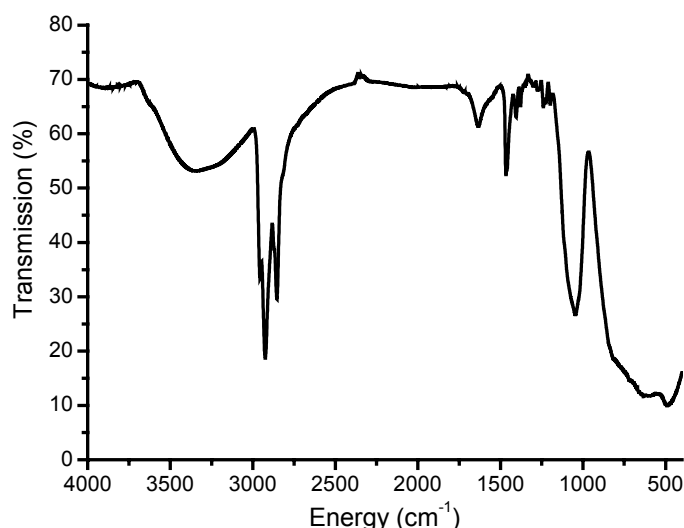


Figure 6.4: FT-IR spectrum of  $\text{TiO}_2:\text{Eu}$  nanoparticles after drying over  $\text{P}_2\text{O}_5$ .

There is a broad band centered at 3300  $\text{cm}^{-1}$ , which can be ascribed to the OH stretching vibration. The TOPO ligand is visible due to the peaks at 2925  $\text{cm}^{-1}$  and 2850  $\text{cm}^{-1}$  of the

stretching vibrations of the CH bonds and the peak at  $1046\text{ cm}^{-1}$  of the PO bond. The band around  $500\text{ cm}^{-1}$  is caused by TiO bonds in the  $\text{TiO}_2$  host.<sup>20a</sup> To investigate the effect of quenching by OH impurities, the nanoparticles were also synthesized by using deuterated solvents. Nanoparticles were synthesized by dissolving the  $\text{EuCl}_3 \cdot 6\text{H}_2\text{O}$  in MeOD and washing the product with MeOD after the reaction. This procedure will convert free OH bonds inside and on the surface of the nanoparticles in OD bonds and thereby reduce the quenching of the  $\text{Eu}^{3+}$  ion. When the luminescence intensity and the luminescence lifetimes of the  $\text{Eu}^{3+}$  ion in nanoparticles synthesized with methanol and with methanol- $d_1$  were compared, no change was found, indicating that OH bonds are present, but not as an important source of quenching. To increase the quantum yield of the nanoparticles, the influence of the reaction time was investigated. A longer reaction time could influence the quantum yield by increasing the crystallinity, improving the surface capping, and by a growth of the nanoparticles. The average luminescence lifetime of  $\text{Eu}^{3+}$  is plotted as a function of the reaction time in Figure 6.5 and an increase in lifetime is clearly observed.

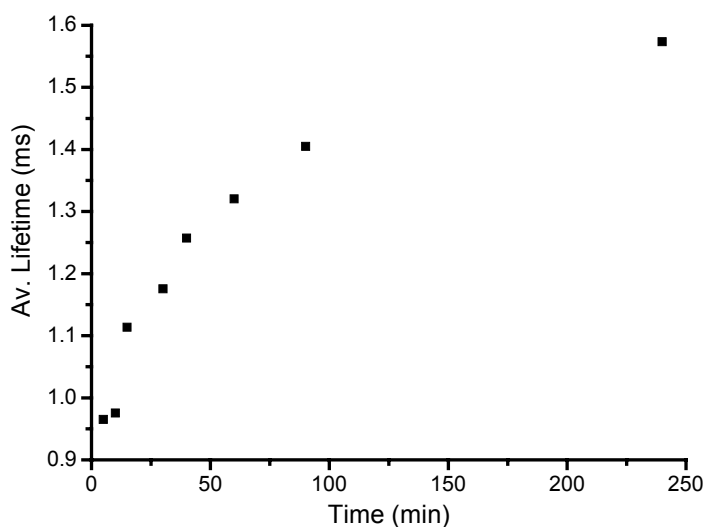


Figure 6.5: Average luminescence lifetime of  $\text{Eu}^{3+}$  in  $\text{TiO}_2$  nanoparticles after different reaction times.

This increase in the luminescence lifetime should correspond to an increase in quantum yield after a longer reaction time, but this was not found. It is possible that un-doped nanoparticles are formed after longer reactions and that they also absorb light, but do not contribute to the lanthanide luminescence. In this case the quantum yield of the doped nanoparticles would be increased, but the result of the quantum yield measurement is disturbed by the presence of un-doped nanoparticles. A change in symmetry around the  $\text{Eu}^{3+}$  ion could also

lead to an increase in the measured lifetime, but this symmetry change should also lead to a different emission spectrum, but this was not observed. The relatively long lifetime of the  $\text{Eu}^{3+}$  ion is an indication that once the energy is transferred to the lanthanide ion, quenching of the  $\text{Eu}^{3+}$  ion is not the dominating process.

### 6.2.3 Lanthanide ions emitting in the Near-Infrared

Other lanthanide ions were also successfully doped in the  $\text{TiO}_2$  nanoparticles. The emission and excitation spectra of  $\text{TiO}_2$  nanoparticles doped with the NIR-emitting lanthanide ions  $\text{Nd}^{3+}$ ,  $\text{Er}^{3+}$ , and  $\text{Yb}^{3+}$  are shown in Figure 6.6.

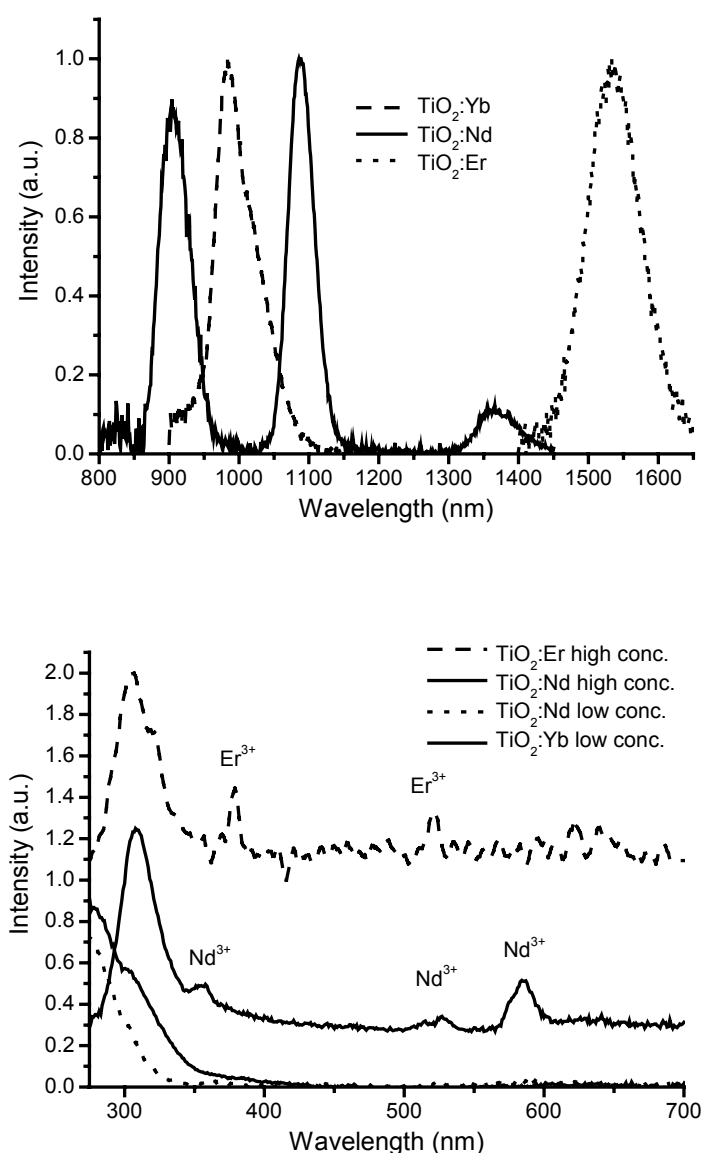


Figure 6.6: Emission (up:  $\lambda_{\text{ex.}}$  300 nm) and excitation (down:  $\lambda_{\text{em.}}$  1060  $\text{Nd}^{3+}$ , 1530  $\text{Er}^{3+}$ , and 980  $\text{Yb}^{3+}$ ) spectra of  $\text{TiO}_2$  nanoparticles doped with  $\text{Yb}^{3+}$ ,  $\text{Nd}^{3+}$ , and  $\text{Er}^{3+}$ . The offset is for clarity.

After excitation in the  $\text{TiO}_2$  absorption band, the emission spectra show the typical luminescence of these lanthanide ions. The  $\text{Nd}^{3+}$  ion emits at 880, 1060, and 1330 nm originating from the  $^4\text{F}_{3/2} \rightarrow ^4\text{I}_J$  ( $J = 9/2, 11/2, 13/2$ ) transitions, respectively. The  $\text{Er}^{3+}$  ion emits at 1530 nm from the  $^4\text{I}_{13/2} \rightarrow ^4\text{I}_{15/2}$  transition and the  $\text{Yb}^{3+}$  ion at 980 nm from the  $^2\text{F}_{5/2} \rightarrow ^2\text{F}_{7/2}$  transition. The excitation spectra show the same broad band starting at 350 nm the same as for the  $\text{TiO}_2:\text{Eu}^{3+}$  particles proving that sensitized emission of these ions also occurs. At high particle concentrations of 50 mg/ml, the excitation spectra also show the direct excitation of  $\text{Er}^{3+}$  and  $\text{Nd}^{3+}$ , because the lanthanide absorption lines become visible in the excitation spectra. In the samples with a high nanoparticle concentration the broad band has a maximum at 310 nm, because below this wavelength all the excitation light is absorbed in the first millimeters of the fluorescence cuvet and the emission is collected at an angle of 90 degrees from the middle of the cuvet. The emission of the  $\text{Nd}^{3+}$  and  $\text{Er}^{3+}$  ions around 1330 and 1530 nm are of special interest for telecommunication purposes, because these wavelengths are in the telecommunication windows.

#### 6.2.4 A LED with $\text{TiO}_2:\text{Eu}$ nanoparticles

A LED doped with  $\text{TiO}_2:\text{Eu}$  nanoparticles was fabricated, with a structure as shown in Figure 6.7.

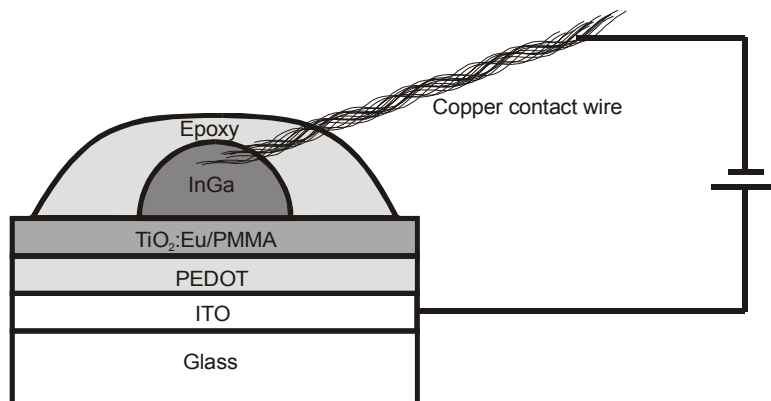


Figure 6.7: LED with  $\text{TiO}_2:\text{Eu}$  nanoparticles. The thickness of the layers are not scaled for clarity.

On the ITO covered glass slides a layer of 80 nm of PEDOT (a mixture of poly(3,4-ethylene dioxythiophene) and poly(styrenesulfonate)) was spin-coated to improve the hole injection from the ITO into the device.<sup>26</sup> When a nanoparticle solution was spin-coated on top of the PEDOT layer cracks appeared in the nanoparticle layer, which can lead to shortcuts in the LED. For this reason a mixture of nanoparticle/PMMA 3/1 was used, because smoother layers



could be spin-coated using the polymer blend. Although the PMMA polymer is a non-conducting polymer a semiconducting layer could be fabricated when the doping ratio of the nanoparticles is high enough. Electroluminescent devices have been fabricated of nanoparticle PMMA blends using ZnS:Cu nanoparticles, which have a slightly larger band gap than our TiO<sub>2</sub> nanoparticles.<sup>27</sup> A drop of InGa eutectic was used as the cathode.<sup>28</sup> The device behaved as a diode, which can be seen by the current-voltage characteristics as shown in Figure 6.8. The turn on voltage of the device is around 12 V. Up to a voltage of 21 V when a significant current of about 5 mA is going through the device no emission could be detected. The low quantum yield of the nanoparticles that was found in the photophysical measurements is probably the reason why it will be very difficult to observe electroluminescence.

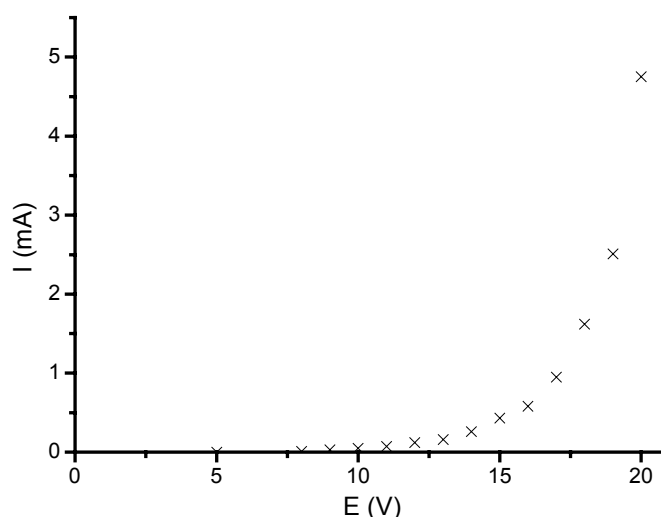


Figure 6.8: Current-voltage characteristics of the TiO<sub>2</sub>:Eu/PMMA LED.

### 6.3 Conclusions

Lanthanide-doped nanoparticles of TiO<sub>2</sub> show energy transfer from the semiconductor host to the lanthanide ions, for lanthanide ions emitting in the visible and in the NIR. The quantum yield of the nanoparticles is low, although the intrinsic quantum yield of the lanthanide ion is high. A LED with the nanoparticles did show diode like behavior, but no lanthanide luminescence was observed. This is probably caused by the low quantum yield of the nanoparticles.

## 6.4 Experimental section

**General.** Photo-physical measurements were performed using the setup described in chapter 3. The spectra of  $\text{Eu}^{3+}$  were measured at a resolution of 1.8 nm and the spectra in the near-infrared were measured at a resolution of 16.2 nm for  $\text{Er}^{3+}$  and 8.1 nm for  $\text{Nd}^{3+}$  and  $\text{Yb}^{3+}$ . The quantum yield of the  $\text{TiO}_2:\text{Eu}$  nanoparticles was determined by comparing the emission intensity with the emission intensity of a solution of ruthenium tris bipyridine with the same optical density at the excitation wavelength ( $\lambda_{\text{ex}}$ , 310 nm). The quantum yield of ruthenium trisbipyridine in deoxygenated water is 4.2 %. For the electroluminescence measurements the same instrument as for the photo-physical measurements was used.

**Nanoparticle synthesis.** Nanoparticles of lanthanide-doped  $\text{TiO}_2$  were prepared by adopting a literature procedure.<sup>21</sup>  $\text{TiO}_2$  nanoparticles were formed by the thermal decomposition of  $\text{Ti}(\text{OPr}^i)_3(\text{dmae})$  (dmae = dimethylaminoethoxide) in hot trioctylphosphine oxide (TOPO). The titanium precursor was synthesized using a literature procedure.<sup>29</sup> Lanthanide-doped nanoparticles were prepared by dissolving 11 mg of  $\text{EuCl}_3 \cdot 6\text{H}_2\text{O}$  in 5 mL of methanol followed by the addition of 3.5 g of TOPO and evaporation of the methanol and water in vacuo. The resulting solution was heated to 315 °C under a nitrogen atmosphere and 200  $\mu\text{L}$  of the titanium precursor was injected, followed by further heating at 300 °C for 10-240 min. The reaction mixture was cooled to 60 °C and the nanoparticles were precipitated by the addition of methanol. The product was separated by centrifugation and further purified by washing with methanol. The resulting lanthanide-doped particles are dispersible in apolar solvents like toluene, dichloromethane, and chloroform, to form optically clear solutions.

**LED fabrication.** A LED with  $\text{TiO}_2:\text{Eu}$  nanoparticles was prepared on ITO covered glass plates. The ITO layer was first cleaned by sonication in water and ethanol, followed by a treatment in an oxygen plasma for 5 min. On top of the ITO a 80 nm thick layer of PEDOT (Aldrich) was spin-coated at 4000 rpm. The layer was dried over  $\text{P}_2\text{O}_5$  in vacuum at 80 °C for 2 days. On top of this layer a 1 % solution of  $\text{TiO}_2/\text{PMMA}$  3/1 in chloroform was spin-coated at 1500 rpm to form a 100 nm thick layer. This layer was also dried over  $\text{P}_2\text{O}_5$  in vacuum at 80 °C for 1 day. The devices were then transferred to a glove box with a dry nitrogen atmosphere and on top of the layers a drop of InGa eutectic was placed. In the drop of InGa eutectic a copper contact wire was placed and the device was protected from the atmosphere by a layer of epoxy glue. The glue was cured at 80 °C for 2 hours.

## 6.5 References and notes

- <sup>1</sup> Blasse, G.; Grabmeier, B. C. *Luminescent materials*; Springer: Berlin, 1994.
- <sup>2</sup> Kenyon, A. J. *Prog. Quant. Electron.* **2002**, *26*, 225.
- <sup>3</sup> (a) Murray, C. B.; Norris, D. J.; Bawendi, M. G. *J. Am. Chem. Soc.* **1993**, *115*, 8706; (b) Harrison, M. T.; Kershaw, S. V.; Burt, M. G.; Rogach, A. L.; Kornowski, A.; Eychmüller, A.; Weller, H. *Pure Appl. Chem.* **2000**, *72*, 295; (c) Du, H.; Chen, C.; Krishnan, R.; Krauss, T. D.; Harbold, J. M.; Wise, F. W.; Thomas, M. G.; Silcox, J. *Nano Lett.* **2002**, *2*, 1321.
- <sup>4</sup> (a) Kang, T. S.; Harrison, B. S.; Bouguettaya, M.; Foley, T. J.; Boncella, J. M.; Schanze, K. S.; Reynolds, J. R. *Adv. Funct. Mater.* **2003**, *13*, 205; (b) Slooff, L. H.; Polman, A.; Cacialli, F.; Friend, R. H.; Hebbink, G. A.; van Veggel, F. C. J. M.; Reinhoudt, D. N. *Appl. Phys. Lett.* **2001**, *78*, 2122.
- <sup>5</sup> Colvin, V. L.; Schlamp, M. C.; Alivisatos, A. P. *Nature* **1994**, *370*, 354.
- <sup>6</sup> Tessler, N.; Medvedev, V.; Kazes, M.; Kan, S.; Banin, U. *Science* **2002**, *295*, 1506.
- <sup>7</sup> (a) Kik, P. G.; Polman, A. *Mat. Sci. Eng. B* **2001**, *81*, 3; (b) Han, H. S.; Seo, S. Y.; Shin, J. H. *Appl. Phys. Lett.* **2001**, *79*, 4568.
- <sup>8</sup> Selvan, S. T.; Hayakawa, T.; Nogami, M. *J. Non-Cryst. Solids* **2001**, *291*, 137.
- <sup>9</sup> Nogami, M.; Enomoto, T.; Hayakawa, T. *J. Lumin.* **2002**, *97*, 147.
- <sup>10</sup> (a) Bhargava, R. N. *J. Lumin.* **1996**, *70*, 85; (b) Kane, R. S.; Cohen, R. E.; Silbey, R. *Chem. Mater.* **1999**, *11*, 90; (c) Ihara, M.; Igarashi, T.; Kusunoki, Y.; Ohno, K. *J. Electrochem. Soc.* **2000**, *147*, 2355; (d) Okamoto, S.; Kobayashi, M.; Kanemitsu, Y.; Kushida, T. *Phys. Stat. Sol. B* **2002**, *1*, 481; (e) Qu, S. C.; Zhou, W. H.; Liu, F. Q.; Chen, N. F.; Wang, Z. G.; Pan, H. Y.; Yu, D. P. *Appl. Phys. Lett.* **2002**, *80*, 3605; (f) Schmidt, T.; Muller, G.; Spanhel, L. *Chem. Mater.* **1998**, *10*, 65.
- <sup>11</sup> Bol, A. A.; van Beek, R.; Meijerink, A. *Chem. Mater.* **2002**, *14*, 1121.
- <sup>12</sup> Raola, O. E.; Strouse, G. F. *Nano Lett.* **2002**, *2*, 1443.
- <sup>13</sup> (a) Wang, Y.; Cheng, H.; Zhang, L.; Hao, Y.; Ma, J.; Xu, B.; Li, W. *J. Mol. Catal. A* **2000**, *151*, 205; (b) Zhang, Y.; Zhang, H.; Xu, Y.; Wang, Y. *J. Mater. Chem.* **2003**, *13*, 2261.
- <sup>14</sup> Conde-Gallardo, A.; García-Rocha, M.; Hernández-Calderón, I.; Palomino-Merino, R. *Appl. Phys. Lett.* **2001**, *78*, 3436.
- <sup>15</sup> Conde-Gallardo, A.; García-Rocha, M.; Hernández-Calderón, I.; Palomino-Merino, R. *Mod. Phys. Lett. B* **2001**, *15*, 813.
- <sup>16</sup> (a) Bahtat, A.; Bouazaoui, M.; Bahtat, M.; Mugnier, J. *Opt. Commun.* **1994**, *19*, 1982; (b) Bahtat, A.; Bouazaoui, M.; Bahtat, M.; Garapon, C.; Jacquier, B.; Mugnier, J. *J. Non-Cryst. Sol.* **1996**, *202*, 16.
- <sup>17</sup> Jeon, S.; Braun, P. V. *Chem. Mater.* **2003**, *15*, 1256.
- <sup>18</sup> Hoffmann, M. R.; Martin, S. T.; Choi, W.; Bahnemann, D. W. *Chem. Rev.* **1995**, *95*, 69.

- <sup>19</sup> Oskam, G.; Nellore, A.; Penn, R. L.; Searson, P. C. *J. Phys. Chem. B* **2003**, *107*, 1734.
- <sup>20</sup> (a) Wu, X.; Wang, D.; Yang, S. *J. Colloid Interf. Sci.* **2000**, *222*, 37; (b) Trentler, T. J.; Denler, T. E.; Bertone, J. F.; Agrawal, A.; Colvin, V. L. *J. Am. Chem. Soc.* **1999**, *121*, 1613.
- <sup>21</sup> Parala, H.; Devi, A.; Bhakta, R.; Fischer, R. A. *J. Mater. Chem.* **2002**, *12*, 1625.
- <sup>22</sup> Frindell, K. L.; Bartl, M. H.; Popitsch, A.; Stucky, G. D. *Angew. Chem. Int. Ed.* **2002**, *41*, 960.
- <sup>23</sup> Werts, M. H. V.; Jukes, R. T. F.; Verhoeven, J. W. *Phys. Chem. Chem. Phys.* **2002**, *4*, 1542.
- <sup>24</sup> *CRC Handbook of Chemistry and Physics 64<sup>th</sup> ed.*, ed. Weast, R. C., 1983-1984, Boca Raton, Florida, USA.
- <sup>25</sup> Haas, Y.; Stein, G. *J. Phys. Chem.* **1971**, *75*, 3668.
- <sup>26</sup> Brown, T. M.; Friend, R. H.; Millard, I. S.; Lacey, D. J.; Butler, T.; Burroughes, J. H.; Cacialli, F. *J. J. Appl. Phys.* **2003**, *93*, 6159.
- <sup>27</sup> Que, W.; Zhou, Y.; Lam, Y. L.; Chan, Y. C.; Kam, C. H.; Liu, B.; Gan, L. M.; Chew, C. H.; Xu, G. Q.; Chua, S. J.; Xu, S. J.; Mendis, F. V. C. *Appl. Phys. Lett.* **1998**, *73*, 2727.
- <sup>28</sup> Gao, F. G.; Bard, A. J. *J. Am. Chem. Soc.* **2000**, *122*, 7426.
- <sup>29</sup> Jones, A. C.; Leedham, T. J.; Wright, P. J.; Crosbie, M. J.; Fleeting, K. A.; Otway, D. J.; O'Brien, P.; Pemble, M. E. *J. Mater. Chem.* **1998**, *8*, 1773.

# CHAPTER 7

## *Polymer waveguide amplifiers doped with LaF<sub>3</sub>:Nd nanoparticles.*

*In this chapter the fabrication of polymer-based optical amplifiers operating at 1319 nm is described. The luminescent material in the polymer waveguides were the LaF<sub>3</sub>:Nd nanoparticles synthesized as described in chapter 3. Two polymer waveguide devices were fabricated. One device with LaF<sub>3</sub>:Nd-doped PMMA as the waveguiding polymer was structured by reactive ion etching. The losses in this waveguide are relatively high, probably due to the rough sidewalls caused by the reactive ion etching process. These waveguides show an optical gain of 0.3 dB at 1319 nm on a 3 cm long device with a pump power of 12 mW at 578 nm. The other polymer waveguide was made of nanoparticle-doped SU-8, a negative photoresist, structured by photolithography. This device showed reduced losses, compared to the PMMA waveguide, but due to the low pump power (5 mW at 795 nm) that could be coupled in the waveguide the measured optical gain was limited to 0.1 dB. However, modeling of the amplification results shows that an optimization of the waveguide structure might lead to optical gain, that is close to the gain obtained in Nd<sup>3+</sup>-doped fiber amplifiers.*

## 7.1 Introduction

Erbium-doped fiber amplifiers (EDFA's) operating at 1530 nm are commercially applied all over the world in long distance telecommunication systems.<sup>1</sup> These optical amplifiers have been used for less than two decades and they are for a large part responsible for the success of optical telecommunication.<sup>2</sup> Optical amplifiers at other wavelengths are currently under investigation, like the praseodymium-doped fiber amplifier for operation around 1300 nm and the thulium-doped fiber amplifier for operation around 1450 nm.<sup>3,4</sup> These wavelengths correspond to the minimum loss window of silica fibers and they are of major interest for optical telecommunication. These glass fiber-based amplifiers function very well for long-range telecommunication, but in short range telecommunication the need for easy integration of a large variety of optical components requires materials, which can be processed more easily and at a lower cost. Polymers are materials with excellent processing properties and with generally low costs.<sup>5</sup> In order to use these polymers in optical systems it is necessary to develop polymer-based optical amplifiers for the compensation of losses in the systems.<sup>6</sup> The active material in these polymer-based optical amplifiers can be lanthanide ions, but then the lanthanide ion has to be shielded from the vibrational energies of the organic bonds surrounding it. In chapter 3, doping of nanoparticles, which are soluble in organic solvents, was proposed as a way to increase the luminescence lifetime of these ions and this strategy was proven to be successful. In this chapter, the realization of polymer-based optical amplifiers doped with these nanoparticles will be discussed. The success of these nanoparticles in polymer-based waveguides will be dependent on the possibility to form homogeneous layers of the polymer nanoparticle composites. The nanoparticles itself are small enough to minimize scattering, but when the nanoparticles aggregate and form large domains, the scattering losses could increase substantially as discussed in chapter 2. The solubility of the nanoparticles in the polymer solution and the polymer itself will determine if aggregation takes place.

The polymer amplifier consists of a polymer waveguide, which is able to guide light by total internal reflection, caused by the higher refractive index of the polymer channel compared to the surrounding medium. Different waveguide designs can be fabricated, of which two are shown in Figure 7.1.

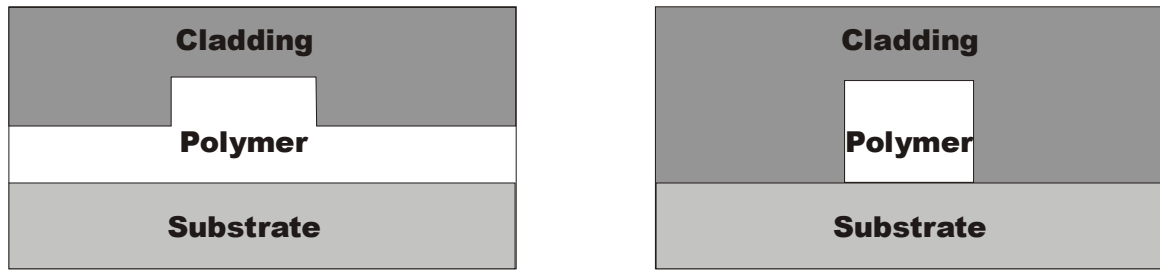


Figure 7.1: Waveguide designs; (left) ridge structure (right) channel structure.

Hebbink showed in previous experiments that these PMMA waveguides made with a channel structure showed high losses of 6 dB/cm, which were ascribed to rough sidewalls, fabricated during the RIE process.<sup>7</sup> In the ridge structure waveguide, the sidewalls have a much smaller surface area, which could reduce the scattering losses of the waveguide. Different cladding materials can be used, from air, leading to a large contrast in refractive index, to polymers with a closely matching refractive index. The refractive index of the cladding and the substrate determine the confinement of the light in the waveguide. A large difference in refractive index confines the light more strongly in the waveguide, making it possible to design curved waveguides, but a high refractive index contrast could also lead to higher losses when the sidewalls are not smooth. In addition to scattering losses, another important source of optical loss are the coupling losses, primarily the coupling losses into the waveguide are of great importance. Careful matching of the incoming light mode and the waveguide mode could reduce these coupling losses. The waveguide mode is dependent on the size of the channels and the refractive index difference between the core and the surrounding material (the cladding).

Before polymers can compete with planar glass technology for the fabrication of planar optical waveguide circuits, some major drawbacks of the polymers have to be overcome. These drawbacks are the generally higher propagation losses and the reduced reliability compared to glass technology. The propagation losses are dominated by absorptions of the vibrations of the polymer. These vibrations are located at energies below  $4000\text{ cm}^{-1}$ , or wavelengths above  $2.5\text{ }\mu\text{m}$ , but the overtones of these vibrations fall in the telecommunication window. With polymers having a large number of CH bonds, this leads to high absorption peaks at wavelengths between  $1.1\text{-}1.2\text{ }\mu\text{m}$  and  $1.35\text{-}1.45\text{ }\mu\text{m}$ . The absorption peaks leave a minimum loss window between  $1.2\text{-}1.35\text{ }\mu\text{m}$ , but also in this region the losses are high compared to glass technology. Substitution of the hydrogens by halogens (F, Br, Cl) can overcome these problems and polymers have been fabricated that can compete with glass in planar optical circuits.<sup>8,9</sup>

In our experiments with lanthanide-doped  $\text{LaF}_3$  nanoparticles we used the polymers PMMA and the negative photoresist SU-8.<sup>10</sup> These polymers have a high CH bond content so they only have a low loss window between 1.25-1.35  $\mu\text{m}$ . The lanthanide ion that shows emission in this region and shows significant emission in the  $\text{LaF}_3$  nanoparticles is  $\text{Nd}^{3+}$ .

Optical gain of  $\text{LaF}_3:\text{Nd}$  nanoparticles was already investigated in a collaboration with the Light Devices Group headed by prof. dr. A. Driessen of the University of Twente. PMMA layers doped with  $\text{LaF}_3:\text{Nd}$  nanoparticles were used as the luminescent material on top of a microring resonator.<sup>11</sup> These microring resonators consist of two identical straight waveguides with a ring placed at a short distance above the waveguides as shown in Figure 7.2 such that light that is coupled into the straight waveguide couples with the microring. The waveguides were made from SiON and on top of the microring a cladding of PMMA doped with  $\text{LaF}_3:\text{Nd}$  nanoparticles was spin-coated.<sup>12</sup>

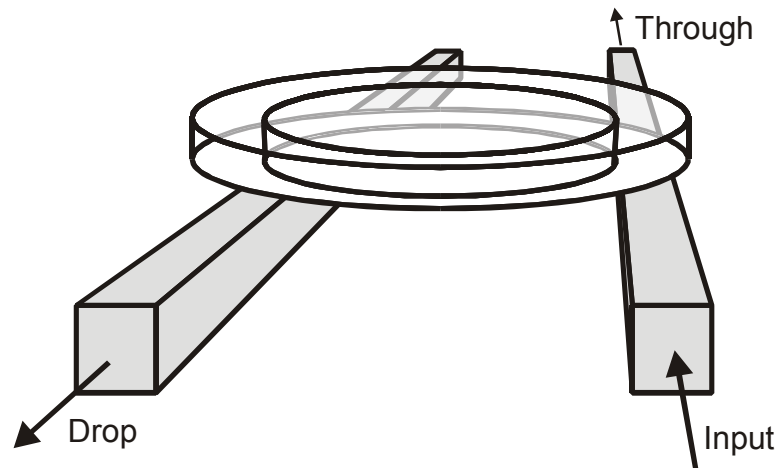


Figure 7.2: Schematic representation of a microring resonator.

The possibility of fabricating a microring laser with this structure was investigated, because this design could offer the possibility for compact and low threshold microring lasers.<sup>13</sup> The ring resonator was designed for pumping at 578 nm and emission around 880 nm. The ring is in resonance when an integral number of wavelengths fit in one roundtrip of the microring and when in resonance, a large amount of pump light can be coupled into the ring from the input waveguide. The threshold for lasing could not be reached in the device, due to the high losses and the low intensity of pump power in the doped cladding layer. However, on the straight waveguide evidence for amplified spontaneous emission was found around 863 nm at a pump power of around 200  $\mu\text{W}$ . This is a very encouraging result that shows that amplification should be possible in an optimized device.



Amplification of neodymium-doped fiber amplifiers around 1300 nm has been reported.<sup>14</sup> Although in glass fibers  $\text{Nd}^{3+}$  cannot compete with  $\text{Pr}^{3+}$ -doped amplifiers for amplification around 1300 nm due to amplified spontaneous emission and excited state absorption, it should be possible to measure sufficient gain using the  $\text{Nd}^{3+}$  ion.

## 7.2 Results and discussion

### 7.2.1 PMMA waveguides

PMMA waveguides doped with 10 % w/w  $\text{LaF}_3\text{:Nd}$  nanoparticles were made by spin-coating a solution of PMMA and the nanoparticles in chlorobenzene on a silicon wafer, covered with a layer of  $3.2\ \mu\text{m}$  of  $\text{SiO}_2$ . Ridge structures with a height of  $1.45\ \mu\text{m}$  were etched in the  $3.3\ \mu\text{m}$  thick polymer layer using reactive ion etching (RIE). The formation of a gray film over the substrate indicated that redeposition of material, probably lanthanide oxides, took place during RIE. The method of RIE relies on the reaction of highly reactive ions and radicals to form volatile products that can be pumped away from the vacuum chamber. Since the lanthanide ions cannot form volatile products in this process, this lead to the redeposition of lanthanide salts. An optical microscope image of waveguide structures made in this way is shown in Figure 7.3. It is clearly visible that the surface of the polymer next to the ridge structures is rough due to the redeposition, but the ridge structures itself seem to be smooth. The final device had air as the top cladding leading to a large difference in refractive index between the polymer ( $\sim 1.49$ ) and the air above the device.

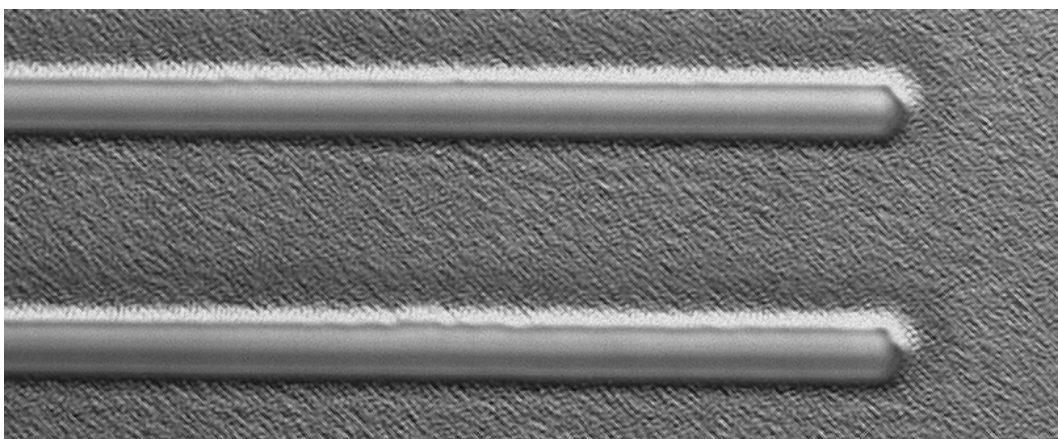


Figure 7.3:  $5\ \mu\text{m}$  wide PMMA/ $\text{LaF}_3\text{:Nd}$  ridge structures on a  $\text{SiO}_2$  wafer.

The endfaces of the polymer waveguide can be made by cleaving the wafer or by dicing the wafer. Due to the weak adsorption of the polymer to the substrate, it was not possible to dice the wafer without destroying the polymer layer and cleaving of the substrate was the only possibility. Low loss endfaces could be made using the cleaving method, but the reproducibility with this method was be low. The PMMA waveguide had a length of 3 cm and contained waveguides with different width, from 10, 5, 4, 3, 2.5, 2  $\mu\text{m}$ . The waveguides of 4  $\mu\text{m}$  and less did not transmit any light at 1300 nm. The 5  $\mu\text{m}$  channel was single-mode at the signal wavelength of 1319 nm and multi-mode at the pump wavelength of 578 nm, but the losses of this waveguide were substantial (18 dB over 3 cm at the signal wavelength). An excitation wavelength of 578 nm was chosen, because at this wavelength the  $\text{Nd}^{3+}$  ion has the strongest absorption peak. The measurements were performed on the 10  $\mu\text{m}$  wide channels, which were multi-mode, both at the signal and pump wavelength. Standard 9/125 optical fibers (core diameter of 9  $\mu\text{m}$ ) were used to couple the light into and out of the waveguide. The total chip losses (propagation and coupling losses) at the pump wavelength were 12 dB on the 10  $\mu\text{m}$  wide channel and at the signal wavelength the losses were about 11 dB. The calculated coupling losses for the signal beam were at least 6 dB, so on the 3 cm device the propagation losses were in the order of 2 dB/cm. These propagation losses were lower compared to the previously prepared PMMA waveguides,<sup>7</sup> but the rough sidewalls of the device still cause substantial propagation losses.

The continuous pump beam was butt-end coupled into the waveguide and the emission was collected at the end of the waveguide. The collected emission spectrum is shown in Figure 7.4. When the emission spectrum of the waveguide is compared with the emission spectrum of  $\text{LaF}_3:\text{Nd}$  nanoparticles in dichloromethane solution, we see that the emission peaks of the  ${}^4\text{F}_{3/2} \rightarrow {}^4\text{I}_{11/2}$  and  ${}^4\text{F}_{3/2} \rightarrow {}^4\text{I}_{9/2}$  transitions of  $\text{Nd}^{3+}$  at 1060 and 1330 nm were observed in both spectra. The emission peak at 880 nm of the  ${}^4\text{F}_{3/2} \rightarrow {}^4\text{I}_{13/2}$  transition was not observed in the waveguide emission spectrum, because an isolator was used to filter out the pump light and this isolator also filtered out the 880 nm emission. The ratio between the intensities of the other two emission peaks was also different, because the isolator filtered out part of the 1060 nm emission. A sharp decrease in the 1330 nm peak was observed above 1340 nm, because of the overtone absorption of the CH bonds in the waveguide. The amplification was measured on the waveguides with a setup as shown in Figure 7.5. In order to measure amplification of the signal beam, the pump and signal light have to be combined before going into the waveguide. The

pump and signal light were combined into a 9  $\mu\text{m}$  core single mode fiber using a WDM and butt-end coupled into the waveguide.

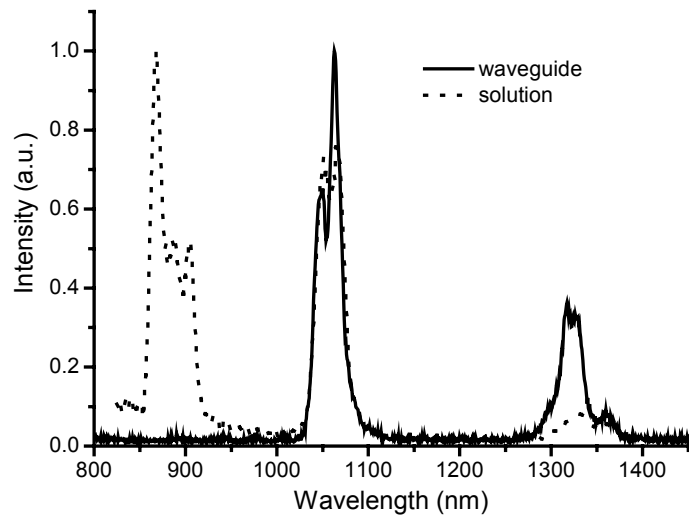


Figure 7.4: Emission spectrum of  $\text{LaF}_3:\text{Nd}$  nanoparticles in solution and in the PMMA waveguide after excitation at 578 nm.

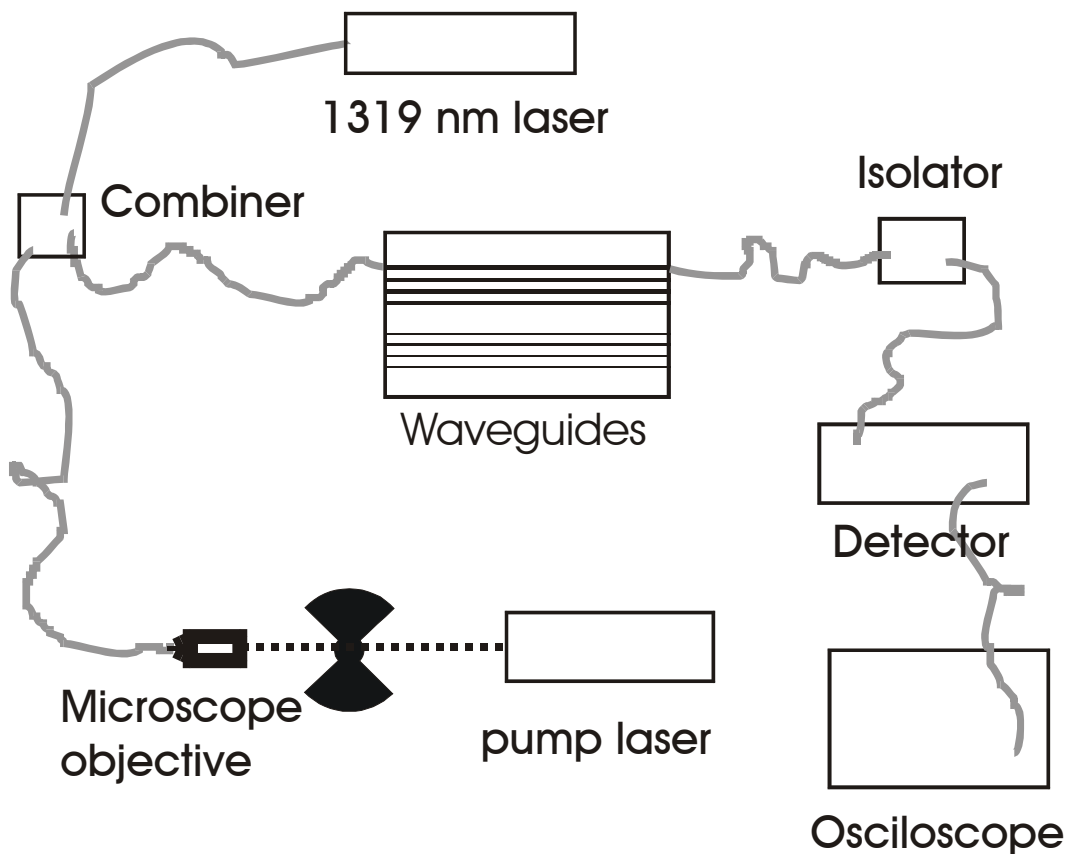


Figure 7.5: Setup for the measurement of optical amplification on the waveguides.

The intensity of the 1319 nm signal laser was unstable, so the pump light was chopped in order to measure the difference in signal intensity when the pump light was on and off. This configuration is only possible when all of the pump light is filtered out before the detector, because otherwise residual pump light will interfere with the amplified emission. The use of an isolator was found sufficient to filter out all of the pump light. The pump beam was chopped at 80 Hz for the amplification measurements and combined with the signal light coupled into the waveguide. The light coming out of the waveguide was collected using a multimode optical fiber with a core diameter of 50  $\mu\text{m}$  and fed to a detector. The detector signal was shown on an oscilloscope. At a pump power of 12 mW coupled into the device and a signal power of about 1  $\mu\text{W}$ , a signal amplification of 0.3 dB was measured. The gain showed a dependence on the pump wavelength between 570 and 590 nm, with the maximum gain corresponding to the absorption peak of the  $\text{Nd}^{3+}$  ion at 578 nm. This amplification is equal to a signal increase of 10 %, using Equation 7.1 for calculation from mW to dB,  $I_{\text{in}}$  is the signal intensity without pump light and  $I_{\text{out}}$  the signal intensity with pumplight, both in mW.

$$\text{dB} = 10 \times^{10} \log\left(\frac{I_{\text{out}}}{I_{\text{in}}}\right) \quad (\text{Eq. 7.1})$$

This signal increase measured with the detector could also be a result of spontaneous emission of the  $\text{Nd}^{3+}$  ions. This was studied by turning off the signal laser and measuring the intensity differences using a chopped pump laser. The effect of the spontaneous emission on the detector signal was approximately 1 % of the amplification signal, so the effect of spontaneous emission could safely be ignored.

Considering the large coupling and propagation losses of the device, net gain will not be possible in this waveguide. The coupling losses can be decreased using a device structure that better fits the fiber light mode with the polymer waveguide mode and the propagation losses can be lowered using other techniques to make the waveguide structures, instead of RIE. SU-8 was used as another polymer that is structured more easily and shows good solubility properties with the  $\text{LaF}_3$  nanoparticles.

### 7.2.2 SU-8 waveguides

Low loss waveguides of SU-8 have been fabricated by Borreman *et al.*<sup>15</sup> The nanoparticle-doped SU-8 waveguides were made by mixing a  $\text{LaF}_3:\text{Nd}$  nanoparticle solution in  $\gamma$ -butyrolactone with a commercially available SU-8 solution in  $\gamma$ -butyrolactone.<sup>10</sup> SU-8 is a negative photoresist that can be patterned by photolithography, thus without RIE. The structures

of the molecules in this photoresist solution are shown in Figure 7.6. The monomer consists of a bisphenol A epoxy resin that can be polymerized by acid catalysis. A sulfonium ion acts as the photoinitiator for the polymerization, which generates protons upon UV irradiation. The solvent used for the photoresist composition is  $\gamma$ -butyrolactone, of which the structure is also shown in Figure 7.6.

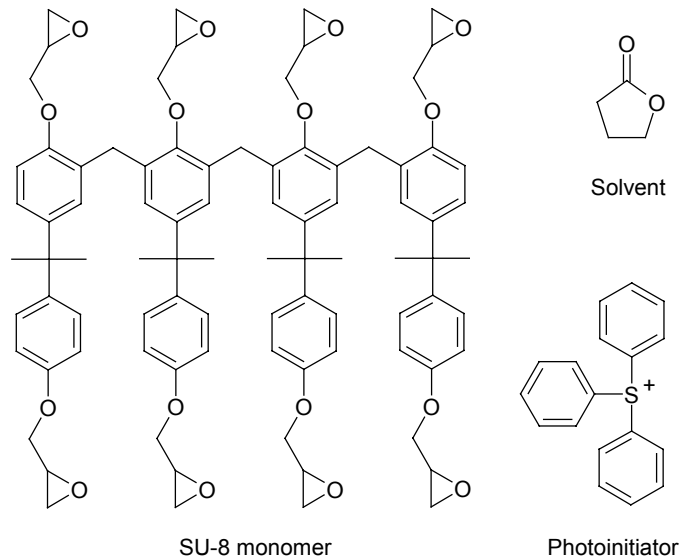


Figure 7.6: Composition of a SU-8 negative photoresist solution.

Due to the high refractive index (1.59) of the polymer, glass can be used as the substrate. The polymer shows good adhesion to glass, making it possible to dice the endfaces. Due to the strong cross-linking of the polymer it is also possible to apply a cladding over the device, without destroying the waveguide structures.

SU-8 layers doped with 20 % w/w of the  $\text{LaF}_3\text{:Nd}$  nanoparticles were spin-coated on 10 cm borosilicate wafers. The processing of the doped SU-8 was similar to the processing of the un-doped photoresist and only a few modifications were necessary.<sup>10,15</sup> First of all, the temperatures at which the spin-coated layers were handled before the development had to be lowered compared to the SU-8 without nanoparticle doping. Temperatures above 75 °C lead to desorption of the ligand from the nanoparticle surface, which has a negative effect on the solubility of the nanoparticles in organic solvents. When the doped layers were handled at temperatures exceeding 75 °C, a thin layer of insoluble nanoparticles remained on the substrate after development. For this reason the layers were heated at 65 °C for two hours after spin-coating to remove the solvent. After the development the layers were hard-baked at the usual temperature of 150 °C, because in the highly cross-linked polymer the nanoparticles will not aggregate anymore. The doped SU-8 layers also needed a longer irradiation time compared to the

SU-8 layers without nanoparticle doping. For the layers without nanoparticles, the irradiation time was 10 seconds, but for the doped layers an irradiation time of 300 seconds was necessary. There can be several reasons for this increase in irradiation time. A possible reason seems the slight desorption of ligand from the nanoparticle surface in the softbake step. This ligand could act as a base during the crosslinking of the polymer, slowing down the reaction rate. Another possibility is that the photoinitiator is not randomly distributed in the polymer film. The ligand monolayer around the nanoparticles creates a hydrophobic film, which could cause an inhomogeneous distribution of the photoinitiator.

The waveguides were finished by spin-coating a layer of HEMA-styrene on top of the device as a cladding, followed by dicing the endfaces. Optical microscope pictures of the waveguides with the cladding on top are shown in Figure 7.7. The left picture shows a top view of some channels covered with the cladding. The picture shows straight and smooth channels. The right picture shows a cross-sectional view of a 5 by 10  $\mu\text{m}^2$  channel. It can be seen that the top of the channel is a bit wider than the bottom of the channel, which can be caused by the un-optimized irradiation conditions. During the irradiation the top of the polymer slab can heat up by the long wavelength components in the UV light source. Due to the higher temperature in the top layer the reaction rate was increased causing the top of the channel to be wider. After dicing the endfaces, the total length of the waveguide was 5.2 cm.

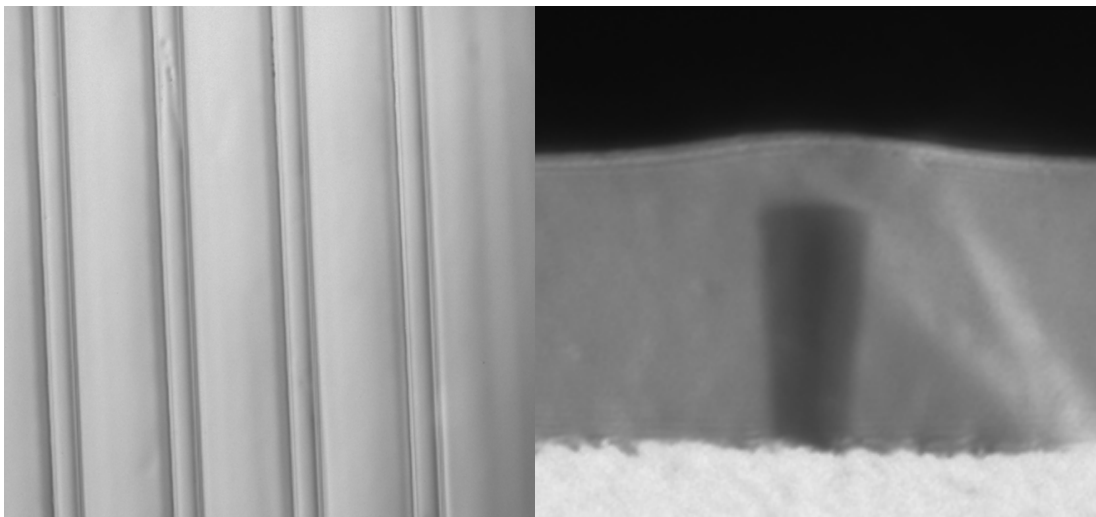


*Figure 7.7: Waveguides of SU-8 doped with 20 % of  $\text{LaF}_3\text{:Nd}$ , (left) top view of waveguide channels, (right) cross-sectional view of a diced  $5 \times 10 \mu\text{m}^2$  channel.*

Optical pumping at 578 nm was not successful for the SU-8 device, because the polymer was not stable under high pump fluxes of this wavelength. Yellowing of the polymer at the high temperatures of the hard bake step is probably the cause of this instability. The yellowing of the

polymer is probably caused by the photoinitiator, leading to absorptions well into the visible part of the spectrum, even at 578 nm.

Another possibility is to excite the  $\text{Nd}^{3+}$  ions at 795 nm. The absorption of this peak is slightly weaker, but an advantage of this wavelength is that pump and signal wavelength are closer together, making it easier to match the light mode of the pump and signal wavelength. For this reason,  $\text{Nd}^{3+}$ -doped fiber amplifiers are usually pumped at this wavelength and because a large variety of cheap pump-lasers are available at this wavelength. It is unlikely that the yellowing in the SU-8 polymer causes high absorption losses at this wavelength. The optical fibers had to be connected to the device for the pumping at 795 nm, because the pump laser and a good alignment setup were not available. Optical fibers (core diameter of 9  $\mu\text{m}$ ) were connected to a 10 by 10  $\mu\text{m}^2$  channel, using UV curable glue. The fibers were aligned using a laser operating at 850 nm. With the glue between the fibers and the waveguide a minimum loss of 7 dB over the 5.2 cm device was measured, including the coupling losses. The propagation losses of this waveguide were in the order of 1 dB/cm or less, assuming coupling losses of 1-2 dB. These losses are very similar to a waveguide without nanoparticles, showing that the nanoparticles are well dispersed in the polymer and that they do not contribute significantly to scattering losses. The losses were increased to 12 dB at 850 nm after curing of the glue by UV irradiation. This increase in the losses could be a result of stress in the glue resulting in an inhomogeneous curing, or as a result of the instability of SU-8 towards UV light.

The chip losses of the waveguide were determined using a white light source and the loss spectrum is shown in Figure 7.8.

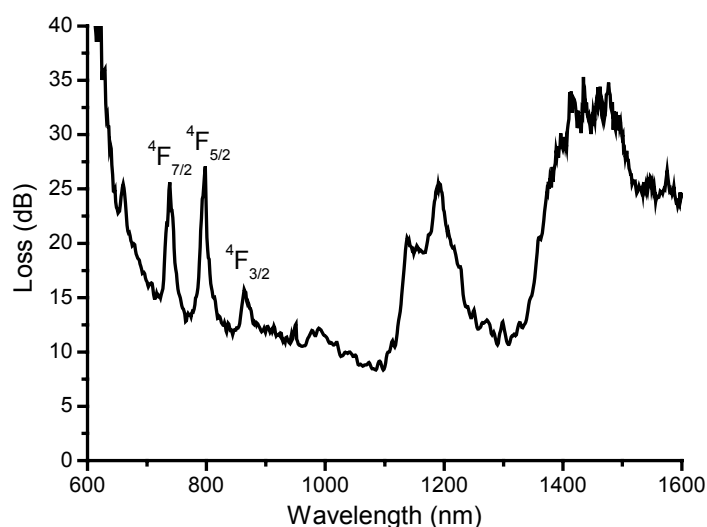


Figure 7.8: Chip losses of a 10 by 10  $\mu\text{m}^2$  waveguide of SU-8/LaF<sub>3</sub>:Nd.

The minimum loss of 8.5 dB over the entire device is around 1100 nm and at the signal wavelength of 1319 nm, the loss is 11.5 dB. At 738, 798, and 863 the  $\text{Nd}^{3+}$  absorption lines are observed originating from absorptions of the ground state level to the  $^4\text{F}_{7/2}$ ,  $^4\text{F}_{5/2}$ , and the  $^4\text{F}_{3/2}$  levels respectively. Below 700 nm the losses of the device increase strongly due to yellowing of the polymer. The overtone absorptions of the CH bonds between 1100-1250 nm and between 1350-1600 nm are observed with a minimal loss window between 1250 and 1350 nm. The high losses around 1500 nm show that this polymer is unsuitable for waveguiding at this wavelength. The emission spectrum of  $\text{Nd}^{3+}$  after pumping the waveguide at 795 nm with 50 mW of input power and collecting the emission at the end of the waveguide structure is shown in Figure 7.9. The ratio of the 1060 and the 1330 nm emission peaks is different from that in solution. This was caused by the filters, the same as for the PMMA device. A small peak of the pump laser at 795 nm is still observed, but this small signal did not interfere with the amplification measurement. Using the same setup as used for the PMMA device (Figure 7.5), amplification of the waveguide was measured. The pump beam and signal beam were coupled in one 9  $\mu\text{m}$  fiber using a 2 x 2 splitter for the amplification measurement. Due to the high losses originating from the splitter, only 5 mW of pump power could be coupled into the device. A signal amplification of 0.1 dB could be measured on the 10 by 10  $\mu\text{m}^2$  channel of 5.2 cm length.

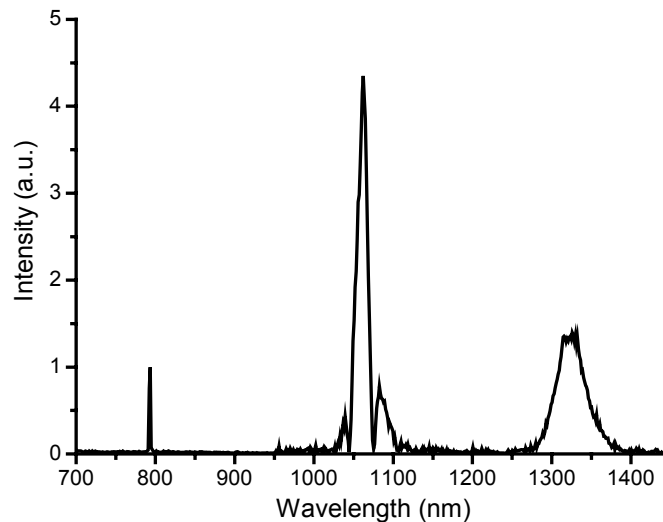


Figure 7.9:  $\text{Nd}^{3+}$  emission spectrum measured at the end of the SU-8/LaF<sub>3</sub>:Nd waveguide after pumping at 795 nm.



### 7.2.3 Modeling of the amplification

There are several models for the calculation of the optical gain in  $\text{Nd}^{3+}$ -doped glass fibers.<sup>16</sup> The simplified model described in the appendix was used to calculate the optical gain that can be reached in the polymer waveguides. This model does not take into account the losses of the chip, the effect of excited state absorption (ESA), and amplified spontaneous emission (ASE). ESA and ASE will deplete the excited state of the  $\text{Nd}^{3+}$  ion by the absorption of a signal photon (ESA), or by amplification of light at another wavelength than the desired signal wavelength (ASE). The occurrence of these processes would lower the actual population of the excited state leading to an overestimation of the actual gain. The energy level scheme of  $\text{Nd}^{3+}$  is a 4-level system (Figure 7.A., see Appendix), because the  $^4\text{I}_{13/2}$  level is not the ground state and non-radiative decay from the  $^4\text{I}_{13/2}$  level to the  $^4\text{I}_{9/2}$  ground state is very fast. As a result, the  $^4\text{I}_{13/2}$  is always empty and a population inversion is always present after photon absorption. Amplification now only depends on the number of ions that are in the  $^4\text{F}_{3/2}$  excited state. The calculated amplification for the PMMA and SU-8 waveguide channels are shown in Figure 7.10, for the pump powers of 12 mW and 5 mW, respectively, and for the channel sizes used in the experiments.

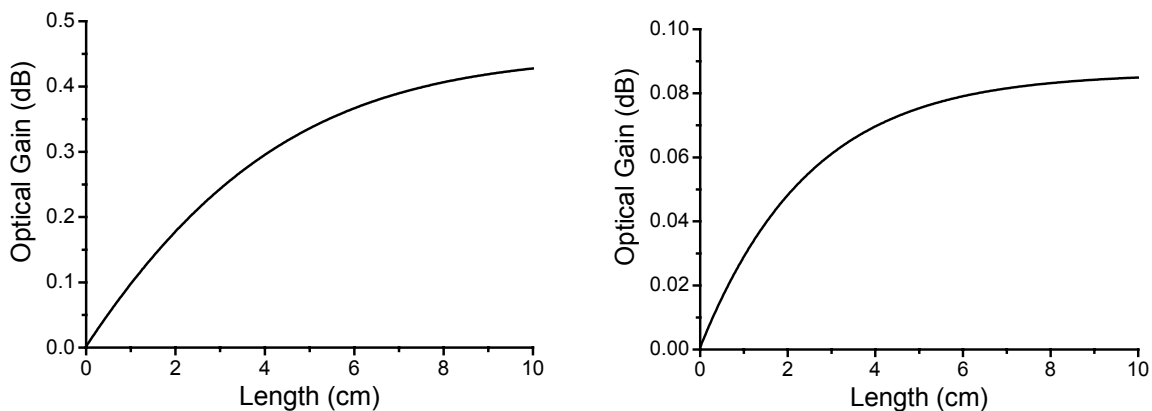


Figure 7.10: Amplification calculated for the PMMA  $10 \times 3.3 \mu\text{m}^2$  waveguide with a pump power of 12 mW at 578 nm (left) and the  $10 \times 10 \mu\text{m}^2$  SU-8 waveguide with a pump power of 5 mW at 795 nm (right).

The PMMA device was only 3 cm long and at this length the maximum amplification is not yet reached. The calculated value of 0.25 dB for a 3 cm chip is only slightly lower than the measured value of 0.3 dB but this is probably within experimental error, considering the approximations in the calculation. At a length of 5.2 cm in the SU-8 waveguide the maximum gain is almost reached. In this case the measured gain of 0.1 dB is also somewhat higher than the

calculated gain of 0.08 dB. The calculated values correspond very well with the measured values indicating that the model gives an accurate description of the actual amplification.

### 7.3 Outlook: Optimization of the device structure

The optical gain measured in the polymer-based waveguide was limited compared to what is reported for Nd<sup>3+</sup>-doped glass fibers (0.3 dB for our polymer-based waveguide compared to 10 dB for glass fibers).<sup>17</sup> However, these results cannot be compared directly, because the experimental conditions that have an influence on the amplification were completely different. The maximum gain of the Nd<sup>3+</sup>-doped fiber was measured at a wavelength of 1343 nm. At 1319 nm a maximum gain of 7 dB was measured, a lot lower as a result of ESA. The pump power and the dimensions of the fiber were also completely different than the conditions we used in our experiments. The Nd<sup>3+</sup>-doped fiber was excited with 100 mW of pump power with a fiber diameter of 6.5  $\mu\text{m}$ . In our experiments the pump power was limited, because of the high losses originating from the coupling and the combining of signal and pump laser. The theoretical model described in the appendix allows for the calculation of the optical gain of the polymer waveguide with varying pump powers and channel dimensions.

The calculated optical gain of an SU-8 waveguide channel, with dimensions of 10 by 10  $\mu\text{m}^2$ , as a function of the pump power is shown in Figure 7.11. The calculations clearly demonstrate that the gain increases substantially when the pump power is increased from 5 mW to 100 mW.

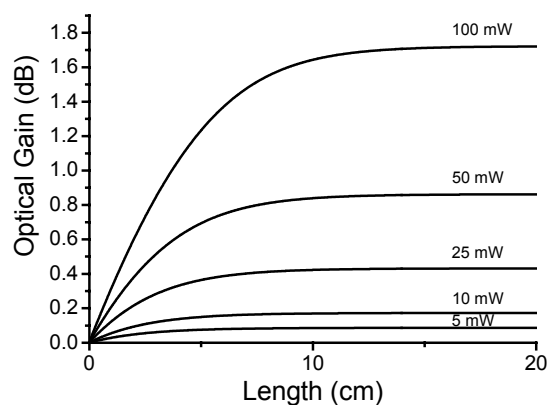


Figure 7.11: Optical gain of a LaF<sub>3</sub>:Nd-doped SU-8 waveguide as a function of pump power for a 10 x 10  $\mu\text{m}^2$  channel pumped at 795 nm.

The length of the device, or the concentration of  $\text{Nd}^{3+}$  ions in the waveguide have to be increased in order to measure the maximum obtainable gain at these higher pump powers. Another large performance increase can be reached when the size of the channel is decreased as shown in Figure 7.12. Decreasing the size of the channel increases the density of the pump power, so the effect is similar to an increase in pump power. These calculations were done with a pump power of 100 mW. The  $\text{Nd}^{3+}$ -doped fiber had a dimension of  $6.5 \mu\text{m}^{17}$  and in a square geometry this corresponds to a  $5.7$  by  $5.7 \mu\text{m}^2$  waveguide channel. The calculated gain in a waveguide of these dimensions is 5.1 dB for a 20 cm long device, close to the value measured in the  $\text{Nd}^{3+}$ -doped fiber of 7 dB. A further decrease of the channel dimensions would result in a further increase of the amplification. Similar results were calculated for the  $\text{Nd}^{3+}$ -doped fiber amplifier.<sup>17</sup> The length of the device and the concentration of  $\text{Nd}^{3+}$  in the waveguide both affect the amplification of the waveguide. When the concentration of the lanthanide ion is doubled, the length of the device can be halved to have the same amplification. This is of course different when losses and the effect of concentration quenching are taken into account. In glass fibers the losses are very low and concentration quenching lowers the luminescent lifetime of the ions even at concentrations below 1 %. As a result, fiber amplifiers are very long, extending to several meters. For integrated devices the length of the amplifier has to be reduced in order to fit the amplifier on a small chip. As a consequence, the concentration of the lanthanide ion has to be increased in order to have sufficient amplification. The optical losses are usually higher for polymers compared to glass materials, making the requirement for a shorter device even more important.

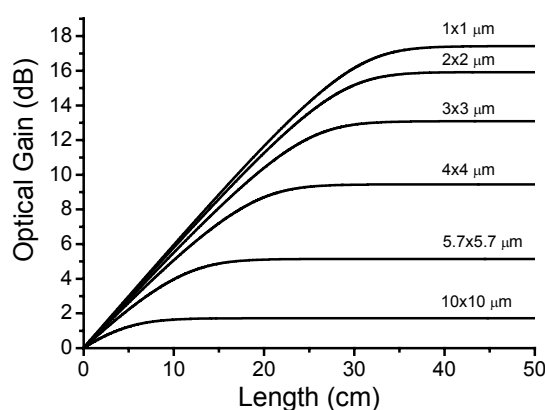


Figure 7.12: Optical gain of a  $\text{LaF}_3:\text{Nd}$ -doped SU-8 waveguide as a function of the dimensions of the waveguide. All calculations were at a constant pump power of 100 mW.

The luminescence lifetime is another important factor in the amplification scheme. It is a measure for the amount of time an ion spends in the excited state and at a fixed pump power it determines directly how much of the population is in the excited state. The emission cross-section determines how much stimulated emission there will be. The higher the emission cross-section the more stimulated emission and the more amplification of the signal. The emission cross-section and the luminescence lifetime are related and this ratio will be the highest when the quantum yield is unity. In order to show that the measured gain is a result of the increase in luminescence lifetime of the  $\text{Nd}^{3+}$  ion in the nanoparticles, compared to organic complexes, the calculated optical gain as a function of the luminescence lifetime is shown in Figure 7.13, for a  $10 \text{ by } 10 \mu\text{m}^2$  waveguide channel and a pump power of 100 mW.

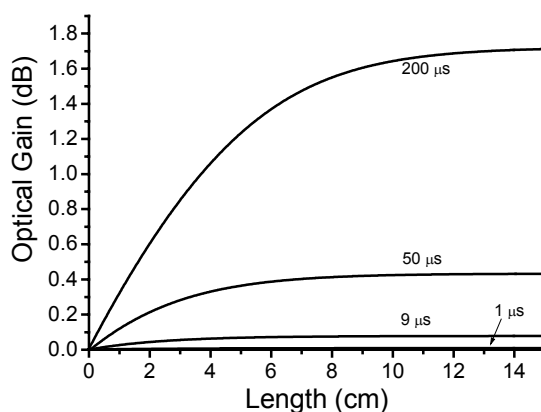


Figure 7.13: Optical gain calculated for different luminescence lifetimes. The pump power is 100 mW and the channel dimensions are  $10 \text{ by } 10 \mu\text{m}^2$ .

The amplification is limited to only 0.009 dB for a luminescence lifetime of 1  $\mu\text{s}$ , which is generally observed for complexes with CH bonds close to the lanthanide ion. The highest luminescence lifetime of  $\text{Nd}^{3+}$  observed in organic systems so far was 9  $\mu\text{s}$  and for this luminescence lifetime the optical gain is still limited to 0.08 dB. For a luminescence lifetime of 200  $\mu\text{s}$  as observed in the  $\text{LaF}_3:\text{Nd}$  nanoparticles the optical gain is already 1.7 dB for this device configuration. In these calculations it is assumed that the absorption and emission cross-sections of  $\text{Nd}^{3+}$  is the same in the different materials. Small differences in these values may be observed due to changes in symmetry, but these differences will not compensate for the large difference in optical amplification that is observed. It is very clear that with the luminescence lifetimes observed in organic complexes it will be difficult to realize net gain. The increase in luminescence lifetime we obtained, by doping the  $\text{Nd}^{3+}$  ion in the  $\text{LaF}_3$  nanoparticles is

responsible for the fact that we were able to measure optical gain. The doping of  $\text{Nd}^{3+}$  ions into the  $\text{LaF}_3$  nanoparticles leads to optical properties that allow amplification close to what is observed in  $\text{Nd}^{3+}$ -doped glass fiber amplifiers.

Amplification with other ions should also be possible. The  $\text{Er}^{3+}$  ion, which is commonly used in optical fiber amplifiers, also shows emission in the  $\text{LaF}_3$  nanoparticles, but for amplification at 1530 nm other polymers have to be used to reduce the optical loss at the signal wavelength. The organic ligand that is protecting the nanoparticles from aggregation also contains a lot of CH bonds, but the total amount of ligand is low in the whole system and a proof of principle should be possible for amplification by  $\text{Er}^{3+}$  ions as well with this ligand and a halogenated polymer. The same holds for the other two lanthanide ions,  $\text{Pr}^{3+}$  and  $\text{Ho}^{3+}$ , that show emissions around 1450 nm.

## 7.4 Conclusions

Optical gain in a polymer-based waveguide doped with nanoparticles synthesized in this thesis in the near-infrared was demonstrated. The pump power that could be coupled in the waveguide was limited and therefore only a small signal gain was observed, but theoretical calculations show that the optical gain could be close to what was observed in  $\text{Nd}^{3+}$ -doped glass fibers, when the same experimental conditions are used.

## 7.5 Experimental section

**General.** Spin-coating of the polymer solutions was performed under standard cleanroom conditions. The thicknesses of the polymer layers were measured using a Dektak surface profiler. Arch, 907/17 was used as the positive photoresist and spin-coated at a speed of 4000 rpm for 20 s and a prebake temperature of 95 °C. The photoresist was developed in standard OPD developer for 50 s. Reactive ion etching was performed using a Elektrotech PF340 etcher. The endfaces of the SU-8 waveguide were made by dicing the substrate using a Disco DAD-321 Dicing Saw.

**$\text{LaF}_3$ :Nd nanoparticles.**  $\text{LaF}_3$ :Nd nanoparticles were synthesized as described in chapter 3. PMMA layers were spin-coated from chlorobenzene and ligand **2** of chapter 3 was used to make  $\text{LaF}_3$ :Nd nanoparticles that are soluble in chlorobenzene. SU-8 is a commercial product with  $\gamma$ -butyrolactone as the solvent. Nanoparticles synthesized with ligand **2** of chapter 4 are soluble in  $\gamma$ -butyrolactone, but for mixing with the SU-8 solution, a mixture of ligand **2** and **5** in the ratio 1:2 was found to give the best solubility properties. The nanoparticle-doped solution was made by dissolving the nanoparticles in  $\gamma$ -

butyrolactone and mixing this solution with commercially available SU-8 25 (solid content 63 %), to end up with a solid content of 52 %.

**Waveguide fabrication.** The PMMA/ LaF<sub>3</sub>:Nd solution was spin-coated on a 3” silicon wafer covered with 3.2 μm SiO<sub>2</sub> (Plasma enhanced chemical vapor deposition; PECVD) on top. The solution consisted of 900 mg PMMA and 100 mg of nanoparticles dissolved in 4 g of chlorobenzene. Spin-coating was performed at 1250 rpm resulting in a layer thickness of 3.3 μm. After spin-coating the wafer was dried at 95 °C followed by spin-coating a 1.2 μm thick layer of positive photoresist on top. Patterns were made with a mask having channels ranging in diameter from 2-10 μm, using a radiation time of 3.7 s. The photoresist was developed in standard OPD developer for 50 sec. After creation of the pattern in the photoresist the polymer was etched using reactive ion etching (RIE). RIE was done for 8 min at a power of 20 W with a pressure of 10 mTorr and 20 sccm O<sub>2</sub>, keeping the wafer at a temperature of 10 °C. Excess photoresist was removed by irradiation and development, leaving ridges with a height of 1.45 μm. The doped SU-8 layers were spin-coated on 10 cm borosilicate wafers that were previously cleaned in fuming nitric acid for 8 minutes. The solid content of the solution of 52 % included the nanoparticles and the composition of the SU-8 solution in a 1:4 weight ratio. Spin-coating was done at 1250 rpm for 30 seconds with an acceleration of 100 rpm/sec. The layers were dried at 65 °C for two hours, followed by exposure for 300 seconds through a mask containing the waveguide structures. The film was postbaked at 65 °C for 2 min followed by development in RER 600 developer for 2 minutes. The structures were washed with isopropanol to remove excess developer and dried with a nitrogen stream. Flood exposure was done for 5 minutes, followed by a hard bake for 2 hours at 150 °C. A cladding of HEMA-styrene was spin-coated on top of the device at a spin speed of 750 rpm.

**Photophysical measurements.** Measurements on the waveguides were performed using an Ar<sup>+</sup>-pumped dye laser as the pump laser at 578 nm and a Ti Sapphire laser was used for pumping at 795 nm. The signal laser was a diode laser operating at 1319 nm. The laser light was coupled into a 9/125 μm single mode fiber using a microscope objective and from the fiber into the waveguide. Alignment of the fibers and chip were done using a butt-end coupling setup. Light coming from the waveguide was collected with a single or multi-mode fiber and lead to a detector or a spectral analyzer for emission spectra.

## 7.6 References and notes

- <sup>1</sup> Becker, P. C.; Olsson, N. A.; Simpson, J. R. *Erbium Doped Amplifiers: Fundamentals and Technology*; Academic Press: San Diego, 1999.
- <sup>2</sup> Polman, A. *Phys. B* **2001**, *300*, 78.

- <sup>3</sup> Whitley, T. J. *J. Lightwave Technol.* **1995**, *13*, 744.
- <sup>4</sup> (a) Percival, R. M.; Szebesta, D.; Williams, J. R.; Lauder, R. D. T.; Tropper, A. C.; Hanna, D. C. *Electron. Lett.* **1994**, *30*, 1598; (b) Komukai, T.; Yamamoto, T.; Sugawa, T.; Miyajima, Y. *IEEE, J. Quant. Electron.* **1995**, *31*, 1880; (c) Taylor, E. R.; Ng, L. N.; Sessions, N. P. *J. Appl. Phys.* **2002**, *92*, 112.
- <sup>5</sup> (a) Ma, H.; Jen, A. K. Y.; Dalton, L. R. *Adv. Mater.* **2002**, *14*, 1339; (b) Zhou, M. *Opt. Eng.* **2002**, *41*, 1631.
- <sup>6</sup> Slooff, L. H.; van Blaaderen, A.; Polman, A.; Hebbink, G. A.; Klink, S. I.; van Veggel, F. C. J. M.; Reinhoudt, D. N.; Hofstraat, J. W. *Appl. Phys. Rev.* **2002**, *91*, 3955.
- <sup>7</sup> Hebbink, G. A. *Luminescent materials based on lanthanide ions* PhD thesis, University of Twente, 2002.
- <sup>8</sup> (a) Schacklette, L. W.; Blomquist, R.; Deng, J. M.; Ferm, P. M.; Maxfield, M.; Mato, J.; Zou, H. *Adv. Funct. Mater.* **2003**, *13*, 453; (b) Eldada, L.; Schacklette, L. W. *IEEE J. Sel. Top. Quant.* **2000**, *6*, 54.
- <sup>9</sup> Ma, H.; Jen, A. K. Y.; Dalton, L. R. *Adv. Mater.* **2002**, *14*, 1339.
- <sup>10</sup> NANO<sup>TM</sup> SU-8-25, Microchem, <http://www.microchem.com>.
- <sup>11</sup> Klunder, D. *Photon physics in integrated optics microringresonators* PhD thesis, University of Twente, 2002.
- <sup>12</sup> Kuiper, V. S. *Feasibility of a microring laser using LaF<sub>3</sub>:Nd nanoparticles as doping* M.Sc. thesis, University of Twente, 2002.
- <sup>13</sup> McCall, S. L.; Levi, A. F. J.; Slusher, R. E.; Pearton, S. J.; Logan, R. A. *Appl. Phys. Lett.* **1992**, *60*, 289.
- <sup>14</sup> (a) Brierly, M. C.; Millar, C. A. *Electron. Lett.* **1988**, *24*, 439; (b) Miyajima, Y.; Komukai, T.; Sugawa, T. *Electron. Lett.* **1990**, *26*, 194; (c) Sugawa, T.; Miyajima, Y.; Komukai, T. *Electron. Lett.* **1990**, *26*, 2042.
- <sup>15</sup> Borreman, A.; Musa, S.; Kok, A. A. M.; Diemeer, M. B. J.; Driessen, A. *Proc. Symp. IEEE/LEOS Benelux Chapter*, **2002**, 83.
- <sup>16</sup> (a) Bjarklev, A. *Optical fiber amplifiers: Design and System Applications*; Artech House: Boston, 1993; (b) Pedereson, J. E.; Brierly, M. C. *Electron. Lett.* **1990**, *26*, 819; (c) Dakks, M. L.; Miniscalco, W. J. *IEEE Photon. Technol. Lett.* **1990**, *2*, 650.
- <sup>17</sup> (a) Miyajima, Y.; Komukai, T.; Sugawa, T. *Electron. Lett.* **1990**, *26*, 194; (b) Sugawa, T.; Miyajima, Y.; Komukai, T. *Electron. Lett.* **1990**, *26*, 2042.

### 7.A.1 Modeling of the Nd<sup>3+</sup> optical amplification.

Theoretically, Nd<sup>3+</sup> can be described as a four-level system as shown in Figure 7.A.1 for pumping at 578 or 795 and optical gain at 1319 nm. This energy scheme is simplified, because in the calculations the excited state absorption (ESA) and amplified spontaneous emission (ASE) are not taken into account.

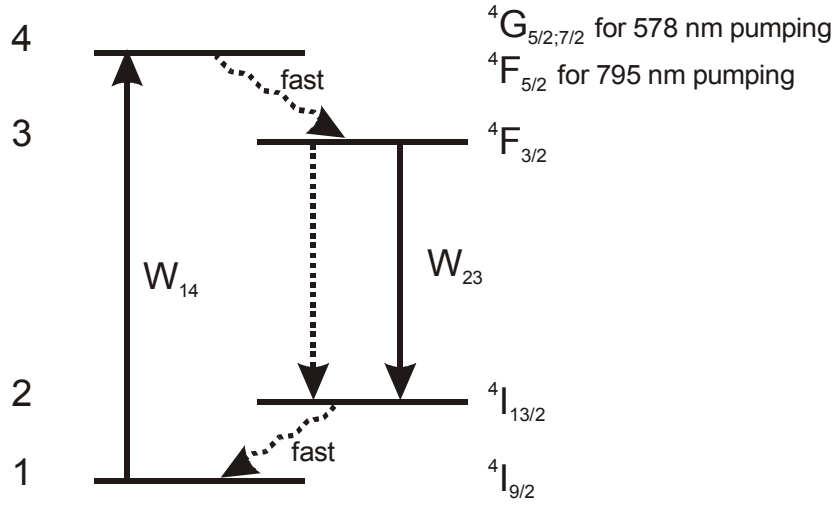


Figure 7.A.1: Simplified 4-level energy scheme of Nd<sup>3+</sup> with the upper level  $^4G_{5/2;7/2}$  for pumping at 578 nm or the  $^4F_{5/2}$  level for 795 nm pumping.

The Nd<sup>3+</sup> ion is excited from the  $^4I_{9/2}$  ground state to the  $^4G_{5/2}$  excited state for 578 nm pumping and to the  $^4F_{5/2}$  excited state for 795 nm pumping followed by a fast decay to the  $^4F_{3/2}$  excited state. Emission at 1319 nm is a transition to the  $^4I_{13/2}$  level, which decays rapidly to the  $^4I_{9/2}$  ground state. Due to the fast decays  $4 \rightarrow 3$  and  $2 \rightarrow 1$ , the levels 4 and 2 are considered empty and the populations of the levels 3 and 1 can be determined using Equation 7.A.1.

$$\begin{aligned} \frac{dN_1}{dt} &= 0 = -W_{14}N_1 + \left( \frac{1}{\tau} + W_{32} \right) N_3 \\ \frac{dN_3}{dt} &= 0 = +W_{14}N_1 - \left( \frac{1}{\tau} + W_{32} \right) N_3 \\ N_1 + N_3 &= N_{\text{tot}} \end{aligned} \quad (\text{Eq. 7.A. 1})$$



With  $N_1$  the population of level 1,  $N_3$  the population of level 3,  $N_{\text{tot}}$  the total population,  $W_{14}$  the rate of absorption,  $W_{32}$  the rate of stimulated emission, and  $\tau$  the luminescence lifetime. In the steady state these equations are equal to zero, but because the sum of both populations is equal to the total population, it is a determined set of equations and thus simplify to

$$\begin{aligned} N_1 &= \left( \frac{W_{32} + 1/\tau}{W_{32} + 1/\tau + W_{14}} \right) N_{\text{tot}} \\ N_3 &= \left( \frac{W_{14}}{W_{32} + 1/\tau + W_{14}} \right) N_{\text{tot}} \end{aligned} \quad (\text{Eq. 7.A.2})$$

The absorption and emission rates  $W_{14}$  and  $W_{32}$  are calculated from the following equations.

$$\begin{aligned} W_{14} &= \sigma_a I_p ; I_p = \frac{P_p}{h\nu_p A} \\ W_{32} &= \sigma_e I_s ; I_s = \frac{P_s}{h\nu_s A} \end{aligned} \quad (\text{Eq. 7.A.3})$$

$I_p$  and  $I_s$  are the photon densities of the pump and signal source and  $\sigma_a$  the absorption cross section and  $\sigma_e$  the stimulated emission cross section. The photon densities are calculated from the pump and signal power  $P_p$  and  $P_s$ , the light frequencies  $\nu_p$  and  $\nu_s$ , Planck's constant  $h$  and the cross section of the waveguide  $A$ . It would be better to use the exact overlap of the pump and signal modes for the cross section, because the overlap of the pump and signal beams will be smaller than the cross-section. The use of the cross-section of the waveguide in these calculation leads to an overestimation of the actual gain.

The power of the signal and pump along the waveguide is given by:

$$\begin{aligned} dI_s &= W_{32} N_3 dz \\ dI_p &= W_{14} N_1 dz \end{aligned} \quad (\text{Eq. 7.A.4})$$

These equations can be solved numerically using the values for the different parameters as shown in Table 7.A.1. Different values for the PMMA and SU-8 device were used. The absorption cross-section at 795 nm is about 0.6 of that at 578 nm and the emission cross-section

is taken the same for both polymers, although there will be a small influence of the refractive index on the emission cross-section. The concentration of the nanoparticles in the SU-8 waveguides is twice as high as in the PMMA waveguide, resulting in a double  $\text{Nd}^{3+}$  ion concentration. The dimensions of the SU-8 channel are also different. A luminescence lifetime of 200  $\mu\text{s}$  was used for the  $\text{Nd}^{3+}$  ions. In chapter 3 the luminescence decay curve of the  $\text{LaF}_3:\text{Nd}$  nanoparticles was found to be bi-exponential with values for the luminescence lifetime of 240 (77 %) and 40 (23 %)  $\mu\text{s}$  were found. The average lifetime of these two is approximated to 200  $\mu\text{s}$ .

*Table 7.A.1: Parameters used in the optical gain calculation*

Parameter	Value 578 nm PMMA waveguide	Value 795 nm SU-8 waveguide	Unit
$P_p$	12	5	mW
$P_s$	0.1	0.1	mW
$\sigma_a$	$2.5 \cdot 10^{-20}$	$1.5 \cdot 10^{-20}$	$\text{cm}^2$
$\sigma_e$	$5 \cdot 10^{-21}$	$5 \cdot 10^{-21}$	$\text{cm}^2$
$\lambda_p$	1319	1319	nm
$\lambda_s$	578	795	nm
$\tau$	200	200	$\mu\text{s}$
$N_{\text{tot}}$	$1.4 \cdot 10^{19}$	$2.8 \cdot 10^{19}$	$\text{cm}^{-3}$
Height	3.3	10	$\mu\text{m}$
Width	10	10	$\mu\text{m}$

The absorption cross-section at 795 nm was taken from the literature for  $\text{Nd}^{3+}$ -doped in  $\text{LaF}_3$ .<sup>1</sup> The absorption cross-section at 578 nm was taken to be 1.7 times as high as the absorption cross-section at 795 nm. The emission cross-section at 1319 nm was calculated from the emission spectrum.<sup>2</sup> The  $\text{Nd}^{3+}$  concentration corresponds to a nanoparticle concentration of 10 and 20 % for the PMMA and SU-8, respectively, taking into account 15 % by weight of organic ligand around the nanoparticles.

## 7.A.2 References

- <sup>1</sup> Bhutta, T.; Chardon, A. M.; Shepherd, D. P.; Daran, E.; Serrano, C.; Yagüe, A. M. *IEEE J. Quant. Electron.* **2001**, *37*, 1469.
- <sup>2</sup> Klunder, D. *Photon physics in integrated optics microringresonators* PhD thesis, University of Twente, 2002.



## Summary

The luminescence of lanthanide ions in organic environment is greatly reduced compared to inorganic materials. This thesis describes the doping of the lanthanide ions in the core of inorganic nanoparticles that are soluble in organic solvents as a way to shield the lanthanide ions from the organic environment and thus to increase the luminescence properties.

The technological importance of lanthanide luminescence in optical amplifiers has been outlined in chapter 1. The integration of optical components requires materials that can be processed easily and at a low cost and polymers are materials that generally have these properties. Optical amplifiers have to be developed for these polymer-based systems and the luminescence of lanthanide ions in polymer environments has to be improved in order for these ions to play a role.

In chapter 2 the luminescence of lanthanide ions in a variety of host materials is described. It explains why lanthanide ions do not show efficient luminescence in organic materials, but are efficient emitters in inorganic materials. The high-energy vibrations of the chemical bonds in organic materials can take up the energy of an excited lanthanide ion very efficiently and thereby quench the luminescence of the ions. In inorganic materials the vibrational energies are substantially lower, making this process less efficient. Nanoparticles are materials with an inorganic core that can be surrounded by organic ligands. These organic ligands can control the growth of the nanoparticles during the synthesis and at the same time they can provide solubility of the particles in organic solvents. Doping of lanthanide ions in the inorganic part of nanoparticles would provide the lanthanide ion with an environment with low vibrational energies, but the nanoparticles itself can be processed as organic materials.

The synthesis of these lanthanide-doped nanoparticles has been described in chapter 3. Nanoparticles of  $\text{LaF}_3$ ,  $\text{LaVO}_4$ , and  $\text{LaPO}_4$  that are soluble in organic solvents were successfully doped with luminescent lanthanide ions. The visible emitting  $\text{Eu}^{3+}$  ion was used to characterize the doping site of the lanthanide ion. The luminescence of the lanthanide ions indicates that the ions are doped in the core of the nanoparticles and that the luminescence spectra are comparable to the bulk materials. The shielding of the lanthanide ion from the organic environment is good, because emissions of lanthanide ions are observed, that are usually quenched in organic complexes. The luminescence decays of the ions are multi-exponential, so not all lanthanide ions have the same probability of decay. The luminescence lifetimes indicate a high quantum yield compared to organic complexes and bulk inorganic compounds. With the emissions of the NIR-

emitting nanoparticles doped with  $\text{Nd}^{3+}$ ,  $\text{Er}^{3+}$ ,  $\text{Ho}^{3+}$ , and  $\text{Pr}^{3+}$  the entire telecommunications window between 1300 and 1600 nm can be covered.

The luminescence decays of lanthanide ions doped in nanoparticles are not mono-exponential. In chapter 4, several factors that are of influence on the decay time and the shape of the decay curve have been identified. These factors include quenching by the solvent, the refractive index of the solvent, and the concentration of the luminescent lanthanide ions. The solvent is the most important source of quenching, causing the deviation from exponential behavior. A model was developed for the fitting of the decay curves, taking into account both the quenching from outside the nanoparticle and the distance of the luminescent ion to the surface of the nanoparticle. The model gives a value for the luminescence lifetime without quenching from outside the nanoparticles and a quenching constant determining the quenching strength of the solvent or ligand. Using this model, concentration quenching and quenching from the solvent can be described. In order to obtain more insight in the size-dependent luminescence properties, nanoparticles with different sizes and with a narrow size distribution had to be prepared. The sizes of the nanoparticles could be varied by changing the concentration of ligand used in the synthesis or by size-selective precipitation. The luminescence lifetime of the lanthanide ions is longer in the larger nanoparticles.

Chapter 5 describes methods to functionalize the surface of  $\text{LaF}_3$  and  $\text{LaPO}_4$  nanoparticles with different ligands. Functionalization has an important influence on the solubility of the nanoparticles, which is important for the processability of the system. The synthesis of core-shell nanoparticles for  $\text{LaF}_3$  was successful, because the sizes of the nanoparticles are increased after growing a shell of un-doped  $\text{LaF}_3$  around the original core. The luminescence properties of the lanthanide ions in the core-shell nanoparticles have been improved compared to nanoparticles without a core-shell structure, as follows from the increase in quantum yield of  $\text{LaF}_3:\text{Ce},\text{Tb}$  nanoparticles and the increase in luminescence lifetime of the emissive levels of the  $\text{Eu}^{3+}$  ion. The results show that it is possible to increase the distance between the quenchers coordinated to the surface and the lanthanide ions by the growth of an inorganic shell around the luminescent core.

In Chapter 6 the synthesis of lanthanide-doped semiconductor nanoparticles has been described. Lanthanide-doped nanoparticles of  $\text{TiO}_2$  show energy transfer from the semiconductor host to the lanthanide ions, for lanthanide ions emitting in the visible and in the NIR. The quantum yield of the nanoparticles is low, although the intrinsic quantum yield of the lanthanide ion is high. A LED with the nanoparticles does show diode like behavior, but no lanthanide

luminescence was observed, which is probably caused by the low quantum yield of the nanoparticles.

Polymer waveguides doped with  $\text{LaF}_3:\text{Nd}$  nanoparticles have been described in chapter 7. The emission spectra of  $\text{Nd}^{3+}$  show that the nanoparticles are in the waveguides and the optical losses of the waveguide indicate that the nanoparticles are not clustered and therefore have a small contribution to scatter in the waveguide. For the PMMA waveguides an amplification of 0.3 dB at 1319 nm at a pump power of 12 mW was measured and for the SU-8 waveguides an amplification of 0.1 dB at a pump power of only 5 mW was measured. Theoretical calculations predict that increasing the confinement of the pump and signal beam and an increase in pump power should lead to an amplification of 5.1 dB for a 5.7 by 5.7  $\mu\text{m}^2$  channel, which is very close to the amplification that is obtained in glass fiber amplifiers doped with  $\text{Nd}^{3+}$  under similar experimental conditions. It has been shown theoretically that this amplification is due to the increase in luminescence lifetime compared to organic complexes and that amplification with the luminescence lifetimes of organic complexes is very limited. The use of these organically soluble nanoparticles is therefore a major breakthrough over the use of lanthanide complexes as the gain material in polymer hosts.





## *Samenvatting*

De luminescentie van lanthanide-ionen in organische materialen is veel zwakker dan over het algemeen in anorganische materialen wordt waargenomen. Dit wordt veroorzaakt door de deactivering van het aangeslagen lanthanide-ion door hoog-energetische vibraties van de chemische bindingen van organische moleculen. Dit proefschrift beschrijft het doteren van lanthanide-ionen in de kern van anorganische nanodeeltjes als een manier om de lanthanide-ionen af te schermen van de organische omgeving en op die manier de luminescentie-eigenschappen van de ionen te verbeteren.

Het technologisch belang van lanthanide-ionen in optische versterkers staat beschreven in hoofdstuk 1. Voor de integratie van optische componenten zijn materialen nodig die gemakkelijk kunnen worden verwerkt en tegen lage kosten. Polymeren zijn materialen die deze eigenschappen gewoonlijk bezitten. Optische versterkers zullen moeten worden ontwikkeld voor polymeren om het mogelijk te maken deze geïntegreerde optische systemen van polymeren te maken. De luminescentie-eigenschappen van lanthanide-ionen in polymeren zullen moeten worden verbeterd om deze ionen in polymere versterkers te kunnen gebruiken.

In hoofdstuk 2 is de luminescentie van lanthanide-ionen in verschillende materialen besproken. Er is uitgelegd waarom lanthanide-ionen geen efficiënte luminescentie vertonen in organische materialen, maar wel in anorganische materialen. De hoog-energetische vibraties van de chemische bindingen in organische materialen kunnen de energie van een geëxciteerd lanthanide-ion efficiënt opnemen en op die manier de luminescentie uitdoven. In anorganische materialen zijn deze vibratie-energiën aanmerkelijk lager waardoor dit proces veel minder efficiënt is. Nanodeeltjes zijn materialen met een anorganische kern die kunnen worden omringd door organische liganden. Deze organische liganden kunnen de groei van de deeltjes reguleren tijdens de synthese en op hetzelfde moment kunnen zij ervoor zorgen dat de deeltjes oplosbaar worden in organische oplosmiddelen. Het doteren van lanthanide-ionen in de anorganische kern van deze nanodeeltjes zorgt ervoor dat de lanthanide-ionen een omgeving hebben met lage vibratie-energiën, maar tegelijkertijd kunnen de nanodeeltjes worden verwerkt als organische materialen.

De synthese van deze lanthanide-gedoteerde nanodeeltjes staat beschreven in hoofdstuk 3. Nanodeeltjes van  $\text{LaF}_3$ ,  $\text{LaVO}_4$  en  $\text{LaPO}_4$  die oplosbaar zijn in organische oplosmiddelen werden succesvol gedoteerd met luminescente lanthanide-ionen. Het  $\text{Eu}^{3+}$  ion dat emitteert in het zichtbare deel van het spectrum werd gebruikt om de omgeving van het gedoteerde ion te

bestuderen. De luminescentie van dit ion leert ons dat het gedoteerde ion in de kern van het nanodeeltje zit en dat de luminescentie spectra vergelijkbaar zijn met die van de bulk materialen. Het afschermen van het lanthanide-ion is succesvol omdat emissies van lanthanide-ionen werden geobserveerd die normaal gesproken worden uitgedoofd in organische complexen. De levensduur van de luminescentie vertoont geen mono-exponentieel verval wat er op duidt dat niet alle ionen dezelfde waarschijnlijkheid tot verval hebben. De luminescente levensduren laten zien dat de lanthanide-ionen een hoge quantum opbrengst hebben in vergelijking met organische complexen en bulk anorganische materialen. De emissies van de nabij-infrarood emitterende  $\text{Nd}^{3+}$ ,  $\text{Er}^{3+}$ ,  $\text{Ho}^{3+}$  en  $\text{Pr}^{3+}$  gedoteerde nanodeeltjes kan het hele telecommunicatie-gebied bestrijken.

Het verval van de luminescentie van lanthanide ionen gedoteerd in de nanodeeltjes is niet mono-exponentieel. In hoofdstuk 4 zijn verschillende factoren onderzocht die een invloed hebben op het verval van de lanthanide-ionen. Deze factoren zijn bijvoorbeeld deactivering door het oplosmiddel, de invloed van de brekingsindex van het oplosmiddel en de concentratie van het luminescerende lanthanide-ion in het nanodeeltje. Van al deze factoren bleek de deactivering door het oplosmiddel de grootste invloed te hebben op het exponentiële verval van de luminescentie. Er werd een model ontwikkeld waarmee de luminescentie-ervallen kunnen worden gefit. Dit model houdt rekening met deactivering van het lanthanide-ion van buiten de nanodeeltjes en met de afstand van het lanthanide-ion tot het oppervlak van het nanodeeltje. Het model geeft een waarde voor de levensduur in afwezigheid van deactivering van buiten het nanodeeltje en een deactiveringsconstante die de mate van deactivering van het lanthanide-ion door organische groepen buiten het nanodeeltje weergeeft. Met dit model kunnen de deactivering door het oplosmiddel en door de concentratie van lanthanide-ionen in het deeltje worden beschreven. De afhankelijkheid van de luminescentie-eigenschappen van de deeltjesgrootte werd bestudeerd door verschillende deeltjes groottes te synthetiseren. Er werd een duidelijke afhankelijkheid van de luminescente levensduur van de deeltjes grootte gevonden met de langste levensduur voor de grootste deeltjes.

In hoofdstuk 5 staan verschillende methoden beschreven om het oppervlak van de  $\text{LaF}_3$  en  $\text{LaPO}_4$  nanodeeltjes te functionaliseren met verschillende liganden. Het oppervlak van de nanodeeltjes bepaald de oplosbaarheid en controle over de oplosbaarheid is belangrijk voor de verwerking van de nanodeeltjes. De synthese van kern-schil deeltjes is beschreven als een manier om de interactie van lanthanide-ionen in het deeltje met deactiverende groepen buiten het deeltje nog meer te verkleinen. De luminescente lanthanide-ionen werden alleen gedoteerd in de kern en daaromheen werd een schil van niet gedoteerd anorganisch materiaal gegroeid. Deze

methode was succesvol want de grootte van de deeltjes nam toe na het groeien van de schil rond de kern en de luminescente eigenschappen van de lanthanide-ionen in de kern verbeteren. De quantum opbrengst van LaF<sub>3</sub>Ce,Tb nanodeeltjes werd verhoogd en de levensduren van de emitterende niveau's van Eu<sup>3+</sup> werden verlengd. Deze resultaten tonen aan dat de afstand tussen het luminescerende lanthanide-ion en de deactiverende groepen die aan het oppervlak van de deeltjes zijn gecoördineerd vergroot kan worden.

In hoofdstuk 6 staat de synthese van lanthanide-gedoteerde halfgeleidernanodeeltjes beschreven. In TiO<sub>2</sub> nanodeeltjes werd energie overdracht van het halfgeleider material naar het lanthanide-ion geobserveerd voor lanthanide-ionen emitterend in het zichtbare en in het nabij-infrarood. De quantum opbrengst van deze nanodeeltjes is laag, hoewel de intrinsieke quantum opbrengst van het lanthanide-ion wel hoog is. Een licht-emitterende diode (LED) met deze nanodeeltjes als luminescent material werd gemaakt en deze gedroeg zich als een diode als er een voltage over werd gezet. Er werd echter geen lanthanide-luminescentie waargenomen, waarschijnlijk door de lage quantum opbrengst van de nanodeeltjes.

Polymere golfgeleiders met LaF<sub>3</sub>:Nd nanodeeltjes staan beschreven in hoofdstuk 7. De emissiespectra van de Nd<sup>3+</sup> ionen laten zien dat de nanodeeltjes in de golfgeleider zitten en de beperkte optische verliezen van de golfgeleider tonen aan dat de nanodeeltjes niet geclusterd zijn en slechts een kleine bijdrage leveren aan lichtverstrooiing in de golfgeleider. Met PMMA golfgeleiders werd een versterking van 0.3 dB gemeten bij 1319 nm bij een pompvermogen van 12 mW en met SU-8 golfgeleiders werd een versterking van 0.1 dB gemeten bij een pompvermogen van slechts 5 mW. Theoretische berekeningen tonen aan dat bij hogere pompvermogens en kleinere golfgeleiders, een versterking van 5.1 dB in een 5.7 bij 5.7 μm<sup>2</sup> golfgeleider mogelijk moet zijn. Dit is een bijna even grote versterking als gemeten voor een glasvezel onder deze experimentele omstandigheden. Er werd bovendien aangetoond dat deze versterking slechts mogelijk is gemaakt door de toename in de levensduur van het Nd<sup>3+</sup> ion door het in de nanodeeltjes te doteren. Het gebruik van deze nanodeeltjes geeft dus een belangrijk voordeel boven het gebruik van organische complexen als versterkend medium in polymere materialen.



## *Dankwoord*

Voor je het weet zijn er al weer vier jaar voorbij en is het aio-schap al weer voorbij. Zonder de hulp van anderen zou dit boekje er heel anders hebben uitgezien, dus wordt het nu tijd om een aantal mensen voor hun bijdrage te bedanken.

David Reinhoudt wil ik bedanken omdat hij mij de mogelijkheid heeft gegeven te promoveren in zijn groep. Hoewel het onderwerp niet jouw directe voorkeur had, heb je toch altijd met veel interesse mijn werk gevolgd. De grote verscheidenheid aan apparatuur beschikbaar in de groep en in het MESA<sup>+</sup> instituut hebben het mogelijk gemaakt om een breed onderwerp als dit toch uit te voeren.

Frank van Veggel wil ik bedanken omdat hij mij het vertrouwen heeft gegeven mij aan te nemen op zijn project. Ik heb je begeleiding altijd als zeer prettig ervaren omdat ik een grote mate van zelfstandigheid van je heb gekregen. Het was een verrassing toen je anderhalf jaar geleden vertelde dat je naar Canada zou gaan, maar ook over lange afstand was je altijd makkelijk bereikbaar.

Gerald Hebbink bedank ik voor de samenwerking die we hebben gehad in het begin van het project. Hij heeft mij veel geleerd over lanthanide-luminescentie, waar ik mij oorspronkelijk helemaal niet mee bezig zou gaan houden. Met jouw kennis van de lanthaniden hebben we samen snel een begin kunnen maken met deze nanodeeltjes.

Voor het meten van de levensduren van de nabij-infrarood emitterende lanthanide-ionen was de hulp van Albert Polman, Jeroen Kalkman en Michiel de Dood van het Amolf instituut in Amsterdam heel belangrijk. Bedankt voor de gastvrijheid die jullie altijd getoond hebben.

Alfred Driessen van de LDG groep bedank ik voor het vertrouwen dat hij had in de materialen die ik heb gemaakt, wat tot enkele samenwerkingen heeft geleid. Eerst was er de samenwerking met Dion Klunder en Vincent Kuiper met de microringresonatoren. Dit was voor mij een zeer nuttige ervaring omdat dit de eerste keer was dat we polymeerlagen hebben gemaakt, gedoteerd met nanodeeltjes. Later heeft Albert Borreman heel veel geholpen met de metingen aan mijn eigen golfgeleiders: onmeunig bedankt daarvoor. Deze mensen en anderen van de LDG groep bedankt voor deze prettige tijd. Belangrijk bij deze metingen was ook de hulp van Liviu Prodan van de laser physica groep met de 795 nm pomplaser die cruciaal bleek te zijn voor de metingen aan de gedoteerde SU-8 polymere golfgeleiders.

Léon Woldering heeft een hoop cleanroomwerk gedaan dat ook voor mijn onderzoek zeer belangrijk was. Deze kennis die jij in de cleanroom hebt opgebouwd, heeft mij in het begin heel veel geholpen.

Mark Brouwer en Marcel de Bruine: bedankt voor het toeleveren van alles wat er in een lab nodig is. Voor de analyse en karakterisering van mijn produkten wil ik Tieme Stevens (massa), Hannie Visser (NMR), Annemarie Montanaro (EA), Louise Vrielink (XRF) en Rico Keim en Mark Smithers (TEM) bedanken. Carla, Rita en Izabel ben ik dankbaar voor alle administratieve ondersteuning.

Dan moet ik natuurlijk nog een heleboel mensen bedanken die in dezelfde periode hier aanwezig waren als ik. Ik zal geen poging doen om ze allemaal bij naam te noemen, maar iedereen die ik heb kunnen lastig vallen met vragen en iedereen die voor gezelligheid op het lab, in de koffiekamer en tijdens volleybal en voetbalwedstrijden heeft gezorgd, bedank ik voor deze mooie tijd! Zeker de mensen die altijd dicht bij me in de buurt hebben gestaan en moesten leven met het valse gezin en gefluit van mijn kant.

Léon en Emiel zullen op de grote dag naast mij op het podium staan als mijn paranimfen waarvoor ik ze alvast hartelijk wil bedanken.

Dan wil ik nog mijn familie bedanken voor de steun en de interesse in mijn onderzoek. In het bijzonder wil ik Siebe bedanken voor het ontwerpen van de voorkant van mijn boekje.

Nathalie als laatste en belangrijkste persoon in mijn leven: bedankt voor de liefde en morele steun tijdens deze vier jaar en dat je voor mijn werk in Tukkerland hebt willen wonen.

## *Curriculum Vitae*

Wiljan Stouwdam werd geboren op 29 december 1974 in Ijsselmuiden. Na het VWO aan het Emelwerda college in Emmeloord begon hij in 1993 aan de studie scheikunde aan de Rijksuniversiteit Groningen. Het hoofdvakonderzoek werd gedaan in de groep van prof. dr. J. B. F. N. Engberts. Hier werd gewerkt aan de synthese en de bestudering van de aggregatie vormen van een lipide. Na het hoofdvakonderzoek heeft hij in 1999 een onderzoeksstage gedaan bij Unilever Research bij de afdeling vloeibare wasmiddelen in Vlaardingen. Hier werd gewerkt aan de binding van calcium aan de verschillende surfactants die in de wasmiddelen worden gebruikt.

In januari 2000 begon hij aan zijn promotie-onderzoek in de vakgroep Supramoleculaire Chemie en Technology onder leiding van prof. dr. ir. D. N. Reinhoudt en dr. ir. F. C. J. M. van Veggel aan de Universiteit Twente. Tijdens dit onderzoek werd gewerkt aan het verbeteren van de optische eigenschappen van lanthanide-ionen in organische materialen voor gebruik in polymere optische versterkers. De resultaten van dit onderzoek staan beschreven in dit proefschrift. Hij zal na zijn promotie als post-doc gaan werken aan de universiteit van Victoria, Canada, waar hij zal werken in de groep van prof. dr. ir. F. C. J. M. van Veggel aan optische materialen voor fotonische kristallen.